1998

Shock-assisted pneumatic injection technology

Ajit Godbole
University of Wollongong

SHOCK-ASSISTED PNEUMATIC INJECTION TECHNOLOGY

A thesis submitted in fulfilment of the
requirements for the award of the degree

Doctor of Philosophy

from

UNIVERSITY OF WOLLONGONG

by

Ajit Godbole

Department of Mechanical Engineering

December 1998

Declaration

This is to certify that the work presented in this thesis was carried out by the author in the Department of Mechanical Engineering of the University of Wollongong and has not been submitted for a degree to any other Institution or University.

Ajit Godbole

Acknowledgments

It is with great pleasure and gratitude that I acknowledge the constant help and encouragement of my supervisors, A/Prof P W Wypych and A/Prof W K Soh, throughout the duration of this work.

I am very grateful to A/Prof P Cooper for his perceptive hints and suggestions concerning the experimental set-up and flow visualisation, and also the analytical work, especially the part involving PHOENICS.

My sincere thanks to Mr David Cook and Mr Peter May of the Centre for Bulk Solids and Particulate Technologies and Mr Stuart Watkins and Mr Martin Morillas of the Engineering Workshop for their great help in building and setting up the experimental facility, and to Mr Ian Frew for his help with the experiments. My heartfelt thanks also go to the Research Office of the University of Wollongong for providing financial support in the form of a UPA scholarship during the latter part of the project.

The basic idea for the device investigated came from Prof R J Krane and Prof W S Johnson, University of Tennessee, Knoxville, U S A.

This work could never have been done without the support and prayers of my wife Neera and my family back home.

Ajit Godbole

Abstract

Analytical and experimental investigations exploring a new, potentially useful idea for a type of particle injector are presented. The injector is designed to work on the principles of gas dynamics, and can be used for transporting dry particulate matter to high pressure destinations and processes. The proposed device is expected to overcome many of the limitations (such as limited operating/back pressure, moving parts, clogging, deterioration due to particle agglomeration) of conventionally used particle feeders. The basic idea involves creation of a zone of relatively low pressure in a supersonic gas stream in a duct, and introducing the particulate matter into this zone. The particulate matter is then conveyed by the gas stream to the high pressure destination through a normal shock.

The aim, motivation and basic concepts of the project are introduced in Chapter 1. The relevant available literature is also surveyed.

Chapter 2 contains an overview of the project. The technique used for the analytical investigation of the flow in the proposed injector is introduced.

Chapter 3 contains an analytical investigation of flow in the Injection Tube.

Chapter 4 presents an analysis of the primary gas flow, which leads to nozzle design.

Flow in the Interaction Region is investigated in Chapter 5.

Chapter 6 introduces a 'Modified-Fanno' model for the pseudo-shock, developed during the course of the analytical investigation of flow in the Compression Region.

In Chapter 7, the 'Modified-Fanno' model is extended to suspension flows.

Chapters 8 and 9 contain two-dimensional and three-dimensional PHOENICS simulations of the flow in the injector duct, respectively.

Chapter 10 contains an account of design considerations and fabrication details of the experimental facility and a description of the flow visualisation technique.

Chapter 11 presents results of the experimental investigation, along with comparisons with theoretical predictions.

Chapter 12 presents conclusions and recommendations for further and related work.

Among the new ideas explored during this study are the application of Generalised Steady One-Dimensional Flow analysis for designing the nozzle duct, modelling of a pseudo-normal shock in a duct as 'Modified-Fanno' flow, and a possible extension of the model to multiple shocks in suspensions.

The study reveals that the proposed injection device is feasible and easily controllable.

Contents

List of Figures

List of Tables

NOMENCLATURE

A	Area of Cross Section	(m^2)
A_{core}	Area of Cross-Section of Core in Shock Region	(m^2)
$A_{\delta u^*}$	Area associated with Boundary-Layer Displacement Thickness	(m^2)
$A_{Frontal}$	Frontal Projected Area of a Particle	(m^2)
AR	Driving potential due to ARea change = $\frac{1}{A}\frac{dA}{dx}$	(m^{-1})
A_{tube}	Area of Cross Section of Injection Tube	(m^2)
a	Sonic Velocity	$(m\ sec^{-1})$
a_s	Sonic Velocity in Suspension	$(m\ sec^{-1})$
B	General Flow Parameter	
b	Width of Shear Layer between two Co-Flowing Streams	(m)
$C_{DStokes}$	Stokes Coefficient of Drag	
C_{Dp}	Coefficient of Drag for Particle	
c_p	Specific Heat at Constant Pressure	$(J\ kg^{-1}K^{-1})$
c_v	Specific Heat at Constant Volume	$(J\ kg^{-1}K^{-1})$
cmp	Specific Heat of Particle Material	$(J\ kg^{-1}K^{-1})$
c	Constant in Shear Layer Growth Equation	
D	Diameter of Duct	(m)
DR	Driving Potential due to Particle Drag	(m^{-1})
d_p	Diameter of a Particle	(m)
D_H	Hydraulic Diameter of Duct	(m)
dx	Increment in Streamwise Distance	(m)
D_p	Drag on a Particle	(N)
EDA	Effect on Density of Area change	
EDFD	Effect on Density of Friction and Drag	
EDEM	Effect on Density of Entrained Mass	
EDEN	Effect on Density of ENergy Transfer	
EMA	Effect on Mach Number of Area Change	
EMFD	Effect on Mach Number of Friction and Drag	
EMEM	Effect on Mach Number of Entrained Mass	
EMEN	Effect on Mach Number of ENergy Transfer	
ENER	Driving Potential due to ENERgy transfer	
EPA	Effect on Pressure of Area Change	
EPFD	Effect on Pressure of Friction and Drag	
EPEM	Effect on Pressure of Entrained Mass	
EPEN	Effect on Pressure of ENergy Transfer	
ESA	Effect on Specific Entropy of Area Change	

ESFD	Effect on Specific Entropy of Friction and Drag	
ESEM	Effect on Specific Entropy of Entrained Mass	
ESEN	Effect on Specific Entropy of ENergy transfer	
ETA	Effect on Temperature of Area Change	
ETFD	Effect on Temperature of Friction and Drag	
ETEM	Effect on Temperature of Entrained Mass	
ETEN	Effect on Temperature of ENergy transfer	
EVA	Effect on Velocity (or Variable) of Area Change	
EVFD	Effect on Velocity (or Variable) of Friction and Drag	
EVEM	Effect on Velocity (or Variable) of Entrained Mass	
EVEN	Effect on Velocity (or Variable) of ENergy transfer	
f	Friction factor = $(\tau_w/0.5\ \rho\ V^2)$	
f'	Friction Factor associated with Core Flow	
f''	Friction Factor associated with Boundary-Layer Flow	
f_{av}	Average Friction Factor associated with Core Flow	
f_{int}	Integrated Friction factor associated with Fanno Flow	
FR	Driving potential due to FRiction = f/D_H	(m^{-1})
H	Total Enthalpy	(J)
h	Specific Enthalpy	$(J\ kg^{-1})$
h_{tube}	Height of Rectangular Cross Section Injection Tube	(m)
k_f	Fluid Thermal Conductivity	$(Jkg^{-1}m^{-1}sec^{-1}K^{-1})$
L*	Length of Duct required to reach Sonic Condition	(m)
M	Mach Number	
mp	Mass of a Single Particle	(kg)
$\dot{m}$	Mass Flow Rate	$(kg\ sec^{-1})$
mfp	Mass Fraction of Particles	
mrp	Mass Ratio of Particles	
Nu	Nusselt Number	
Nu_{Stokes}	Nusselt Number in Stokes Flow Regime	
Nu_{dp}	Nusselt Number based on Particle Diameter	
p	Static Pressure	(Pa abs)
p_0	Stagnation Pressure	(Pa abs)
p_b	Back Pressure	(Pa abs)
p_e	Exit Pressure	(Pa abs)
$\dot{Q}$	Rate of Total Heat Transfer	$(Jsec^{-1})$
$\dot{q}$	Rate of Heat Transfer per Unit Mass	$(Jkg^{-1}sec^{-1})$
R	Gas Constant	$(J\ kg^{-1}K^{-1})$
R_s	Gas Constant for Suspension	$(J\ kg^{-1}K^{-1})$
Re_{d_p}	Reynolds Number based on Particle Diameter	

Re_{D_H}	Reynolds Number based on Duct Hydraulic Diameter	
r	Radius	(m)
r_{tube}	Radius of Circular Cross Section Injection Tube	(m)
S	Total Entropy	($J\ K^{-1}$)
s	Specific Entropy	($J\ kg^{-1}K^{-1}$)
T	Static Temperature	(K)
T_0	Stagnation (Total) Temperature	(K)
T_p	Particle Temperature	(K)
t	Time	(sec)
V	Fluid Velocity	($m\ sec^{-1}$)
V	Mass-Averaged Velocity	($m\ sec^{-1}$)
V_p	Particle Velocity	($m\ sec^{-1}$)
V_1	Velocity of Stream 1 of Two Co-Flowing Streams	($m\ sec^{-1}$)
V_2	Velocity of Stream 2 of Two Co-flowing Streams	($m\ sec^{-1}$)
$\bar{V}$	Ratio of Velocities = V_2/V_1	
vfp	Volume Fraction of Particles	
Vol_{inf}	VOLume (of Suspension) INFluenced (by Primary Gas Stream)	(m^3)
WK	Driving Potential due to WorK Transfer	
w	Work Transfer Rate per Unit Mass	($J\ kg^{-1}sec^{-1}$)
w_{tube}	Width of Injection Tube of Rectangular Cross Section	(m^2)
x	Streamwise Distance	(m)
x_c	Length of Potential Core	(m)
β	Flow Parameter per Unit Mass	
γ	Ratio of Specific Heats = c_p/c_v	
δD	Drag on Fluid in Control Volume	(N)
δ_u	Boundary-layer thickness upstream of shock	(m)
δ_u^*	Boundary-Layer Displacement Thickness upstream of Shock	(m)
θ_u	Boundary-Layer Momentum Thickness upstream of Shock	(m)
ρ	Fluid Density	($kg\ m^{-3}$)
ρ_1	Fluid Density of Stream 1 of Two Co-Flowing Streams	($kg\ m^{-3}$)
ρ_2	Fluid Density of Stream 2 of Two co-Flowing Streams	($kg\ m^{-3}$)
ρ_s	Suspension Density	($kg\ m^{-3}$)
ρ_{mp}	Particle Material Density	($kg\ m^{-3}$)
$\bar{\rho}$	Ratio of Densities (ρ_2/ρ_1)	
σ_p	Particle Concentration	(m^{-3})
τ_w	Shear Stress at Duct Wall	($N\ m^{-2}$)
ψ	Recurring function of γ and M ($= 1 + \frac{\gamma - 1}{2} M^2$)	

Chapter 1

BASIC CONCEPTS

1.1 Introduction

Pneumatic conveying of particulate matter finds important applications in many industrial processes ranging from food-processing to power plants. These applications include drying and pneumatic transport of grain and other solid material, catalytic cracking in the petroleum industry, production of synthetic fuels from coal in energy conversion systems, etc. [A5]. Many applications require continuous feeding of particulate matter to high-pressure regions or processes. For example, in some coal gasification plants, coal is fed in the form of pulverised solid to gasifiers which operate at pressures between about 6 and 18 bar (g) [H5]. In the 'Lurgi' gasifier, crushed coal and a counter-current of gas react in chambers at pressures up to 30 bar (g) [B7]. In the 'Koppers-Totzec' gasifier, dried pulverised coal and a mixture of steam and oxygen is fed to coaxial burners. Coal gasification with steam is an endothermic process, so that the required heat must be provided. Complete entrainment of the feed material needs high gas velocities, and the reaction requires temperatures between 1825 and 1925 °C. In the 'Winkler' gasifier, crushed and dried coal is fed into chambers operating at temperatures from 1000 to 1100 °C [B7]. In coal-fired furnaces, pulverised coal is carried to the burners in an air stream and blown into the furnace, where it is burned in suspension. Such devices use pre-heated air at 200 to 320 °C [B7].

Conventionally used devices for 'continuous' bulk transport are [M4]:

1 Gravity Conveyors
2 Belt/Apron Conveyors
3 Bucket Conveyors
4 Flight/Drag Conveyors
5 Spiral/Screw Conveyors
6 Vibrating/Oscillating Conveyors

and

7 Pneumatic Conveyors.

Some conventional particle feeders are shown in Figure 1.1.

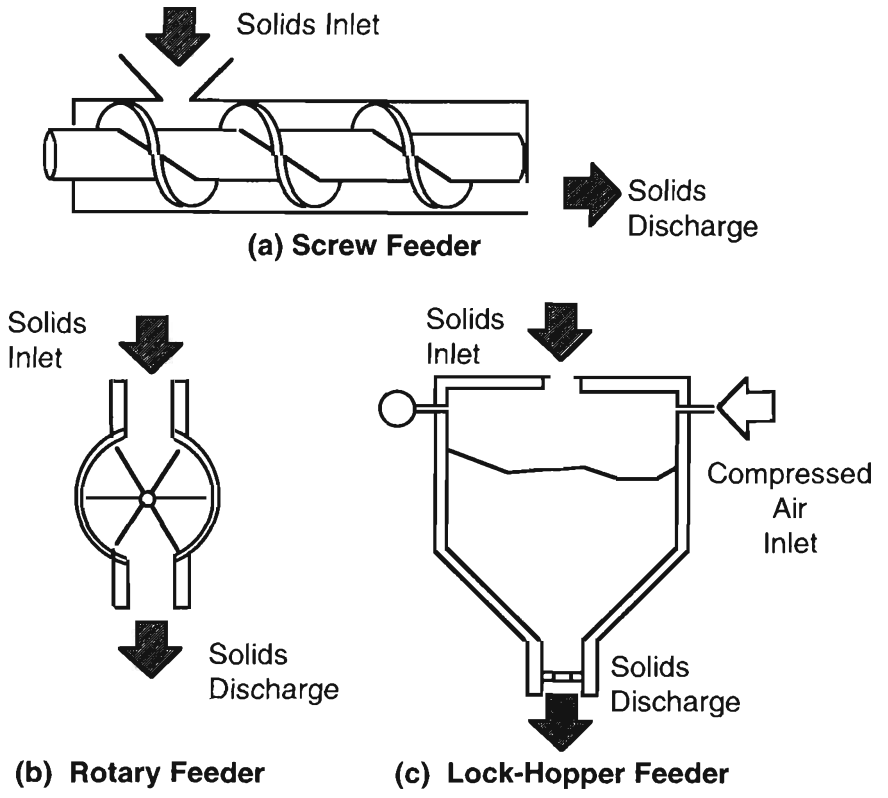

Figure 1.1 Some Conventional Solids Feeders

Most conventional feeders suffer from one or more of the following drawbacks:

1 Moving parts;
2 Intermittent and discontinuous feeding process;
3 Frequent clogging due to particle agglomeration and/or material build-up;
4 Large frictional losses, accompanied by excessive wear of close-tolerance machined parts;
5 Inability to transport particulate matter to high-pressure destinations;
6 Complicated design;
7 Preheating, if required, by additional means.

Besides these drawbacks particular to particle feeders, it should be mentioned that in the flow of compressible fluids and gas-solids mixtures, the occurrence of shocks is generally regarded as detrimental to the flow, due to the losses involved. Therefore, shocks are avoided as far as possible.

1.2 Motivation

'It is of considerable advantage to use feeders with no moving parts rather than applications with rotating parts such as rotary valves and screw feeders. Injectors have a large energy consumption often exceeding the energy required for the actual conveying of the solid material. In order to benefit from the latest progress in pneumatic injectors, it is essential to improve the performance of gas-solids injectors. At present, there is no reliable design procedure for this type of feeder owing to lack of theoretical and experimental data' [B5]. The proposed injector device (hereafter referred to as the Shock-Assisted Injector or SAI - this nomenclature will be justified in due course) is expected to overcome most of the demerits of conventional feeders, for the following reasons:

1 It has no moving parts.
2 A carefully designed injector should ensure smooth and continuous feeding.
3 The particles to be injected are less likely to come into contact with the injector walls for most of their flight path. This will ensure a minimum of clogging, so that the attendant losses are minimised.
4 Thus, minimal wear is expected. The device should therefore require only occasional maintenance, reducing operational costs.
5 The SAI is specifically designed to transport a pre-determined quantity of particulate matter to high-pressure destinations and processes.
6 The design of the proposed device is relatively simple, consisting of a de Laval nozzle with a centrally located injection tube.
7 Shock-assisted injection will prove useful in applications requiring pre-heating of the stream [B7], because a shock is accompanied by rise in temperature across it. The shock can also be used as an effective mixing device [Y2].

Finally, in an initially supersonic flow, subsequent rapid deceleration and recompression must necessarily occur through a shock. Thus, it is proposed that the occurrence of this otherwise undesirable flow feature be 'used' as a thermodynamic compression device to achieve the desired high pressure levels, and hence the term "Shock-Assisted Injector". Controlled use of shock wave production for desagglomeration in dispersed two-phase flows has been reported [eg. B7].

Motivation for the present project is provided by the possibility of testing several new ideas, both theoretical and practical.

On the theoretical side, it gives the researcher an opportunity of finding novel applications of known theories such as 'Generalised Steady One-Dimensional Flow Theory' [Z1] (see Chapters 3 to 5). The properties of gas-solids suspensions must be investigated in detail. A new model to account for the 'pseudo-shock' in duct flows (Chapters 6, 7) is proposed, and can be applied to situations where such multiple shocks are observed.

On the practical side, there is the possibility of producing a new conceptually simple injection device based on a definite design procedure, thus filling the lacuna mentioned above [B5]. Measurement of relevant flow parameters such as pressure offer additional challenges, as does the possibility of setting up a flow visualisation apparatus which may find uses apart from that in the present project.

1.3 Schematic Design

Some existing designs for pneumatic particle feeders are shown in Figure 1.2.

'In order to obtain a satisfactory performance and a high efficiency in transforming kinetic energy into static pressure energy, a detailed fluid dynamic calculation and correct dimensioning are necessary. The most advantageous aerodynamic solution is an injector with central solids feed and a ring nozzle' [B5].

In existing designs with 'central solids feed and ring nozzle', the solids are introduced into the nozzle flow upstream of the throat. This imposes a restriction on the achievable suction levels attained at the injection tube exit. One of the aims of the proposed SAI design is overcoming this limitation. A schematic diagram of the proposed injector is shown in Figure 1.3. The SAI consists of the following parts/regions :

1 A **de Laval (converging-diverging) Nozzle**, in which the 'primary' gas stream flows.

2 An **Injection Tube**, carrying the particulate matter in suspension, borne by a 'secondary' gas stream. This tube is centrally located in the nozzle duct and opens in the divergent (low-pressure) region of the nozzle.

3 The **Region of Interaction** between the primary and secondary streams where a limited amount of physical mixing is expected to take place.

4 The **Shock-Compression Region**, characterised by the occurrence of a normal shock. The possibility of a 'pseudo-normal' shock must be taken into account. Most of the physical mixing is likely to take place here.

5 The **Diffuser Region**, bringing about further deceleration and compression and conveying the composite stream to the final high-pressure destination.

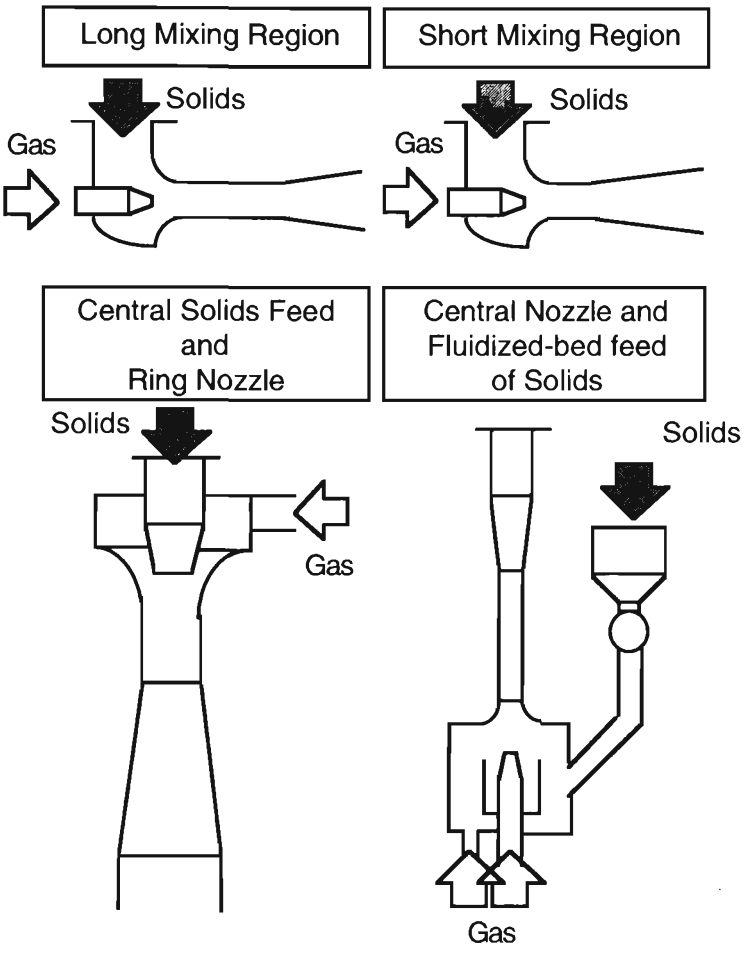

Figure 1.2 Different Pneumatic Injector Designs [B5]

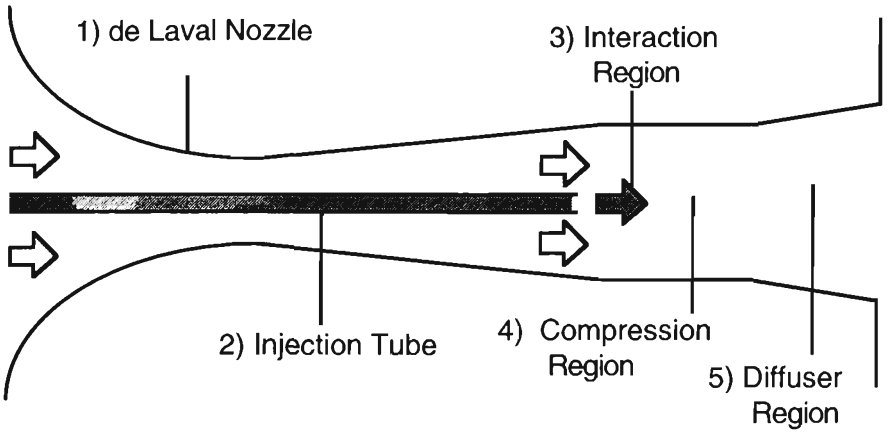

Figure 1.3 Schematic Diagram of Shock-Assisted Injector

The proposed injector is different in design from the devices sketched in Figure 1.2 in that the injector tube opens in the *divergent* part (downstream of the throat) of a de Laval nozzle duct in a *supersonic* primary gas stream. The nozzle duct is designed expressly to convey a pre-determined quantity of particulate matter to a high-pressure destination, as shown later. In a supersonic flow, subsequent deceleration to the final destination must occur via a shock; therefore the occurrence of a shock is used as a thermodynamic compression device to achieve the desired high-pressure levels. Compression across a single normal shock can be considered more *effective* than isentropic compression in that for the same density increase, shock compression is accompanied by a greater increase in pressure [A2] (See Figure 1.4). Compression across a single shock also occurs over a much shorter duct length than isentropic compression, which is the ideal case with no losses. This will continue to be true even in case of a multiple shock in the duct.

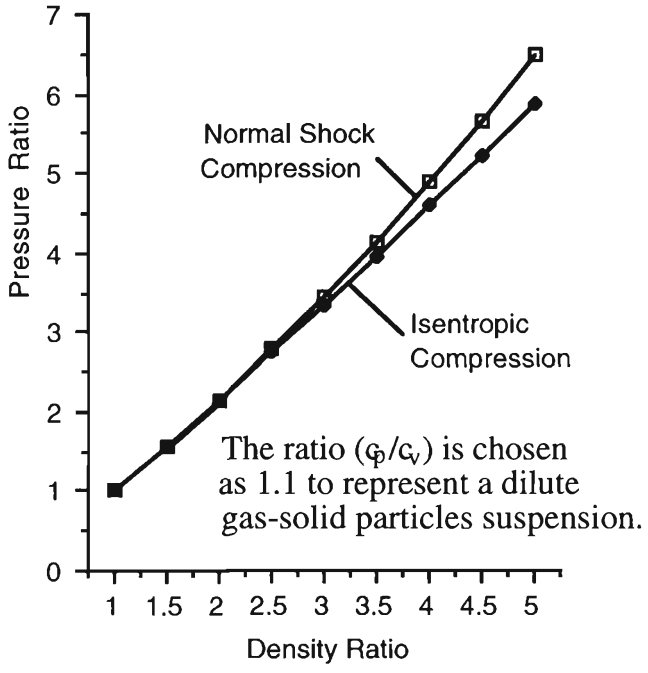

Figure 1.4 Shock Compression vs Isentropic Compression [A2]

1.4 SAI Flow Characteristics

The overall axial pressure variation in an SAI is sketched qualitatively in Figure 1.5. It is seen that the suspension is conveyed to a destination which is at a higher pressure than its starting point. There is, however, a net drop in the primary gas pressure, due to frictional losses and irreversibilities in the system.

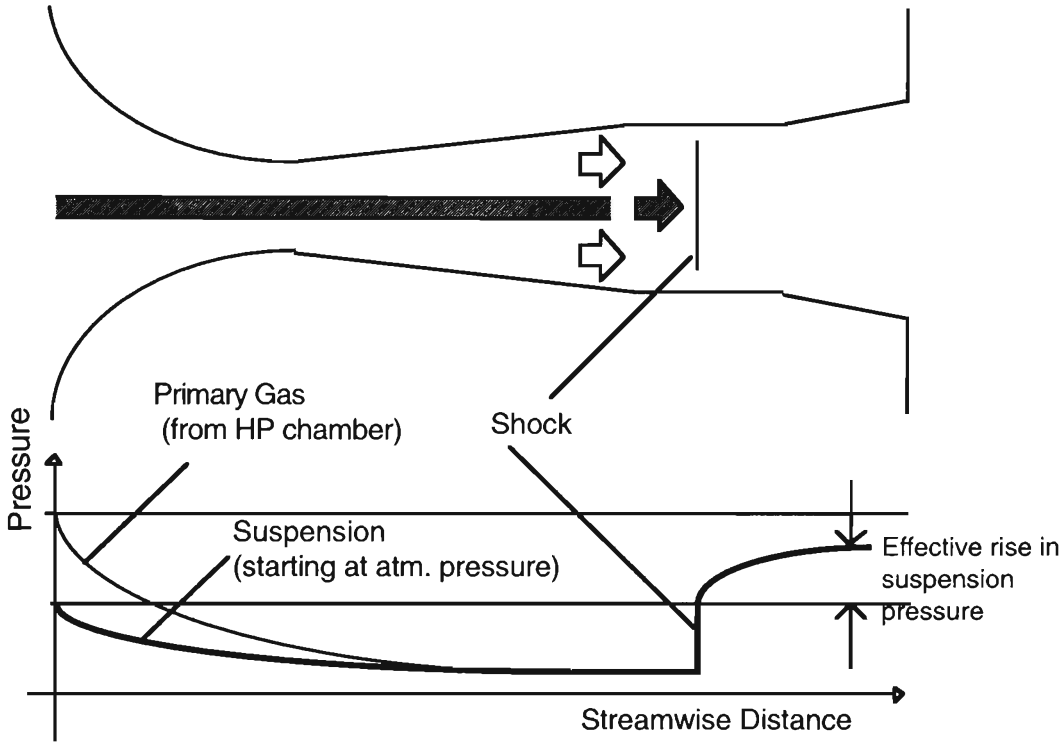

Figure. 1.5 Pressure Variation in SAI

It is convenient to study the different regions of the flow in the SAI separately . In the following sections, qualitative features of the flow in the different regions are described. Useful assumptions associated with the study of flow in each region are set down, along with preliminary qualitative descriptions.

1.4.1 Injection Tube

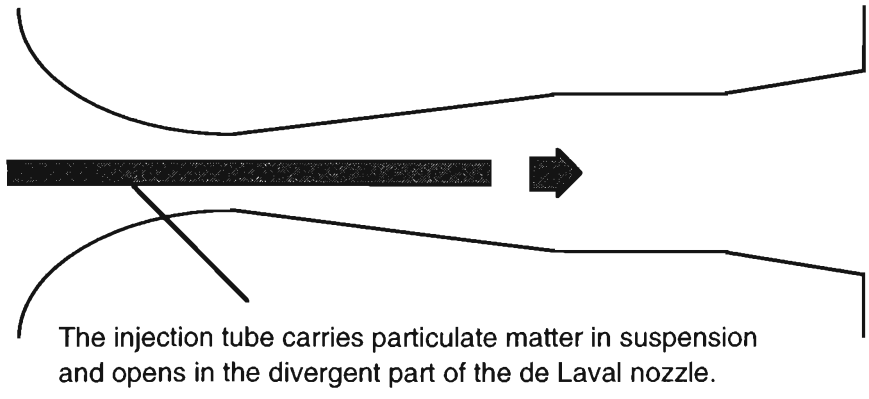

Figure 1.6 Injection Tube

As recommended in [B5], the injection tube is centrally located in the de Laval nozzle. It opens into the divergent (low-pressure) portion of the nozzle (Figure 1.6). The injection tube carries the particles in suspension, borne by a 'secondary' gas. For

the secondary gas-particles suspension to lend itself to analysis, it must satisfy certain requirements. Of the various phases of the flow of a gas-solids suspension, the one relevant to this study is the 'dilute' phase. In this phase, the solid particles occupy a small volume (say up to 5%) of the total mixture, and mix well with the secondary gas, forming a homogeneous mixture [S2].

A detailed enumeration of the properties of such dilute suspensions appears in Chapter 3.

1.4.2 de Laval Nozzle

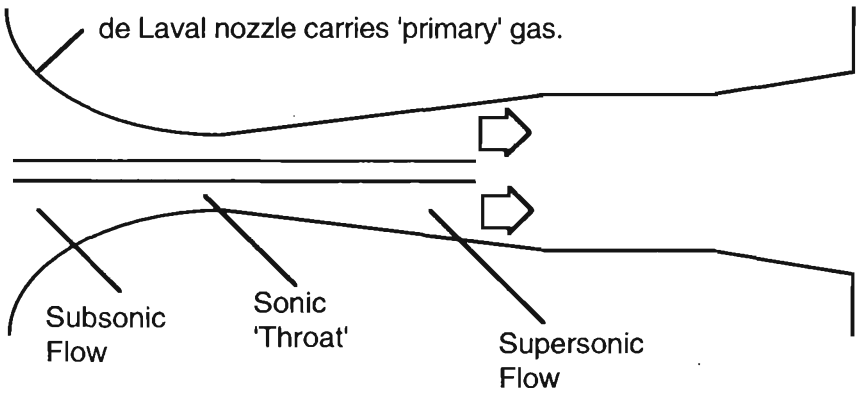

Figure 1.7 Flow of Primary Gas

The primary gas flows in a de Laval nozzle duct till the onset of interaction between the primary gas and the suspension. This duct can be designed (ie. the duct cross section areas at successive specified downstream locations can be calculated) using a one-dimensional approach, as demonstrated later. The aim is to produce a supersonic primary gas stream with a corresponding low pressure zone. The suspension can be introduced into this low-pressure zone. The injection tube thus opens in the divergent part of the de Laval nozzle. The cross-section of the de Laval nozzle can be circular or rectangular.

Interaction between the two streams starts when the suspension emerges from the injection tube and finds itself enveloped by the faster primary gas stream.

1.4.3 Interaction Region

At the onset of the interaction region, starting at the exit plane of the injection tube, a supersonic primary gas stream meets a co-flowing suspension stream, emerging at its sonic speed. At this stage, the velocity of the suspension is necessarily smaller than that of the primary gas stream. The slower suspension stream is to be accelerated by the primary gas stream. (If the injection tube is itself shaped like a de Laval nozzle, the suspension will emerge at *its supersonic* speed, which will still be *less* than the supersonic velocity of the primary gas - See Chapter 2.)

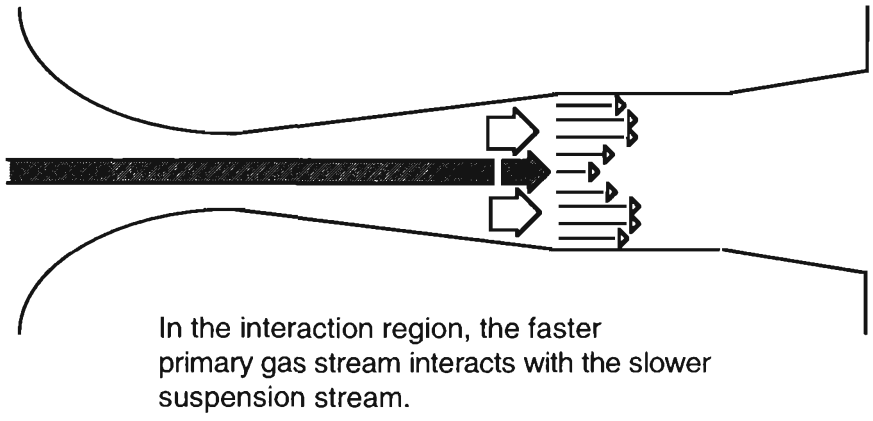

Figure 1.8 Interaction Region

It can be anticipated that the velocity profile in this region will be as shown in Figure 1.8. A limited amount of physical mixing between the suspension and the primary gas is likely to take place here. In this region, the duct should be designed such that the interaction is of a *constant-pressure* type, to prevent the formation of expansion or compression waves (Figure 1.9).

The presence of solid particles makes the suspension heavy - in applications involving pulverised coal, for example, the density of coal particles exceeds that of the secondary gas by a factor of about 1000. Therefore, due to their inertia, the particles in the suspension are not likely to spread to a great extent in the cross-stream direction. The general velocity profile is expected to be akin to a wake flow, as shown in Figure 1.8. The interaction can be allowed to continue till the combined stream reaches a supersonic speed.

Thereafter, the combined stream can undergo compression initially in the shock-compression region, then in the diffuser.

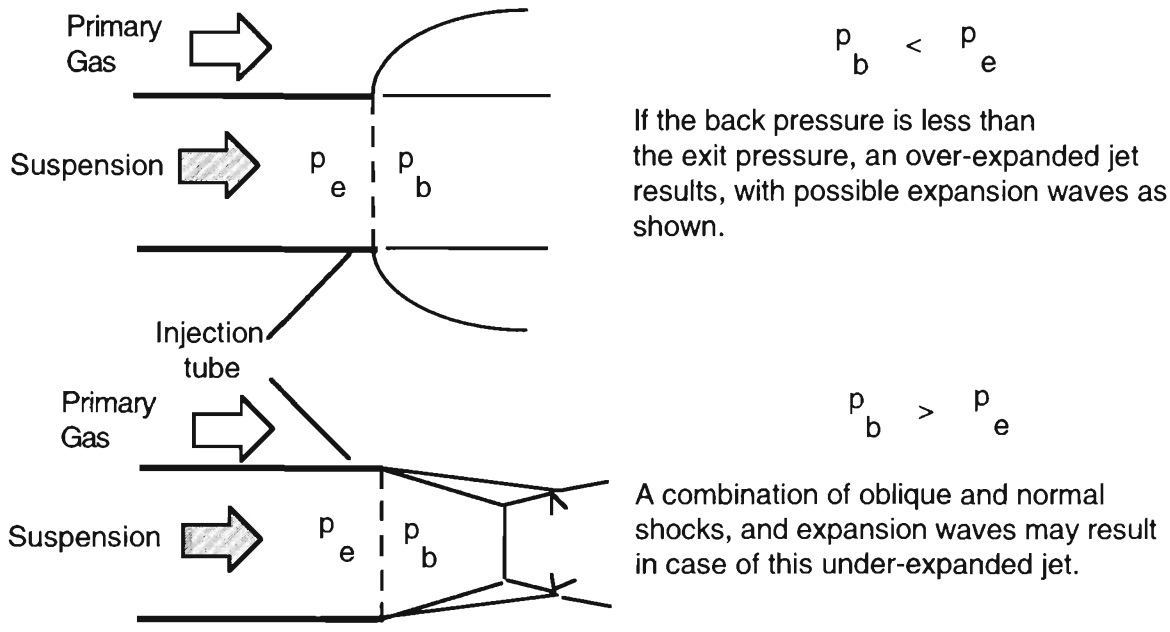

Figure 1.9 Unequal Pressures at Start of Interaction Region

1.4.4 Shock compression region

The interaction between the primary gas stream and the secondary gas-particles suspension continues until the combined stream reaches supersonic speed. Depending upon the desired pressure at the final destination, a normal shock can be made to stand at a specific point in the duct. In an unbounded or ideal inviscid flow, a single normal shock is expected, with the accompanying abrupt rise in pressure across the shock.

In a narrow channel flow such as the SAI, however, severe interaction is expected between the initial shock and the boundary layer growing along the walls of the duct. The resulting flow is such that the pressure rise associated with a normal shock occurs over an extended length of the duct [eg. S11]. The core of the flow (around the centerline and away from the confining walls of the duct) is characterised by the occurrence of a succession of progressively weaker shocks, if the initial 'blockage' (effective reduction in flow area due to boundary-layer growth) is high enough [O1, O2] (Fig. 1.10). The core flow is accompanied by large spatial fluctuations in flow parameters such as Mach number, pressure, etc. because of the shock train. These fluctuations are damped out at distances closer to the confining walls. At the wall of the duct, the pressure shows a steady rise throughout the shock compression region [I1, O1, O2, T2, T3].

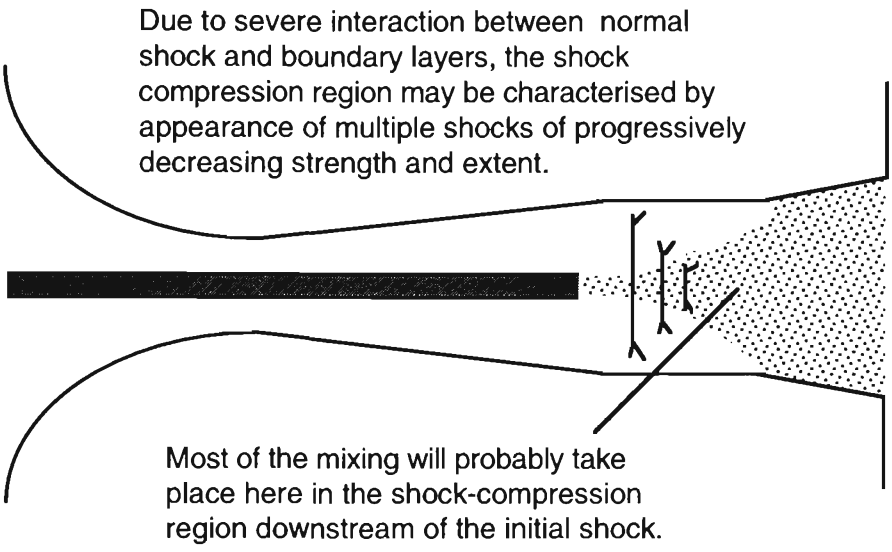

Figure 1.10 Shock Compression Region

It is estimated that a duct length of the order of 10 diameters is required for the pressure rise [eg. O1]. In the SAI, most of the physical mixing between the particles and the primary gas is expected to take place here. Thereafter, the composite stream enters the diffuser region, where the pressure continues to rise.

Because of the strong possibility of a pseudo-shock occurring in a flow such as the SAI, a study of this flow becomes an important part of the project. This need is accentuated by the fact that to date there is no comprehensive analytical model which accounts for the trends seen in a pseudo-shock pattern even in single-phase flows, which is also observed in a number of other situations [eg. O1].

1.4.5 Diffuser Region

The stream entering the diffuser region is assumed to be completely homogeneous. It is now a gas-particle suspension more dilute than the suspension in the injection tube. The additional dilution is due to the presence of the primary gas in the mixture. Thus, the characteristic properties of this stream can be defined in a way analogous to that used for the secondary gas-particle suspension. Based on these properties, the diffuser region can be designed (ie. the flow cross section areas at successive locations can be calculated). As before, the first set of calculations can be based on a one-dimensional approach.

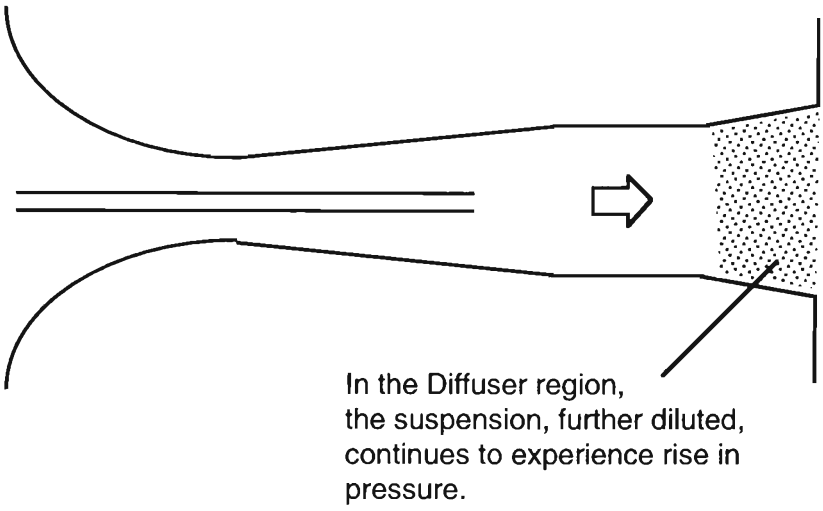

Figure 1.11 Diffuser Region

1.5 Brief Literature Survey

References to the relevant literature are cited and discussed at appropriate places in the following chapters. In this section, a brief literature survey is presented.

A qualitative comparison of the effectiveness of shock compression with respect to isentropic compression appears in [A2]. The significance of entropy generation in fluid flows is highlighted in [B6]. The suggestion is made that the second law should receive more careful attention in process equipment design, as it imposes fundamental restrictions on what can be achieved in practice. Reference [W7] provides an explicit formula for wall friction factor as a function of Reynolds number (Haaland's formula). This accurate formula is slightly more convenient to apply in the computational procedure than other conventionally used formulae which have the friction factor appearing on both sides of the equation, and hence require an iterative procedure for evaluation. Extensive wall friction factor measurements in pipe flows are reported in [K1]. [P3] investigates boundary layer development in a de Laval nozzle. This is significant in the present project for estimating the 'blockage' effect which may lead to formation of a pseudo-shock pattern. [S11] gives a short account of the theory involved in optical investigations of flows, especially those with density gradients. Shock-boundary layer interaction is identified as cause of the pseudo- shock. Discussion of the Fanno line appears in the section on normal shocks. This connection, in part, led to the development of the 'modified-Fanno' model for the pseudo-shock (Chapters 6, 7).

A design procedure for sub-sonic gas-solids injectors is given in [B5], and the recommendation made that a central solids feed with a 'ring' nozzle is the most efficacious design.

Development of models for the 'Driving Potentials' is based on the theoretical treatment in [A1]. In general, this model development is in agreement with findings reported in particular experimental situations, such as [A3], [C1-C7] and [K2]. [Z1, vol 1] gives a detailed account of the "Generalised Steady One-Dimensional Flow Analysis" procedure, along with some FORTRAN routines which can be used in specific flow situations. Lagrangian equations of particle motion in a gas-particles suspension are given in [Z1, vol 2], and these can be combined with the Eulerian equations for gas motion in the analytical treatment used in the present project, leading to a one-dimensional form of discrete particle modelling. The Runge-Kutta fourth-order scheme for solving simultaneous first-order differential equations appears, for example, in subroutine form in [P7], and is used in the present project.

An enumeration of significant parameters in gas-particle flows appears in [eg. W1, P1]. The suggestion that dilute gas-particle suspensions can be treated as ideal gases with modified properties such as gas constant, ratio of specific heats, etc. is put forth. However, experimental investigations particularly aimed at confirming this theory have been impossible to locate. The effect of small particles on the dynamic viscosity of the mixture is analysed in [E1], and [J1] reports the apparently contradictory influence of small particles on the eddy viscosity of suspensions. The importance of gas-particle flows in many different branches of modern technology are pointed out in [B1]. The fundamental mechanics of flowing suspensions is developed. The effect of finite particle size on the dynamics of suspensions is studied [L4] and [R3]. These and other studies suggest that particle volume fraction can be used to define the so-called 'dilute' suspension. However, the threshold value of 5% may be arbitrary, and can perhaps be doubled to 10% [eg W9].

[A5] gives a detailed account of various facets of pneumatic transport of solids, and the latest developments in the pneumatic transport of bulk solids are reported in [W9].

Experimental Investigations of pseudo-shock in clean air flow are reported in [O1, O2], [C9-C12], and [T2, T3], in which the distinction between 'λ-type' and 'X-type' pseudo-shocks is pointed out. An account of Crocco's 'Shockless' model for the pseudo-shock appears in [I1], along with an improved version called the 'Diffusion model'. A description of the phenomenological 'Shock-reflection' model is given in [Y3, Y4]. Exact details of the pseudo-shock model reported in [M5, M6 (Japanese

language)] are not available, but from the information available, it appears that the model is not unlike the Diffusion Model [I1]. [G5] outlines the 'Modified-Fanno' model and defines a 'friction factor' for the core flow in the pseudo-shock pattern. A preliminary second-law analysis of the pseudo-shock is also reported. The passage of solid particles across a single normal shock is analysed in [C6, K3, R4 and W1]. There appear to be no reports of studies of the pseudo-shock in suspensions in the available literature, as also no reports of studies on the passage of solid particles through a pseudo-shock pattern.

An overview of the present project is given in Chapter 2. Calculations based on the one-dimensional approach are taken up in detail in the subsequent chapters.

Chapter 2

PROJECT OVERVIEW

A breakdown of the analytical and experimental investigations of the SAI is provided in Figure 2.1.

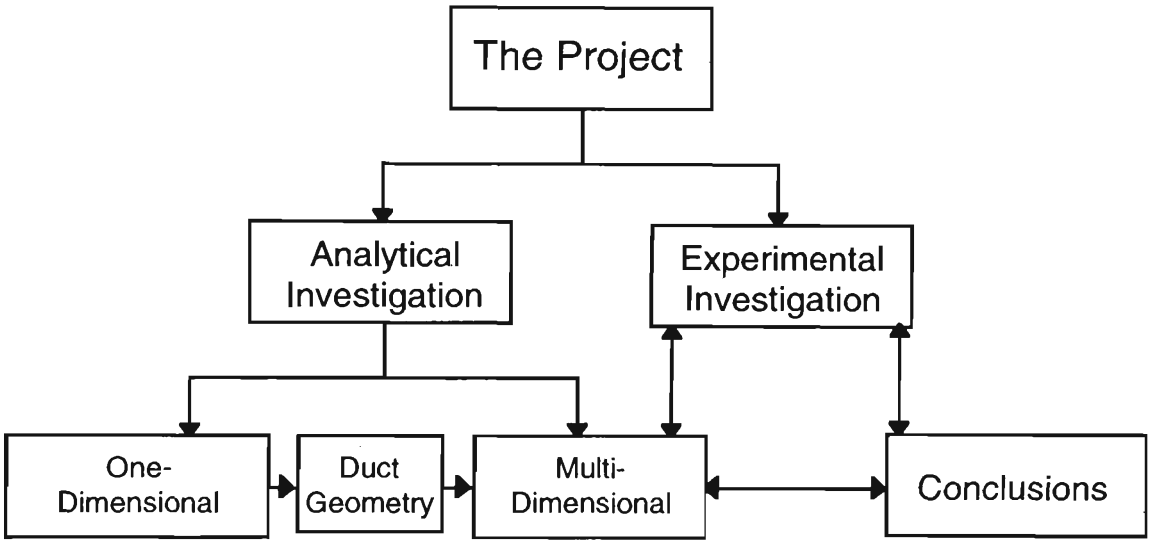

Figure 2.1 Project Overview

From the qualitative investigation in Chapter 1, it is clear that many different types of flow occur in different regions of the SAI. The method of analytical investigation must be such that these flows can be studied in a consistent way, and yet be simple enough to be the starting point of the investigation.

2.1 One-Dimensional Analysis

In one-dimensional analysis, the variation of flow parameters along the axis of the device is studied. Variations in the cross-stream direction are neglected. It is assumed that the flow is steady, ie. flow parameters at a particular point in the flow field do not change with time.

2.1.1 Analytical Technique

The method chosen is 'Generalised Steady One-Dimensional Flow' analysis' [Z1]. The main attractive feature of this method is its adaptability to different flow regimes in the SAI. Evolution of the flow in the downstream direction is described primarily in terms of equations of conservation of mass, momentum and energy. Other considerations such as entropy production can also be brought into play if required. The equations are written for a control volume which spans the flow and extends over a differential distance in the downstream direction (Figure 2.2). The conservation equations are supplemented by auxiliary equations such as the equation of state for an ideal gas and definitions of 'stagnation' (total) quantities (eg. stagnation pressure). These equations are cast in the form of a set of first-order ordinary differential equations in terms of 'Influence Coefficients' and 'Driving Potentials'. There are as many equations as there are flow parameters to be studied, so that they can be solved simultaneously.

As seen later, this analysis is used to 'size' the device. Once the overall shape (the geometrical boundary) of the device is known, it is possible to extend the analysis to a multi-dimensional study by constructing a computational domain to conform to the boundaries.

Main details of the method of analysis are given below. A full derivation of the governing equations is given in Appendix A. Expressions for significant driving potentials are derived at appropriate places in the following chapters, and are tabulated in Appendix A.

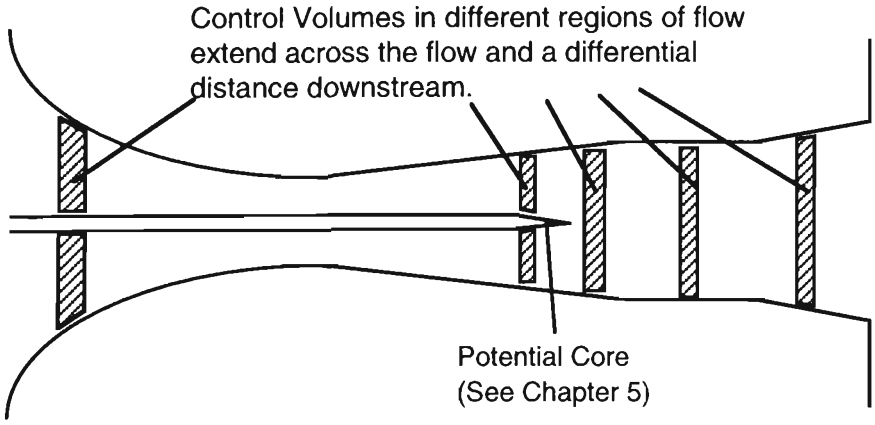

Figure 2.2 Control Volumes

2.1.2 Governing Equations

The rate of change of each flow variable ('var') with distance ('x') is described in terms of 'Influence Coefficients' and 'Driving Potentials' in the following form :

$$\frac{d(var)}{dx} = \sum_{\text{all effects}} (\text{Influence Coefficient}) \cdot (\text{Driving Potential}) \qquad (2.1)$$

The Driving Potentials are agents which bring about changes in flow parameters. For compressible fluid flow in a duct, these agents are recognised to be [Z1]:

1 Area of cross section of flow;
2 Friction at confining walls and Drag due to embedded/conveyed objects;
3 Energy transfer as Heat or Work to or from the fluid stream;
4 Mass entrained into the fluid stream.

Thus, the general equation describing the variation of any flow variable can be written as:

$$\frac{d(var)}{dx} = EVA \cdot AR + EVFD \cdot FD + EVEN \cdot ENER + EVEM \cdot EM \qquad (2.2)$$

Here, 'var' = any general flow variable such as pressure, velocity, etc.

The 'Influence Coefficients' are:

EVA = Effect on the Variable of Area change;
EVFD = Effect on the Variable of Friction and Drag;
EVEN = Effect on the Variable of ENergy transfer (Heat and/or Work);
EVEM = Effect on the Variable of Entrained Mass.

and the 'Driving Potentials':

AR = Driving Potential due to ARea change;
FD = Driving Potential due to Friction and Drag;
ENER= Driving Potential due to ENERgy transfer;
EM = Driving Potential due to Entrained Mass.

This yields a set of simultaneous first-order differential equations, equal in number to the flow variables investigated. The equations are solved by the Fourth-order Runge-Kutta technique [P7], starting from a set of known (or assumed) initial conditions and marching downstream in small increments.

One of the aims of the present project is to establish a design procedure for the injector device. This means having to design the shape of the converging-diverging nozzle duct, that is, to calculate the area of cross-section of the duct at specified locations along its length. If the equations of Generalised Steady One-Dimensional Flow analysis are used exactly in the form derived [Z1], it is assumed that this area variation is *given*, so that it can only be used as an independent variable (See Appendix A). In the present project, however, this is not the case. Thus the area variation must be treated as an unknown, and some other variable must be treated as known or given. Referring back to Figure 1.5, 'Pressure Variation in a Shock-Assisted Injector', it is seen that the variation of static pressure in the SAI can be specified, and thus treated as given along the length of the duct. The duct shape compatible with this pressure variation can then be determined from the above one-dimensional analysis.

Initially, it is desirable to study the flow in the different regions of the device separately (Figure 2.3). For these different regions, forms of the 'Influence Coefficients' in the above equations remain the same. However, for each region, it is necessary to recognise and derive expressions for the operative driving potentials. This feature makes the chosen analytical technique adaptable to different types of flows.

2.1.3 Connecting Link

It is noticed from the account in Chapter 1 that the flow of primary gas in the converging-diverging nozzle and that of the gas-particle suspension in the injection tube occur concurrently but independently until the onset of interaction between the two. Thus it is necessary to establish a connecting link between the two flows, so that the link can be used in the nozzle design procedure. Again, Figure 1.5 suggests that a possible connecting link is equality of pressure in the two flows at the onset of the interaction region.

In Chapter 3, flow of gas-particle suspension is studied in detail. It is also suggested that this flow approximates a Fanno-type flow. This establishes the pressure of the suspension at the end of the injection tube in a unique way and furnishes the connecting link between suspension flow and primary gas flow.

In subsequent chapters, the analytical technique is applied in turn to each region of the SAI.

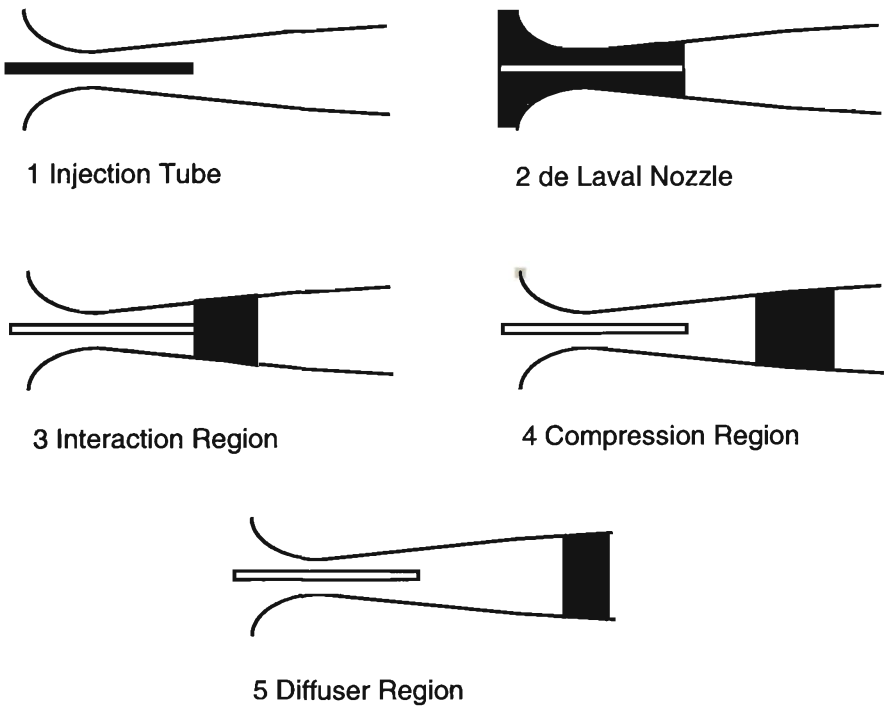

Figure 2.3 Flow Regions

2.3 Multi-Dimensional Analysis

Once the overall dimensions (the geometrical boundaries) of the device have been decided upon from the results of the one-dimensional analysis, it is possible to construct a 'computational domain', fitted so as to conform to the boundaries and divided into a convenient number of parts or 'cells'. Geometrical symmetry allows the construction of a two-dimensional computational domain (Chapter 8). Equations of conservation of mass, momentum and energy are solved for the contiguous computational cells, and thus for the entire computational domain. Results are obtained primarily in the form of plots of velocity vectors, and contour plots of such scalar variables as pressure, temperature, etc.

Two-dimensional analysis is carried out using the PHOENICS flow simulation system.

For the sake of completeness, a three-dimensional analysis is also carried out using PHOENICS, this being an extension of the previous step (Chapter 9).

Details of the PHOENICS simulation system are given in Chapters 8 and 9. The corresponding input data files, supplemented by explanatory comments, appear in Appendices C7 to C9.

Analysis of flow in each of the regions of the SAI begins with flow in the injection tube in the next chapter.

Chapter 3

FLOW IN INJECTION TUBE

The injection tube carries particulate matter in the form of a dilute gas-particle suspension, starting at atmospheric conditions.

For the secondary gas-particle suspension to lend itself to analysis, it must satisfy certain requirements. Various phases of the flow of a gas-solid particles suspension are described in the literature, such as low-velocity slug flow, plug flow, single-slug flow, extrusion, etc. [W9]. The particular phase relevant to this study is the 'dilute' phase, in which the particles are fully suspended, and occupy at most 5% of the suspension volume [S1]. With this assumption, the suspension can be treated as a pseudo-ideal gas with properties such as gas constant, ratio of specific heats, etc. modified due to the presence of particles [S1, W1].

3.1 Dilute Gas-Particle Suspensions

The analysis of a dilute suspension is based on the following assumptions:

1) The particles are small in size. Small as an individual particles may be, the molecules of the surrounding fluid are many orders of magnitude smaller. The behaviour of the suspended particles is therefore determined by the mechanics of a 'continuum' around it.

2) The particles are spherical in shape. In the SAI, combustion of the particles is not considered, so that each particle retains its size and mass throughout its journey. In the possible application in a coal gasification plant, for instance, combustion does not commence till the particles reach their final destination. Moreover, in this application, the particle size *distribution* may be assumed unimportant because this will affect the design only in minor details, so that the analysis can be based on the statistical average particle diameter.

3) As the particles are carried by the secondary gas, inter-particle collisions are assumed negligible. This will be approximately valid for a *dilute* small particle suspensions, in which inter-particle distances will be large compared to particle size. The suspension is considered as a mixture of two 'gases': one, the real gas, and the other, a 'pseudo-gas', consisting of particles only. (With this assumption, it is possible to define a 'molecular weight' of the pseudo-gas. See Equation 3.10).

3.1.1 Definition of Suspension Properties

The following basic properties of the gas-particle suspension are identified as relevant [P1, S2]:

1 Gas Density $= \rho_G = \dfrac{\text{mass of gas}}{\text{unit volume of gas}}$ (3.1)

2 Gas 'Concentration' $= \sigma_G = \dfrac{\text{mass of gas}}{\text{unit volume of gas-particle mixture}}$ (3.2)

3 Particle material density $= \rho_{mp}$ (constant) (3.3)

4. Particle 'Concentration' $= \sigma_p = \dfrac{\text{mass of particles}}{\text{unit volume of gas-particle mixture}}$ (3.4)

5 $\left[\begin{matrix}\text{Mass Fraction}\\ \text{of Particles}\end{matrix}\right] = \text{mfp} = \dfrac{\left[\begin{matrix}\text{Mass of Particles in}\\ \text{Unit Mixture Volume}\end{matrix}\right]}{\left[\begin{matrix}\text{Total Mass in Unit}\\ \text{Mixture Volume}\end{matrix}\right]} = \dfrac{\sigma_P}{\sigma_P+\sigma_G}$ (3.5)

6 $\left[\begin{matrix}\text{Mass Ratio}\\ \text{of Particles}\end{matrix}\right] = \text{mrp} = \dfrac{\left[\begin{matrix}\text{Mass of Particles in}\\ \text{Unit Mixture Volume}\end{matrix}\right]}{\left[\begin{matrix}\text{Mass of Gas in Unit}\\ \text{Mixture Volume}\end{matrix}\right]} = \dfrac{\sigma_p}{\sigma_G} = \dfrac{\text{mfp}}{1-\text{mfp}}$ (3.6)

7 $\left[\begin{matrix}\text{Particle}\\ \text{volume}\\ \text{fraction}\end{matrix}\right] = \text{vfp} = \dfrac{\text{volume of particles in unit mixture volume}}{\text{unit volume of mixture}} = \dfrac{\sigma_p}{\rho_{mp}}$ (3.7)

8 $\left[\begin{matrix}\text{Volume Fraction}\\ \text{of Gas}\end{matrix}\right] = \text{vfg} = \dfrac{\text{volume of gas in unit mixture volume}}{\text{unit volume of mixture}}$ (3.8)

9 Suspension density $= \rho_S = \dfrac{\text{total mass contained in unit volume of mixture}}{\text{unit volume of mixture}}$

Thus,

$$\rho_S = \sigma_P + \sigma_G = (vfp)\,\rho_{mp} + (1 - vfp)\,\rho_G \tag{3.9}$$

10 'Molecular Weight' of particle 'gas' = MWP = $\dfrac{\text{mass of a particle}}{\text{mass of a hydrogen atom}}$

(The particles are considered as 'very large molecules' [E1].)

11 Molecular Weight of Gas = MWG

12 Molecular Weight of Suspension = MWS = $\dfrac{1}{\dfrac{mfp}{MWP} + \dfrac{1 - mfp}{MWG}}$ (3.10)

13 Gas constant of suspension = R_S = $\dfrac{\text{Universal Gas Constant}}{\text{Mol. Wt. of suspension}}$ = $\dfrac{R_{univ}}{MWS}$

14 Specific heat of particle material = cmp

15 Constant - pressure specific heat of gas = cpg

16 Constant - volume specific heat of gas = cvg

17 Specific Heat ratio of gas = γ_G = $\dfrac{cpg}{cvg}$

18 $\left[\begin{matrix}\text{Constant-pressure specific heat} \\ \text{of suspension}\end{matrix}\right]$ = cps = $\dfrac{cpg + mrp \cdot cmp}{1 + mrp}$ (3.11)

19 $\left[\begin{matrix}\text{Constant-volume specific heat} \\ \text{of suspension}\end{matrix}\right]$ = cvs = $\dfrac{cvg + mrp \cdot cmp}{1 + mrp}$ (3.12)

20 $\left[\begin{matrix}\text{Specific Heat ratio} \\ \text{of suspension}\end{matrix}\right]$ = γ_S = $\dfrac{cps}{cvs}$ = $\gamma_G \dfrac{1 + mrp\dfrac{cmp}{cpg}}{1 + \gamma_G \cdot mrp\dfrac{cmp}{cpg}}$ (3.13)

21 Sonic Speed in suspension = a_S = $\sqrt{\gamma_S R_S T_S}$ (3.14)

22 $\left(\begin{matrix}\text{Suspension} \\ \text{Pressure}\end{matrix}\right)$ = $\left(\begin{matrix}\text{Gas} \\ \text{Pressure}\end{matrix}\right)$ + $\left(\begin{matrix}\text{Particle} \\ \text{Pressure}\end{matrix}\right)$

or,

$$p_s = p_g + p_p$$

It is now assumed that the contribution of the particles to the suspension pressure is taken into account automatically by the equation

$$p_S = \rho_S R_S T_S \tag{3.15}$$

expressing the assumption that the suspension behaves as an ideal gas. This assumption appears to be valid because the mechanism of exerting pressure must be identical for both gas molecules and suspended small particles - random impacts on the containing walls [B7].

In addition, the dynamic and kinematic viscosities of the suspension are included in this list of basic suspension properties. Doing so seems to remove an apparent contradiction in a simple way: experimental studies indicate that the presence of solid particles in a gas results in the *reduction in eddy viscosity* of the suspension [J1]. At the same time, other studies show that the *dynamic viscosity increases* due to the presence of suspended particles [eg. E1]. This apparent discrepancy is removed once it is recognised that eddy viscosity is the turbulent counterpart of *kinematic* viscosity, and that, by definition,

$$\text{kinematic viscosity} = \frac{\text{dynamic viscosity}}{\text{density}}$$

The presence of solid particles increases the dynamic viscosity. However, this increase is more than compensated for by the increase in suspension density, so that the ratio of the two quantities decreases. This is shown in Figure (3.1).

In general, the dynamic viscosity of gases depends strongly on temperature and only slightly on pressure. An equation describing the temperature dependence is the 'Sutherland viscosity law' [W7]:

23 Dynamic viscosity of gas = μ_G = Constant $\cdot \left[\frac{T^{1.5}}{T+110} \right]$ (3.16)

24 Dynamic viscosity of suspension = $\mu_S = \mu_G \cdot (1+2.5\text{vfp})$ [E1] (3.17)

25 $$\begin{bmatrix}\text{Kinematic viscosity} \\ \text{of suspension}\end{bmatrix} = \nu_S = \frac{\mu_S}{\rho_S} = \nu_G \frac{1+2.5\text{vfp}}{1+\text{vfp}\left(\rho_{mp}/\rho_G - 1\right)} \tag{3.18}$$

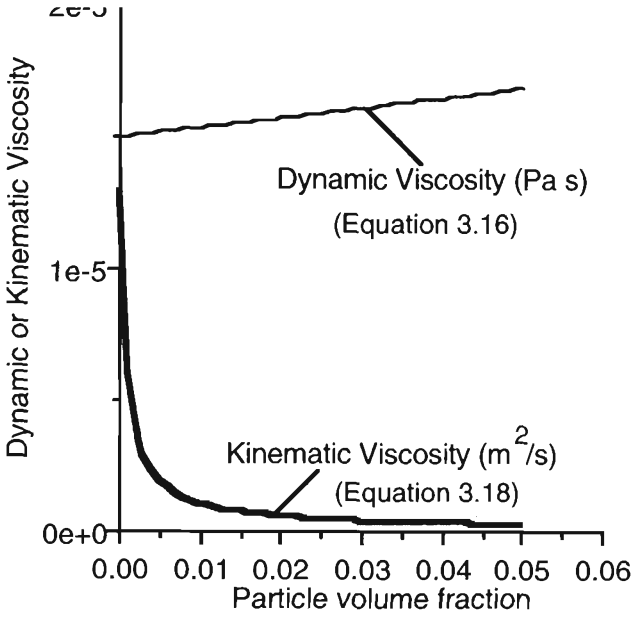

Figure 3.1 Dynamic and Kinematic Viscosities of Suspension

3.2 Suspension Flow Analysis

The suspension is assumed to flow in an injection tube of constant cross-sectional area and having an impermeable wall which is assumed rigid and perfectly insulated. With no transfer of energy as either heat or work across such a boundary, the stagnation (total) enthalpy (or stagnation temperature, if the suspension behaves as an ideal gas) remains constant. An additional assumption is made that the particles are thoroughly mixed with the secondary gas, so that there is no difference between the velocities and temperatures of the particles and the secondary gas. The suspension approximates 'homogeneous equilibrium flow' [W1]. (It may be mentioned that if this assumption is found invalid, it is still possible to treat the suspension as an ideal gas with its properties such as gas constant expressed in terms of (constant) velocity and temperature lags [W1]). The flow is thus adiabatic but irreversible - wall friction is the sole driving potential bringing about property changes in the streamwise direction. In other words, the suspension undergoes a 'Fanno-type' flow (Appendix B) in the injection tube.

3.2.1 Significant Driving Potentials

For such a flow, the equations describing it are obtained from the most general equations (Appendix A) by making the following observations about the relevant driving potentials:

5. Rate of Change of Velocity:

$$\frac{dV_S}{dx} = V_S \left\{ \frac{\gamma_S M_S^2}{2} \right\} \frac{c_{f_S}}{D_{H_{tube}}} \tag{3.27}$$

6. Rate of Change of Stagnation (total) Pressure:

$$\frac{dp_{0s}}{dx} = p_{0s} \left\{ \frac{-\gamma_S M_S^2}{2} \right\} \frac{c_{f_S}}{D_{H_{tube}}} \tag{3.28}$$

7. Rate of Change of Specific Entropy (optional) :

$$\frac{ds_S}{dx} = c_{p_S} \left\{ \frac{(\gamma_S - 1) M_S^2}{2} \right\} \frac{c_{f_S}}{D_{H_{tube}}} \tag{3.29}$$

3.3 Alternative Analytical Approach

Under the assumption of adiabatic flow of a suspension in a rigid-walled tube, the suspension undergoes a 'Fanno-type' flow, with wall friction as the only operative driving potential. At the exit, the suspension attains its sonic condition, with the corresponding values of flow parameters. In particular, the static pressure corresponding to the suspension's sonic condition is given by p_S^* (Appendix B). Alternatively, by ensuring that the pressure at the exit of the injection tube is p_S^*, the suspension can be made to emerge at its sonic speed. This effectively ties together the analyses of flows in the injection tube and the de Laval nozzle, as explained in the next chapter. This connection is depicted in Figure 3.2.

The constants associated with the suspension (gas constant, specific heats, ratio of specific heats, etc) and suspension flow parameters at the end of the injection tube are a function of particle 'loading' (particle volume fraction). Following the assumption made above that a suspension can be considered 'dilute' if the volume fraction of the particles is less than 5%, the suspension parameters are calculated for the range of volume fractions $0 < vfp < 0.05$. It may be noted that this assumption can be relaxed, because the 5% figure seems arbitrary.

Suspension parameters expressed as functions of particle volume fraction are shown in Figures 3.4 to 3.9.

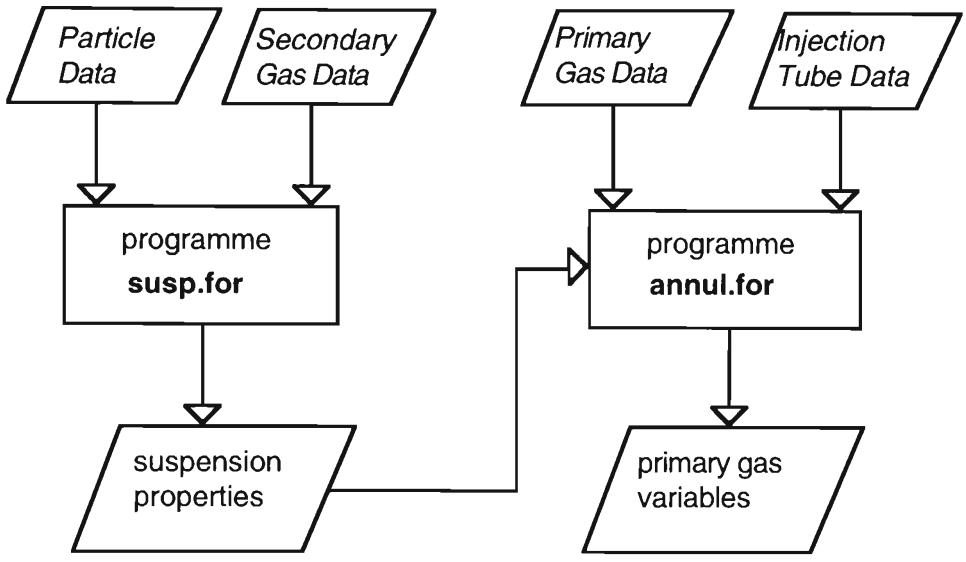

Figure 3.2 Link between Suspension Flow and Primary Gas Flow

3.4 Suspension Flow Parameters

In the experimental part of this project, the gas-particle suspension is composed of air at standard atmospheric conditions and spherical glass 'beads' of an average size 150 μm (Figure 3.3). These particles were chosen because of their availability. They also have the desirable property of not being sticky and are capable of free flow. The computer program 'susp.for' [Appendix C] calculates suspension properties as a function of particle volume fraction. It is significant that particle size is not an important variable in the definitions of suspension properties. This lends justification to the assumption that particle size distribution is an unimportant variable as far as suspension properties are concerned.

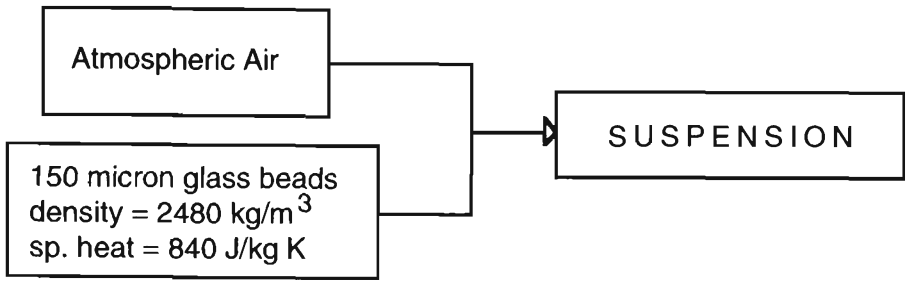

Figure 3.3 Gas-Particle Suspension

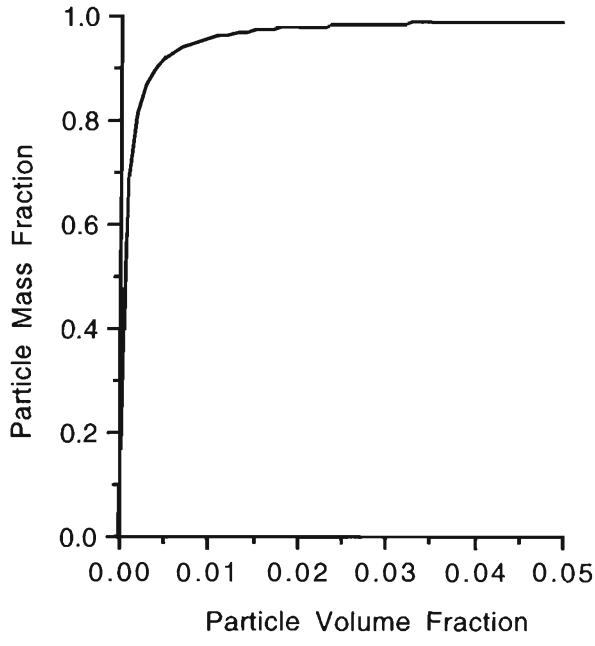

Figure 3.4 Particle Mass Fraction vs Particle Volume Fraction

It is seen in Figure 3.4 that as particle volume fraction increases, particle mass fraction also increases and eventually approaches the value '1' asymptotically. The limiting value implies an 'all solids' state.

Figure 3.5 below shows that particle mass ratio for the suspension increases almost linearly with increasing particle volume fraction. Particle Mass Ratio attains very high values even for small values of particle volume fraction. This is due to the high value of particle material density, and implies that even relatively dilute suspensions carry a large quantity of solid particles. This result therefore is compatible with one of the aims of the project - to convey large quantities of particulate matter pneumatically.

If the 'diluteness' assumption (particle volume fraction < 5%) is relaxed, the resulting particle mass ratio values will be even better for the present project. The diluteness 'threshold' has been variously defined, and perhaps a value of 10% can be considered acceptable.

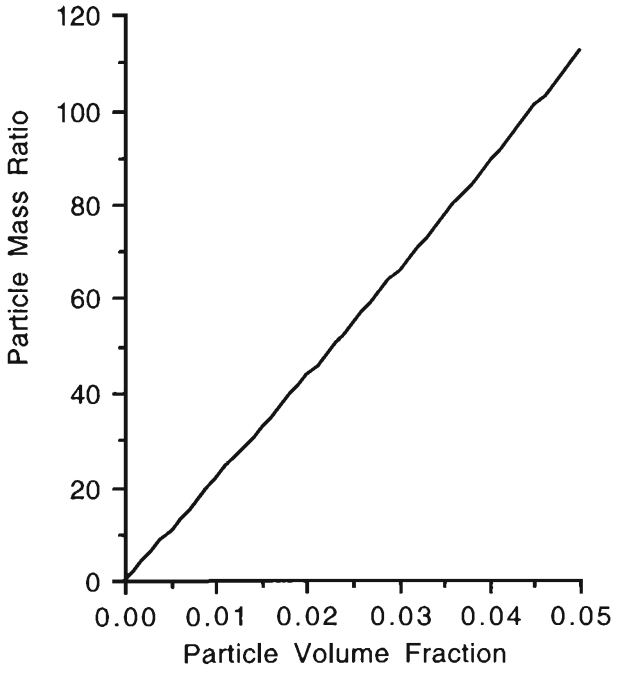

Figure 3.5 Particle Mass Ratio vs Particle Volume Fraction

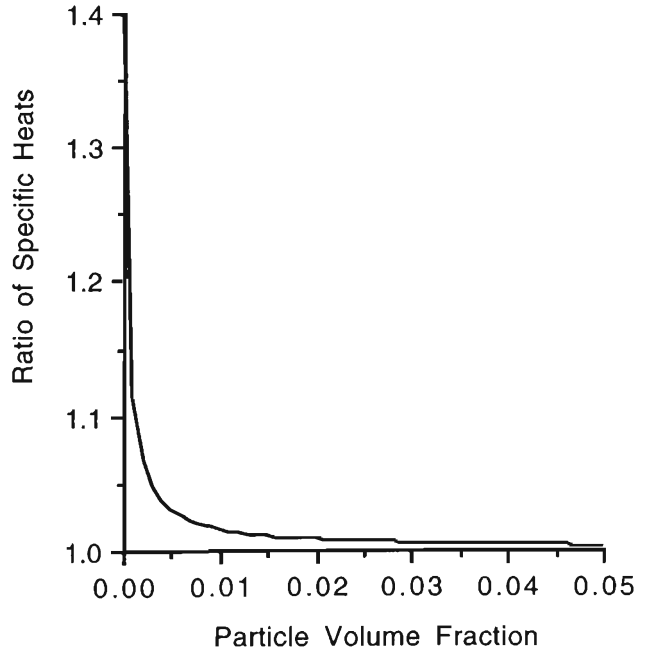

Figure 3.6 Specific Heat Ratio vs Particle Volume Fraction

It is seen from Figure 3.6 that the ratio of specific heats for the suspension decreases with increasing particle volume fraction. This ratio approaches '1' asymptotically,

signifying that for the limiting 'all-solids' state, there is no qualitative difference between 'specific heat at constant pressure' and 'specific heat at constant volume'.

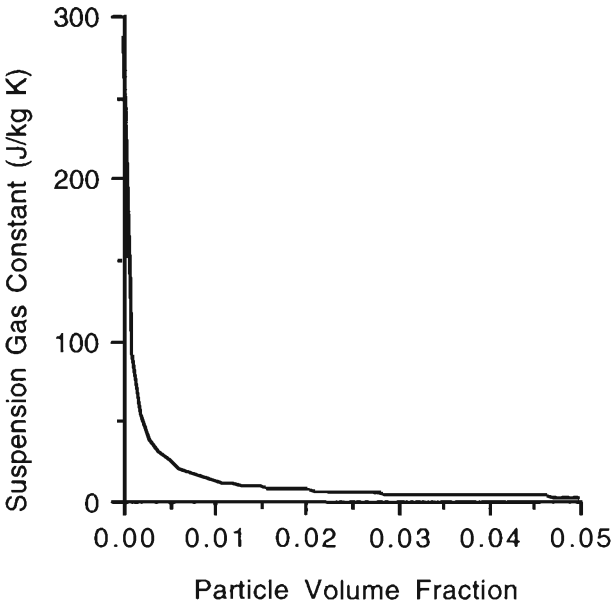

Figure 3.7 Suspension Gas Constant vs Particle Volume Fraction

Figure 3.7 shows that the suspension gas constant decreases asymptotically with increasing particle volume fraction, approaching the value zero at larger particle volume fractions. This is compatible with the relationship (Gas Constant = c_p - c_v), and that for large particle volume fractions, the qualitative difference between c_p and c_v is progressively obliterated.

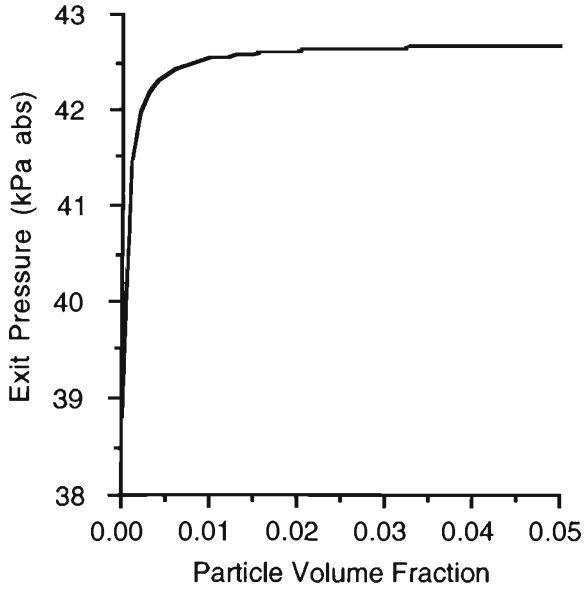

Figure 3.8 Suspension Exit Pressure vs Particle Volume Fraction

Figure 3.8 shows a somewhat surprising result: the suspension exit pressure increases with increasing particle volume fraction and approaches a value of about 42.5 kPa abs asymptotically. This assumes that the suspension stagnation pressure is 1 atm abs. The practical implication of this trend is that different quantities of particulate matter can be easily conveyed by the same injector merely by making small changes in the location of the injection tube exit plane in the divergent part of the nozzle, to adjust the pressure at the injection tube exit. This is because pressure in the de Laval nozzle varies with distance along the duct as seen qualitatively in Figure 1.5.

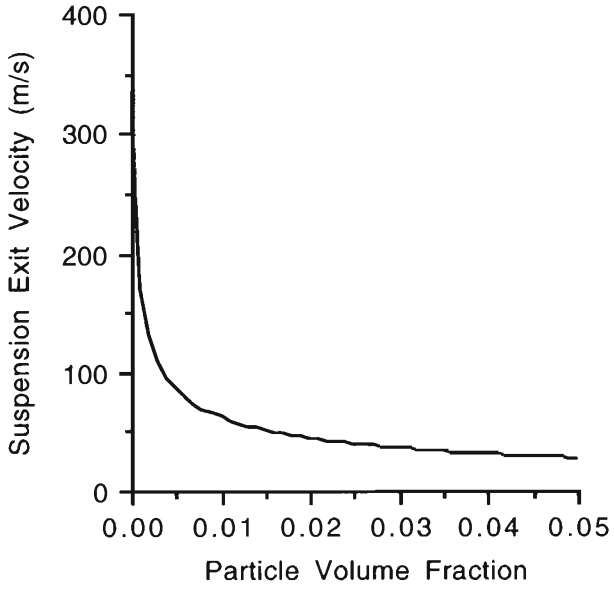

Figure 3.9 Suspension Exit Velocity vs Particle Volume Fraction

The sonic speed associated with a gas-particle suspension shows a drastic decrease with increasing particle volume fraction, as seen in Figure 3.9. This leads to the reasonable conclusion that heavier suspensions will experience greater initial velocity lag with respect to the primary gas stream, and will therefore be increasingly difficult to convey.

3.5 Injection Tube Length

A parametric study is carried out to estimate the injection tube length required to attain sonic conditions at its exit. As shown in Appendix B, this length is a function of the initial Mach number of the flow entering the tube (property of the flow), the ratio of specific heats of the gas (property of the fluid), and the friction factor [W7]:

$$f_{int}\frac{L^*}{D} = \frac{1 - Ma^2}{\gamma\, Ma^2} + \frac{\gamma + 1}{2\gamma}\ln\frac{(\gamma + 1)\, Ma^2}{2 + (\gamma - 1)\, Ma^2} \tag{3.30}$$

Theoretically, considerably slender (high length/diameter ratio) ducts are required for attainment of sonic conditions at the exit. Figure 3.10 is a graphical representation of Equation 3.30, and gives a rough estimate of the lengths required. This is done to ascertain whether such lengths are feasible in the present project, and may influence the design.

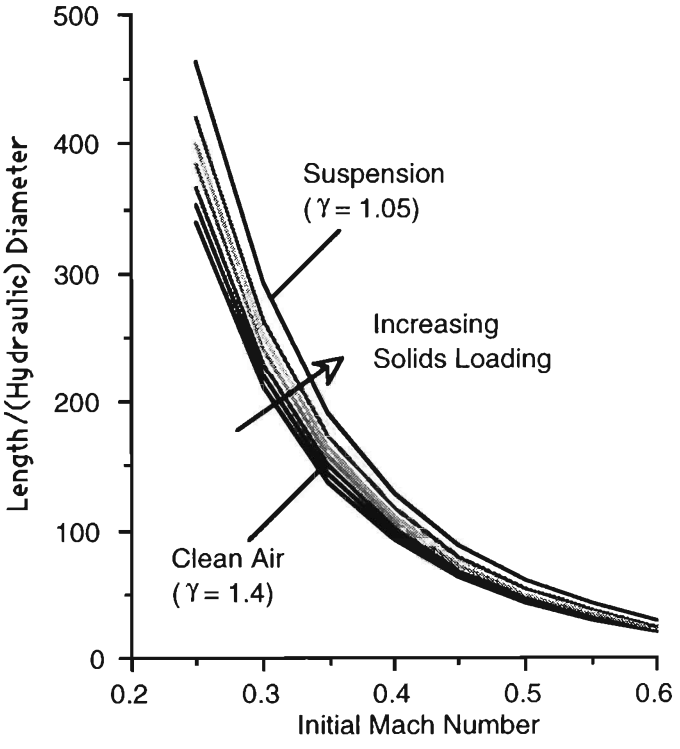

Figure 3.10 Injection Tube Length/Diameter Ratio

It can be seen that for high initial Mach numbers of the entering flow, shorter tubes are sufficient for attainment of sonic conditions at the exit. Also, for the same initial Mach number, a gas-solids suspension requires a longer tube to attain sonic conditions, compared to clean gas. These considerations suggest that a suitable accelerating device such as a converging nozzle is required at the injection tube inlet (See Chapter 10).

The suspension, emerging from the centrally located injection tube, is enveloped by the primary gas stream flowing in the nozzle region. Analysis of flow in the nozzle region is carried out in the next chapter.

Chapter 4

PRIMARY GAS FLOW IN NOZZLE

As seen in Chapter 3, the assumption that suspension flow in the injection tube approximates a 'Fanno' flow implies that the suspension emerges from the injection tube at its sonic speed. This condition determines suspension flow parameters at the end of the injection tube. In particular, for a given value of particle 'loading' in the suspension, the value of suspension static pressure at the exit of the injection tube is fixed. To avoid compression or expansion waves at the start of the interaction region, it must be ensured that the primary gas in the nozzle also attains the same value of static pressure at this point in the flow. Thus, this equality of static pressures effectively ties together the analyses of flows in these two regions (See Figure 3.2).

4.1 Flow Characteristics and Driving Potentials

The characteristics of primary gas flow in the nozzle region and the corresponding Driving Potentials are (See Table A1, Appendix A):

1 No Drag due to objects in relative motion, obstacles, etc.:

$$DR = 0 \tag{4.1}$$

so that

$$FD = FR \tag{4.2}$$

2 No entrained mass into the stream:

$$EM = 0 \tag{4.3}$$

3 No transfer of energy either as heat or work to the stream:

$$ENER = 0 \tag{4.4}$$

Thus, area change AR and wall friction FR are the only driving potentials responsible for bringing about changes in flow properties. Of these, wall friction can be

calculated using Haaland's formula for friction factor [W7] (Appendix A). As seen earlier in Chapter 2, area change has to be treated as an unknown, at the expense of some other flow parameter which may be specified. In the present application, this parameter is static pressure. By rearranging the equation for static pressure in such a way that the pressure gradient term appears on the right hand side of the equation, it is possible to solve for area change. This is equivalent to designing the nozzle:

$$\frac{dA}{dx} = \frac{A}{EPA}\left\{\frac{dp}{dx} - (EVFD \cdot FD + EVEM \cdot EM + EVEN \cdot ENER)\right\} \qquad (4.5)$$

It is clear that for a particular specification for static pressure (dp/dx in Eq. 4.5), a unique nozzle shape will result. There are many conceivable ways of specifying static pressure variation along the nozzle. These are investigated in the following section, and the most appropriate specification chosen.

4.2 Specification of Pressure Variation

Emergence of the suspension at its sonic speed fixes the flow parameters at the injection tube exit plane. Also, as explained in Chapter 1, interaction between the primary gas and the suspension starts at this point, and this interaction is required to be of the *constant-pressure* type. It follows that the pressure of the primary gas must also be p_S^* at the end of the nozzle region. If the stagnation pressure of primary gas (total pressure p_{01} at the start of primary gas flow) is assumed, this gives the pressures at the start (p_{01}) and the end (p_S^*) of the nozzle region. Between these two points, the pressure variation can be specified in a number of ways. Some of these choices are shown in Figure 4.1.

The resulting nozzle shape is to be compatible to the specified pressure variation. In other words, depending on the assumed expression for (dp/dx), the resulting (dA/dx) and therefore the area variation will be different.

To ensure smooth flow in the nozzle, three requirements must be satisfied:

1 Smooth entry into the nozzle from the primary gas stagnation chamber;
2 Smooth passage through the sonic 'throat' section;
3 Smooth blending into the interaction region.

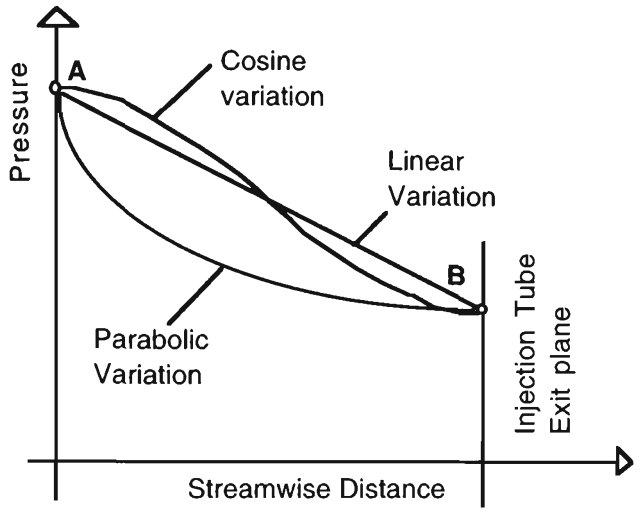

Figure 4.1 Nozzle Pressure Specification Options

It was found that specifying a linear pressure drop in the nozzle leads to abrupt area changes at points A and B. This does not satisfy requirements 1 and 3, and therefore this option has to be discarded. The 'Cosine' pressure variation option leads to a nozzle shape which ensures smooth blending with the interaction region (point B), thus satisfying condition 3. However, it was found that the resulting area variation A(x) also has a cosine curve-like shape. At the point of entry into the nozzle from the ideally large stagnation chamber, there is an abrupt change in area (point A). Thus this option also must be discarded because it does not satisfy requirement 1.

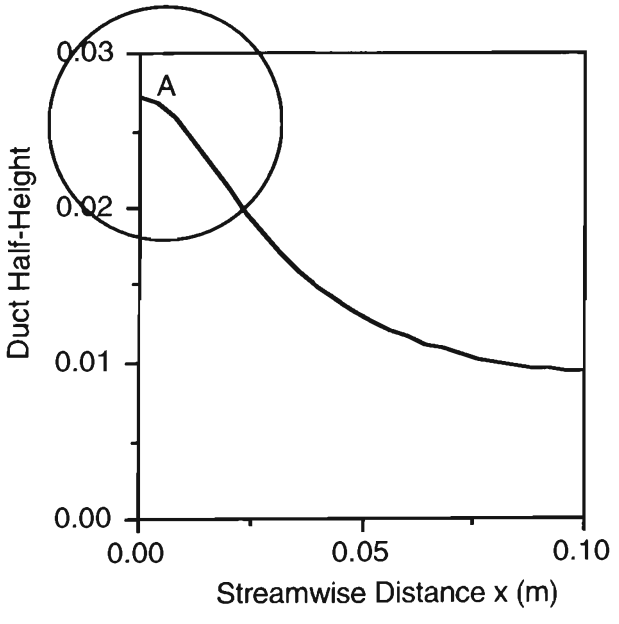

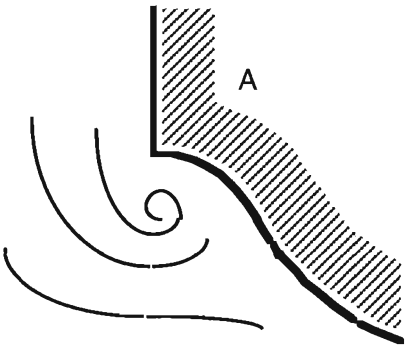

Abrupt area change from a large stagnation chamber would lead to eddies and non-uniformities in the flow at the inlet to the nozzle.

Figure 4.2 Nozzle Shape for 'Cosine' Pressure Variation

As an example, the duct shape corresponding to the 'Cosine' variation of pressure is shown in Figure 4.2. It is found that the resulting nozzle shape is such that there is an abrupt change in area at the inlet from the large stagnation chamber. This would lead to eddy formation in the flow, and would destroy uniformity of the velocity profile. In order to ensure no such 'jumps' in area variation, the static pressure drop from the stagnation chamber to the end of the nozzle region is specified as *parabolic*. It was found that this results in a nozzle design with smooth entry (at A) and smooth blending with interaction region (at B). See Figures 4.5 and 4.10.

4.3 Nozzle Design Parameters

The actual physical shape of the nozzle depends upon the following variables :

1 Primary Gas Mass Flow Rate;
2 Primary Gas Stagnation Pressure;
3 Suspension Stagnation Pressure;
4 Particle Loading in Suspension
and
5 Length of Injection Tube (which is also the length of the nozzle region).

Theoretically, there are over a hundred different combinations possible among these five design parameters. Each combination leads to a unique nozzle shape. However, many of these combinations can be automatically ruled out, because they do not lead to *supersonic* flow at the end of the nozzle region. (It is clear that if the primary gas does not attain supersonic speed at the end of the nozzle region, subsequent formation of a normal shock is impossible.) This restriction still leaves many different combinations of the above parameters which do lead to supersonic flow at the end of the nozzle region. From these combinations, the following set of (achievable) parameters was chosen as the basis for designing the experimental facility (Chapter 10):

Primary Gas Mass Flow Rate	=	0.25	kg sec^{-1}
Primary Gas Stagnation Pressure	=	2.0	bar (abs)
Suspension Stagnation Pressure	=	1.0	bar (abs)
Suspension Particle Volume Fraction	=	0.01	
Length of Injection tube	=	0.20	m.

Table 4.1 Nozzle Design Parameters

These values were selected for the following reasons :

1 An air mass flow rate of 0.25 kg/sec could be achieved easily with the facilities available, without being too high.

2 Similarly, the primary air stagnation pressure of 2 atm abs could also be easily attainable without having to place too stringent restrictions on the design of the stagnation chamber pressure vessel. Alternatively, it is also theoretically possible to produce supersonic flow with a primary air stagnation pressure of 1 atm abs, provided the downstream end of the nozzle is at a sufficiently low (below atmospheric) pressure. It was found that with the facilities available, sufficiently low pressures could not be attained. It was much easier to keep the downstream end at 1 atm abs, and design the nozzle accordingly.

3 It is most typical to start the flow of the suspension at atmospheric conditions.

4 A particle volume fraction of 0.01 would imply a suspension sufficiently dilute to be regarded as an ideal gas with modified properties. At the same time, due to the high material density of the particles, the transport of a sufficiently large quantity of particulate matter can be studied (see Figure 3.5).

5 A 20 cm long injection tube would be long enough without making heavy demands on space requirements. This is also the length of the primary gas nozzle region. (As seen later in Chapter 10, design considerations require the length of the injection tube as such to be about a meter.)

The FORTRAN programme listing (with explanatory comments) which calculates flow parameters in the nozzle region is given in Appendix C1. The programme also computes nozzle cross section areas at successive downstream locations. Results of the calculations appear in Figures (4.3-4.10).

4.4. Nozzle Flow Parameters

Figure 4.3 below shows the variation of primary gas Mach number with downstream distance. Starting at an arbitrarily assumed low value of 0.2, the Mach number increases smoothly through the sonic 'throat' to about 1.5 at the injection tube exit plane. This can be considered adequate for the present purpose, as it is sufficiently

supersonic without being too high, and is accompanied by a sufficiently low pressure at the injection tube exit plane for adequate suction of suspension.

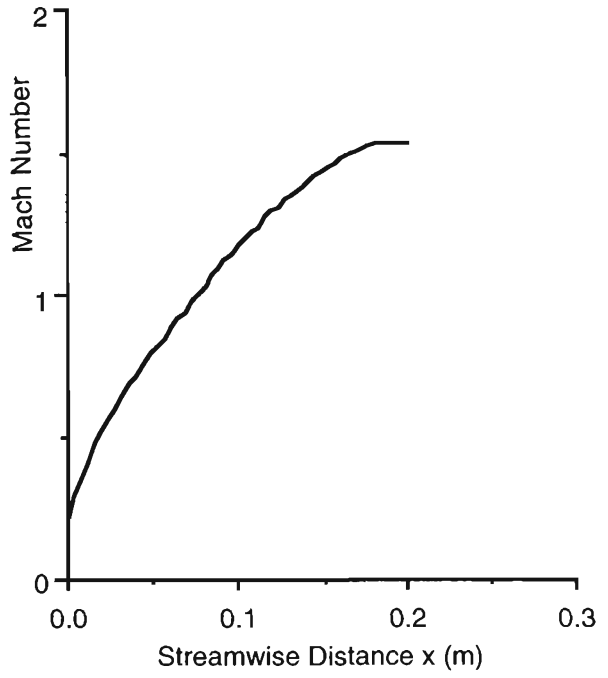

Figure 4.3 Primary Gas Mach Number vs Distance

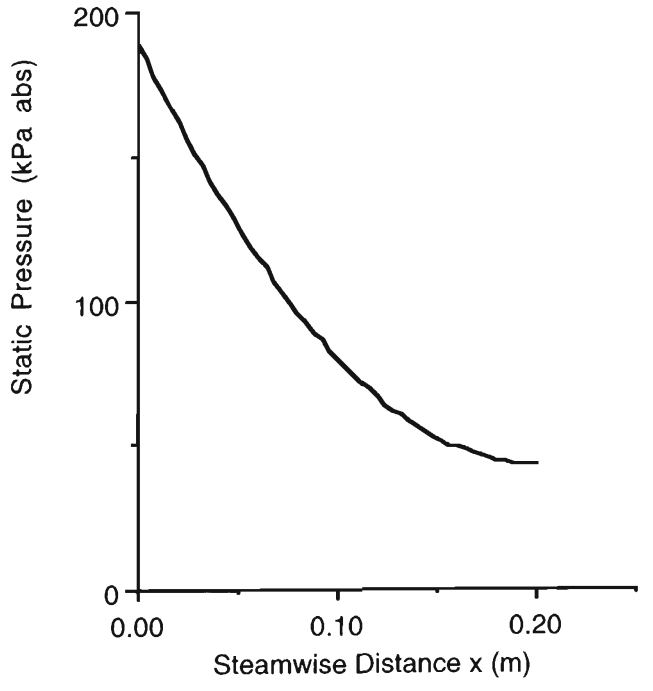

Figure 4.4 Primary Gas Static Pressure vs Distance

Figure 4.4 shows the variation of primary gas static pressure with downstream distance. This variation was specified so as to satisfy the three requirements for smooth primary gas flow, as mentioned in Section 4.3. It is seen that the slope of the curve

gradually reduces to zero at the end of the nozzle region. This enables smooth blending into the constant-pressure interaction region (Chapter 5).

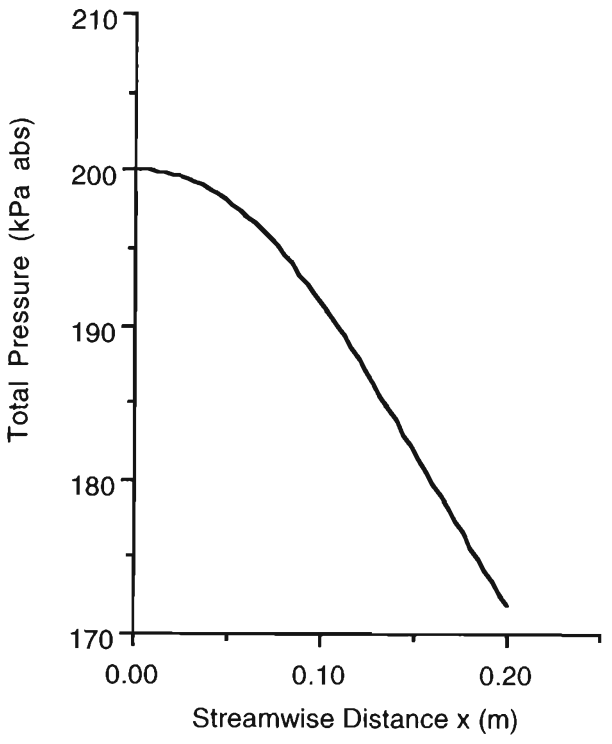

Figure 4.5 Primary Gas Stagnation Pressure vs Distance

Figure 4.5 depicts the variation of primary gas stagnation (total) pressure with downstream distance. Starting at the specified value of 2.0 bar abs, the stagnation pressure undergoes gradual reduction. The reduction reflects flow irreversibilities such as friction at the nozzle walls, as seen from the equation describing variation of stagnation pressure with distance (Eq A6 in Appendix A). The very gradual change near the inlet shows that the losses there are small, indicative of smooth flow at entry point. This is a consequence of the specified pressure variation, and the resulting area variation. The actual value of stagnation pressure at each cross-section depends on the friction factor and the assumed roughness parameter for the walls of the nozzle. Since frictional effects are thus accounted for, it is not necessary to adjust the flow area for growth of boundary-layer displacement thickness in the streamwise direction.

The effects of compressibility are reflected in primary gas density variation in the downstream direction, shown in Figure 4.6. The density continues to drop throughout the nozzle region as the flow passes though the sonic throat into the divergent supersonic part. The density variation is akin to the specified static pressure variation, because of the assumption that the primary gas (air) behaves as an ideal gas ($p = \rho RT$).

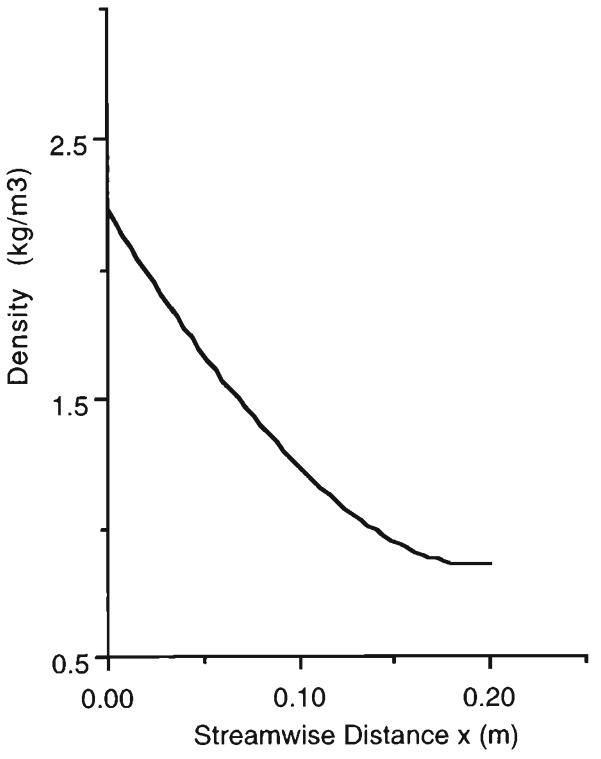

Figure 4.6 Primary Gas Density vs Distance

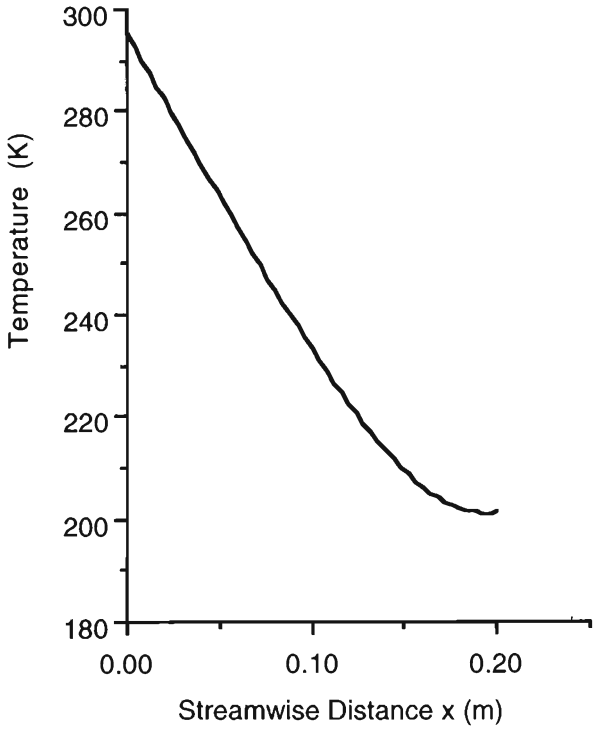

Figure 4.7 Primary Gas Temperature vs Distance

Compatible with density decline, the static temperature also drops continuously through the nozzle (Figure 4.7). The primary gas is assumed to start its journey at an atmospheric temperature of 293.15 K. If necessary, this initial condition can be

modified by providing some initial heating. It is likely that the cooling can lead to condensation of moisture in the ambient secondary air.

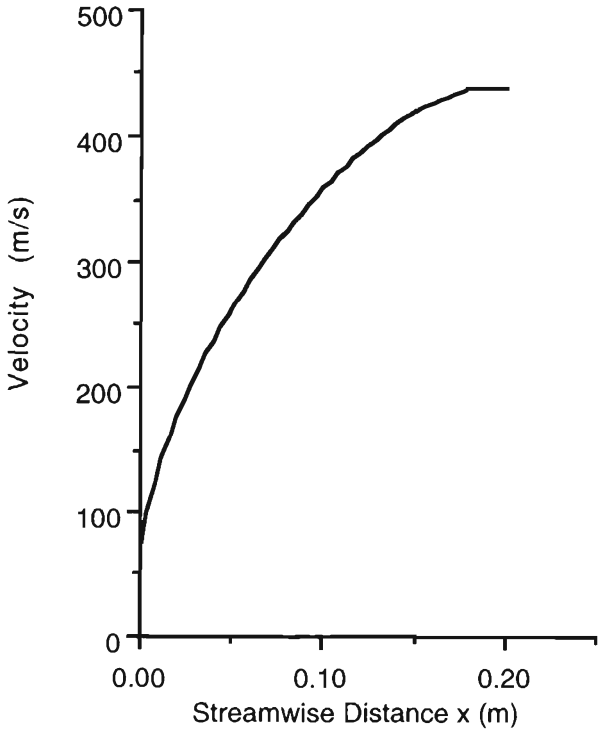

Figure 4.8 Primary Gas Velocity vs Distance

Figure 4.8 shows the variation of primary gas velocity with downstream distance in the nozzle. Starting at an arbitrarily selected low value (compatible with the assumed initial Mach number and initial sonic velocity), the velocity attains a value of about 450 m/s at the end of the nozzle region. This corresponds to a Mach number value of about 1.5 at that section.

Figure 4.9 below shows the nozzle cross-sectional area variation with downstream distance. In keeping with the experimental requirement that the flow should approximate a two-dimensional flow, the cross-sectional area is assumed rectangular, with constant width and variable height (See Section 10.1). Such a cross section makes flow visualisation possible. Unlike the area variation shown in Figure 4.2, the steepest half-height variation is seen to be at the starting point, which enables smooth entry from the ideally large stagnation chamber.

The minimum area (throat) of the nozzle is at approximately 0.075 m from the starting point. Comparing this with Figure 4.3, 'Primary Gas Mach Number vs Streamwise Distance', it can be readily seen that at the throat, the flow Mach number is very close to unity. This provides a check for the validity of the nozzle design procedure. At the end of the nozzle region, the primary gas attains a Mach number of

about 1.5, and a pressure equal to that of the suspension emerging from the injection tube. The constant-pressure interaction between these two streams commences here.

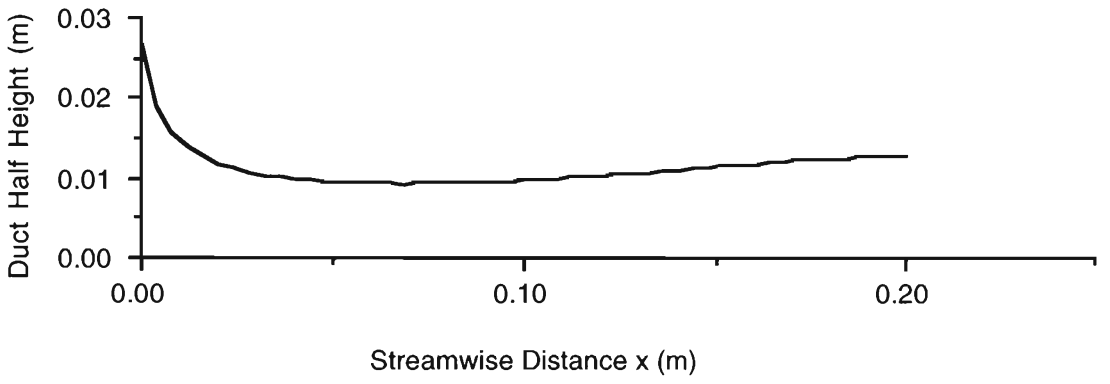

The nozzle area variation is shown in terms of the variation of duct half height. The nozzle shape is symmetrical, and the cross-sectional area is rectangular in shape, with a constant width (30 mm). The width was chosen so as to simulate an approximately two-dimensional flow in the duct, bounded on two sides by glass walls.

Figure 4.10 Primary Nozzle Half Height vs Distance

The next chapter outlines the analysis of flow in the Interaction Region.

Chapter 5

FLOW IN INTERACTION REGION

As seen from the foregoing analyses of the suspension flow in the constant-area injection tube and the primary gas stream in the nozzle region, at the onset of the interaction region a supersonic primary gas stream meets a co-flowing suspension stream which emerges at *its* sonic speed. At this stage, the velocity of the suspension is necessarily less than that of the primary gas. Also, in general, the suspension emerges at a temperature higher than that of the primary gas stream. The slower, hotter suspension is now to be accelerated by interaction with the primary gas stream.

5.1 Mixing between Co-flowing Streams

It is necessary to anticipate the nature of the mixing process between the two compressible co-flowing streams. Assuming that the velocities of the primary gas and the suspension are uniform just before the onset of the interaction region, a shear layer now develops at the interface between the two streams. The rate of growth of this shear layer is a measure of the extent of mixing (Figure 5.1).

The rate of growth of the shear layer with distance can be expressed as [A1]:

$$\frac{db}{dx} \propto \frac{V_1 - V_2}{V} \tag{5.1}$$

where V_1 and V_2 are the velocities at the boundaries of the mixing zone, and V is a characteristic velocity in the mixing zone. In the general case, the characteristic velocity V is expressed as the 'mass-averaged velocity' [A1] :

$$V = \frac{\rho_1 V_1 + \rho_2 V_2}{\rho_1 + \rho_2} \tag{5.2}$$

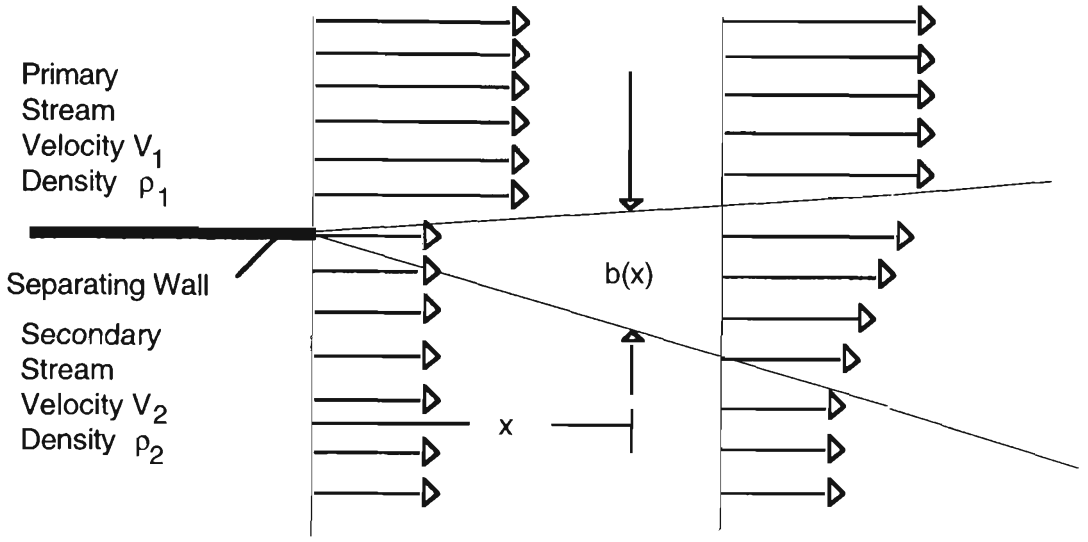

Formation of Shear Layer at the interface
between two compressible fluid streams.

The lateral extent of mixing is b(x).
Thickness of the separating wall is assumed negligible.

Figure 5.1 Shear Layer between Co-flowing Streams

Equation (5.2) takes into account the difference in densities of the interacting streams. (If the streams are assumed incompressible and of the same fluid, $\rho_1 = \rho_2 = \rho$, and the characteristic velocity is simply the arithmetic mean $\frac{V_1+V_2}{2}$).

The rate of growth of the shear layer is given by [A1]

$$\frac{db}{dx} = \frac{c}{2}\frac{(1-\bar{V})(1+\bar{\rho})}{(1+\bar{\rho}\bar{V})}. \qquad (5.3)$$

with $\bar{V}=V_2/V_1$ and $\bar{\rho}=\rho_2/\rho_1$

The constant 'c' is experimentally estimated to be about 0.25 [A1]. The '2' in the denominator is introduced so that the incompressible case may be written as a special case of the general compressible formula. This device makes the same formula applicable to a wide range of velocities and densities. It is also reported that this formula is applicable to both plane and axisymmetric flows [A1]. This adaptability is relevant to the present project, because although the analytical treatment is carried out with a circular cross section duct in mind, a rectangular cross-section duct is used in the experimental setup to make flow visualisation possible (Chapter 10).

For reasons stated earlier, the mixing process in the SAI must be of the constant-pressure type. The presence of the solid particles makes the suspension dense and heavy - the density of the solid particles being greater than that of the gas by a factor of about 1000. It is reported in the literature [eg. A1] that the lateral components of velocity in a flow field such as this are negligibly small. In view of these considerations, it is not unnatural to expect that the particles in the suspension will not spread appreciably in the cross-stream direction.

A picture of the mixing zone between the primary gas and the suspension can now be formed (Figure 5.2). Due to gradual mixing between the two streams, the interaction region itself must be divided into two parts.

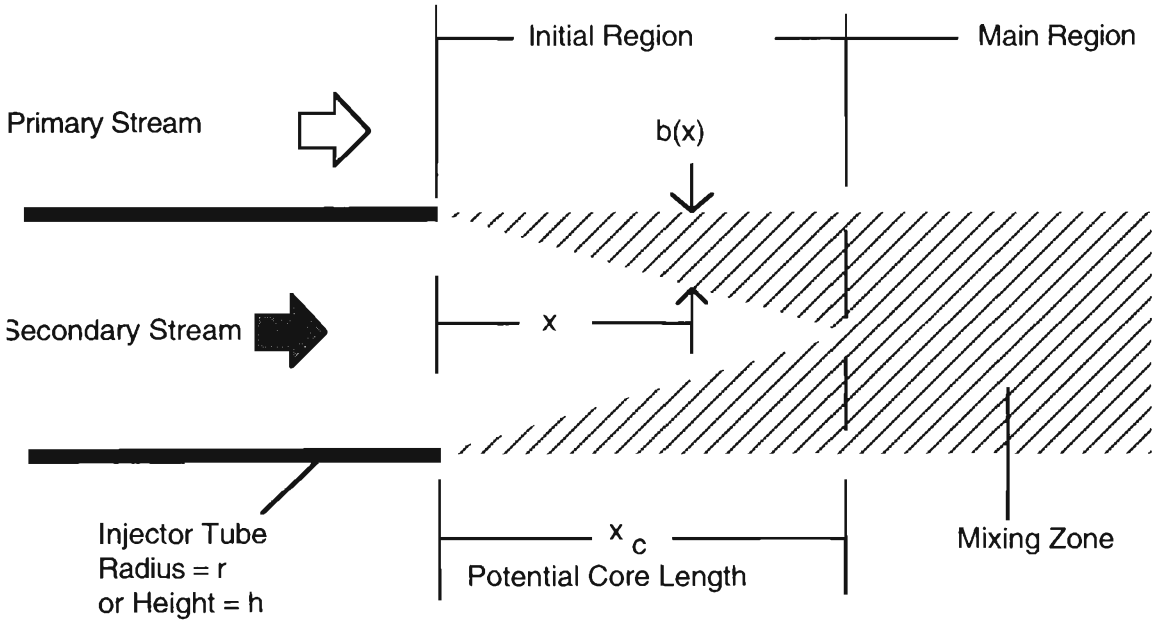

Model for the mixing between suspension and primary stream.
The length of the potential core is also the length of the initial region.

Figure 5.2 Mixing between Suspension and Primary Gas

5.2 Sub-Regions of Interaction

The jet-like flow of the suspension after emerging from the injector tube can be divided into two regions:

1) An Initial Region : the region in which the lateral extent (width) of the shear layer increases with increasing downstream distance. In the axisymmetric case, the shear layer grows inward until it reaches the axis of symmetry. This forms a cone-shaped

region of suspension flow called the 'potential core'. (In a 2-dimensional flow, the potential core would be shaped like a triangular prism.) The suspension velocity inside the potential core is not affected by the action of the primary gas stream. In fact, due to the requirement that the mixing must be of the constant-pressure type, the velocity of suspension throughout the potential core is constant, equal to the velocity at which the suspension emerges from the injector tube.

From the point of view of the suspension, it is thus seen that all of the particles in it at any cross section do *not* 'feel' the accelerating influence of the primary gas stream at the same time. Only the particles in the shaded part in Figure 5.2 feel the effect. The number of such particles is proportional to the local width of the shear layer, b(x). More particles are influenced at greater distances from the injection tube exit plane.

From the point of view of the primary gas stream, on the other hand, it is as if there is *continuous mass entrainment* into it in this initial region of interaction. This mass entrainment takes place across the surface of the potential core.

2) The Main Region: begins where the Initial Region ends. From this point onwards, all the particles borne by the suspension are 'within the grasp' of the primary gas stream. All particles feel the accelerating influence of the primary gas stream. There is no more mass entrainment into the primary gas stream, but the primary stream continues to feel the drag due to the slower moving suspension, due to the velocity difference between the (particles in the) suspension, and the faster primary gas.

An analysis of flow in the interaction region can now be carried out. In the following sections, the 'driving potentials' affecting the flow parameters of the primary gas stream are recognised.

5.3 Significant Driving Potentials

5.3.1 Potential Core (Initial Region)

In the Initial Region, agents causing property changes in the primary gas stream, (and the corresponding driving potentials) are :

1 Area Change; (AR)

2 [Friction at Duct Wall] + [Drag due to an increasing number of particles]; (FD = FR + DR)

3 [Heat transfer from an increasing number of particles] + [Work transfer to an increasing number of particles] (ENER = HT - WK)

(Note: For brevity, 'Energy Transfer as Work' is shortened to 'Work Transfer'.)

4 Mass Entrainment across potential core surface; (EM).

5.3.2 Main Region

In the Main Region, agents causing property changes in the primary gas stream, (and the corresponding driving potentials) are :

1 Area Change; (AR)

2 [Friction at Duct Wall] + [Drag due to all particles]; (FD = FR + DR)

3 [Heat transfer from all particles] + [Work transfer to all particles]; (ENER = HT - WK)

There is no more 'mass entrainment' into the primary gas, so that

4 EM = 0.

Having identified the significant driving potentials, analytical expressions for the driving potentials are developed in the following sections.

5.4 Derivation of Driving Potentials

5.4.1 Potential Core Length

As seen earlier, the rate of growth of the width of the shear layer at the interface between the co-flowing streams is:

$$\frac{db}{dx} = 0.125 \frac{(1 - \bar{V})(1 + \bar{\rho})}{(1 + \bar{\rho}\bar{V})} \tag{5.6}$$

If the simplifying assumption is now made that V_1, V_2, and ρ_1, ρ_2 are all independent of x in the initial region, integration yields, with b(x = 0) = 0,

$$b(x) = 0.125 \frac{(1 - \bar{V})(1 + \bar{\rho})}{(1 + \bar{\rho}\bar{V})} x \tag{5.7}$$

The above assumption is necessary as a starting point. As seen earlier, V_2 is required to be constant, and variations in the other parameters can be assumed negligible, especially for short potential core lengths.

At the end of the initial region, $x = x_c$ and $b(x = x_c) = r_{tube}$ for axisymmetric flow, and $x = x_c$ and $b(x = x_c) = 0.5\ h_{tube}$ for plane flow (neglecting the thickness of injection tube wall), so that

$$r_{tube} = 0.125 \frac{(1 - \bar{V})(1 + \bar{\rho})}{(1 + \bar{V}\bar{\rho})} x_c \text{ (axisymmetric flow)} \tag{5.8}$$

and

$$\frac{h_{tube}}{2} = 0.125 \frac{(1 - \bar{V})(1 + \bar{\rho})}{(1 + \bar{V}\bar{\rho})} x_c \text{ (plane flow)} \tag{5.9}$$

where x_c is the length of the potential core. At this point, the lateral extent of the shear layer is specified to be equal to the injector tube radius in the axisymmetric case, and half the height of the tube in the rectangular cross-section case. This is a result of the crucial assumption that the suspension does not spread in the lateral direction. This assumption can be relaxed if experimental results reveal otherwise.

This yields the length of the potential core in terms of the injection tube radius and the flow properties at the start of the interaction region :

$$x_c = 8\ r_{tube} \frac{1 + \bar{V}\bar{\rho}}{(1 - \bar{V})(1 + \bar{\rho})} \quad \text{(axisymmetric flow)} \tag{5.10}$$

and

$$x_c = 4\ h_{tube} \frac{1 + \bar{V}\bar{\rho}}{(1 - \bar{V})(1 + \bar{\rho})} \quad \text{(plane flow)} \tag{5.11}$$

The above analysis thus yields the downstream extent of the initial region in terms of a known geometrical parameter, viz. size of injection tube.

5.4.2 Particle Drag in Initial Region

In the Initial Region, the number of particles influenced by the primary gas stream increases with downstream distance x, so that

$$\begin{bmatrix}\text{Total Drag exerted}\\ \text{by affected particles}\\ \text{on Primary Stream}\end{bmatrix} = \delta D(x) \tag{5.12}$$

Now,

Total Drag = $\delta D(x)$ = (Drag per particle)(Number of Particles Influenced)

or,

$$\delta D(x) = (\text{Drag per particle}) \frac{(\text{number of particles})}{(\text{unit volume of suspension})} \begin{pmatrix}\text{Volume of}\\ \text{suspension}\\ \text{influenced by}\\ \text{primary}\\ \text{stream}\end{pmatrix}$$

In terms of particle 'concentration' (σ_p) and particle mass (m_p) (see Chapter 3),

$$\frac{\text{Number of particles}}{\text{Unit volume of suspension}} = \frac{\text{Total mass of particles per unit suspension volume}}{\text{mass of a single particle}} = \frac{\sigma_p}{m_p} \tag{5.13}$$

Therefore,

$$\delta D(x) = D_p \frac{\sigma_p}{m_p} V_{inf}(x) \tag{5.14}$$

An expression for the influenced volume must now be sought.

5.4.3 Volume of Suspension influenced by Primary Stream

The expression for $V_{inf}(x)$ can be derived as follows: At a distance $x < x_c$ from the injector tube exit plane, the volume $V_{inf}(x)$ is the shaded volume shown in Figure 5.3.

$$V_{inf}(x) = [A_{tube} - A_{core}(x)]\,dx = A_{tube}\left[1 - \frac{\pi r^2}{\pi r_{tube}^2}\right] dx$$

From similar triangles $\quad \dfrac{r}{r_{tube}} = \dfrac{x - x_c}{x_c}$

so that

$$V_{inf}(x) = A_{tube}\left[1 - \left(1 - \frac{x}{x_c}\right)^2\right] dx \qquad \text{in the Initial Region.} \qquad (5.15)$$

This formula can be verified thus: When $x = 0$, $V_{inf}(x) = 0$, implying that none of the particles have been swept into the primary stream. When $x \geq x_c$, $V_{inf}(x) = A_{tube}.dx$, implying that at the start of the Main Region, all of the particles 'feel' the accelerating influence of the primary stream, without spreading laterally.

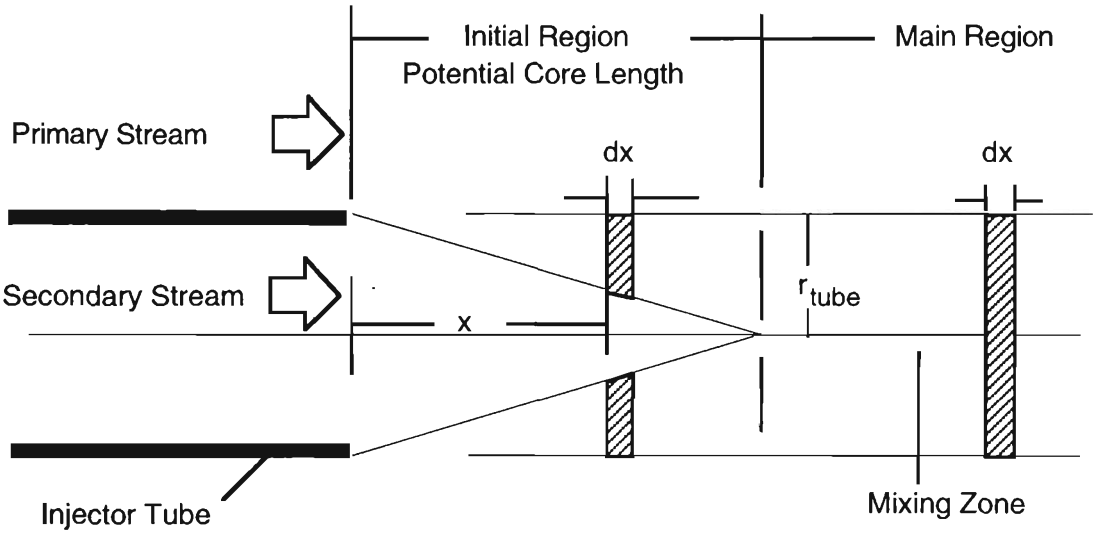

Figure 5.3 Volume of Suspension influenced by Primary Stream

Substituting for $V_{inf}(x)$ in Equation (5.14),

$$\delta D(x) = D_p \frac{\sigma_p}{m_p} A_{tube}\left[1 - \left(1 - \frac{x}{x_c}\right)^2\right] dx \qquad \text{(Initial Region)} \qquad (5.16)$$

and

$$\delta D(x) = D_p \frac{\sigma_p}{m_p} A_{tube}\, dx \qquad \text{(Main Region)} \qquad (5.17)$$

An expression for 'D_p', drag on an individual particle, is derived next.

5.4.4 Drag on Individual Particle

For a spherical particle of diameter d_p, moving at velocity V_p in a fluid stream moving at velocity V in the same direction,

$$D_p = \frac{1}{2} \rho V_{rel}^2 C_{D_p} A_{frontal} \tag{5.18}$$

Following the nomenclature in [Z1], let

$$C_D = \frac{C_{D_p}}{C_{D\ Stokes}} = \frac{\text{Actual Particle Drag Coefficient}}{\text{"Stokes" Drag Coefficient}} \tag{5.19}$$

where

$$C_{D\ Stokes} = \frac{24}{Re_{d_p}} \tag{5.20}$$

Here, $C_{DStokes}$ is the 'Stokes' drag coefficient applicable to the Stokes flow regime [W7] based on particle Reynolds Number Re_{dp} only, and $Re_{d_p} = \frac{\rho V_{rel} d_p}{\mu}$.

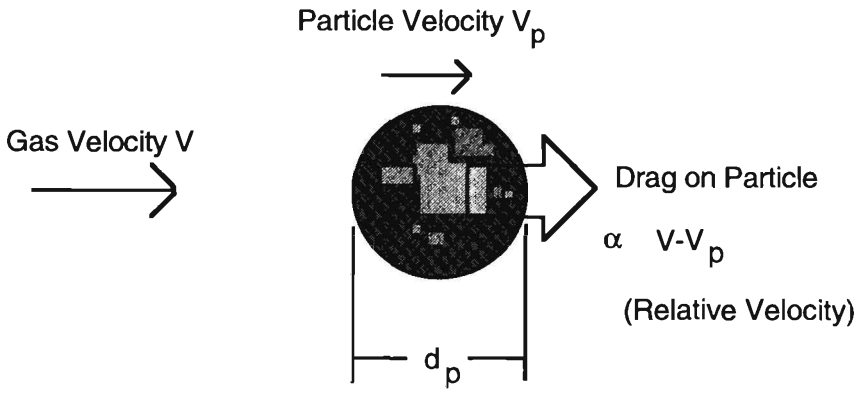

Figure 5.4 Drag on a Spherical Particle

Then,

$$C_{Dp} = (C_D).(C_{DStokes}) = (C_D).(24/Re_{dp}) = C_D \frac{24\ \mu}{(V - V_p)\ \rho\ d_p} \tag{5.21}$$

The expression for the drag D_p thus assumes the form

$$D_p = \frac{1}{2} \rho (V - V_p)^2 C_D \frac{24\ \mu}{(V - V_p)\ \rho\ d_p} \frac{\pi}{4} d_p^2 = 3\ \pi\ \mu\ C_D\ d_p\ (V - V_p) \tag{5.22}$$

An equation of motion for the particles can now be derived.

5.4.5 Equation of Motion of a Particle

Drag force on the particle causes it to accelerate:

Drag per particle = (Mass of particle) (Acceleration of particle)

$$D_p = m_p \frac{dV_p}{dt} = m_p \frac{dV_p}{dx}\frac{dx}{dt} = m_p V_p \frac{dV_p}{dx} \qquad (5.23)$$

interpreting $\frac{dx}{dt}$ as the velocity *of the particle* [Z1].

Then,

$$3 \pi \mu C_D d_p \left(V - V_p\right) = m_p V_p \frac{dV_p}{dx}$$

and

$$\frac{3 \pi \mu C_D d_p \left(V - V_p\right)}{m_p} = V_p \frac{dV_p}{dx} \qquad (5.24)$$

For a spherical particle of material density ρ_{mp},

$$m_p = \rho_{mp} \frac{\pi d_p^3}{6} \qquad (5.25)$$

Hence the momentum equation for the particle takes the form :

$$\frac{dV_p}{dx} = \frac{18 \mu C_D}{\rho_{mp} d_p^2} \left(V - V_p\right) \qquad (5.26)$$

Thus, in the Initial Region,

$$\delta D(x) = 3 \pi \mu C_D d_p \left(V - V_p\right) \frac{\sigma_p}{m_p} A_{tube} \left[1 - \left(1 - \frac{x}{x_c}\right)^2\right] dx \qquad (5.27)$$

and in the Main Region,

$$\delta D(x) = 3 \pi \mu C_D d_p \left(V - V_p\right) \frac{\sigma_p}{m_p} A_{tube} \, dx \qquad (5.28)$$

These formulae do not take into account the fact that the relative velocity responsible for producing the drag on the particles is *not* $(V\text{-}V_p)$ for *all* particles in the shear layer. To remedy this defect, it is seen that (Figure 5.2):

$V_{rel} = (V - V_p)$ at the outer edge of the shear layer;
and
$V_{rel} = 0$ at the inner edge of the shear layer.

Assuming a linear velocity profile across the shear layer, the effective relative velocity featured in the formula can be approximated as:

$$V_{rel,effective} = \frac{V - V_p}{2} \qquad (5.29)$$

With this change, the expressions for particle drag become:

In the Initial Region,

$$\delta D(x) = \frac{3}{2} \pi \mu C_D d_p \left(V - V_p\right) \frac{\sigma_p}{m_p} A_{tube} \left[1 - \left(1 - \frac{x}{x_c}\right)^2\right] dx \qquad (5.30)$$

and in the Main Region,

$$\delta D(x) = \frac{3}{2} \pi \mu C_D d_p \left(V - V_p\right) \frac{\sigma_p}{m_p} A_{tube} \, dx \qquad (5.31)$$

This yields expressions for the Driving Potential DR in the Initial and Main Regions of interaction :

$$DR \, dx = \frac{2 \, \delta D(x)}{\gamma M^2 \, p \, A}$$

so that

$$DR = \frac{2}{\gamma M^2 \, p \, A} \frac{\delta D(x)}{dx}$$

Thus, substituting for the expressions for particle drag $\delta D(x)$, in the Initial Region,

$$DR = \frac{3}{\gamma M^2 \, p \, A} \pi \mu C_D d_p \left(V - V_p\right) \frac{\sigma_p}{m_p} A_{tube} \left[1 - \left(1 - \frac{x}{x_c}\right)^2\right] \qquad (5.32)$$

and in the Main Region,

$$DR = \frac{3}{\gamma M^2 \, p \, A} \pi \mu C_D d_p \left(V - V_p\right) \frac{\sigma_p}{m_p} A_{tube} \qquad (5.33)$$

5.4.6 Heat Transfer from Suspension

At the onset of the interaction region, in general, temperature of the (particles in the) suspension is higher than that of the primary gas stream. This results in energy transfer as heat from the suspension to the primary gas.

As seen earlier, in the Initial Region, the number of particles influenced by the primary gas stream increases with downstream distance x, so that:

$$\begin{bmatrix}\text{Total rate of}\\ \text{heat transfer}\\ \text{from particles}\\ \text{to primary gas}\end{bmatrix} = \begin{bmatrix}\text{Rate of}\\ \text{heat transfer}\\ \text{from a}\\ \text{single particle}\end{bmatrix} \cdot \begin{bmatrix}\text{Number of}\\ \text{particles taking}\\ \text{part in}\\ \text{heat transfer}\end{bmatrix}$$

that is,

$$\delta\dot{Q}(x) = \begin{bmatrix}\text{Heat transfer}\\ \text{rate}\\ \text{per particle}\end{bmatrix} \cdot \begin{bmatrix}\text{Number of}\\ \text{particles}\\ \text{influenced}\end{bmatrix}$$

or

$$\delta\dot{Q}(x) = \begin{bmatrix}\text{Heat transfer}\\ \text{rate}\\ \text{per particle}\end{bmatrix} \cdot \frac{\begin{bmatrix}\text{Number of}\\ \text{particles}\end{bmatrix}}{\begin{bmatrix}\text{unit volume}\\ \text{of suspension}\end{bmatrix}} \cdot \begin{bmatrix}\text{Volume of}\\ \text{suspension}\\ \text{influenced by}\\ \text{primary stream}\end{bmatrix}$$

or,

$$\delta\dot{Q}(x) = \delta\dot{Q}_p \frac{\sigma_p}{m_p} V_{inf}(x)$$

Using the formula for $V_{inf}(x)$ as derived earlier ,

$$\delta\dot{Q}(x) = \delta\dot{Q}_p \frac{\sigma_p}{m_p} A_{tube} \left[1 - \left(1 - \frac{x}{x_c}\right)^2\right] dx \qquad (5.34)$$

An expression for $\delta\dot{Q}_p$,heat transfer from a single particle, is now needed.

5.4.7 Heat Transfer from a Particle

For a single spherical particle of diameter d_p, at temperature T_p, in an ambient fluid at temperature T:

$$\begin{bmatrix}\text{Heat Transfer}\\ \text{rate}\\ \text{per particle}\end{bmatrix} = \begin{bmatrix}\text{Exposed}\\ \text{surface area}\end{bmatrix} \cdot \begin{bmatrix}\text{Temperature}\\ \text{difference}\end{bmatrix}$$

In terms of 'h', the coefficient of convective heat transfer from the particle surface:

$$\dot{Q}_p = h\, A_{exposed} (T_p - T) \qquad (4.35)$$

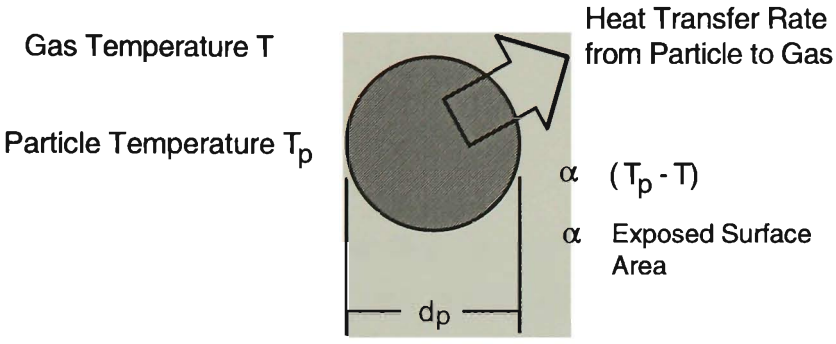

Figure 5.5 Heat Transfer from a Spherical Particle

The coefficient 'h' is expressed in terms of a non-dimensional parameter, the Nusselt Number, based on the diameter of the particle and defined as:

$$Nu_{d_p} = \frac{h\, d_p}{k_{fluid}}$$

Here (as was necessary in the case of particle drag coefficient C_{Dp}), an assumption is required to be made about the estimation of Nu_{Dp}. Let

$$Nu = \frac{Nu_{d_p}}{Nu_{Stokes}} = \frac{\text{Actual Particle Nusselt Number}}{\text{"Stokes" Nusselt Number}}$$

where Nu_{Stokes} = Nusselt Number in the Stokes flow region of low values of particle Reynolds Number, and is equal to 2.0 [Z1].

Then,

$$Nu_{d_p} = Nu_{Stokes} \cdot Nu = 2 \cdot Nu$$

so that

$$h = \frac{Nu_{d_p}\, k_{fluid}}{d_p} = \frac{2 \cdot Nu \cdot k_{fluid}}{d_p}$$

and

$$\delta \dot{Q}_p = \frac{2\, Nu\, k_{fluid}}{d_p} \pi\, d_p^2 \left(T_p - T\right) = 2\, Nu\, k_{fluid}\, \pi\, d_p \left(T_p - T\right) \qquad (5.36)$$

As a consequence of this heat transfer, each particle undergoes a change in its energy (enthalpy) :

$$\begin{bmatrix}\text{Rate of}\\ \text{heat transfer}\\ \text{from a particle}\end{bmatrix} = \begin{bmatrix}\text{Rate of}\\ \text{decrease of}\\ \text{particle enthalpy}\end{bmatrix}$$

or,

$$\delta\dot{Q}_p = - m_p\, c_{mp} \frac{dT_p}{dt} \tag{5.37}$$

The negative sign accounts for the fact that each particle *loses* energy due to heat transfer. An implicit assumption made here is that the temperature of the particle has the same value throughout its volume. This assumption is valid for small particles. For a spherical particle of diameter d_p and particle material density ρ_{mp},

$$-\delta\dot{Q}_p = \rho_{mp} \frac{\pi}{6} d_p^{\,3}\, c_{mp} \frac{dT_p}{dt} = \rho_{mp} \frac{\pi}{6} d_p^{\,3}\, c_{mp} \frac{dT_p}{dx}\frac{dx}{dt} \tag{5.38}$$

Again, interpreting the term $\frac{dx}{dt}$ as the velocity, *of the particle* [Z2],

$$-\delta\dot{Q}_p = \rho_{mp} \frac{\pi}{6} d_p^{\,3}\, c_{mp} \frac{dT_p}{dx} V_p \tag{5.39}$$

or,

$$2\cdot Nu \cdot k_{fluid}\, \pi\, d_p \left(T - T_p\right) = \rho_{mp} \frac{\pi}{6} d_p^{\,3}\, c_{mp} \frac{dT_p}{dx} V_p \tag{5.40}$$

In the Initial Region,

$$\delta\dot{Q}(x) = 2\cdot Nu \cdot k_{fluid} \cdot d_p \left(T_p - T\right) \frac{\sigma_p}{m_p} A_{tube}\left[1 - \left(1 - \frac{x}{x_c}\right)^2\right] dx \tag{5.41}$$

and in the Main Region,

$$\delta\dot{Q}(x) = 2\cdot Nu \cdot k_{fluid} \cdot d_p \left(T_p - T\right) \frac{\sigma_p}{m_p} A_{tube}\, dx \tag{5.42}$$

Now the expression for the driving potential due to heat transfer can be derived:

$$HT \cdot dx = \frac{\delta q}{\psi\, c_p T}$$

$$= \frac{\delta\dot{Q}(x)/\dot{m}}{\psi\, c_p T} = \frac{2\ Nu\ k_{gas}\ d_p \left(T_p - T\right) \frac{\sigma_p}{m_p} A_{tube}\left[1 - \left(1 - \frac{x}{x_c}\right)^2\right]}{\psi\, c_p T \cdot \rho\, V\, A} dx$$

so that, in the Initial Region,

$$HT = \frac{2\ Nu\ k_{gas}\ d_p\ (T_p - T)\ \frac{\sigma_p}{m_p}\ A_{tube}\left[1 - \left(1 - \frac{x}{x_c}\right)^2\right]}{\psi\ c_p T \cdot \rho\ V\ A} \tag{5.43}$$

and in the Main Region,

$$HT = \frac{2\ Nu\ k_{gas}\ d_p\ (T_p - T)\ \frac{\sigma_p}{m_p}\ A_{tube}}{\psi\ c_p T \cdot \rho\ V\ A} \tag{5.44}$$

In addition to energy transfer as heat between primary and secondary streams, there is energy transfer as work from primary stream to the suspension.

5.4.8 Work Transfer to Suspension

In the Initial Region, the primary gas stream has to perform work on an increasing number of particles in the suspension.

$$\begin{bmatrix}\text{Total rate of}\\ \text{work transfer}\\ \text{to particles}\\ \text{from primary gas}\end{bmatrix} = \begin{bmatrix}\text{Rate of}\\ \text{heat transfer}\\ \text{to a}\\ \text{single particle}\end{bmatrix} \cdot \begin{bmatrix}\text{Number of}\\ \text{particles taking}\\ \text{part in}\\ \text{heat transfer}\end{bmatrix}$$

That is,

$$\delta\dot{W}(x) = \begin{pmatrix}\text{Work}\\ \text{Transfer rate}\\ \text{per particle}\end{pmatrix} \cdot \begin{pmatrix}\text{Number of}\\ \text{particles}\\ \text{influenced}\end{pmatrix}$$

As before,

$$\delta\dot{W}(x) = \delta\dot{W}_p\ \frac{\sigma_p}{m_p}\ V_{inf}(x) \tag{5.45}$$

so that, in the Initial Region,

$$\delta\dot{W}(x) = \delta\dot{W}_p\ \frac{\sigma_p}{m_p}\ A_{tube}\left[1 - \left(1 - \frac{x}{x_c}\right)^2\right] dx \tag{5.46}$$

and in the Main Region,

$$\delta\dot{W}(x) = \delta\dot{W}_p \frac{\sigma_p}{m_p} A_{tube}\, dx \tag{5.47}$$

An expression for $\delta\dot{W}_p$, work performed on a single particle, is now derived.

5.4.9 Work Transfer to a Particle

The basic definition of the amount of work done on an object is :

(Work done) = (Net External Force)•(Displacement parallel to Force)

so that

$$\begin{bmatrix}\text{Time rate}\\ \text{of}\\ \text{work done}\end{bmatrix} = \begin{bmatrix}\text{Force}\\ \text{on object}\end{bmatrix} \cdot \begin{bmatrix}\text{velocity}\\ \text{of object}\end{bmatrix}$$

For a particle moving at velocity V_p under the action of Drag force D_p, assuming that D_p and V_p are the same direction,

$$\delta\dot{W}_p = D_p V_p = 3\pi\mu C_D d_p \left(V - V_p\right) V_p \tag{5.48}$$

The expression for total work transfer for the influenced particles is found by substituting for $\delta\dot{W}_p$ in the equation for $\delta\dot{W}(x)$:

In the Initial Region,

$$\delta\dot{W}(x) = 3\pi\mu C_D d_p \left(V - V_p\right) V_p \frac{\sigma_p}{m_p} A_{tube} \left[1 - \left(1 - \frac{x}{x_c}\right)^2\right] dx \tag{5.49}$$

and in the Main Region,

$$\delta\dot{W}(x) = 3\pi\mu C_D d_p \left(V - V_p\right) V_p \frac{\sigma_p}{m_p} A_{tube}\, dx \tag{5.50}$$

Now the expressions for driving potentials due to work transfer can be derived.

$$WK \cdot dx = \frac{\delta w}{\psi\, c_p T}$$

$$= \frac{\delta \dot{W}(x) / \dot{m}}{\psi\, c_p T}$$

$$= \frac{3\,\pi\,\mu\, C_D\, d_p \left(V - V_p\right) V_p \frac{\sigma_p}{m_p} A_{tube} \left[1 - \left(1 - \frac{x}{x_c}\right)^2\right]}{\psi\, c_p T \cdot \rho\, V\, A} dx$$

so that, in the Initial Region,

$$WK = \frac{3\,\pi\,\mu\, C_D\, d_p \left(V - V_p\right) V_p \frac{\sigma_p}{m_p} A_{tube} \left[1 - \left(1 - \frac{x}{x_c}\right)^2\right]}{\psi\, c_p T \cdot \rho\, V\, A} \tag{5.51}$$

and in the Main Region,

$$WK = \frac{3\,\pi\,\mu\, C_D\, d_p \left(V - V_p\right) V_p \frac{\sigma_p}{m_p} A_{tube}}{\psi\, c_p T \cdot \rho\, V\, A} \tag{5.52}$$

Next, an expression for mass entrainment into the primary stream is sought.

5.4.10 Mass Entrainment

In the Initial Region, mass is continuously added to the primary gas stream. This mass is entrained through the lateral surface of the cone-shaped potential core.

Entrained mass through a differential surface element

$$d\dot{m} = \rho_s\, V_s \left(dA_{cone} \perp V_s\right) = \rho_s\, V_s\, (2\,\pi\, r \cdot dr) \tag{5.53}$$

or

$$d\dot{m} = \rho_s\, V_s \left(2\,\pi\, r \frac{dr}{dx} dx\right) = \rho_s\, V_s\, 2\,\pi \left[r_{tube} \left(1 - \frac{x}{x_c}\right)\right] \left(\frac{r_{tube}}{x_c}\right) dx$$

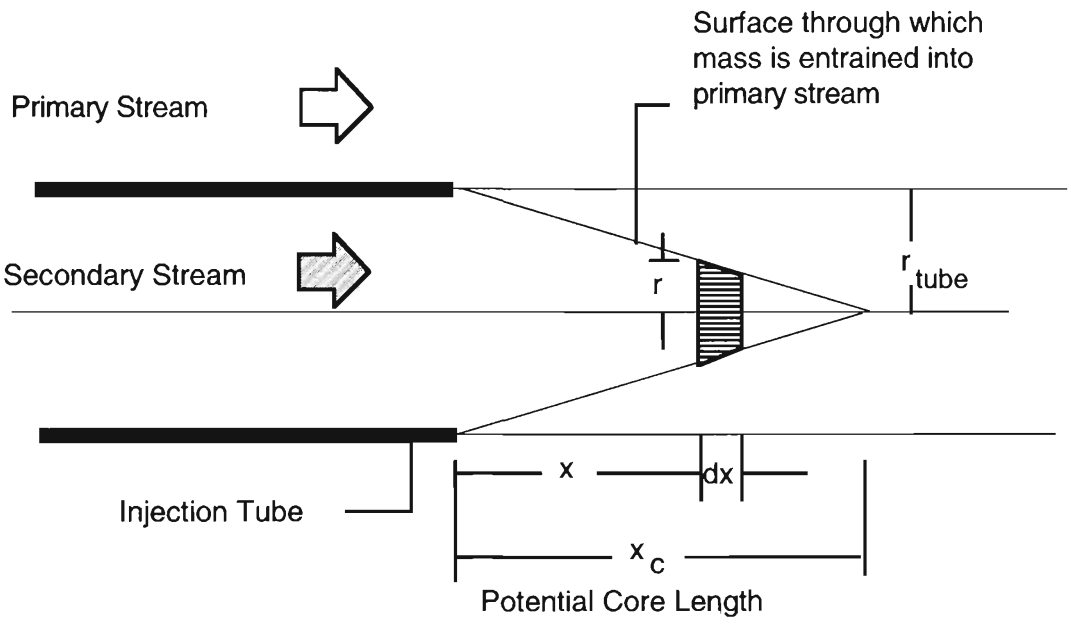

Figure 5.6 Mass Entrainment in the Initial Region

That is,

$$d\dot{m} = \rho_s V_s 2 \pi r_{tube}^2 \left(\frac{1}{x_c}\right)\left(1 - \frac{x}{x_c}\right) dx$$

Now the expression for driving potential due to mass entrainment can be derived:

$$EM \cdot dx = \frac{1}{\rho V A} \rho_s V_s 2 A_{tube} \frac{1}{x_c}\left(1 - \frac{x}{x_c}\right) dx \qquad (5.54)$$

so that, in the Initial Region,

$$EM = \frac{1}{\rho V A} \rho_s V_s 2 A_{tube} \frac{1}{x_c}\left(1 - \frac{x}{x_c}\right) \qquad (5.55)$$

and, in the Main Region,

$$EM = 0. \qquad (5.56)$$

Equation 5.56 results from the observation that in the main region, all the particles have been entrained into the primary stream, and that the area through which such entrainment can occur has reduced to zero.

5.4.11 Different Stagnation Enthalpies

Finally, if the interacting streams have different initial stagnation temperatures, and hence different stagnation enthalpies, this leads to additional energy transfer between them, which is related to mass entrainment:

$$DH0I \cdot dx = \frac{c_p T_0 - c_{p\,i} T_{0\,i}}{\psi\, c_p T} \cdot \frac{d\dot{m}}{\dot{m}}$$

$$= \frac{\rho_s\, V_s\, 2\, A_{tube}\, \frac{1}{x_c}\left(1 - \frac{x}{x_c}\right)\left(c_p T_0 - c_{p\,i} T_{0\,i}\right)}{\psi\, c_p T \cdot \rho\, V\, A}\, dx$$

The associated driving potentials are

In the Initial Region,

$$DH0I = \frac{\rho_s\, V_s\, 2\, A_{tube}\, \frac{1}{x_c}\left(1 - \frac{x}{x_c}\right)\left(c_p T_0 - c_{p\,i} T_{0\,i}\right)}{\psi\, c_p T \cdot \rho\, V\, A} \qquad (5.57)$$

and, in the Main Region,

$$DH0I = 0 \qquad (5.57)$$

5.5 Governing Equations

The governing equations describing the flow in the interaction region can now be written. Expressions for the Influence Coefficients are as derived in Appendix A, and are the same for any compressible fluid flow. Expressions for the driving potentials are as derived above.

The equations are:

Rate of Change of Mach Number

$$\frac{dM}{dx} = EMA \cdot AR + EMFD \cdot FD + EMEN \cdot ENER + EMEM \cdot EM \qquad (5.58)$$

Rate of Change of Density

$$\frac{d\rho}{dx} = EDA \cdot AR + EDFD \cdot FD + EDEN \cdot ENER + EDEM \cdot EM \tag{5.59}$$

Rate of Change of Temperature

$$\frac{dT}{dx} = ETA \cdot AR + ETFD \cdot FD + ETEN \cdot ENER + ETEM \cdot EM \tag{5.60}$$

Rate of Change of Fluid Velocity

$$\frac{dV}{dx} = EVA \cdot AR + EVFD \cdot FD + EVEN \cdot ENER + EVEM \cdot EM \tag{5.61}$$

Rate of Change of Stagnation (Total) Pressure

$$\frac{dP_o}{dx} = EP0A \cdot AR + EP0FD \cdot FD + EP0EN \cdot ENER + EP0EM \cdot EM \tag{5.62}$$

Rate of Change of Specific Entropy (optional)

$$\frac{ds}{dx} = ESA \cdot AR + ESFD \cdot FD + ESEN \cdot ENER + ESEM \cdot EM \tag{5.63}$$

Rate of Change of Impulse Function (optional)

$$\frac{dF}{dx} = EFA \cdot AR + EFFD \cdot FD + EFEN \cdot ENER + EFEM \cdot EM \tag{5.64}$$

Rate of Change of Particle Velocity

$$\frac{dV_p}{dx} = \frac{18\mu C_D}{\rho_{mp} d_p^{\,2}} \left(\frac{V - V_p}{V_p} \right) \tag{5.65}$$

Rate of Change of Particle Temperature

$$\frac{dT_p}{dx} = \frac{18 \cdot Nu \cdot k_{fluid}}{\rho_{mp} \cdot d_p^{\,2} \cdot c_{mp}} \left(\frac{T - T_p}{V_p} \right) \tag{5.66}$$

and finally,

Rate of Change of Static Pressure

$$\frac{dp}{dx} = EPA \cdot AR + EPFD \cdot FD + EPEN \cdot ENER + EPEM \cdot EM \tag{5.67}$$

However, as stated earlier, the flow in the entire Interaction Region is required to be of the *constant-pressure* type. It follows that:

$$\frac{dp}{dx} = 0$$

This allows the driving potential due to Area Change (AR) to be evaluated in terms of the other driving potentials :

$$AR = - \frac{EPFD \cdot FD + EPEN \cdot ENER + EPEM \cdot EM}{EPA} \tag{5.68}$$

As before, this amounts to using the requirement of constant pressure in the interaction region to treat the problem as one of designing the duct geometry (calculating the cross-sectional areas at successive downstream locations) in the interaction region of the SAI. Thus :

Rate of Change of Area

$$\frac{dA}{dx} = - \frac{A}{EPA} [EPFD \cdot FD + EPEN \cdot ENER + EPEM \cdot EM] \tag{5.69}$$

Equations (5.58) to (5.66) and (5.69) form a set of ten first-order differential equations which must be solved simultaneously. It is not necessary to solve Equation (5.67), the pressure equation. This is because the pressure is constant, equal to the initial specified value.

5.6 Flow Parameters

Results of the analysis of the flow in the nozzle and interaction region are presented in Figures 5.7 to 5.12. The following points should be noted:

1 These analytical results are presented as a continuation of those in Chapter 4, ie., they cover a longer axial distance from the starting point at the stagnation chamber.
2 This makes it possible to assess the smooth blending between flows in the nozzle and interaction regions.

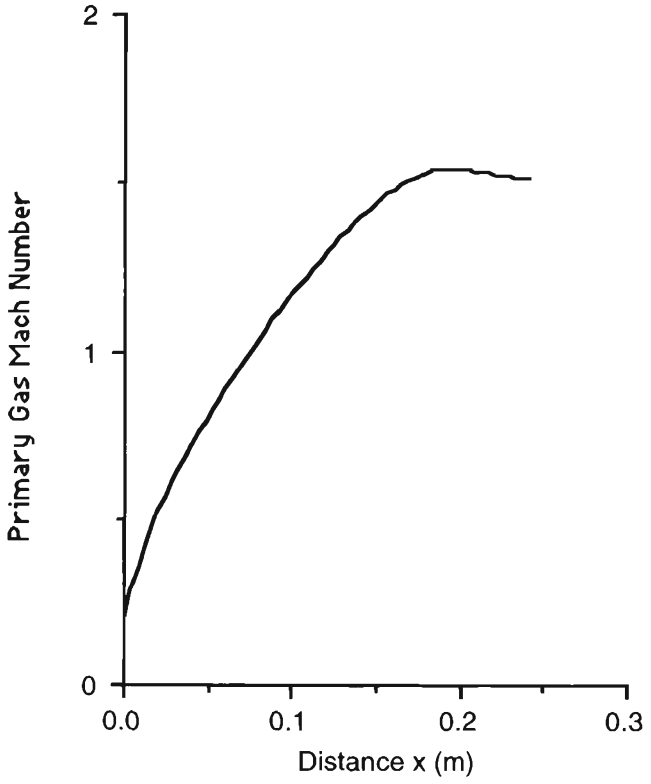

Figure 5.7 Primary Gas Mach Number vs Distance

Figure 5.7 shows the variation of primary gas Mach number in the nozzle region followed by the interaction region. In the interaction region, (0.2 m $\leq$ x $\leq$ 0.24 m), the decelerating influence of the secondary stream brings about a slight drop in the Mach number value, although it remains substantially supersonic.

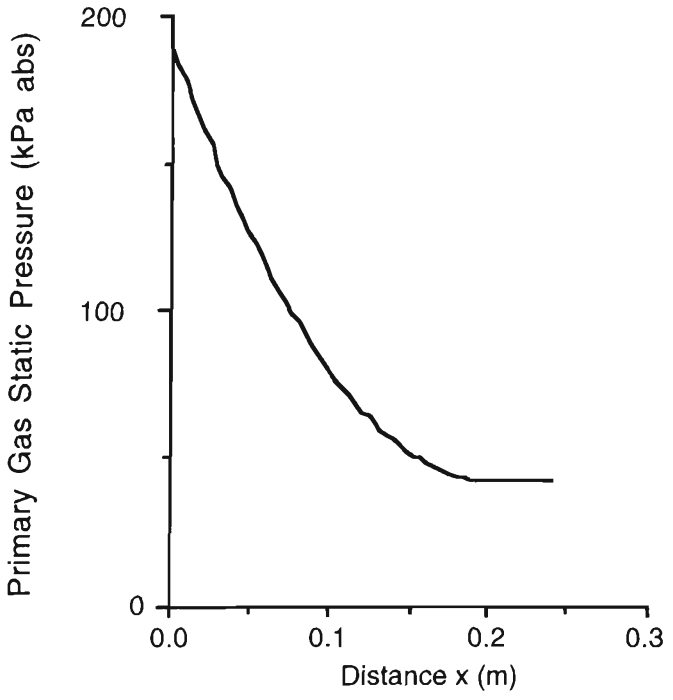

Figure 5.8 Primary Gas Static Pressure vs Distance

Variation of static pressure in the nozzle and interaction regions is depicted in Figure 5.8. The interaction is seen to be of the constant pressure type (0.2 m $\leq$ x $\leq$ 0.24 m), as was specified.

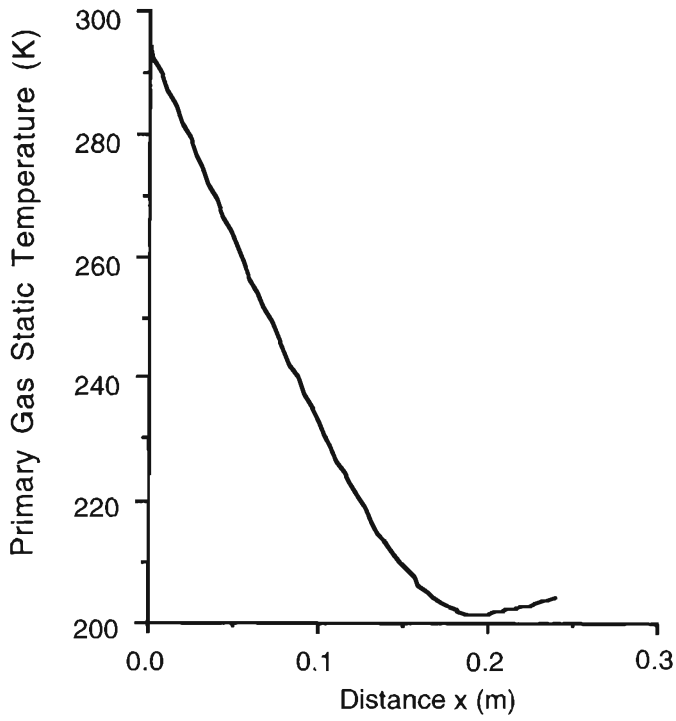

Figure 5.9 Primary Gas Static Temperature vs Distance

Figure 5.9 shows the effect of heat transfer between the primary gas and the secondary stream in the interaction region. After a continuous decline in the nozzle region, (0 $\leq$ x $\leq$ 0.2 m), the temperature shows a steady upward trend in the interaction region due to heat transfer from the hotter secondary stream.

Like the Mach number variation, primary gas velocity also drops due to the decelerating influence of the slower secondary stream in the interaction region, as shown in Figure 5.10. It is necessary in the present project to maintain the velocity of the combined stream sufficiently above the sonic, so that subsequent shock formation may be possible. This suggests that the length of the interaction region is a crucial parameter.

A limited amount of physical mixing between the primary and secondary streams brings about a slight rise in density of the combined stream in the interaction region, as depicted in Figure 5.11. This will be more noticeable in case of a heavier suspension.

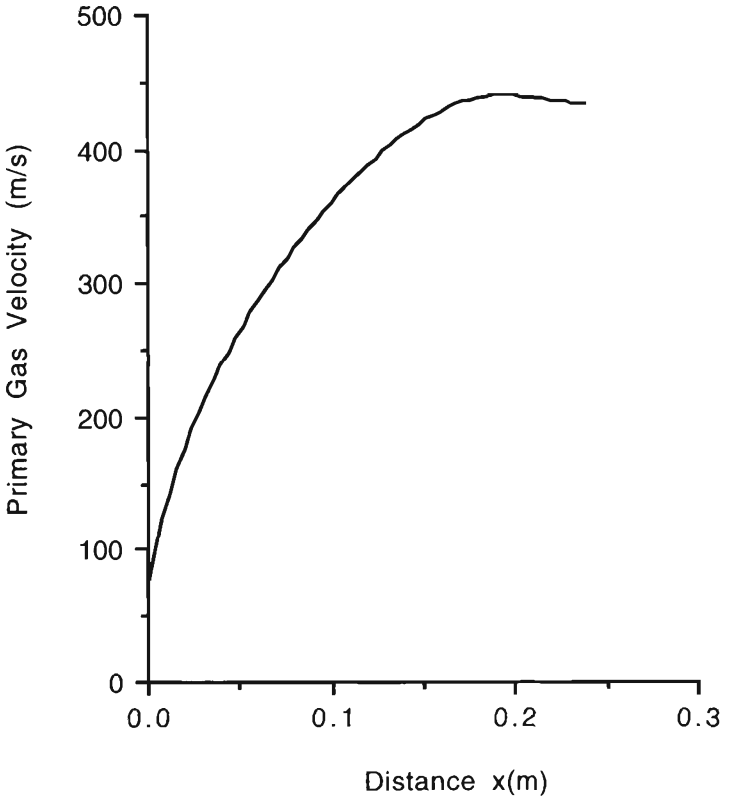

Figure 5.10 Primary Gas Velocity vs Distance

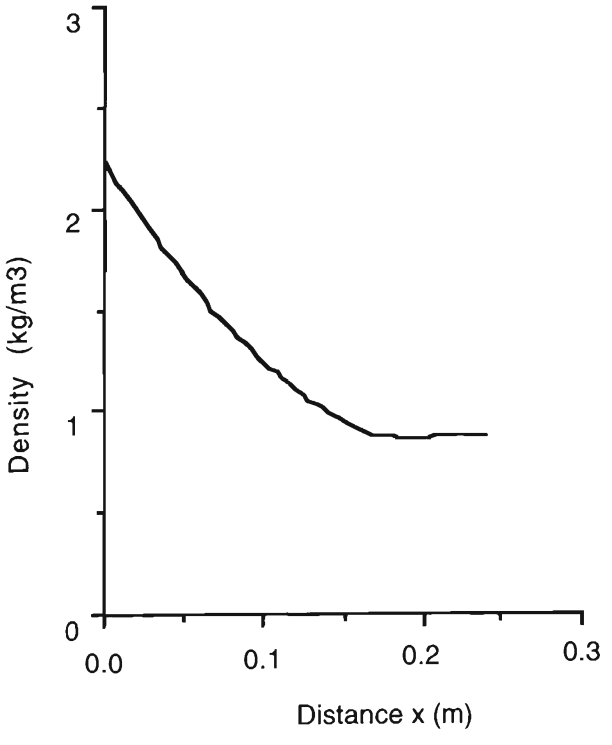

Figure 5.11 Primary Gas Density vs Distance

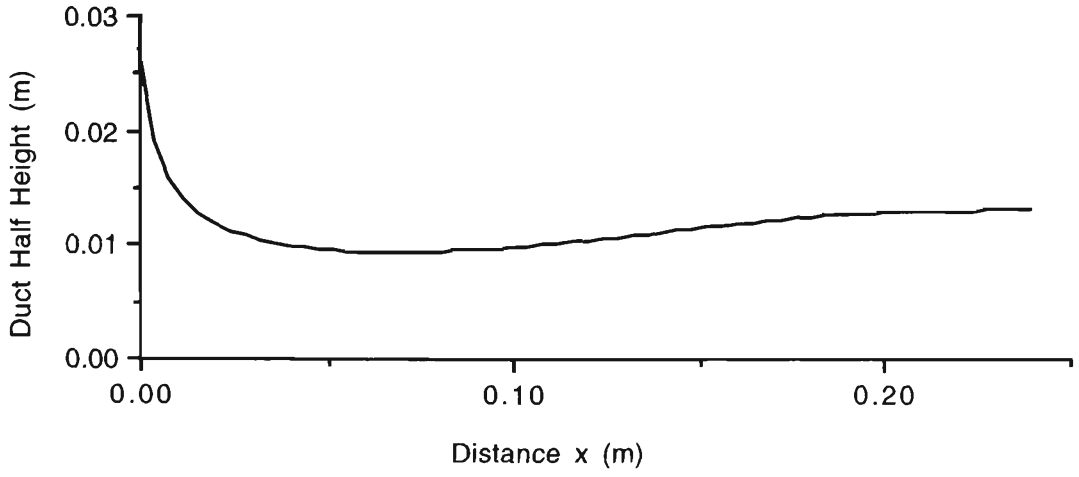

Figure 5.12 Duct Half Height vs Distance

Variation of duct half height with distance in the nozzle and interaction regions is shown in Figure 5.12. It can be seen that a constant-pressure interaction is possible only if the duct opens up to the appropriate extent to admit the additional mass flow rate of the secondary stream. There is also no noticeable jump in duct height at the cross-over point between nozzle and interaction regions, a desirable feature from the design point of view.

At the end of the interaction region, depending upon the pressure at the final destination and also the area of flow, a shock will appear in the flow. This marks the commencement of the compression region. Analysis of flow in the compression region is taken up in the next chapter.

Chapter 6

FLOW IN COMPRESSION REGION

6.1 Shock-Compression Region

It was mentioned briefly in Chapter 1 that the structure of a normal shock in a duct is very different from that in an ideal, unconfined flow. This is due to a severe interaction between the boundary layer on the duct walls and the normal shock. This results in the so-called 'pseudo-shock' or 'multiple shock' pattern. Because the present project involves supersonic flow in a narrow channel, it is very likely that such a shock pattern will appear in the SAI duct.

It is the purpose of this chapter to propose a conceptually simple model for the pseudo-shock. A detailed outline of the model for a single-phase (gas-only) case is presented here. In Chapter 7, the proposed model is extended to a two-phase (gas-particle) flow.

6.2 Introduction

When the pressures at the inlet and the exit of a duct in which a gas flows supersonically are adjusted so that a compression shock appears in the duct, the shock is found to be radically different from a plane discontinuity. This difference arises as the result of an interaction between the shock wave and the boundary layer on the walls of the duct [S11]. When such an interaction occurs in a supersonic diffuser, the overall static pressure rise is much less than that expected from inviscid theory, rendering a design based on such a theory almost useless [Y3]. The pseudo-shock is encountered in the inlets of air-breathing engines and SCRAMjet engines, and poses a basic problem in supersonic compressors and high-pressure power-plants [Y4]. A study of the interaction is also important for diffuser applications of gas-dynamic lasers, where relatively thick boundary layers may be present in narrow channels [O1]. In the present

project, the possibility of a multiple shock occurring in the duct must be taken into it involves supersonic flow in a narrow channel with relatively thick boundary layers.

6.3 Pseudo-shock Structure

Depending upon the degree of 'blockage' (effective reduction in flow cross-section area) caused by the growth of boundary layers on the duct walls, the interaction between the shock and the boundary layer leads to a series of shocks in the core of the flow. The multiple shocks are successively weaker, and the core flow velocity tends towards the sonic velocity at the end of the so-called 'shock region'. For relatively low blockage (ratio of boundary-layer thickness to half duct height d/h = about 0.1 [O2]), the shocks are normal to the duct centerline and bifurcated near the walls, (called 'λ-type'). For greater degrees of blockage, the central normal part disappears, leaving an 'X-type' pseudo-shock. After attaining sonic speed in the core, due to further mixing with the low-speed flow near the duct walls, the flow continues to be decelerated to subsonic speed, and the stream static pressure continues to rise. It is thus seen that the flow in the pseudo-shock can be divided into two parts [T2] (See Figure 6.1):

1 An upstream 'shock region' in which the initial supersonic flow is gradually decelerated to sonic conditions through a series of successively weaker shocks in the core, and
2 the downstream 'mixing region' in which there is large-scale mixing between the core flow and the boundary-layer flow.

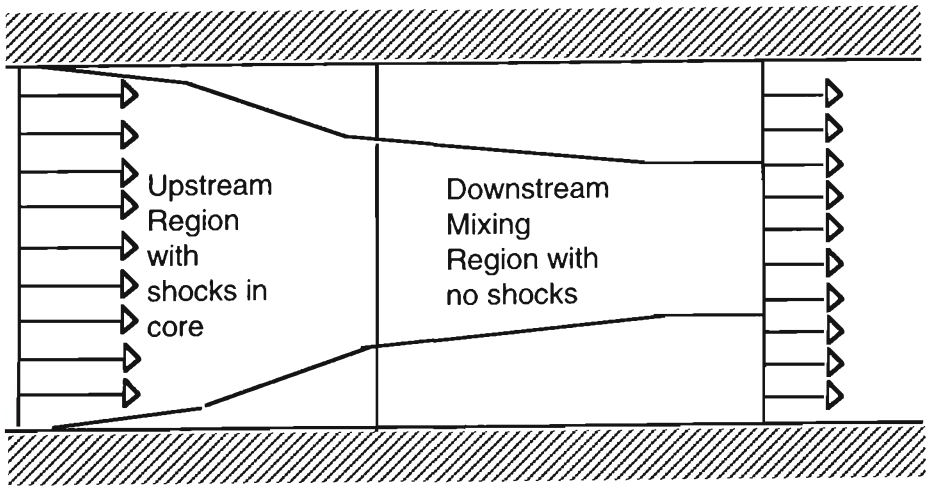

Figure 6.1 Regions of Pseudo-shock Flow

In this chapter, attention is focussed on the upstream region characterised by the occurrence of multiple shocks.

6.4 Motivation

The oldest known model for the pseudo-shock pattern is 'Crocco's Shockless Model' [I1]. In this model, the overall flow is divided into two parts :

1 Core flow,
2 Flow near the solid walls.

The core flow is assumed to be isentropic. The width of the core reduces to zero at the end of the pseudo-shock. All the dissipative effects are assumed to be confined to the flow near the walls (Figure 6.2).

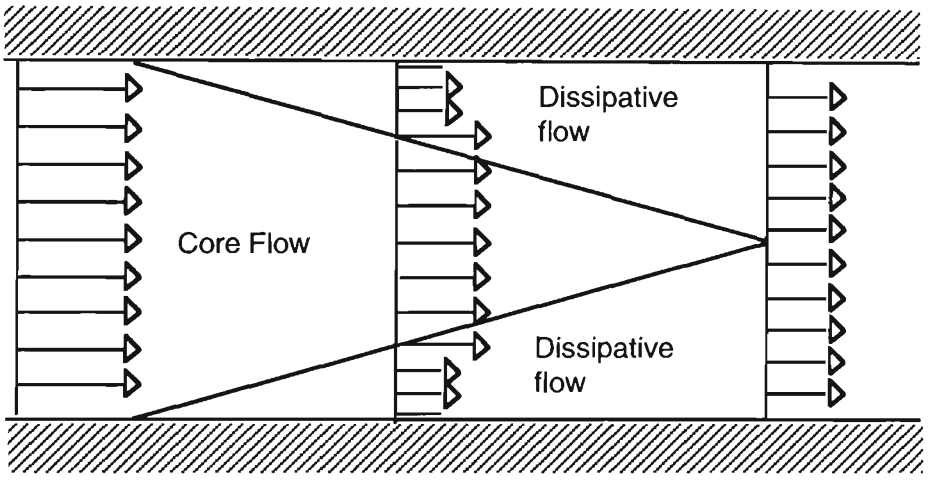

Figure 6.2 Crocco's 'Shockless' Model [I1]

Assuming the core flow to be 'shockless' and therefore isentropic seems to be the main drawback of Crocco's model. Due to the occurrence of multiple shocks, the core flow is far from isentropic. Other drawbacks are:

1 Crocco's model cannot predict the distribution of various quantities related to the distance along the duct and the length of the pseudo-shock, since all quantities are calculated as functions of the ratio of the mass flow rate of the dissipative low-velocity flow to the total mass flow rate;

2 How this ratio itself varies with downstream distance is not predicted;

3 There is a discrepancy in predicted velocities between the high- and low-speed regions at the final section of the pseudo-shock.

Ikui et al [I1] recognised these drawbacks, and proposed an improved version, called the 'Diffusion Model' (Figure 6.3). In the Diffusion Model, it is assumed that the high-speed flow in the core and the low-speed flow near the wall diffuse into each other and both flow velocities become equal at the end of the mixing region. Using the Diffusion Model it is possible to estimate, for a given initial Mach number, the overall length of the pseudo-shock, and the ratio of mass flow rate of the dissipative low-velocity flow to the total mass flow rate as a function of distance (normalised with respect to the duct diameter). The core flow is not assumed isentropic. However, the occurrence of many shocks in the upstream core of the flow is still left unaccounted for. It is also assumed in this model that the static pressure is constant across the flow, as in a boundary layer. This is contrary to experimental findings. It is reported [O2, etc] that the occurrence of many successively weaker shocks in the core of the flow brings about large fluctuations in pressure (and consequently other flow parameters) in the core flow. These fluctuations are damped out at points closer to the solid boundary.

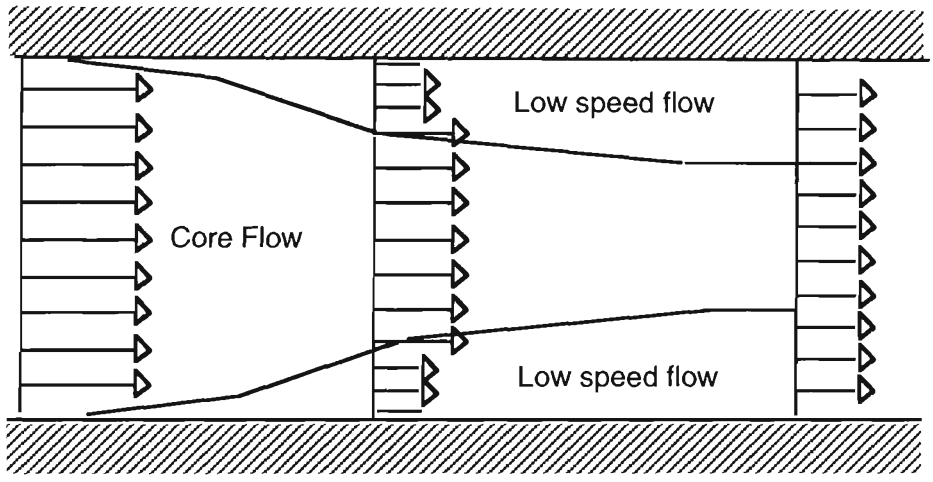

Figure 6.3 Diffusion Model

Tamaki et al [T2] propose a 'Shock-reflection model' which accounts for the occurrence of successive shock waves in the upstream core of the flow in a phenomenological and mostly qualitative way [Y5]. This model is based on the idea that in the upstream region, the shock wave repeats a kind of reflection on the boundary surface between the main flow and the low-speed region near the wall. An actual determination of this boundary surface is not carried out.

There seems to be, as yet, no model which accounts for all the major quantitative trends seen in multiple shock patterns. On the other hand, a number of experimental findings have been reported in the literature [eg. C9-C12, O1, O2]. In this chapter, a simple model for the pseudo-shock pattern consisting of multiple normal shocks in the core is presented. It is hoped that this model combines tested features of the above-

mentioned models with a new idea which has not been explored yet. This may form a useful basis for an alternative way of studying the pseudo-shock phenomenon and initiate more detailed research along the line suggested. Although the model is developed for multiple normal (or λ-type) shocks, it is conceivable that it can be extended to multiple oblique (or X-type) shocks by considering only the components normal to the oblique shocks. It is also possible to extend the model to dilute gas-particle flows, so that it may be applied to the present project. This extension is outlined in Chapter 7.

6.5 'Modified-Fanno' Model

The overall characteristics of the flow in the upstream shock region are :

1 Constant cross section passage leading to a constant mass flux;

2 Adiabatic and rigid duct wall;

3 Sonic condition at the end of this region.

The first two attributes generally have been supported by experimental work reported in the literature [eg O1], and the third is a characteristic of the pseudo-shock pattern itself. *It is noticed at this point that these attributes are exactly the same as those of a 'Fanno' flow.* In a Fanno flow, wall friction is the sole agency which brings about progressive changes in the flow properties in the downstream direction. The similarity in the overall features of the two flows, however, prompts the question: "Would it be possible to describe the flow in the pseudo-shock pattern as a 'modified-Fanno' flow?" Changes in flow properties in this version of Fanno flow would be brought about not only by the frictional effects at the walls, but also due to the occurrence of multiple shocks in the core of the flow.

The possibilities suggested by this question are explored in the following pages of this chapter.

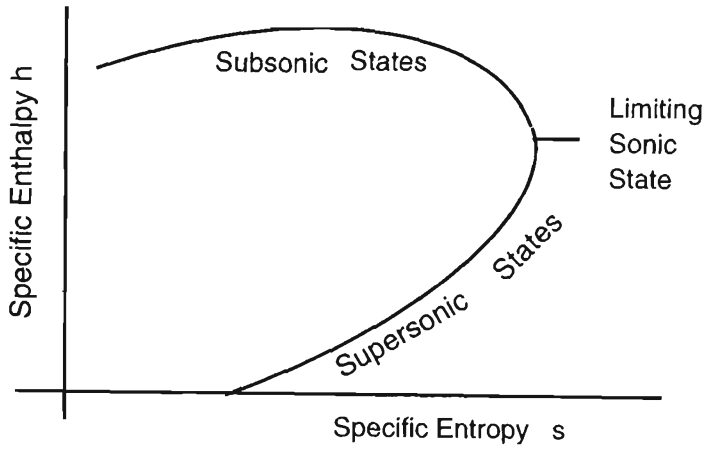

Figure 6.4 Fanno Line

The following equation describes the rate of change of specific enthalpy h with respect to specific entropy s for a Fanno flow (Figure 6.4):

$$\frac{dh}{ds} = h(\gamma - 1)\frac{M^2}{M^2 - 1} \tag{6.1}$$

Characteristic features of the Fanno line are:

1 For $M < 1$, $M^2 < 1$, and $(M^2\text{-}1) < 0$, so $\frac{dh}{ds} < 0$ (Upper limb of Fanno line)

2 For $M > 1$, $M^2 > 1$, and $(M^2\text{-}1) > 0$, so $\frac{dh}{ds} > 0$ (Lower limb of Fanno line)

3 $M = 1$ is the limiting case where $\frac{dh}{ds}$ becomes indeterminate, because in any realistic flow, it is required that entropy be *produced* ($ds > 0$).

If the flow is initially supersonic, the effect of friction will be to decrease the velocity and Mach number and to increase the enthalpy and pressure of the stream (lower limb of Fanno line). On the other hand, if the flow is initially subsonic, the effect of friction will be such that the velocity and Mach number will increase, and the enthalpy and pressure will fall (upper limb of Fanno line). This latter feature of Fanno flow suggested that the suspension flow the injection tube in the SAI could be modelled as a Fanno flow. In general, frictional effects are required to pass continuously along the Fanno line to any other state on the line [S11]. If, however, a more general meaning is attached to 'frictional effects', viz. that they are dissipative effects leading to entropy production, it is possible to pass discontinuously from a point on the lower limb to a point on the upper limb through a compression shock. It is thus seen that the same physical mechanism, frictional dissipation, can account for both the deceleration and reacceleration of the flow, such as is seen in the case of a pseudo-shock pattern.

Because of boundary layer growth along the duct walls, mass flow rate in the core (subjected to the successively weaker shocks) decreases in the downstream direction. At the same time, the area available to the core flow also decreases in the downstream direction, for the same reason. *It is now assumed that these two effects combine in such a way that the successive states attained by the core flow are represented by points on the Fanno line*. A crude-sounding argument for this assumption is: the mass flow rate in the core flow and the area available to it decrease at the same rate, so that the *mass flow rate per unit area*, or mass *flux*, remains constant in the core. the validity of this assumption is tested in the following sections using data reported in the literature. This suggests the following view of changes taking place in the core of the flow (Figure 6.5):

1 Starting at '1', a condition of supersonic flow, the flow is decelerated to a subsonic condition '2' through the first normal shock.
2 Due to boundary-layer development, the core fluid now effectively undergoes flow in a converging-diverging nozzle, attaining the next supersonic condition '3'. (The phenomenon is referred to as an 'aerodynamic converging-diverging nozzle' [C10], and 'effective area modulation arising from displacement thickness buildup' [O1].) Reacceleration in the core flow may be assumed isentropic as a first approximation.
3 The processes described in steps (1) and (2) are repeated such that the core flow is continuously driven to the sonic condition: '3' to '4' to '5', and so on.

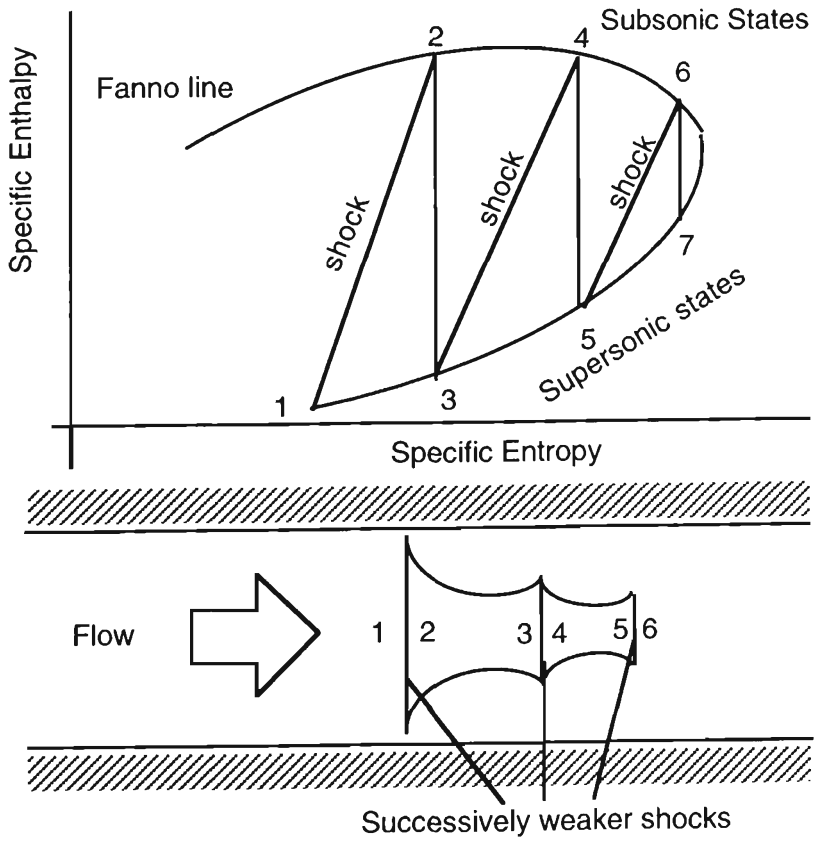

Figure 6.5 Pseudo-shock as 'Modified-Fanno' flow

6.6 Core Flow

To test this model, experimental results reported in [O1] (Table 6.1) are compared with analytical results obtained for the same initial conditions.

Axisymmetric Flow (Radius = 25.95 mm)	
p_0 = 0.3325 atm (assumed gauge)	δ_u = 5.15 mm
T_0 = 300 K	δ_u^* = 1.001 mm
Re/m = 4.90 (10)^6	θ_u = 0.399 mm

Blockage $B = \dfrac{A_{\delta_u^*}}{A} = \left[1 - \left(1 - \delta_u^*/R\right)^2\right] = 0.0515$

Then, $\dfrac{A_{core_u}}{A} = 1 - B = 0.9485$

Table 6.1 Experimental Conditions in [O1]

1 Using experimental results reported in [O1], related to growth of boundary layer displacement thickness δ^* in the shock region, progressive reduction in core flow area can be estimated.

Figure 6.6 shows the growth of boundary layer displacement thickness δ^*, reproduced from Figure 8 in [O1], and using δ_u^* = 1.001 mm (Table 6.1). Then, using R = 25.95 mm, the ratio A_{core}/A in the shock region of this axisymmetric flow is :

$$\frac{A_{core}}{A} = \left(1 - \frac{\delta^*}{R}\right)^2 \qquad (6.2)$$

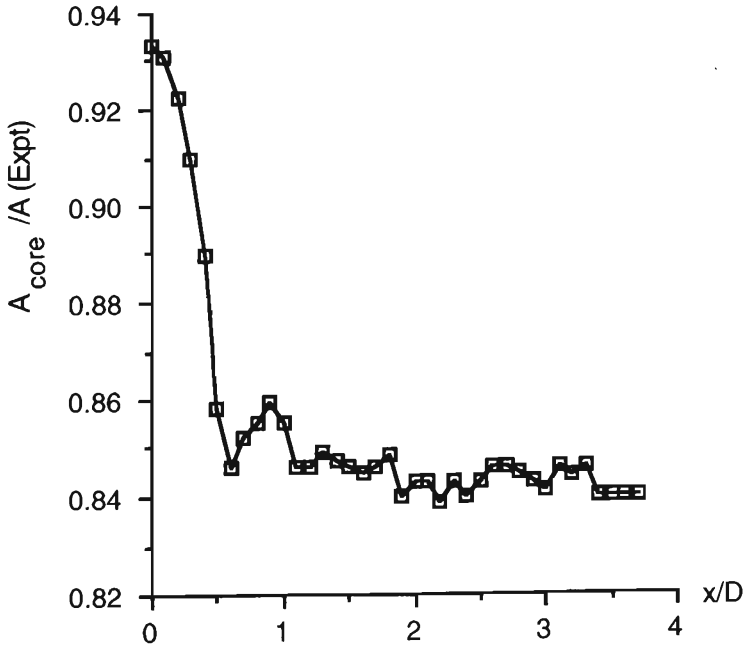

Figure 6.6 (Core Area/Total Area) in Shock Region [O1]

2 Using the theoretical development reported in the 'Diffusion Model' of Ikui et al [I1], it can be estimated how the mass flow rate available to the core flow decreases in the shock region due to the growth of the boundary layer on the duct wall, for the same initial Mach number as in [O1]. This yields values of the ratio $\frac{\dot{m}_{core}}{\dot{m}}$ at successive downstream stations in the shock region. The steps are as follows :

According to Ikui et al [I1], and using the same notation as [I1], the ratio of the mass flow rate in the slower, dissipative layer to the total mass flow rate is given by :

$$\mu = \frac{\text{Mass flow rate in boundary layer}}{\text{Total Mass flow rate}}$$

$$= \frac{\left(w^{*2}/w' + w'\right) - \left(w^{*2}/w_1 + w_1\right)}{\left(w^{*2}/w' + w'\right) - \left(w^{*2}/w'' + w''\right)} \tag{6.3}$$

where

$$w = \text{Dimensionless Velocity} = \text{Crocco Number}$$

$$= \frac{\text{Velocity}}{\sqrt{2\, c_p\, T_0}} \tag{6.4}$$

and

$$w^{*2} = \frac{\gamma - 1}{\gamma + 1} \tag{6.5}$$

and the superscripts (') and (") refer to flow in the core and boundary layer respectively. The subscript '1' refers to the condition immediately upstream of the shock region [I1].

It is shown by Ikui et al [I1] that , in the pseudo-shock region,

$$w' = w_1\, e^{-c\,x}$$

$$w'' = \frac{w^{*2}}{w_1 - w^{*2}/w_1}\left(1 - e^{-c\,x}\right) \tag{6.6}$$

with c = 0.114, an experimentally determined constant, and x the distance from the commencement of the shock region, normalised with respect to duct diameter D.

It is thus possible to calculate the ratio

$$\frac{\dot{m}_{core}}{\dot{m}} = 1 - \mu \tag{6.7}$$

for the experimental conditions in [O1]. It is interesting to note that this ratio, according to the Diffusion Model, is only a function of the gas (c_p, γ), the stagnation condition (T_0) and the upstream Mach number, and is independent of the particular geometrical parameters of the experimental setup.

3 At each station, the ratio of the above two ratios is obtained. That is,

$$\frac{\dot{m}_{core}/\dot{m}}{A_{core}/A} = \frac{\dot{m}_{core}/A_{core}}{\dot{m}/A} = \frac{\text{Mass Flux in core}}{\text{Total Mass flux}} \tag{6.8}$$

If at all stations for which experimental data are available in [O1], this ratio is approximately 1.0, the assumption of constant mass flux in the core can be considered validated.

Figure 6.7 shows the variation of $(1 - \mu) = \frac{\dot{m}_{core}}{\dot{m}}$ with distance in the shock region for the experimental conditions in [O1]. The Diffusion Model predicts that the overall length of the pseudo-shock (= length of the shock region + length of the mixing region) is 5.46 diameters, as can be verified from Table 1 in [I1].

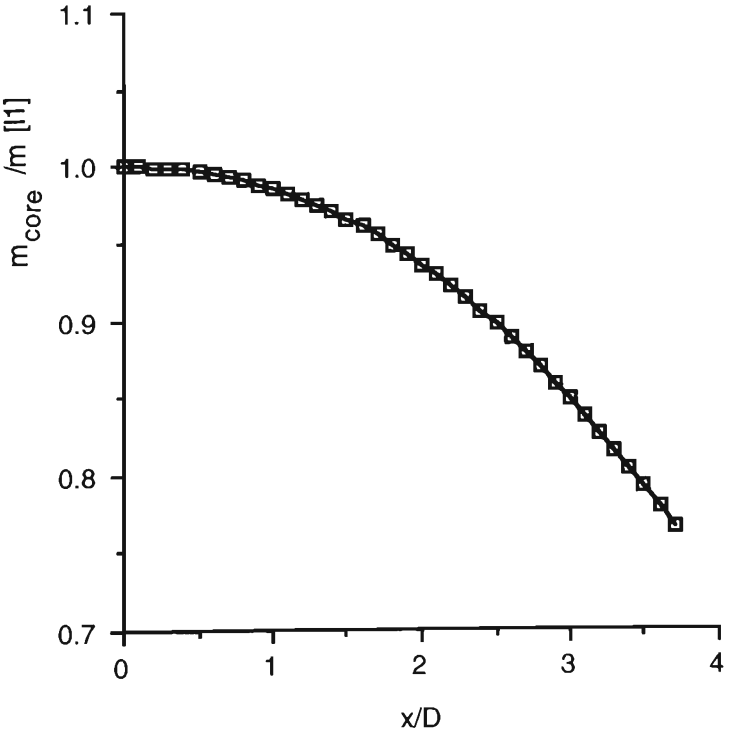

Figure 6.7 Core Mass Flow Rate/Total Mass Flow Rate (Diffusion Model)

From Figures 6.6 and 6.7, it is now possible to estimate the variation of the ratio

$$\frac{\dot{m}_{core}/\dot{m}}{A_{core}/A} = \frac{\dot{m}_{core}/A_{core}}{\dot{m}/A} = \frac{\text{Mass Flux in core}}{\text{Total Mass flux}} \qquad (6.9)$$

in the shock region. This ratio is plotted in Figure 6.8. As can be seen, throughout the shock region, this ratio does not differ appreciably from unity.

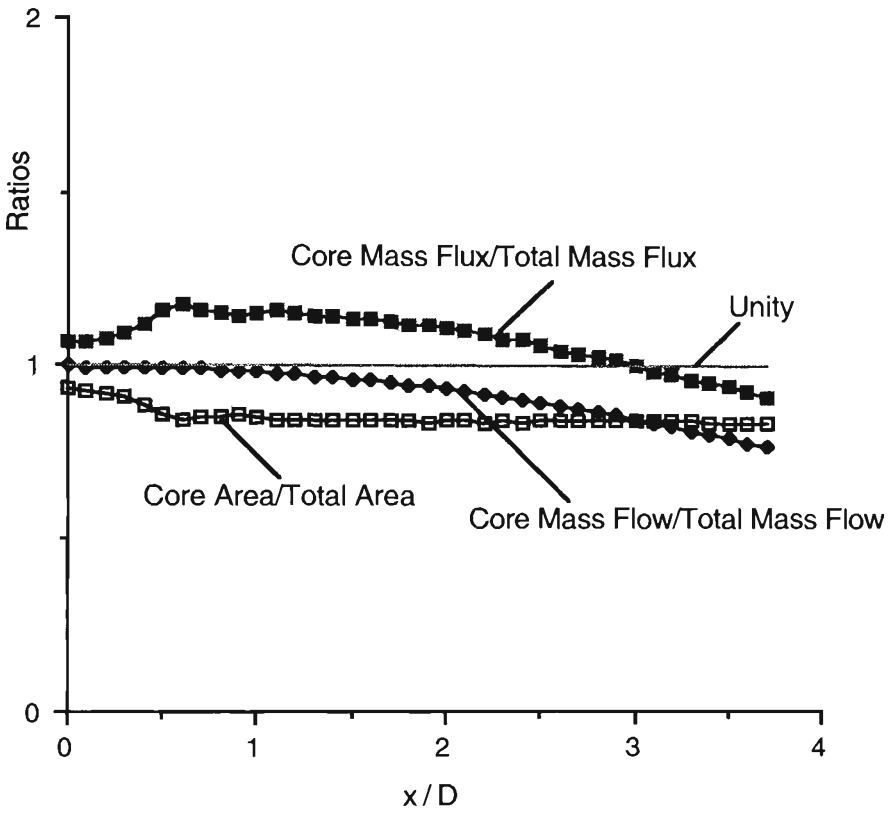

Figure 6.8 Verification of Constant Mass Flux Assumption for Core Flow

It is thus seen that the core flow approximately satisfies the assumption of constant mass flux. This allows modelling of the shock region flow as a 'modified Fanno' flow.

6.7 Distances between Successive Shocks

The shocks are progressively weaker in the downstream direction as the core flow is driven to the sonic condition. Consequently, the rise in specific entropy associated with each shock is smaller than that accompanying the preceding shock. It is assumed that the core flow *between* shocks is isentropic. This allows the following approximation for the flow between sections '1' and '3', for example,

$$\begin{aligned} \Delta s_{1-3} &= \Delta s_{1-2} + \Delta s_{2-3} \\ &\approx \Delta s_{1-2} \\ &= \text{Entropy rise associated with } 1^{st} \text{ shock only} \end{aligned}$$

Then, the distance between sections '1' and '3', that is, the distance between the first and second shocks can be estimated from a value of 'core friction factor' f, using the following relation :

$$ds = \frac{c_p\,(\gamma - 1)\,M^2}{2}\,\frac{f}{D_H}\,dx \tag{6.10}$$

or,

$$\Delta s_{1-3} = \int_1^3 ds = \int_1^3 \frac{c_p\,(\gamma - 1)\,M^2}{2}\,\frac{f}{D_H}\,dx$$

$$\approx \frac{c_p\,(\gamma - 1)}{2}\,M_{av,1-3}{}^2\;f\;\Delta\left(\frac{x}{D_H}\right)_{1-3}$$

so that

$$\Delta\left(\frac{x}{D_H}\right)_{1-3} \approx \frac{\Delta s_{1-3}}{\frac{c_p\,(\gamma - 1)}{2}\,M_{av,1-3}{}^2\;f'_{av}} \tag{6.11}$$

The distances between each successive pair of shocks can be calculated in the same way, provided an estimate is available for the core friction factor f'_{av}. Such an estimate can be obtained from a Second-Law Analysis of the shock region. This represents an extension of the Diffusion Model of Ikui et al [I1].

6.8 Second Law Analysis

Following the nomenclature adopted by Ikui et al [I1], the law of entropy production [B5] can be written for the shock region as :

$$\dot{S}_{gen} = \frac{\partial S}{\partial t} - \frac{\dot{Q}}{T} + (\dot{m}\,s)_2 - (\dot{m}\,s)_1 \tag{6.12}$$

Under the assumptions of steady ($\frac{\partial S}{\partial t} = 0$) and adiabatic ($\frac{\dot{Q}}{T} = 0$) flow and that the specific entropy associated with the incoming flow (s_1) is zero,

$$\dot{S}_{gen} = (\dot{m}\,s)_2$$

$$= (\dot{m}'\,s')_2 + (\dot{m}''\,s'')_2$$

or,

$$\dot{m}_1\,s_{gen} = (\dot{m}'\,s')_2 + (\dot{m}''\,s'')_2 \tag{6.13}$$

(It may be noted that the steady flow assumption ($\partial S/\partial t = 0$) may be relaxed to include findings about the unsteady oscillations of the pseudo-shock [eg. I3] without destroying the basic argument in this model.)

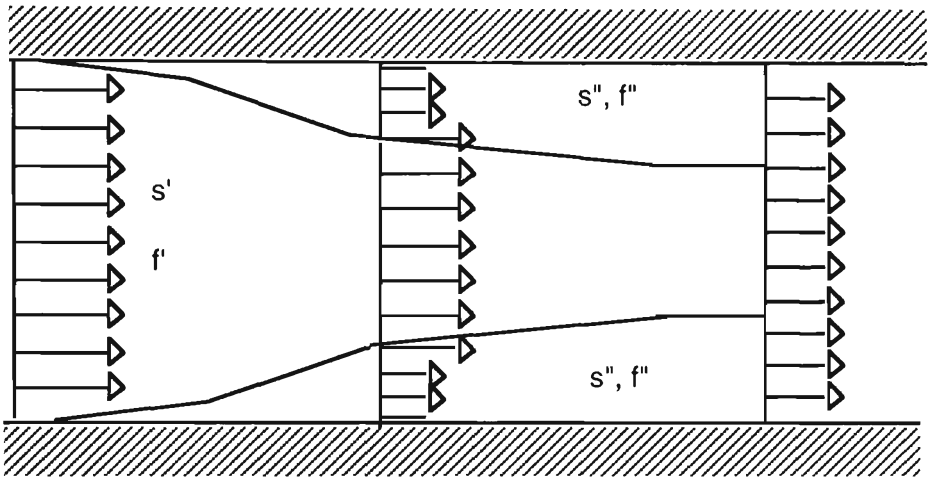

Figure 6.9 Extension of Diffusion Model

Dividing through by $\dot{m}_1$,

$$s_{gen} = ((1 - \mu)\, s')_2 + (\mu\, s")_2$$
$$= (1 - \mu)_2\, s'_2 + \mu_2\, s"_2$$

We can now define frictional dissipation factors f' and f" associated with the core flow and the boundary-layer flow. In terms of these friction factors,

$$s_{gen} = (1 - \mu)_2\, f'_{av} \int_1^2 c_p \frac{\gamma - 1}{2} Ma'^2\, dx + \mu_2 \int_1^2 c_p \frac{\gamma - 1}{2} Ma"^2\, f"\, dx \qquad (6.14)$$

in which the dissipative effect in the core is represented by the average friction factor f'_{av}, and there are experimental data available for friction factor associated with the boundary-layer flow f" [O1].

From Equation 6.14, the average core flow friction factor is given by :

$$f'_{av} = \frac{s_{gen} - \mu_2 \int_1^2 c_p \frac{\gamma - 1}{2} Ma"^2\, f"\, dx}{(1 - \mu)_2 \int_1^2 c_p \frac{\gamma - 1}{2} Ma'^2\, dx} \qquad (6.15)$$

An estimate of s_{gen} can be obtained from the 'Integrated Friction Factor' value as follows: For a supersonic flow at an initial Mach Number 'Ma' to be driven to sonic speed by frictional dissipative effects in a constant-flux flow [W7],

$$f_{int} \frac{L^*}{D} = \frac{1 - Ma^2}{\gamma\, Ma^2} + \frac{\gamma + 1}{2\,\gamma} \ln \frac{(\gamma + 1)\, Ma^2}{2 + (\gamma - 1)\, Ma^2} \tag{6.16}$$

where L^* is the duct length required, and D its diameter. f_{int} is the 'integrated friction factor', which can be looked upon as a weighted average of f' and f''. It is experimentally seen in [O1] that a length of about 3.5 diameters is required to decelerate the core flow from a Mach number 1.49 to 1. So that,

$$f_{int}\,(3.5) = \frac{1 - 1.49^2}{(1.4)\,1.49^2} + \frac{1.4 + 1}{2\,(1.4)} \ln \frac{(1.4 + 1)\,1.49^2}{2 + (1.4 - 1)\,1.49^2} \tag{6.17}$$

yielding

$f_{int} = 0.04$

and

$$s_{gen} \approx c_p \frac{\gamma - 1}{2} Ma_{av}^2\, f_{int}\,(3.5) \approx 41.1 \quad \frac{J}{kg\ K}$$

so that, from Equation 6.15,

$f'_{av} = 0.062.$ (6.18)

6.9 Model Validation

Using this value of f'_{av} , the distance between successive shocks can be calculated. It is seen that this distance decreases for each successive pair of shocks, in agreement with experimental findings. With these distances known, a more meaningful graphical comparison of the variation of some flow parameters in the shock region can be made. This is done in Figures 6.10 and 6.11.

Although there is some discrepancy between experimental values and those calculated from the model, it can be seen that the model reproduces all the trends quantitatively and in a natural way. It is crucially important for a meaningful comparison to predict the distances between successive shocks in the core more accurately. This can be achieved by a more accurate determination of the frictional dissipation factor f'_{av} associated with the core flow. It was assumed that f'_{av} is constant throughout the shock region, whereas it may be a function of distance and such parameters as upstream Mach number.

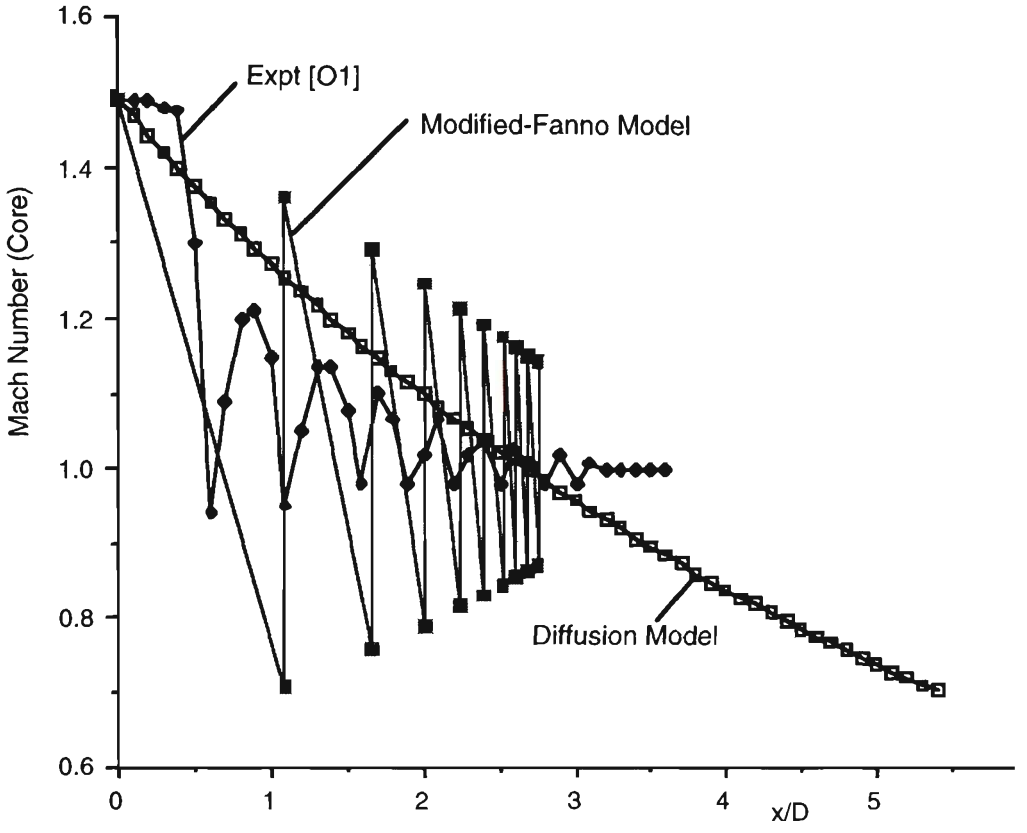

Figure 6.10 Core Mach Number

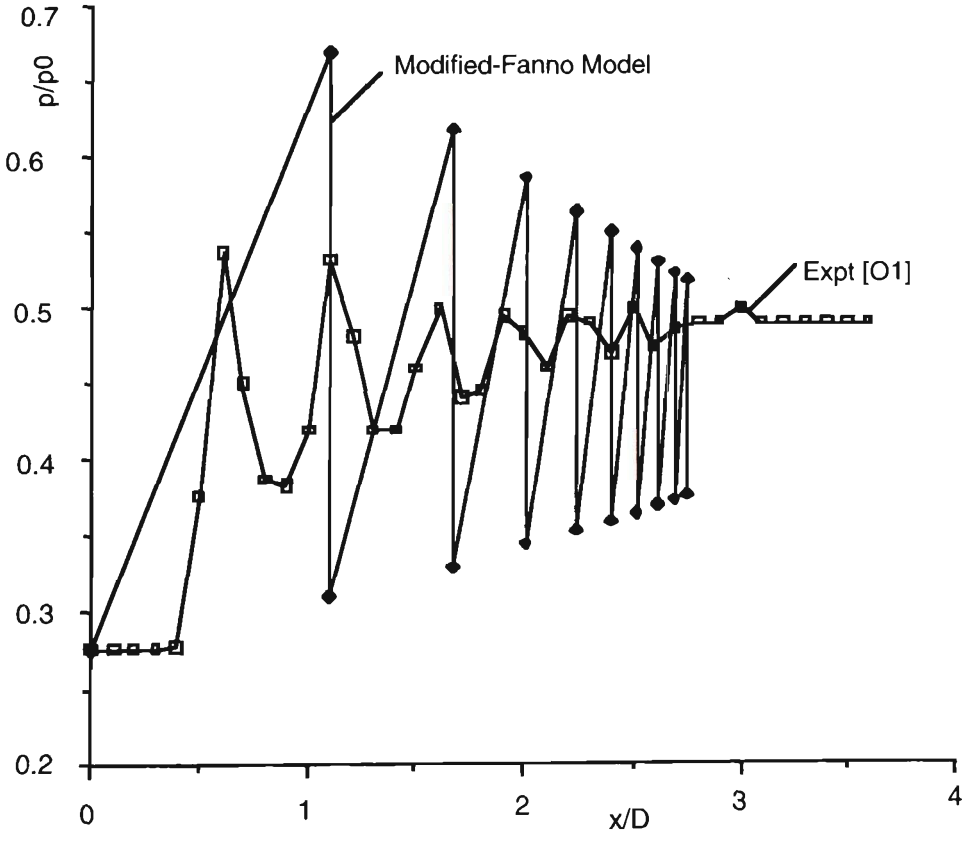

Figure 6.11 Core (Static Pressure/Initial Total Pressure)

6.10 Aerodynamic Nozzle between Shocks

For the subsonic flow immediately after each normal shock to be reaccelerated to a supersonic velocity just before the next shock, the core flow must pass through an aerodynamic nozzle [C10]. The shape of the nozzle is the shape of the line between the core flow and the boundary layer flow along the duct walls.

Under the assumption that the core flow between shocks is isentropic, the shape of the aerodynamic nozzle can be determined from a simple isentropic flow analysis. For this analysis, the smooth variation describing ($\frac{\dot{m}_{core}}{\dot{m}} = 1 - \mu$)(Figure 6.7) can be approximated as a stepwise variation, with the core mass flow rate remaining constant between shocks. One such possible approximation is shown in Figure 6.12.

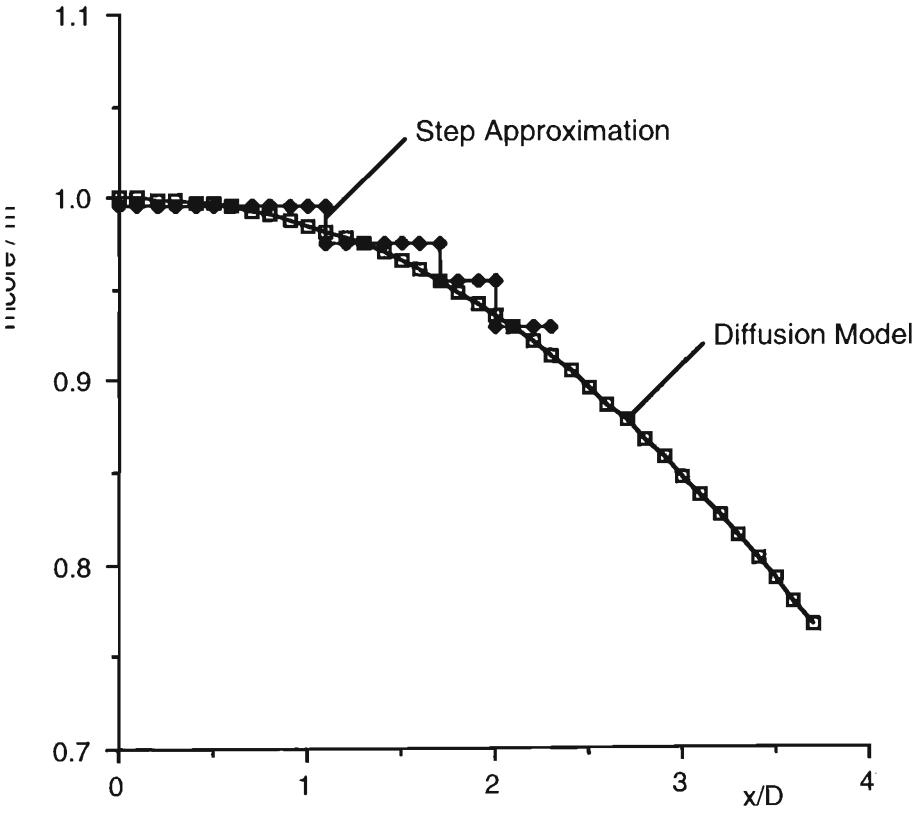

Figure 6.12 Step Approximation - Core Mass Flow

Figure 6.13 shows a comparison between the experimental and calculated variations of (A_{core}/A) in the shock region, for flow between the first three shocks. The shape of the aerodynamic nozzle after the first (and strongest) shock is clearly seen.

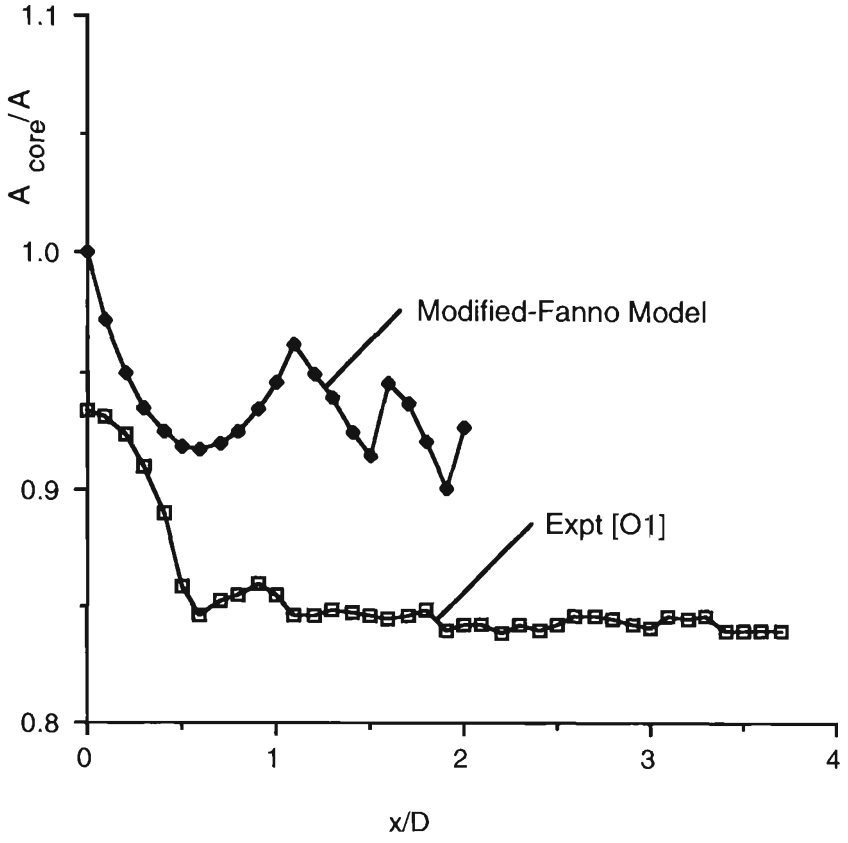

Figure 6.13 'Aerodynamic Nozzle' between Successive Shocks

Considering that this is a result of approximate cross-plotting between experimental data in [O1], the Diffusion Model [I1] and the present model, the overall agreement seems reasonable.

6.11 Summary

From the foregoing analysis, it appears that the upstream shock region of the pseudo-shock in a confined flow can be modelled as a 'modified-Fanno' flow. The model is based fundamentally on the observation that the overall flow characteristics of a Fanno flow and that in a pseudo-shock pattern are similar, and involves a re-interpretation of the well known Fanno line equation. Details of the pseudo-shock structure are obtained using a second law analysis of the flow.

Considering the complexity of the flow and the basic conceptual simplicity of the model, the comparison between experimental and calculated flow parameters seems adequate. It may be possible to use this model for non-circular cross-section duct flows by using the 'hydraulic diameter' concept. A more thorough second law analysis of the shock region is required to provide a more accurate determination of the shock

structure and the crucial new parameter, the dissipative friction factor f'_{av} for the core flow, defined by Equation (6.15).

In the next chapter, the above analytical treatment is extended to pseudo-normal shocks in dilute gas-particle suspensions.

Chapter 7

PSEUDO-SHOCK IN DILUTE SUSPENSIONS

In this chapter, the Diffusion Model and the Modified-Fanno model are extended to dilute gas-particle suspensions. Under the assumption of 'diluteness', the gas-particles suspension behaves as an ideal gas with modified properties. As seen in Chapter 3, the relevant parameters (gas constant, etc.) associated with the suspension can be expressed in terms of the particle volume fraction (vfp). Therefore the simplest extension of the models outlined in the previous chapter would be to use these modified suspension properties.

Before extending the Diffusion Model and the Modified-Fanno Model to dilute suspensions, it is instructive to consider an analytical comparison between the length of a pseudo-shock in a dilute suspension with that of a similar shock in 'clean' gas.

7.1 Pseudo-Shock Length

The connection between entropy rise 'ds' over a duct length dx, and the compatible friction factor f is:

$$ds = \frac{c_p (\gamma - 1) M^2}{2} \frac{f}{D_H} dx \qquad \text{for 'clean' gas} \tag{7.1}$$

and

$$ds_S = \frac{c_{p_s} (\gamma_S - 1) M^2}{2} \frac{f_S}{D_H} dx_S \qquad \text{for a dilute suspension} \tag{7.2}$$

Assuming a comparison between pseudo-shocks in the same duct (D_H same) and with the same initial Mach number (M same), the ratio of pseudo-shock lengths in a dilute suspension (subscript 'S') to that in a clean gas can be approximated as:

$$\frac{\Delta x_S}{\Delta x} = \frac{c_p}{c_{p_s}} \frac{(\gamma - 1)}{(\gamma_S - 1)} \frac{f}{f_S} \frac{\Delta s_S}{\Delta s} \tag{7.3}$$

Using the basic definitions of the ratio of specific heats

$$\gamma = \frac{c_p}{c_v} \; ; \; \gamma_S = \frac{c_{p_s}}{c_{v_s}} \tag{7.4}$$

and gas constant

$$R = c_p - c_v \; ; \; R_S = c_{p_s} - c_{v_s} \tag{7.5}$$

it can be shown that

$$\frac{\Delta x_S}{\Delta x} = \left(\frac{\gamma}{\gamma_S}\right)\left(\frac{R}{R_S}\right)\left(\frac{f}{f_S}\right)\left(\frac{\Delta s_S}{\Delta s}\right) \tag{7.6}$$

The ratio of pseudo-shock lengths thus depends upon the four ratios (γ/γ_S), (R/R_S), (f/f_S) and $(\Delta s_S/\Delta s)$. These ratios can be examined individually to determine their cumulative effect upon the ratio of pseudo-shock lengths $(\Delta x_S/\Delta x)$.

7.1.1 The Ratio γ/γ_S

Following the analysis of the properties of dilute suspensions(Chapter 3), it can be shown that:

$$\frac{\gamma}{\gamma_S} = \frac{1 + \gamma \; mrp \; \dfrac{cmp}{c_p}}{1 + \; mrp \; \dfrac{cmp}{c_p}} \tag{7.7}$$

It is seen that the numerator and the denominator differ only by the factor γ in the second term. Since the numerical value of γ for both clean gases and suspensions is greater than 1 (eg, 1.4 for air), the ratio γ/γ_S will have a value greater than unity. Thus, $\gamma/\gamma_S > 1$.

7.1.2 The Ratio R/R_S

Again using the formulae derived in Chapter 2, it can be shown that

$$\frac{R}{R_S} = 1 + mrp \tag{7.8}$$

For any positive value of mrp, it is obvious that $R/R_S > 1$.

7.1.3 The Ratio f/f_S

An estimate of this ratio can be obtained by using the basic definition of friction factor:

$$\text{Friction Factor } f = \frac{\text{Wall Shear Stress}}{\text{Dynamic Pressure}} = \frac{2\tau_w}{\rho V^2} = \frac{2\,\mu\,\partial u/\partial y}{\rho V^2} \tag{7.9}$$

In terms of the *kinematic viscosity,* $\nu = \mu/\rho$,

$f = 2\,\nu\,\dfrac{\partial u/\partial y}{V^2}$ for a clean gas, and

$f_S = 2\,\nu_S\,\dfrac{\partial u/\partial y}{V^2}$ for a dilute suspension.

Comparing friction factors in similar flows of clean gas and suspension (same velocity gradient $\partial u/\partial y$ and same freestream velocity V):

$$\frac{f}{f_S} = \frac{\nu}{\nu_S} \tag{7.10}$$

As seen in Chapter 3, $\nu > \nu_S$ for all values of particle loading (Figure 3.1), so that the ratio of friction factors $\dfrac{f}{f_S} = \dfrac{\nu}{\nu_S} > 1$.

7.1.4 The Ratio $\Delta s_s/\Delta s$.

For similar flows of clean gas and dilute suspension, it is inconceivable that the relative rise in entropy will be such that this ratio can have a numerical value less than unity. In fact, it is most likely that the presence of particles leads to a greater entropy rise in the suspension. In any case, the relative entropy rise is expected to be such that

$$\frac{\Delta s_S}{\Delta s} \geq 1 \tag{7.11}$$

Combining the results obtained in sections 7.1.1 to 7.1.4, we see that

$$\frac{\Delta x_S}{\Delta x} > 1 \qquad (7.12)$$

Thus it is possible to predict analytically that, in similar flows (for example, with similar velocity profile upstream of the shock), the length of the pseudo-shock in a dilute suspension will be greater then that in a clean gas. In the following sections, this gross qualitative prediction is investigated further by extending the Diffusion Model and the Modified-Fanno model to dilute gas-particle suspensions.

7.2 Extension of Diffusion Model

Following the nomenclature in [I1], the length of a pseudo-shock normalised with respect to duct diameter is given by

$$l = \frac{L}{D_H} = \frac{1}{c} \ln\left(\frac{\omega_1^2}{\omega^{*2}}\right) \qquad (7.13)$$

where 'c' is an experimentally determined constant [I1], ω_1 is the non-dimensional velocity (Crocco Number) just upstream of the pseudo-shock, and ω^* is a function of the isentropic exponent γ:

$$\omega_1 = \frac{u_1}{\sqrt{2\, c_p\, T_0}} = \frac{M_1 \sqrt{\gamma\, R\, T_1}}{\sqrt{2\, c_p\, T_0}} = M_1 \sqrt{\frac{\gamma\, R}{2\, c_p}} \frac{1}{\sqrt{1 + \frac{\gamma - 1}{2} M_1^2}} \qquad (7.14)$$

$$\omega^{*2} = \frac{\gamma - 1}{\gamma + 1} \qquad (7.15)$$

Since the parameters c_p, R and γ are all seen to be functions of particle loading (volume fraction) for dilute suspensions (Chapter 3), it can inferred that the parameters ω_1 and ω^* are also functions of particle loading. Consequently, from Equation 7.13, the length of the pseudo-shock is also a function of particle loading in the suspension and the upstream Mach number. As a first approximation, and in the absence of any experimental evidence, it must be assumed that the constant 'c' is the same as recommended in [I1].

Figure (7.1) depicts the variation of pseudo-normal shock length with particle volume fraction in the suspension, with the initial Mach number as parameter. It is seen that for a particular initial Mach number, the length of the pseudo-shock increases rapidly at first, and then seems to level off. The length is always greater than that in case of a pseudo-normal shock in clean gas at the same initial Mach number (given by the intercepts of

each curve on the vertical axis). This corroborates the comparative analysis in the previous section, based on the expression for entropy rise.

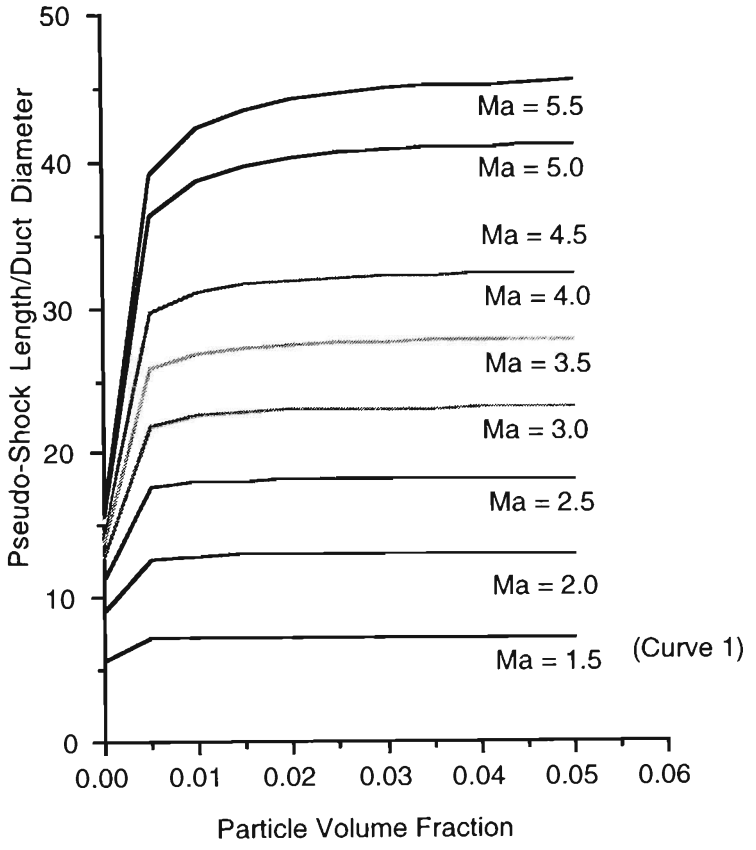

Figure 7.1 Particle Volume Fraction vs Pseudo-Shock Length

A typical curve (Curve 1) from Figure 7.1 is singled out for closer examination in Figure 7.2.

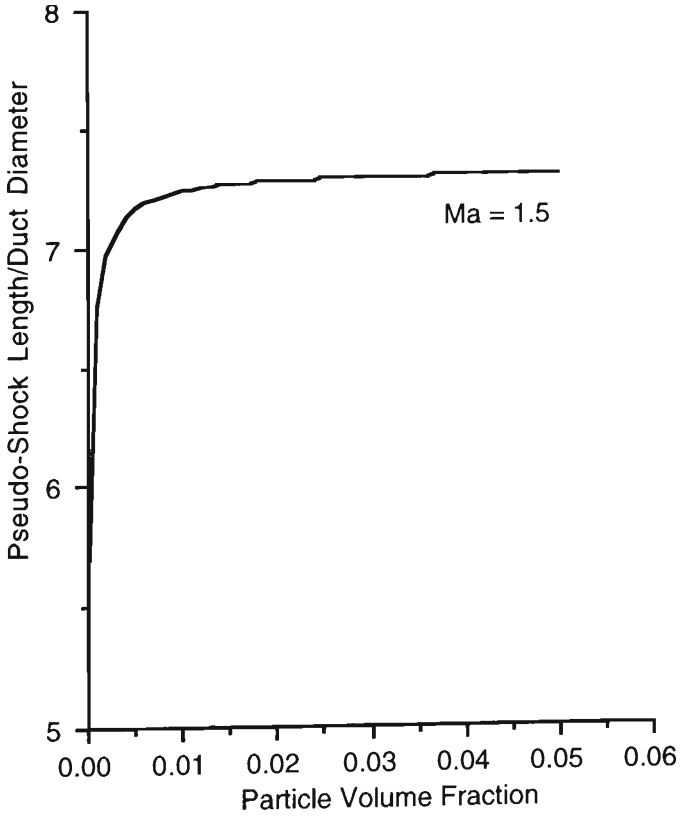

Figure 7.2 Detail of Figure 7.1

It is seen from Figure 7.2 that starting at the 'clean air' value of about 5.5 duct diameters (as can be verified from [I1]), the pseudo-shock length increases with increased particle loading and seems to level off at about 7.25 duct diameters for high loading values.

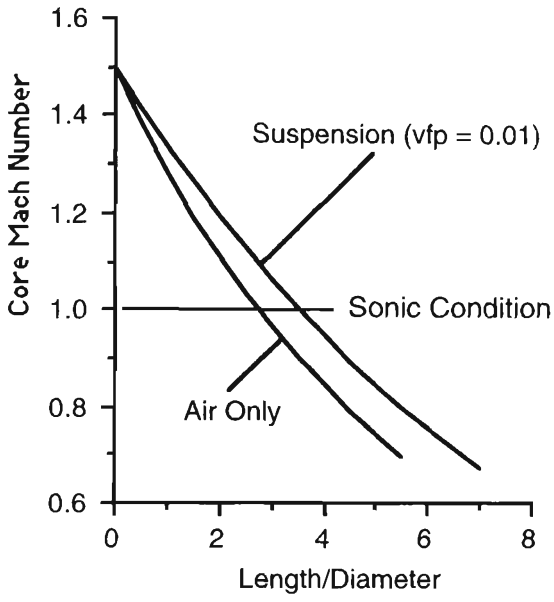

Figure 7.3 Core Mach Number (Extended Diffusion Model)

Figure 7.3 shows a comparison between core Mach number variation in clean air according to the Diffusion Model, and Mach number variation in a dilute suspension (particle volume fraction = 0.01), for the same initial Mach number. It is seen that whereas clean air requires an overall length of about 5.5 diameters, the suspension requires about 7.2 diameters. Sonic condition (M = 1) is reached in clean air in about 3 diameters, and about 3.5 diameters in the suspension. It can be expected that this difference will be more pronounced for suspensions with higher particle loadings.

The Diffusion Model, being an improved version of the 'shockless' model, does not predict fluctuations in core flow parameters, and further details of variations in flow parameters such as core Mach number, core pressure, etc. in the upstream shock region of a pseudo-shock can be provided by extending the Modified-Fanno model to dilute gas-particle suspensions.

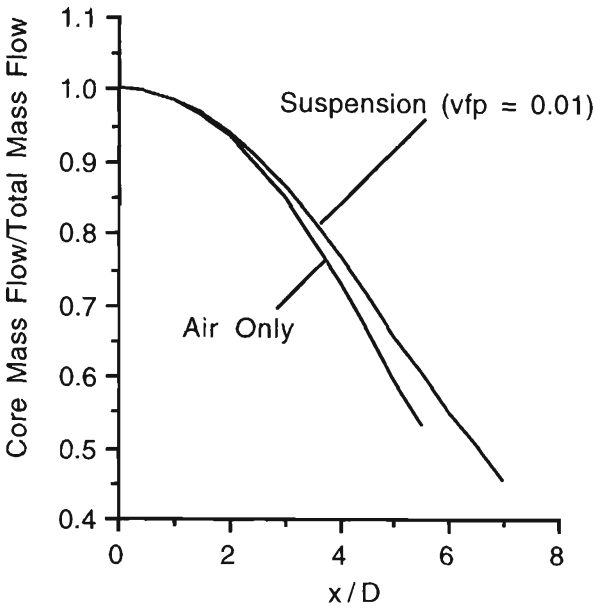

Figure 7.4 Core Mass Flow (Extended Diffusion Model)

Figure 7.4 depicts a comparison between core mass flow rates for clean air and dilute suspension. It is seen that at the same distance downstream of the initial shock, the core mass flow in the suspension is greater than that in clean air. This is to be expected, since the suspension is heavier due to the presence of particles.

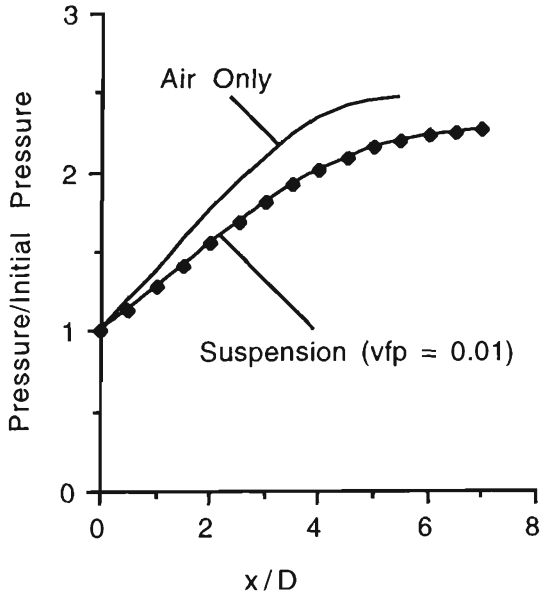

Figure 7.5 Core Pressure (Extended Diffusion Model)

Figure 7.5 compares the pressure rise in the core in a pseudo-shock in clean air with that in a dilute suspension for the same initial Mach number. It shows that the suspension undergoes a smaller pressure rise at the same distance from the initial shock, as compared

to pressure rise in clean air. This is perhaps due to the fact that the same value of the constant 'c' in Equation 7.13 is assumed for the suspension. This constant defines the rate of change of pressure with distance, according to the Diffusion Model.

7.3 Extension of 'Modified-Fanno' Model

As seen in Chapter 6, the 'Modified-Fanno' model for the pseudo-shock is based on a Second Law Analysis of the shock region. It also makes use of tested features of the Diffusion Model. It was noted in Chapter 6 (Section 6.2.5) that the important parameters affecting flow in the pseudo-shock were the gas properties (c_p and γ). This suggests a simple way of extending the 'modified-Fanno' model to a dilute suspensions which behaves like an ideal gas with modified properties. These properties, such as the two specific heats and their ratio, etc., were expressed in terms of particle volume fraction in Chapter 3. These definitions are used to extend the modified-Fanno model outlined in Chapter 6 to dilute suspensions. This extension scheme is outlined in Figure 7.6. The corresponding FORTRAN programme appears in Appendix C5.

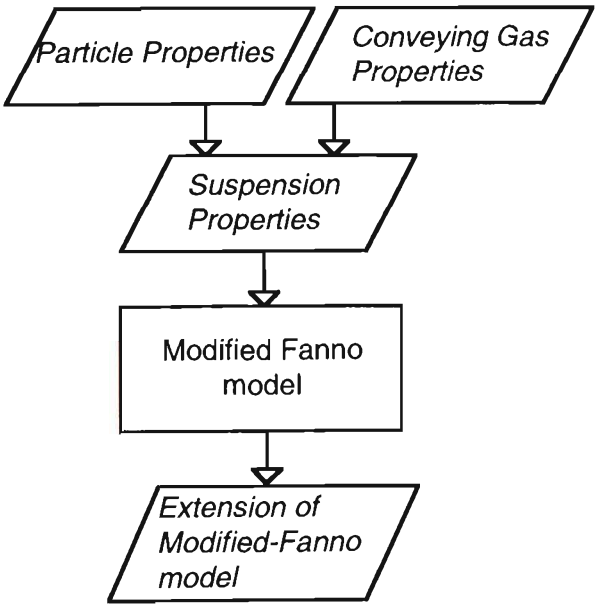

Figure 7.6 Extension of Modified-Fanno Model

Figures 7.7 and 7.8 show a comparison between pseudo-shocks in clean gas (air) and suspension. As before, the suspension is assumed to be made up of heavy particles which occupy 1% of the total suspension volume. Figure 7.7 shows a comparison between Mach number variation in the core and Figure 7.8 compares the normalised static pressures in the two flows. It is again obvious that the length of the pseudo-shock in the suspension is more than that in clean air. At present, however, no comparison with experimental data is possible.

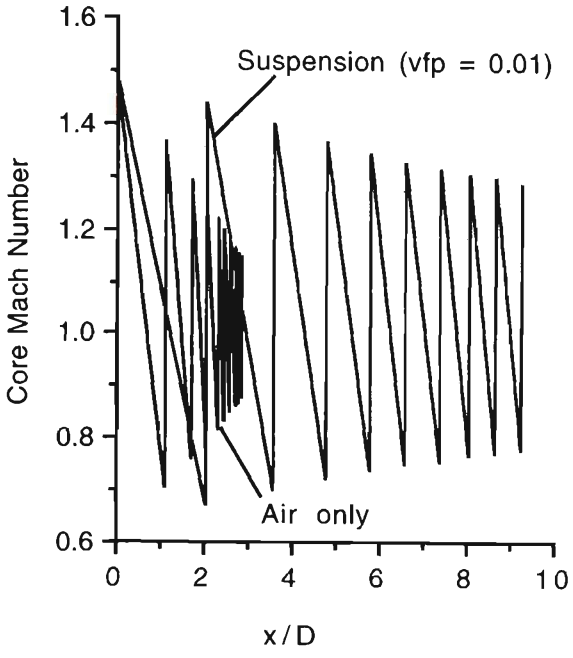

Figure 7.7 Core Mach number in Air and Suspension

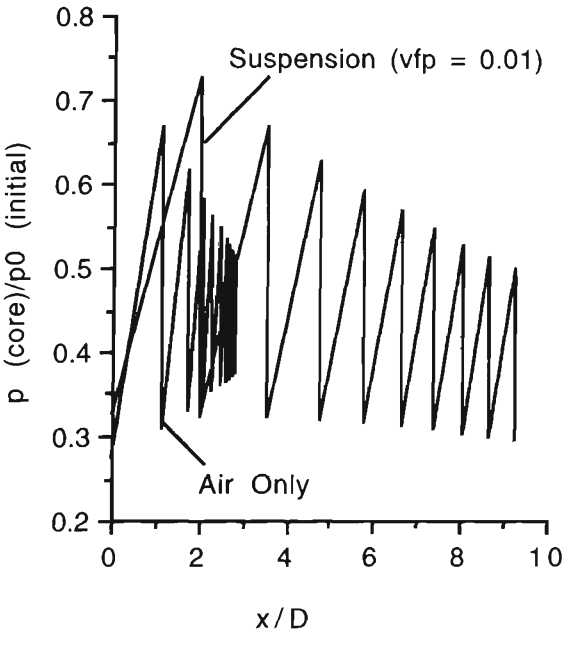

Figure 7.8 Core Static Pressure in Air and Suspension

It was emphasised in Chapter 6 that the crucial parameter determining the structure of the pseudo-shock is the newly defined 'core friction factor'. A complete extension of the modified-Fanno model to dilute suspensions should therefore include an extension of the core friction factor concept to dilute suspensions. A possible method for such an extension is outlined below.

7.3.1 Core Friction Factor in Suspensions

The 'integrated' friction factor f_{int} in Fanno flow [W7] is given by

$$f_{int} \frac{L^*}{D} = \frac{1 - Ma^2}{\gamma\, Ma^2} + \frac{\gamma + 1}{2\,\gamma} \ln \frac{(\gamma + 1)\, Ma^2}{2 + (\gamma - 1)\, Ma^2} \qquad (7.16)$$

where Ma is the initial (supersonic) Mach number, L* the length required for deceleration to the sonic condition and D the duct diameter. γ is the ratio of specific heats of the gas. Using the analysis in Chapter 3 and the result in Figure 7.3 that a suspension with vfp = 0.01 requires a length of about 3.5 - 4 duct diameters to attain sonic condition starting at an initial Mach number of 1.5, Equation 7.16 gives

$$f_{int} = 0.071 \qquad (7.17)$$

for the suspension. This value can be compared with f_{int} = 0.04 for a similar pseudo-shock in clean air, as found in Chapter 6. If an experimental value of wall friction factor for the suspension is available, an analysis similar to that reported in Chapter 6 and leading to Equation (6.18) can be carried out to establish the core friction factor for the suspension.

Verification of this theory has to await further experiments with pseudo-shocks in suspensions.

Chapter 8

TWO-DIMENSIONAL SIMULATION

In the previous chapters, a one-dimensional analysis of the flow in different regions of an SAI was carried out. A main aim was to obtain quantitative estimates of the flow parameters involved. At the same time, the analysis provided a method of 'sizing' the device, that is, determining its geometrical parameters. The next logical step is to conduct a more detailed investigation of the flow parameters by carrying out a multi-dimensional analysis. Initially, this can be done without having to actually fabricate the experimental facility, by simulating the flow on a computer.

8.1 Analytical Technique

The flow simulation system used in the present project is PHOENICS. A typical PHOENICS flow simulation consists of the following steps:

1 Construction of Computational Grid
2 Specification of Fluid Characteristics
3 Specification of Flow Characteristics
4 Specification of Boundary Conditions (and Special Sources)
5 Specification of Solution Criteria
6 Specification of Output Requirements
7 Flow Simulation
8 Interpretation of Results.

All the specifications are contained in an input file called the 'Q1' file, written in the PHOENICS Input Language (PIL). The Q1 file is interpreted by the 'Satellite' module in PHOENICS, and the input data is stored in a file called 'EARDAT' (EARth DATa). The main flow solver in PHOENICS, called EARTH, receives input information from EARDAT, and carries out the flow simulation analysis. Results of the analysis are

produced in the form of two files, called the 'PHI' file and the 'RESULT' file respectively. The PHI file is read by the post-processor PHOTON, and its results rendered in visual form, mainly in terms of velocity vectors and contours of scalar variables. The RESULT file contains information about the simulation in terms of tabular numerical output. A typical computer operation is shown in Figure 8.1, and a typical PHOENICS flow simulation in simplified form in Figure 8.2.

Figure 8.1 Typical Computer Operation

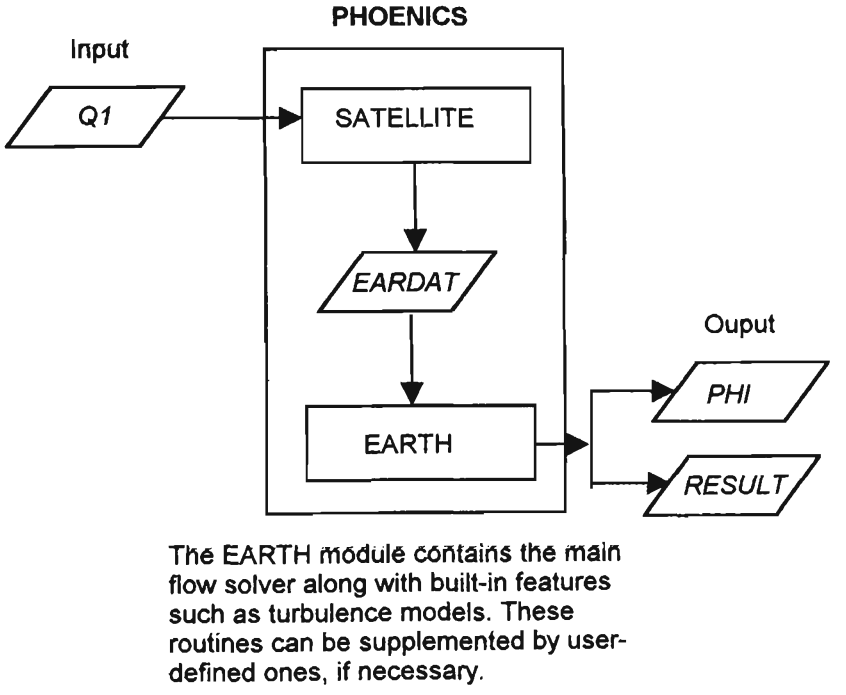

Figure 8.2 Typical PHOENICS Simulation

The above steps as applied to flow in the SAI are described in detail in the following sections. Since establishing a supersonic primary gas (air) flow and its subsequent entry into the high-pressure destination are central to the operation of the SAI, an 'air-only' simulation is conducted. One of the main objectives of the simulation is to determine the probable structure of the shock in the compression region, ie., whether a pseudo-shock pattern may be expected in the flow being investigated.

8.2 SAI Flow Simulation

8.2.1 Computational Grid

Since the most important part of the flow in the SAI is that in the de Laval nozzle followed by the main test section, these regions are chosen to form the 'computational domain', that is, the region of the flow chosen for detailed computational analysis.

The physical boundaries of this region are:

1 Inlet from Stagnation Chamber
2 Outlet to High-Pressure Destination
3 Upper Wall of the Nozzle
4 Lower Wall of the Nozzle
5 Side Walls of the Nozzle

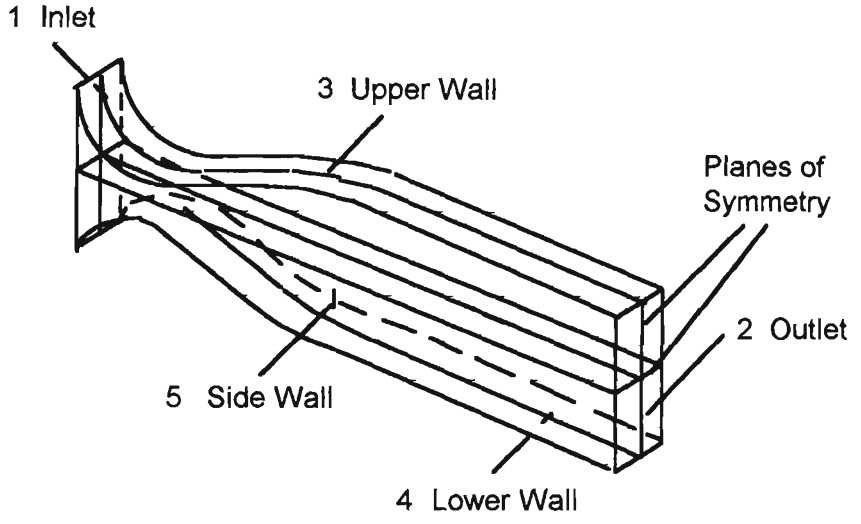

Figure 8.3 Boundaries of Flow Domain

Figure 8.3 shows the physical boundaries of the flow domain. It also shows the vertical and horizontal planes of symmetry in the flow domain. In order to minimise memory requirements in the PHOENICS simulation, a plane of symmetry can be assumed as one of the boundaries of the computational domain. With this provision, the memory requirements are reduced by 50% for each plane of symmetry because now a computational domain need only be constructed for part (say the top) of the actual physical region of the flow. Figure 8.4 shows the computational domain with the horizontal plane of symmetry as the bottom boundary. The flow is along the positive x axis.

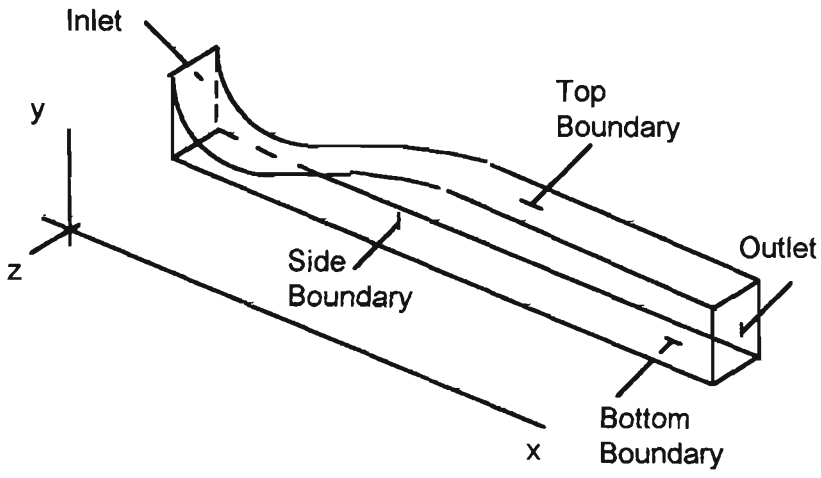

Figure 8.4 Boundaries of Computational Domain

The computational domain thus has six faces, and as such can be regarded as a deformed (called 'body-fitted') unit cube. This 'body-fitted-coordinate' or 'BFC' domain must now be divided into smaller parts, called 'cells', each of which is also a figure with six faces. Each cell must be as small as possible, to simulate a 'differential' element of dimensions dx, dy (and dz, for a three-dimensional case). However, reduction in cell size entails a larger number of cells required to cover the entire computational domain, and hence larger memory requirements and longer computation times. A compromise is needed between these two requirements. A further compromise can be achieved by having the cells distributed non-uniformly. Cells can be crowded together in regions where large changes in flow variables are expected, and thus a more detailed analysis is desirable. In the present simulation, there are two such regions: (1) adjacent to the solid wall, and (2) mixing between interacting shear layers.

A computational domain constructed according to the above considerations is shown in Figure 8.5. There are 120 cells in the x-direction, 36 in the y-direction, and only one in the z-direction. The z-direction specification corresponds to a two-dimensional flow simulation, in the x-y plane. It should be mentioned that while the nozzle region in Figure 8.5 conforms exactly to the duct shape which results from the one-dimensional analysis in Chapter 4, the regions downstream of the injection tube do not correspond exactly to the experimental facility (Chapter 10). In particular, the flared diffuser does not exist in the final experimental facility. This is because the objective of this preliminary simulation is to initiate an investigation of the effect of boundary layers on shocks. This preliminary study was conducted before the final design and fabrication of the experimental facility. If this study provides any evidence of a multiple-shock pattern, a more detailed study can be conducted at a later stage (See section 8.4 and Chapter 9).

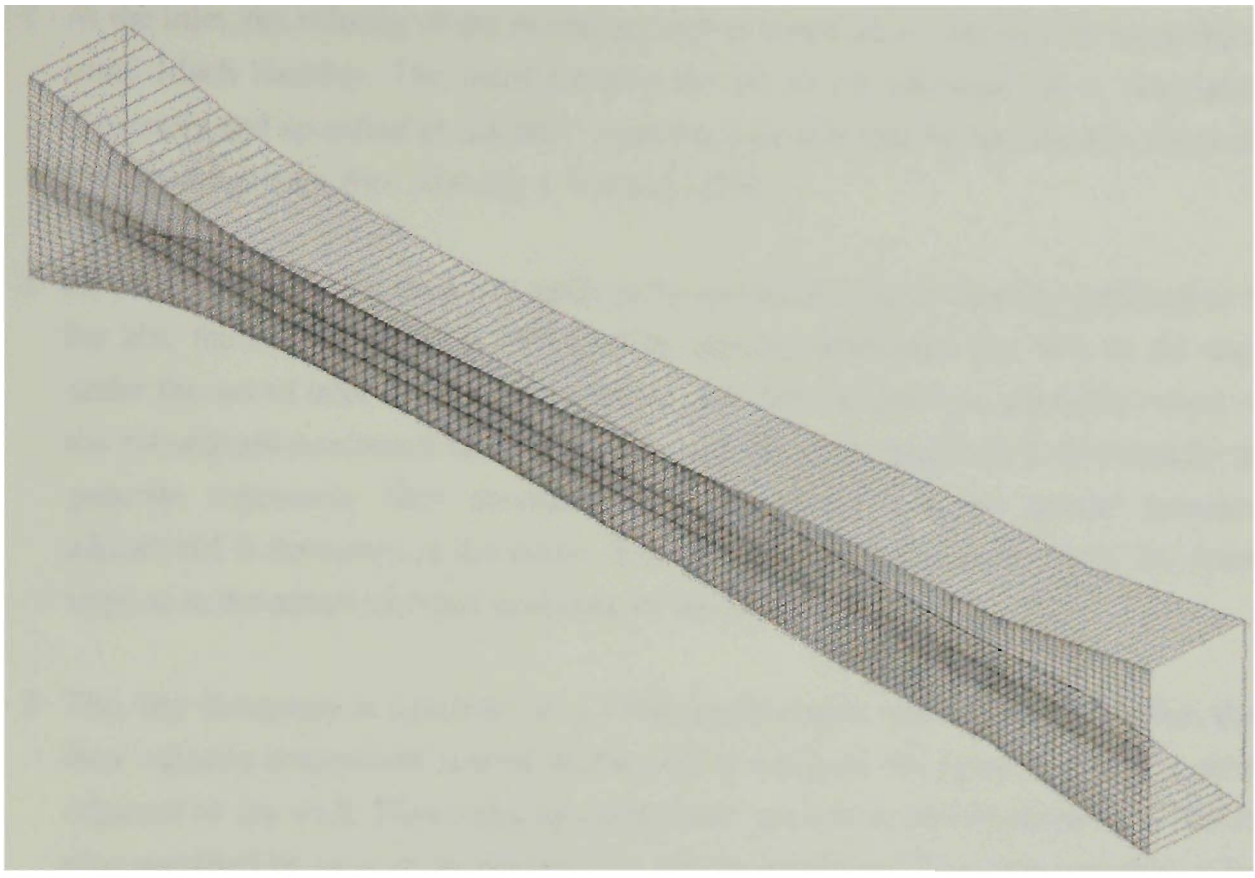

Figure 8.5 Computational Grid - Full - 2D

8.2.2 Fluid Characteristics

For this preliminary simulation, it is assumed that only air flows in the duct. The fluid is thus assumed to be an ideal gas, satisfying the equation of state $p = \rho RT$. The corresponding PHOENICS specification appears in the Q1 file (Appendix C7).

8.2.3 Flow Characteristics

The flow is assumed to be turbulent, the effective viscosity being calculated according to the k-ε model. This built-in feature of PHOENICS is invoked in the Q1 file. The dynamic viscosity is calculated using the Sutherland viscosity law (Eq. 3.16).

8.2.4 Boundary Conditions

Boundary conditions for the chosen computational domain must be specified at the Inlet, Outlet, Upper Wall, Side Boundaries, and the boundary made up by the plane of symmetry.

1 At the Inlet, the velocity of the incoming high-pressure air is specified by assuming a small Mach Number. The corresponding density of the incoming air is calculated separately and specified at the inlet. Inlet pressure can thus be specified in terms of the incoming mass flux (Density x Velocity) [P6].

2 At the Outlet, only the pressure needs to be specified. This is initially specified as 1 bar abs, the default option in PHOENICS. Having established the flow in the duct under this set of inlet and outlet conditions, the outlet pressure is gradually raised in the subsequent continued runs. It is seen that the duct shape itself is adequate to generate supersonic flow downstream of the throat, and no special pressure adjustment is necessary at the outlet. The simulation thus follows exactly the same steps as in the actual physical operation of the SAI.

3 The Top Boundary is specified as a solid impermeable wall. This implies that the flow velocity component normal to the wall is assigned the value zero in the cells adjacent to the wall. Flow velocity component parallel to the (stationary) wall can also specified be as zero, to simulate the no-slip condition. This is accomplished by the built-in 'wall' condition in PHOENICS (but see Section 8.3.2).

4 No particular boundary conditions need to be specified for the sides and the plane of symmetry. PHOENICS interprets such boundaries as 'walls with slip'. Velocity components normal to these walls are zero, simulating an impervious wall. But velocity components parallel to these walls are not forced to be zero. This default interpretation works well for the side boundaries in this two-dimensional simulation, and also for the boundary made up by the plane-of-symmetry. In the two-dimensional simulation, boundary layer growth occurs only on the upper wall (and the symmetrical lower wall) of the computational domain.

8.2.5 Solution Criteria

PHOENICS solves the equations of conservation of mass, momentum and energy in discretised form, by an iterative technique. It is necessary to avoid large changes in the values of flow parameters from iteration to iteration, which may lead to a diverged and hence unrealistic solution. This is accomplished by specifying a 'false-time-step' and 'linear relaxation' for the pressure term. The 'false-time-step' can be physically interpreted as the time required for the flow to cross a computational cell. This provision slows the changes between iterations to avoid divergence. The corresponding specifications appear in Group 17 of the Q1 file in Appendix C7.

8.2.6 Output Specifications

The results of the simulation in tabular form appear in the RESULT file created at the end of every simulation. The type of record during the run (spot values, field values, etc) are specified in the Q1 file. The most useful output is, however, obtained from the 'PHI' file, which can be read by the graphics post-processor package PHOTON.

8.2.7 Flow Simulation

PHOENICS simulates the flow thus specified in terms of geometrical parameters (for the computational grid) and boundary conditions (for the flow) by using a "control volume approach". The differential form of the laws of conservation of mass, momentum and energy are discretised and integrated over the volume of each cell in the computational domain. These discretised equations are solved iteratively, starting from an initial field of values which can be specified. If a certain initial field is not specified, built-in values are assumed. The conservation laws are thus satisfied for each individual cell, and therefore for the entire computational domain, since the cells are contiguous and are 'body-fitted' to conform to the shape of the computational domain.

8.3 Results of Flow Simulation

8.3.1 Full Flow Field

The computational grid for the full flow field is shown in Figure 8.5. The nozzle shape corresponds to that resulting from specifying a 'Cosine-type' pressure variation (Figure 4.2). This is done because the shape results in near-orthogonal cells in the computational domain, a feature which is conducive to good calculations. It must be emphasised that this does not affect the realism of the resulting nozzle flow is in any way.

Figure 8.6 shows the velocity vectors in the complete flow field corresponding to the computational grid in Figure 8.5, and shows clear evidence of a complex pseudo-shock-like flow pattern. In this two-dimensional simulation, the velocity vector associated with each cell is plotted at the mid-point of the cell.

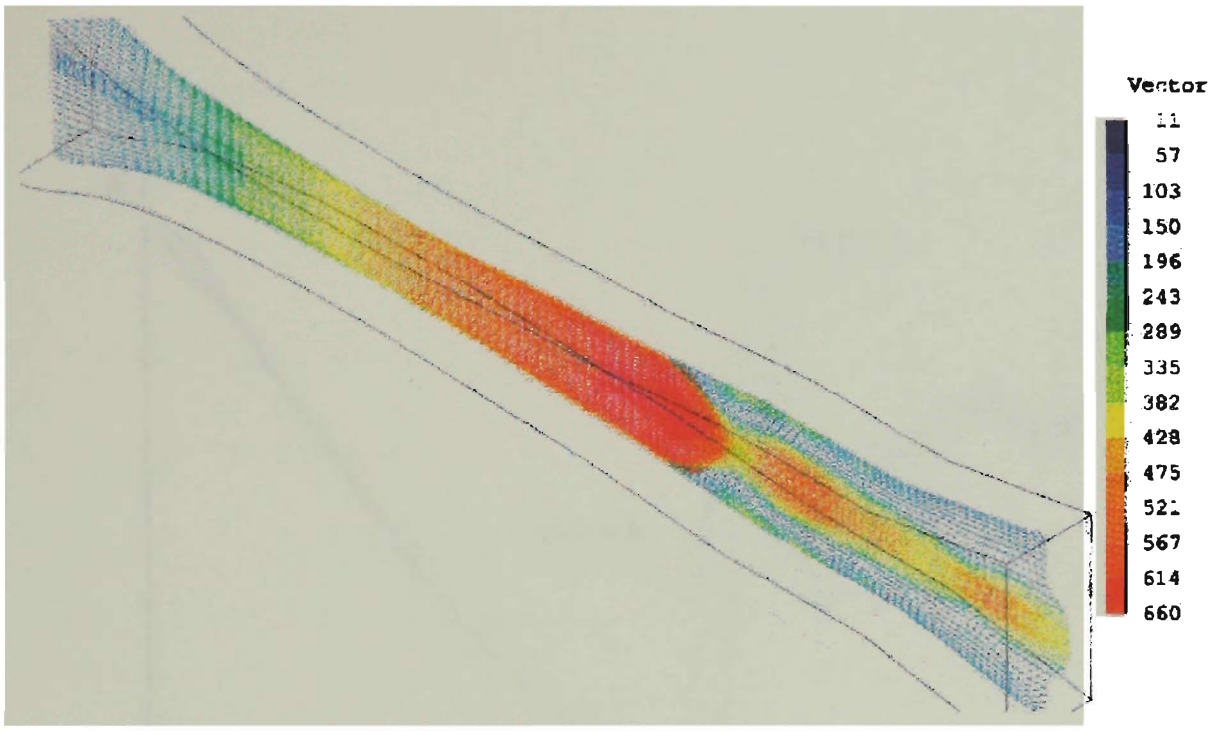

Figure 8.6 Velocity Vectors - Full - 2D

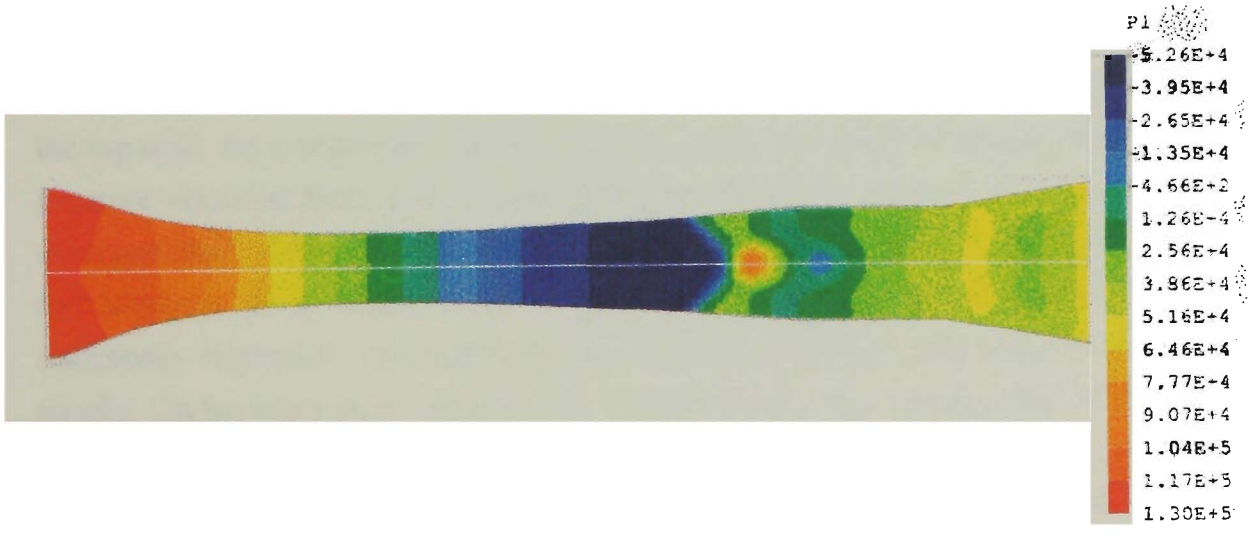

Figure 8.7 Static Pressure Contours - Full - 2D

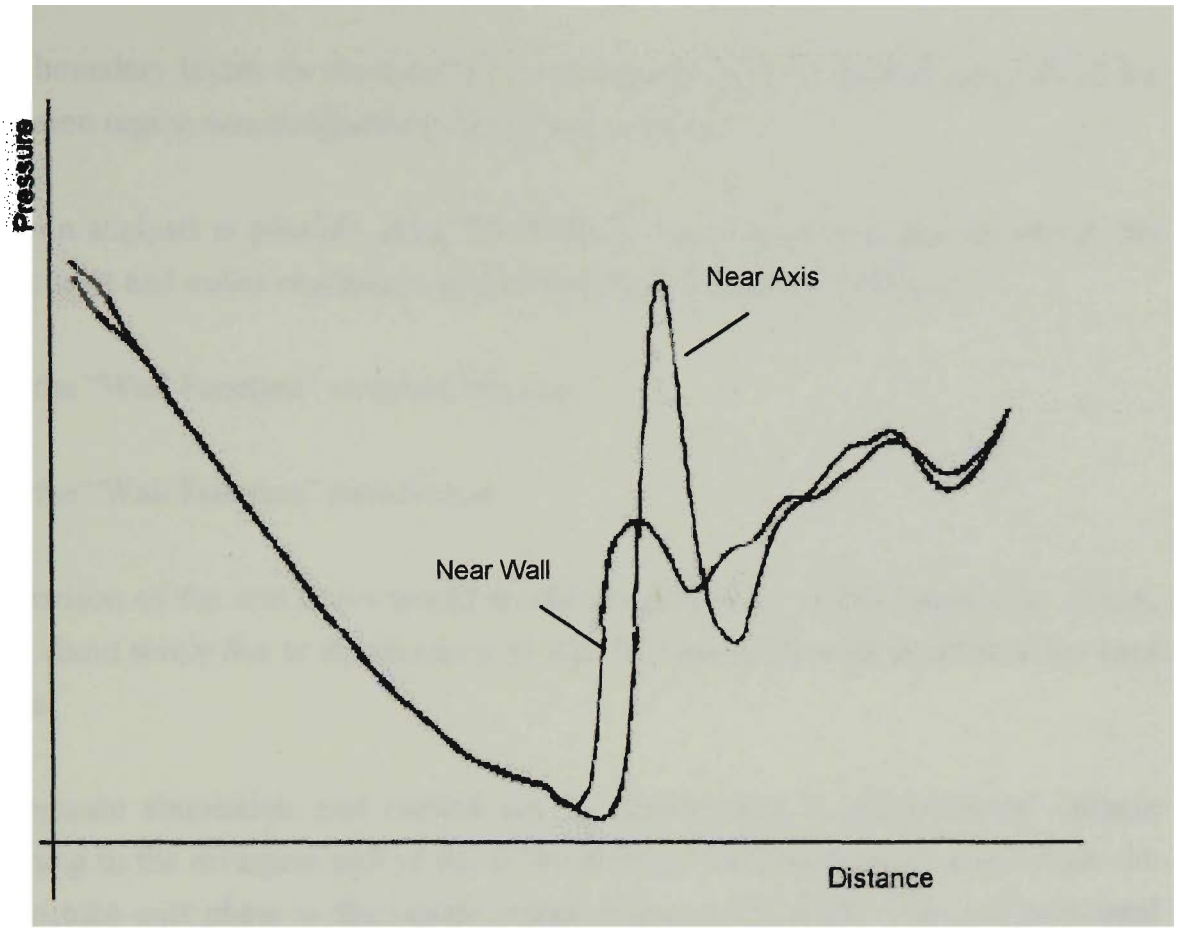

Figure 8.8 Wall and Axis Pressure Variation

Figure 8.8 shows a comparison between the static pressures on the duct axis and on the top wall. As was pointed out in Chapter 6, there is a strong evidence of cross-stream pressure variation from axis to wall. After the initial fall corresponding to flow in the divergent part of the de Laval nozzle, pressure on the axis shows a steep rise indicating the presence of a shock. This is followed by fluctuations of smaller amplitude indicating repeatedly reaccelerating and decelerating flow, suggesting further weaker shocks. On the other hand, the pressure variation in the slab of cells adjacent to the wall superimposes exactly upon the former curve in the initial divergent part of the nozzle. Downstream of the shock, however, the two curves are markedly different. The latter curve also shows fluctuations in pressure, although these are smaller in amplitude. This can be interpreted as being due to viscous damping effects which are predominant

8.3.2 Air-Only Compression Region

Figures 8.6, 8.7 and 8.8 provide the first visual evidence of a complex flow very similar to the pseudo-shock reported in the literature [eg. O1]. It is theorised that this flow results entirely from the interaction between the initial shock and the slower-

moving boundary layers on the solid walls of the duct [S1]. A detailed analysis of the compression region was conducted to test this hypothesis.

Such an analysis is possible using PHOENICS, since the simulation can be run for the same inlet and outlet conditions, under two sets of boundary conditions:

1 with the "Wall Function" switched off, and

2 with the "Wall Function" switched on.

A comparison of the two flows would reveal the difference in flow structures, if any, brought about solely due to the presence of wall friction, if all other conditions are kept the same.

A separate simulation was carried out by constructing a computational domain conforming to the divergent part of the of the nozzle, covering the duct length from the injection tube exit plane to the nozzle outlet. (Figures 8.9, 8.10). This computational domain is made up of 350 cells evenly distributed in the x-direction; 40 non-uniformly distributed cells in the y-direction with smaller cells near the wall, and only one cell in the z-direction (Figure 8.10).

It must be emphasised that a still finer grid will be necessary for more detailed study, although the number of x-cells in this study is more than twice that in the earlier case, and cover a much smaller length of computational domain. The cells are thus much finer, and the objective is to 'capture' shocks as accurately as possible without taxing memory requirements excessively.

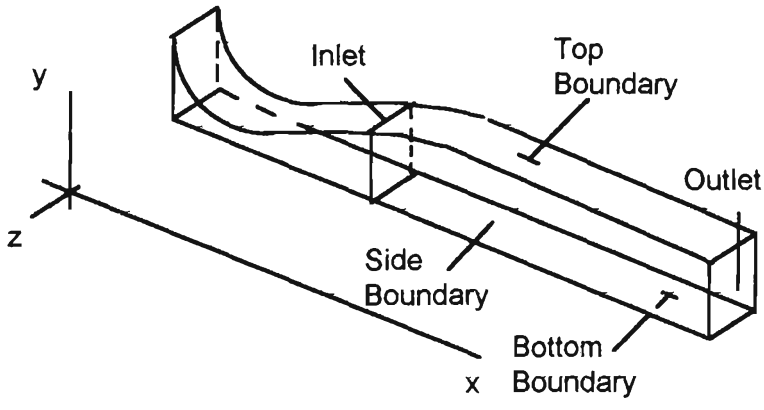

Figure 8.9 Computational Domain for Detailed Study

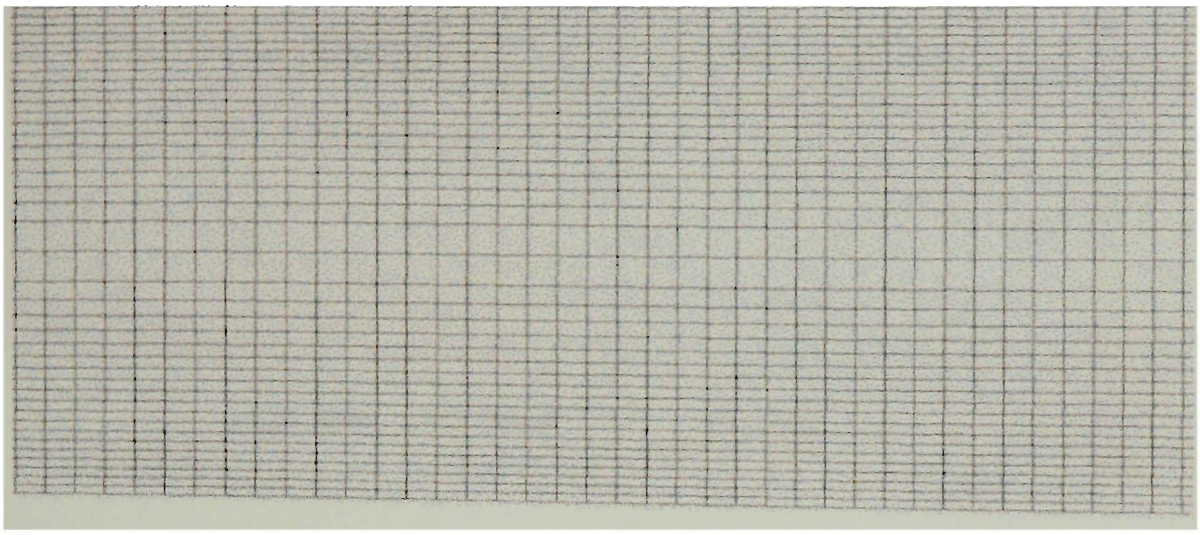

Figure 8.10 Computational Grid for Detailed Study

A comparison of the results of the above simulations reveals the crucial role played by the boundary layers in the formation of the pseudo-shock pattern. Figure 8.11 shows the velocity vectors in the nozzle showing that there is an abrupt change in the velocity across the shock, as the flow suddenly decelerates from a supersonic velocity to a subsonic. (A finer grid will reveal the 'step-change' better.) Figure 8.12 shows a magnified view of the velocity vectors in Figure 8.11, in the vicinity if the shock. It is seen that the velocity drops from supersonic to subsonic in the space of about three cells. This abrupt change will be even more apparent with a finer computational grid. Figure 8.13 shows the corresponding near-step-change in static pressure across the shock. The shock is perpendicular to the flow direction.

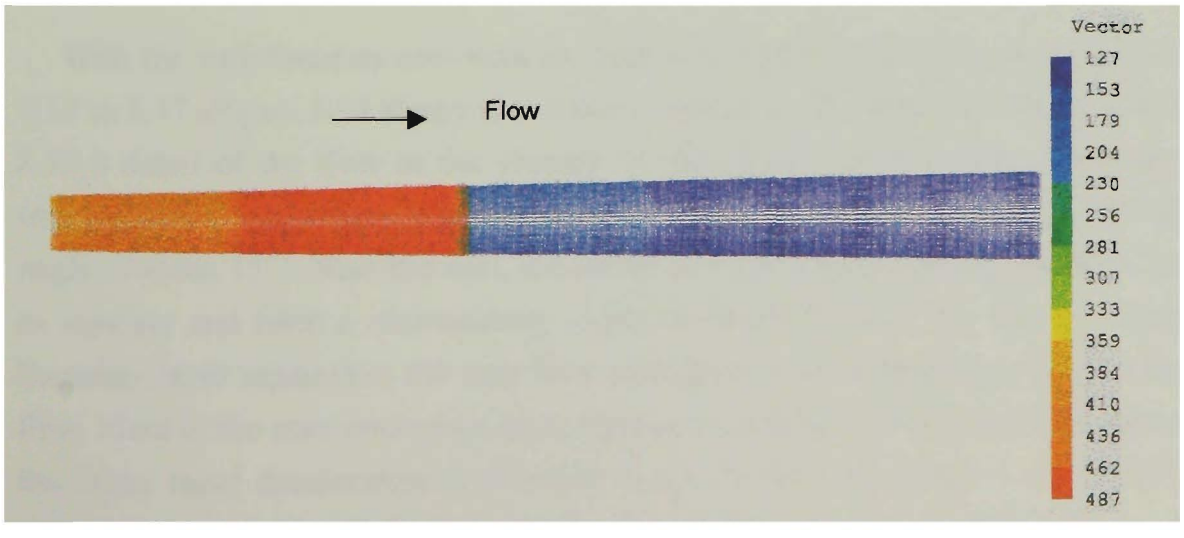

Figure 8.11 Velocity Vectors -Without Wall Condition -

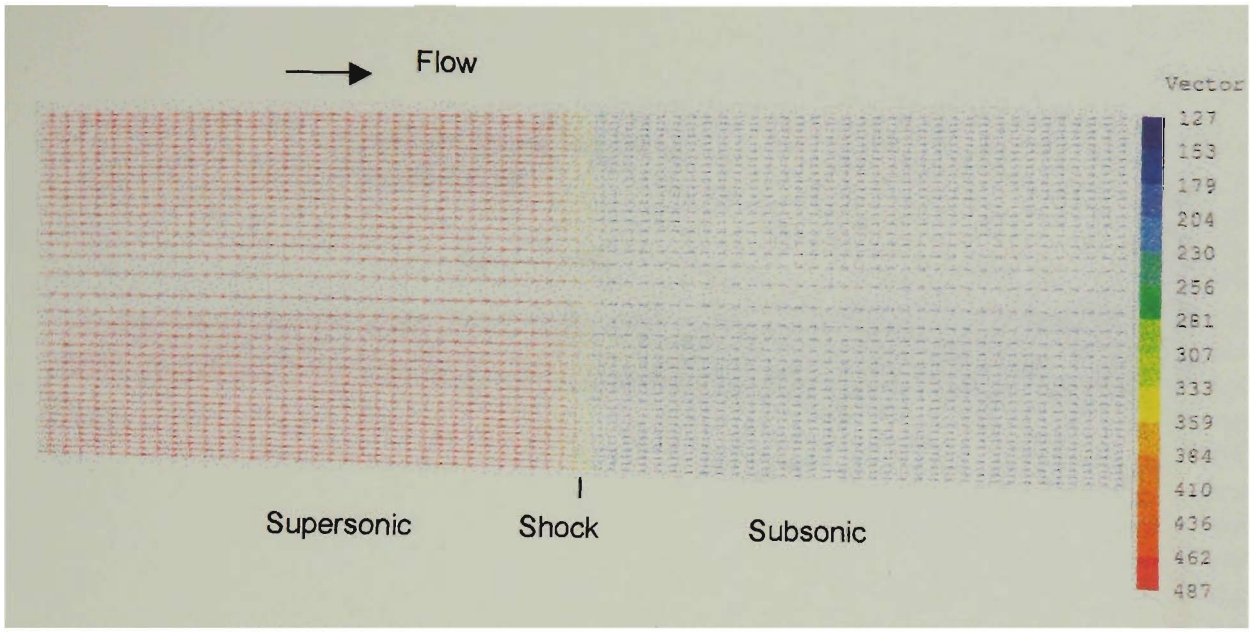

Figure 8.12 Detail of Figure 8.11

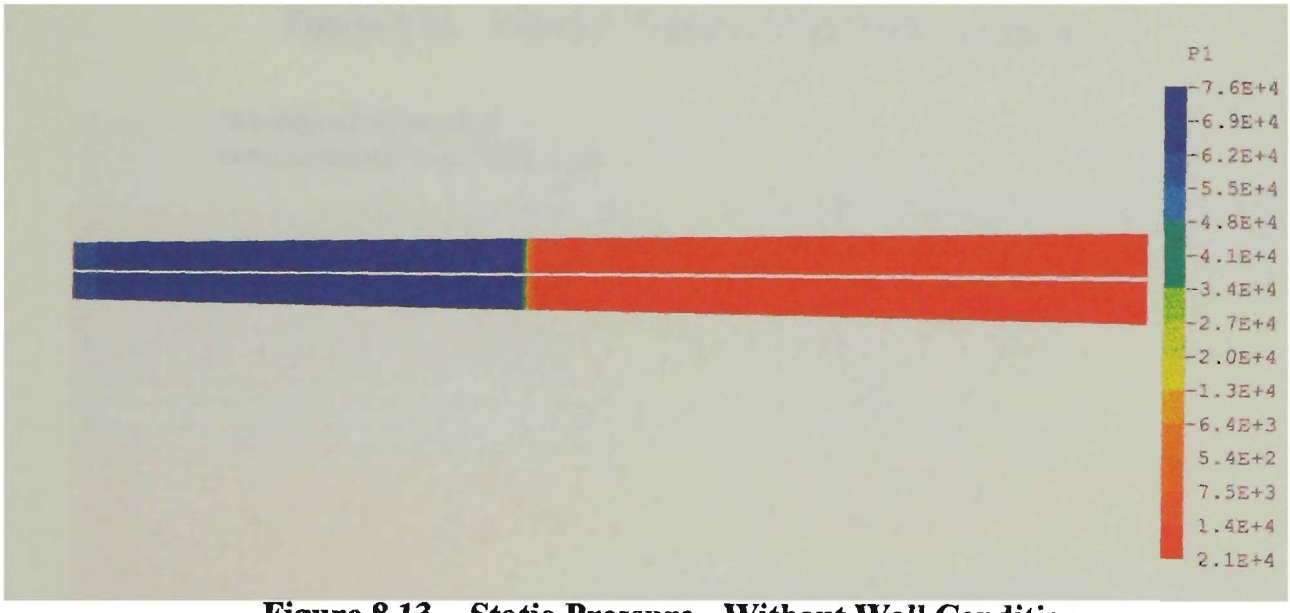

Figure 8.13 Static Pressure - Without Wall Condition-

With the wall function activated, the flow is completely different, as seen in Figures 8.14 to 8.17. Figure 8.14 shows the velocity vectors in the entire flow field, and Figure 8.15 a detail of the flow in the vicinity of the shock. There is clear evidence of an oblique shock near the wall as the flow undergoes a sudden inward turn through an angle of about 15□. Near the wall, the abrupt adverse pressure gradient causes the flow to separate and form a recirculating region immediately after the shock. Because of boundary-layer separation, the core flow undergoes a converging-diverging nozzle-like flow. Fluid in the core undergoes reacceleration, reaching supersonic speeds again after the initial rapid deceleration to subsonic speed through the shock. It is interesting to compare Figure 8.15 with Figure 6.5, which is the basis for the 'modified-Fanno' model for the pseudo-shock. Figures 8.16 and 8.17 show the corresponding pressure pattern for the entire flow field, and in the vicinity of the shock, respectively.

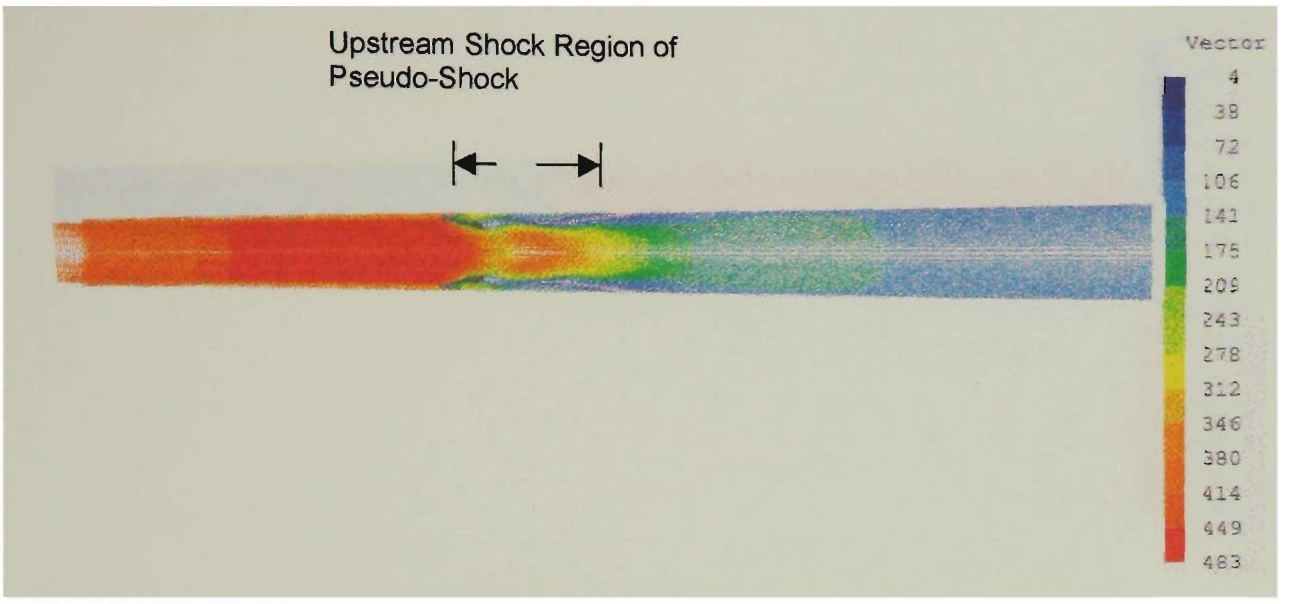

Figure 8.14 Velocity Vectors - With Wall Condition-

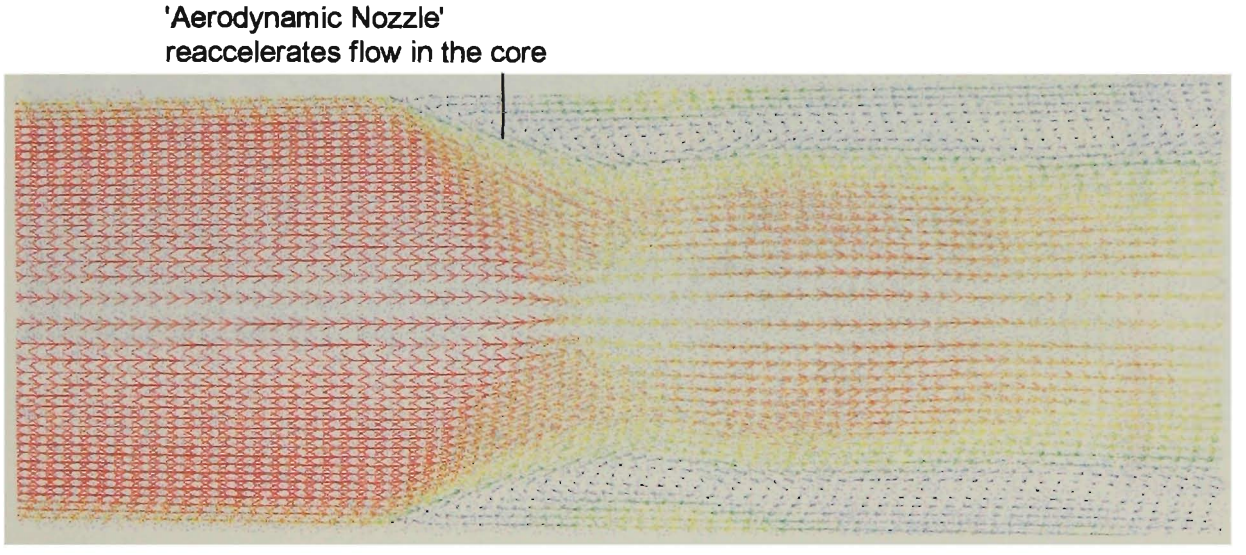

Figure 8.15 Detail of Figure 8.14

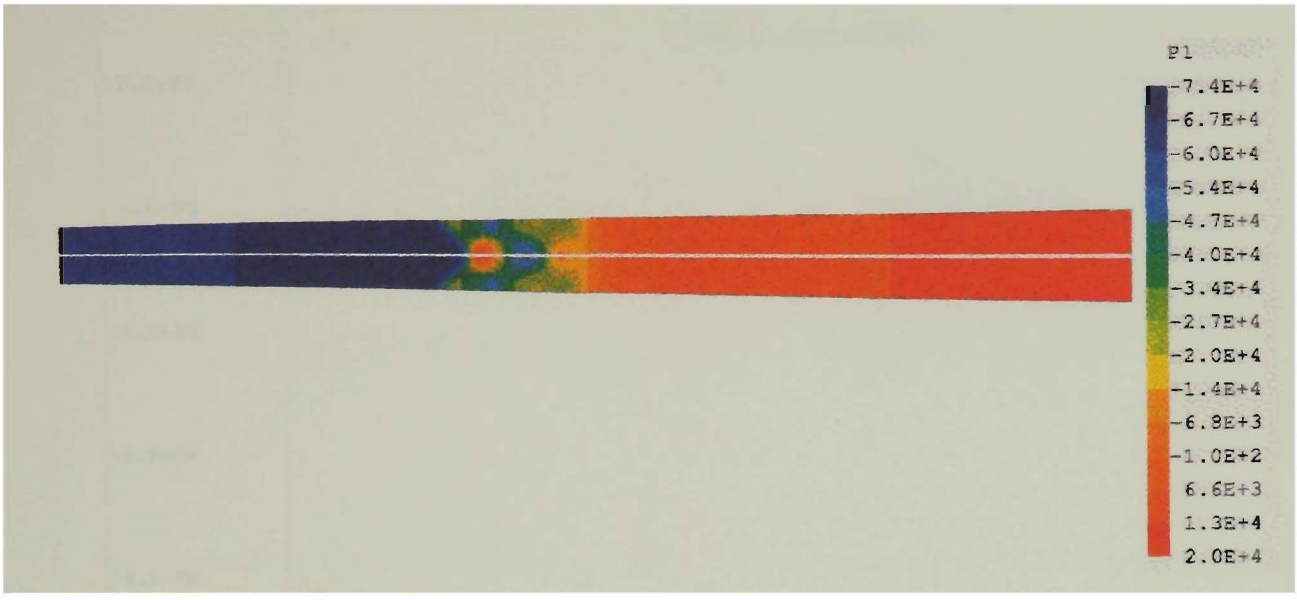

Figure 8.16 Static Pressure Contours - With Wall Condition -

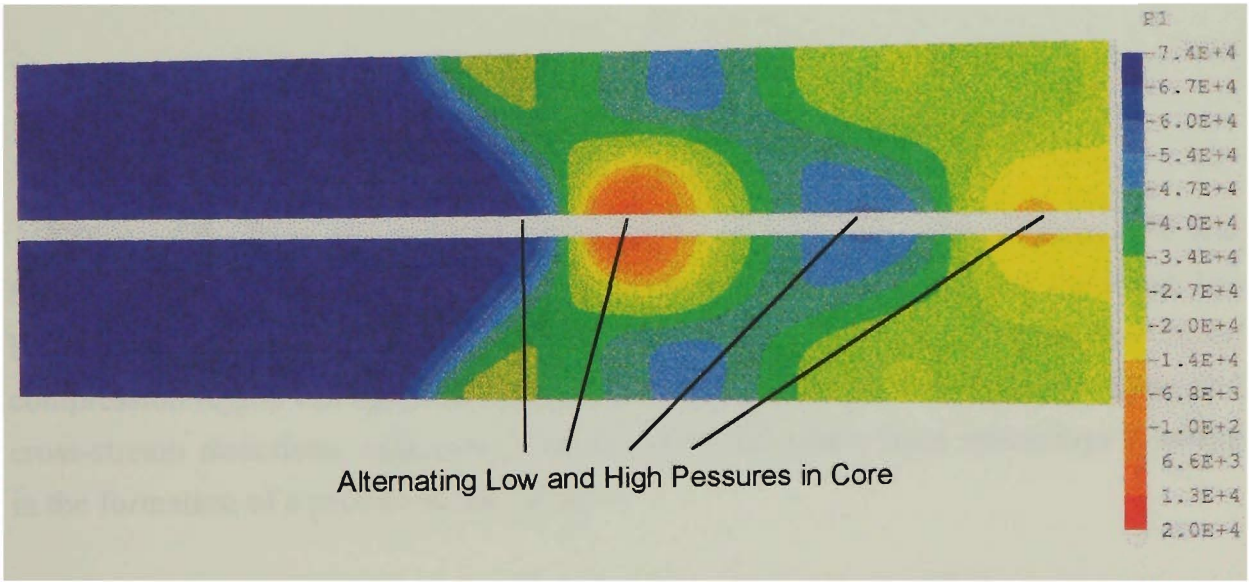

Figure 8.17 Detail of Figure 8.16

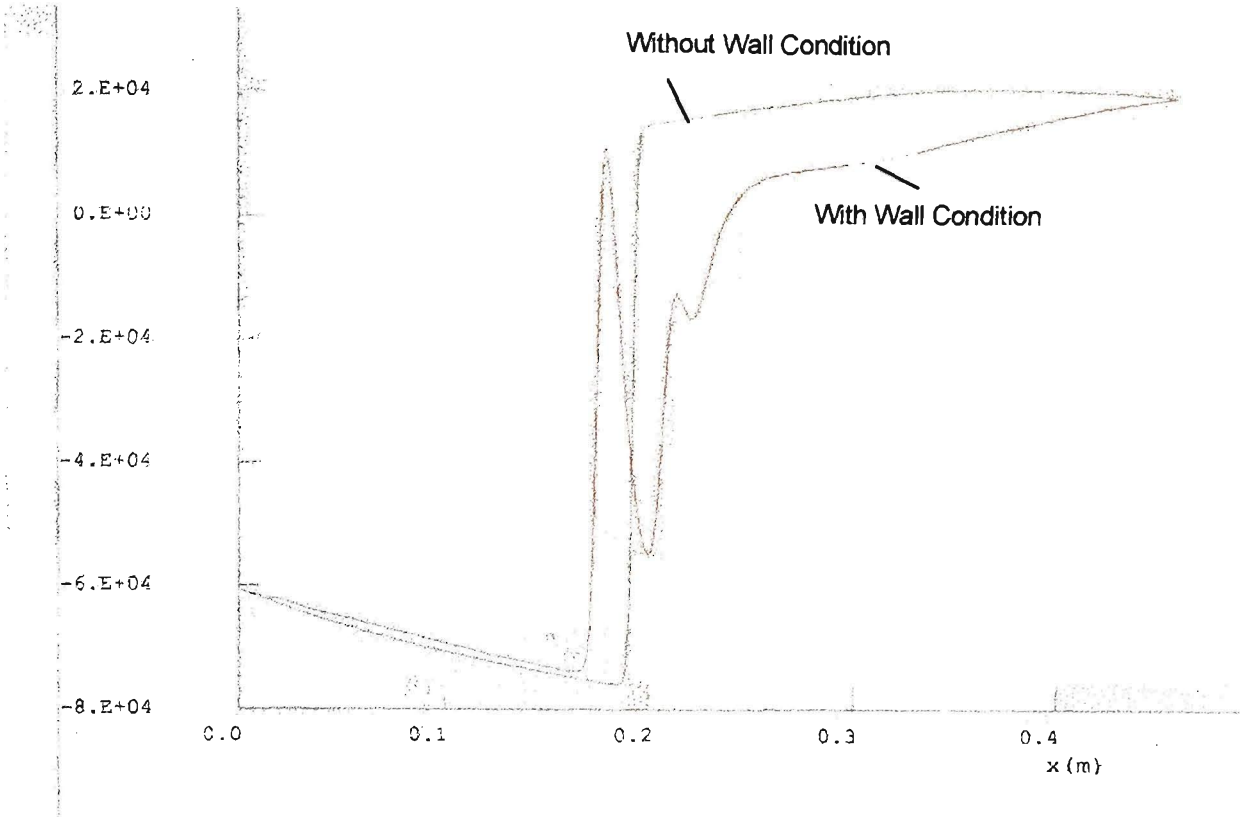

Figure 8.18 Static Pressure - With and Without Wall

Effect of the finer computational grid can be seen by comparing Figures 8.18 and 8.8. In Figure 8.18, the much sharper rise in core pressure indicates that the shock has been captured more precisely with the finer grid. The overall features of the flow in the compression region can again be seen: pressure fluctuations in both the downstream and cross-stream directions, indicating a severe shock-boundary layer interaction resulting in the formation of a pseudo-shock pattern.

For the sake of completeness, a three dimensional simulation was carried out next. Chapter 9 outlines this simulation, followed by an account of the experimental investigation in Chapters 10 and 11.

Chapter 9

THREE-DIMENSIONAL SIMULATION

In this chapter, a more detailed, three-dimensional analysis of the flow in the SAI is carried out. The analytical technique is the same as that in Chapter 8, viz. the PHOENICS flow simulation system.

9.1 Computational Domain

The flow region chosen for analysis is the one between the injection tube exit plane and the final exit from the nozzle. This region is the same as that chosen for a more detailed study of air-only flow in section 8.3.2. Unlike the computational domain in that section, the new computational domain is as shown in Figure 9.1. In order to economise on the number of cells needed and still carry out as detailed an analysis as possible, a computational domain which covers only a quarter of the actual flow region is constructed. In doing so, the fact that the flow region has two planes of symmetry, horizontal and vertical, is used. Besides the Inlet and Outlet, the top and left-hand boundaries of this computational domain are now specified as impermeable walls, and the bottom and right-hand boundaries, corresponding to the two planes of symmetry, are 'walls with slip'.

The axis system for this three-dimensional study is as shown in Figure 9.1. The distribution of cells along the z-axis is the same (250 cells, evenly distributed) as that along the x-axis in the previous simulation. The distribution of cells in the y-direction is exactly the same as earlier (17 cells, smaller cells near the top wall). Along the third, x, direction, there are now 16 cells in place of the single cell in the z-direction in the previous case. These cells are unevenly distributed, and are smaller near the side left-hand-side wall, and larger in the vicinity of the axis. This is necessary because in reality, the solid glass side walls act as additional impermeable boundaries to the flow

along which the no-slip condition must be satisfied. Figure 9.2 shows the three-dimensional computational grid.

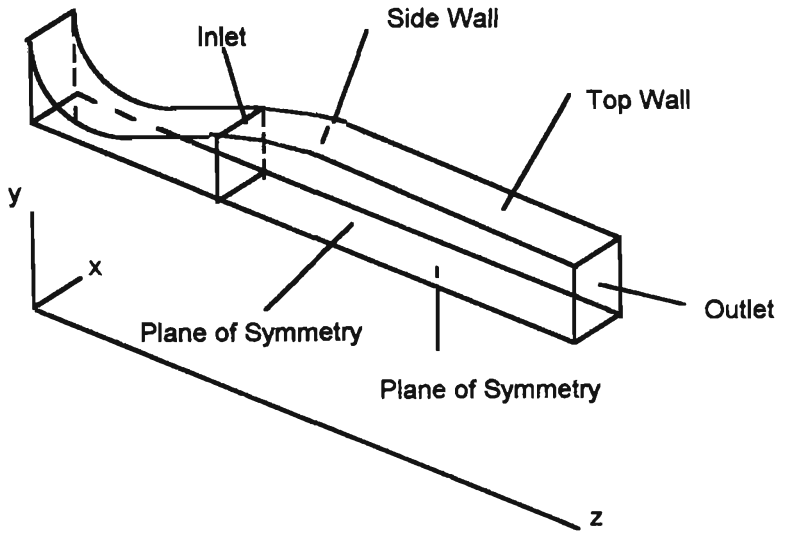

Figure 9.1 Computational Domain

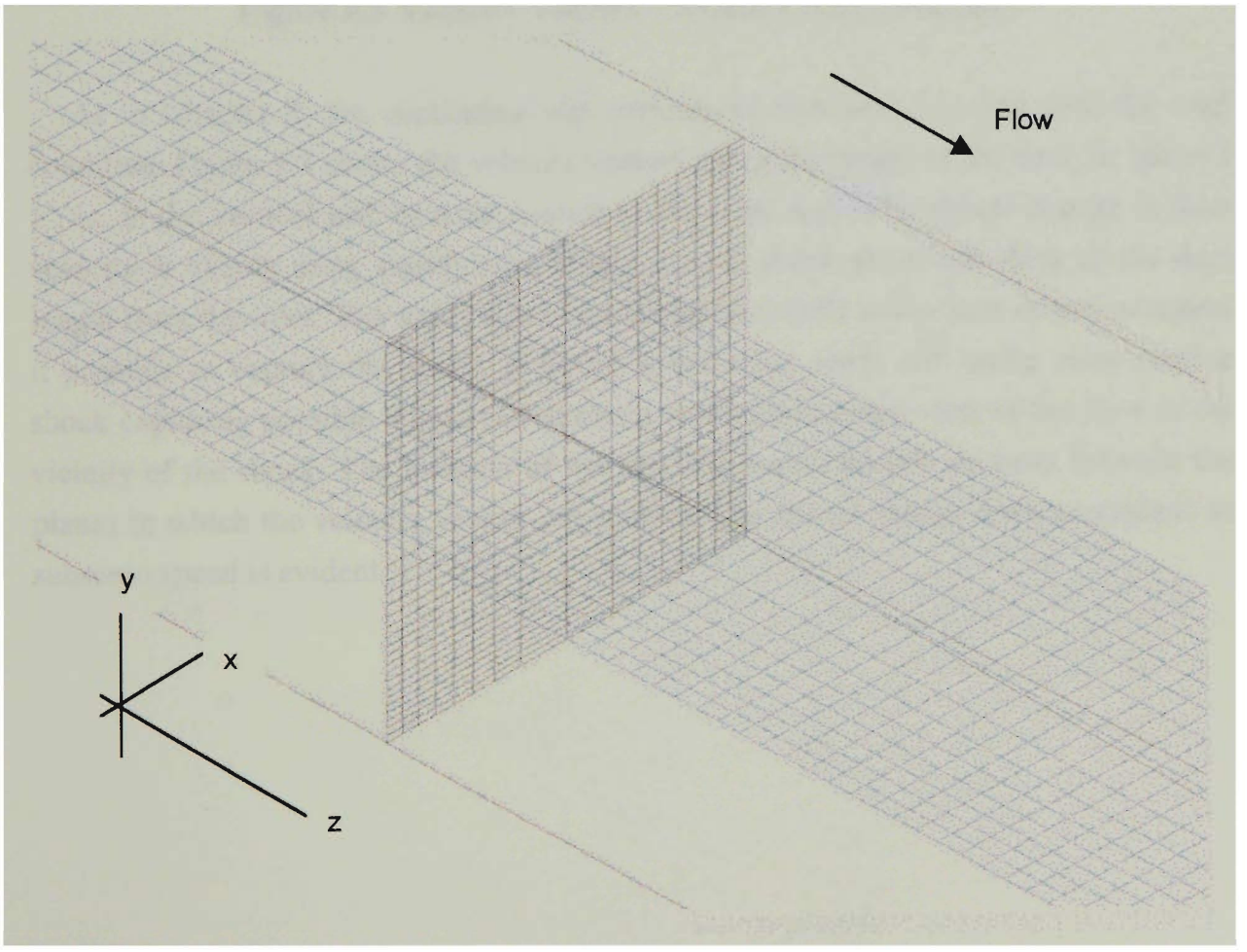

Figure 9.2 Computational Grid

Other settings for this simulation are similar to those in the two-dimensional simulation, and are not repeated here. The Q1 files appear in Appendices C8 and C9.

9.2 Results of Simulation

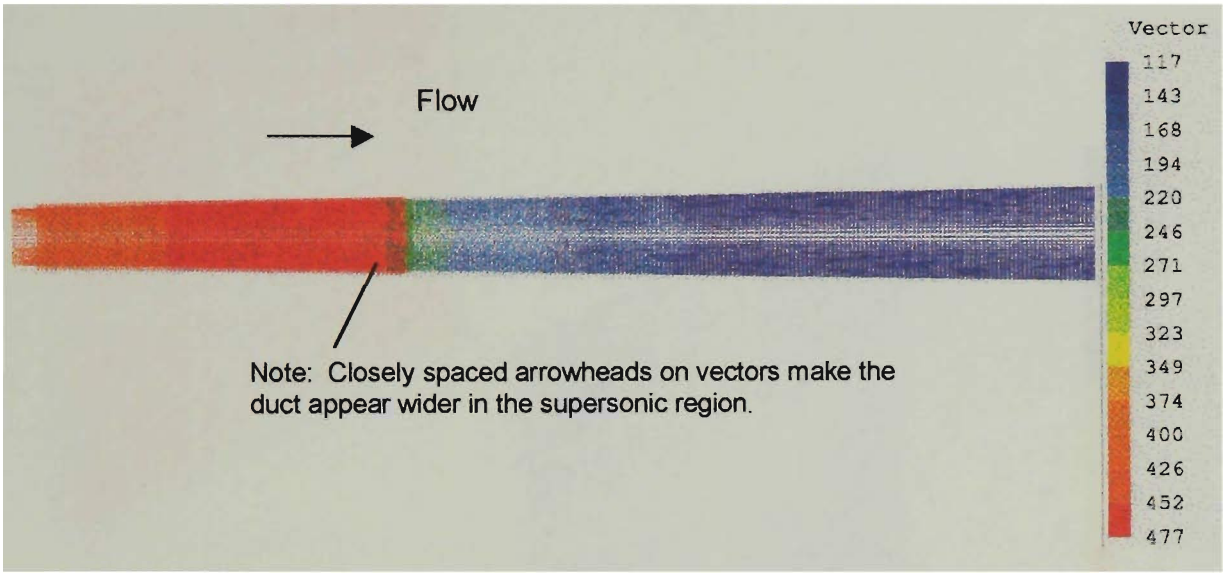

Figure 9.3 Velocity Vectors - Without Wall Function -

As in Chapter 8, the simulation was carried out first without, then with the wall condition. Figure 9.3 shows the velocity vectors along the length of the duct, in 'plane I 1', ie. in the vertical slab of cells nearest to the solid wall. The abrupt change in flow velocity is clearly seen, signifying a single normal shock about one-third of the duct length from the inlet. The small size of computational cells in the flow direction makes it possible to capture the shock, although a still finer mesh will make more precise shock capturing possible. Figure 9.4 shows a three-dimensional view of the flow in the vicinity of the shock. The location of the shock is approximately midway between the planes in which the velocity vectors are plotted. The abrupt change from supersonic to subsonic speed is evident.

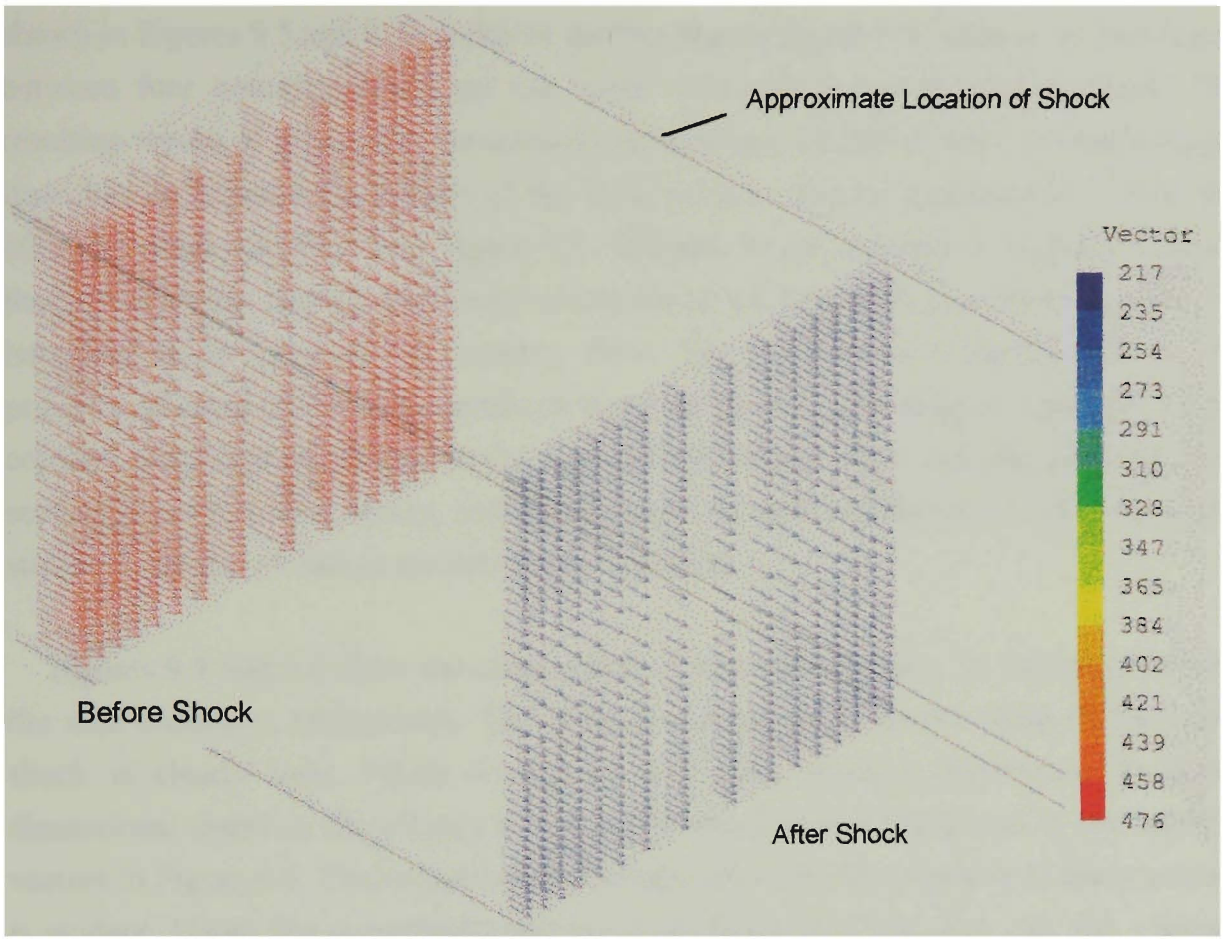

Figure 9.4 Velocity Vectors before and after Shock - Without Wall -

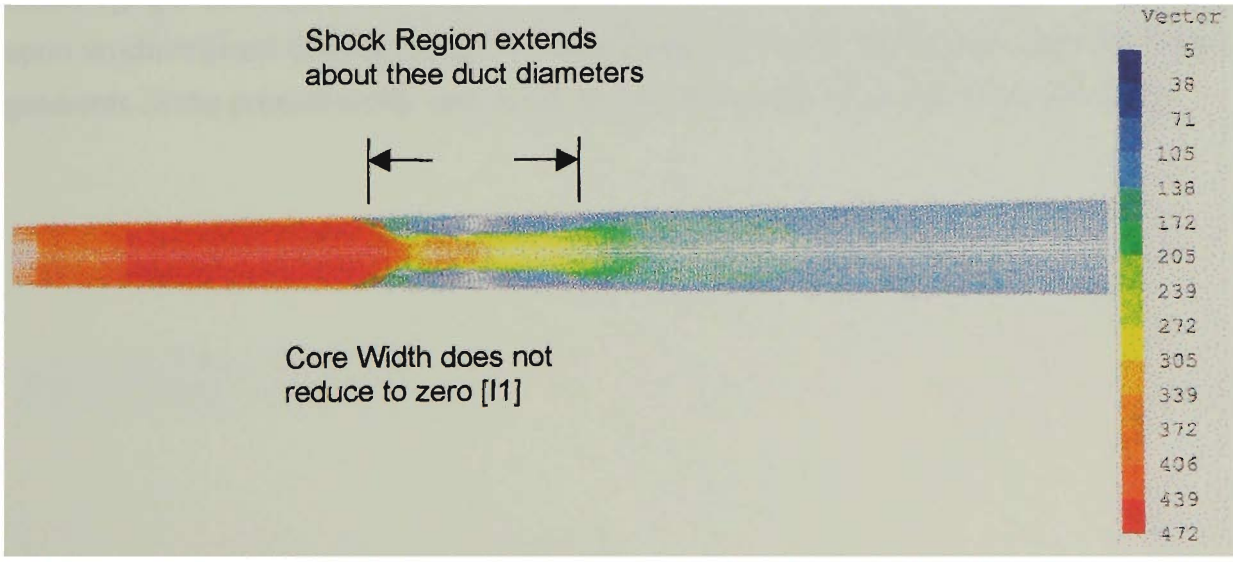

Figure 9.5 Velocity Vectors - With Wall Function -

When the wall function is activated, the resulting flow is completely different, as was seen in Chapter 8. Figure 9.5 shows the velocity vectors in the SAI duct, and once again the picture invites comparison with Figure 6.5. The difference in the flow patterns

shown in Figures 9.5 and 8.14 is due to the fact that in Figure 9.5, there is an interaction between four boundary-layers on the walls of the duct and the initial shock. The resulting region of separation immediately downstream of initial shock is clearly larger than that in Figure 8.14. Details of the flow velocity vectors immediately before and after the shock are shown in Figure 9.6. Whereas in the absence of boundary layers, there is an abrupt change in velocity across the shock (Figure 9.4), interaction with the boundary layers produces a complex flow. The complexity is heightened by the presence of sharp corners, and results in larger zones of separated flow, especially in the corners. The slight asymmetry in the flow patterns is due to the fact that the duct cross section is not a perfect square, and also because the cell distributions in the two cross-stream directions (x and y) are not exactly identical.

Figures 9.7 and 9.8 show the static pressure contours in plane I 1 without and with the wall condition, respectively. The zone of reacceleration downstream of the initial shock is clearly seen. Figure 9.9 shows the static pressure distribution in three-dimensional detail in the vicinity of the initial shock, and corresponds to the velocity vectors in Figure 9.6. The complications brought about by the presence of sharp corners is evident. Under the assumption that the fluid behaves as an ideal gas, the constant density contours also should be similar to the isobars in Figure 9.9. This observation may have some bearing upon the experimental investigation reported in Chapter 11, in which an attempt is made to visualise the pseudo-shock in the duct using the shadowgraph technique. Successful observation of a clear shadowgraph is dependent upon unidirectional density gradients in the medium, and it seems likely that the density gradients in the present study may result in loss of clarity in the shadowgraph image.

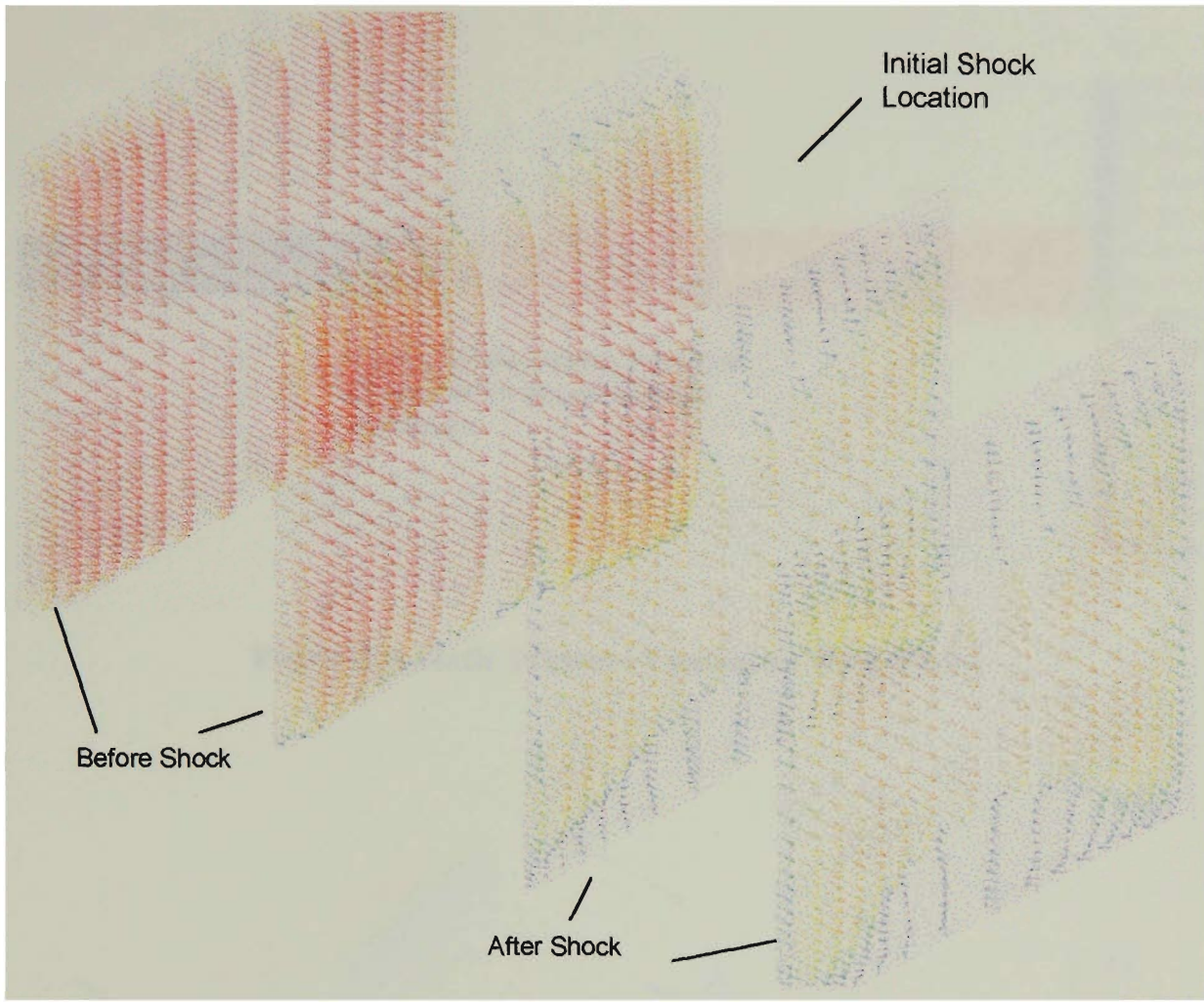

Figure 9.6 Velocity Vectors before and after Shock - With Wall -

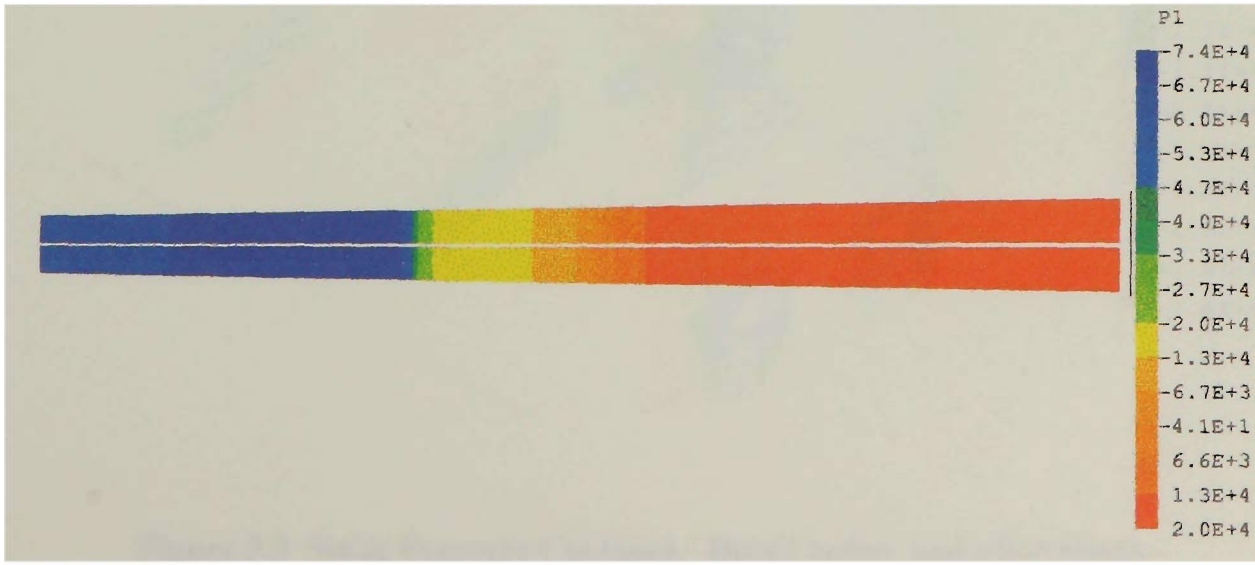

Figure 9.7 Static Pressure Contours - Without Wall -

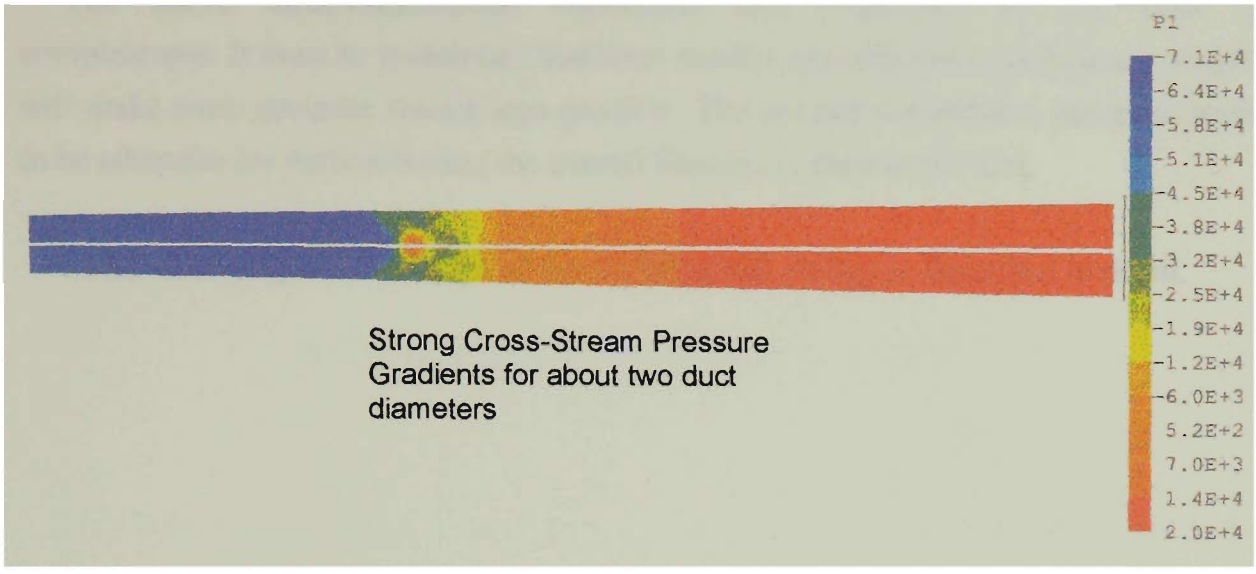

Figure 9.8 Static Pressure Contours - With Wall -

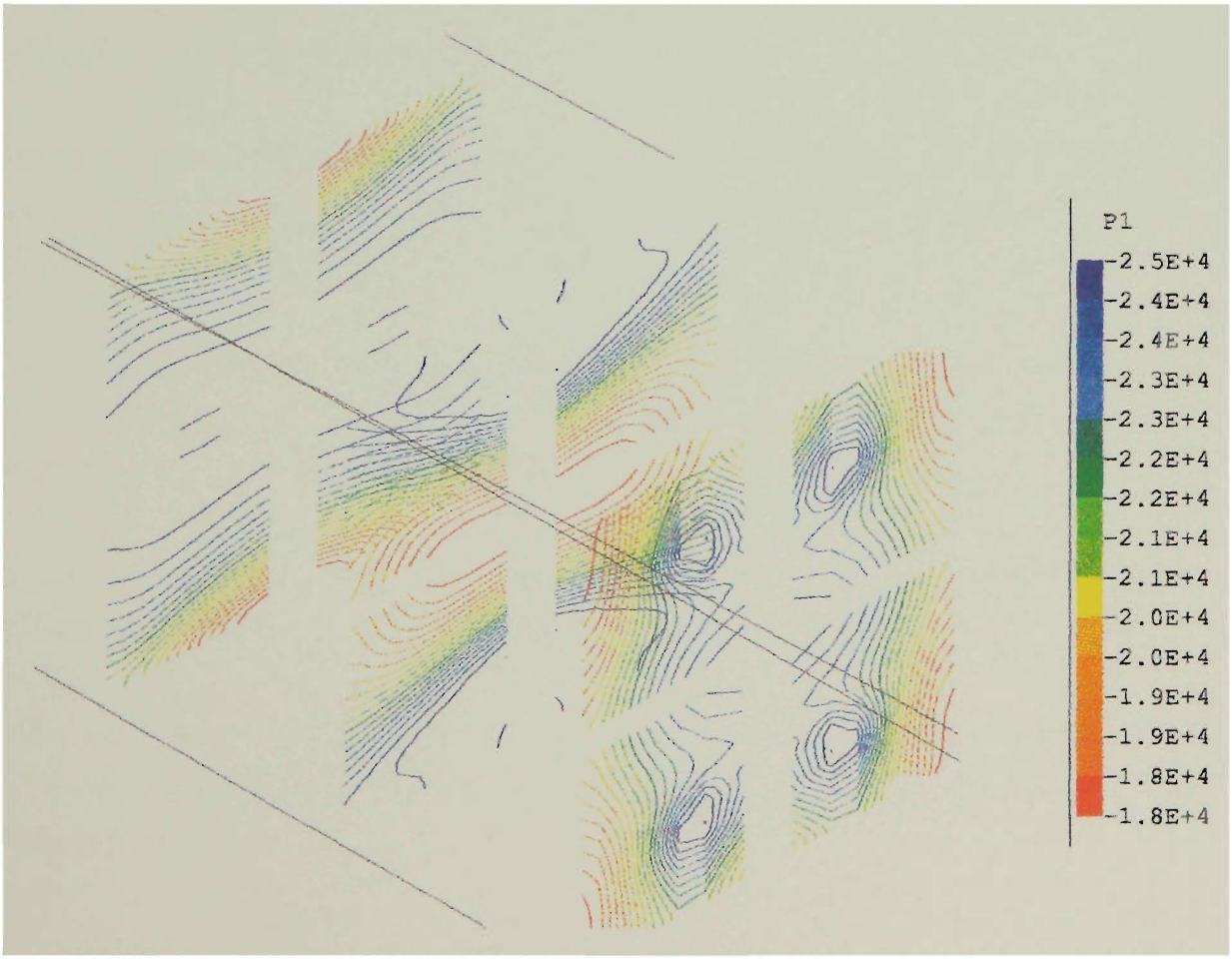

Figure 9.9 Static Pressure Contours - Detail before and after Shock -

The above three-dimensional simulation was conducted for the sake of completeness. It must be mentioned that finer meshes and alternative turbulence models will make more accurate simulations possible. The present simulations, however, seem to be adequate for demonstrating the overall features of flow in the SAI.

In the next chapter, the design of the experimental facility is described in detail.

Chapter 10

EXPERIMENTAL FACILITY

Recapitulating the steps which were taken in the previous chapters during analytical investigation of flow in the SAI:

1 Some design flow parameters, such as stagnation pressures for primary gas and suspension, and some geometrical parameters such as injection tube length, were selected, based on feasibility (Chapters 2, 3).

2 A generalised one-dimensional analysis was conducted to 'size' the SAI. This step also yielded an estimate of the evolution of important flow parameters along the length of the SAI (Chapters 3, 4, 5, 6 and 7).

3 Based on the calculated overall dimensions of the SAI, a two-dimensional study was conducted using the PHOENICS flow simulation system. This study provided preliminary visual evidence of a pseudo-shock in the duct (Chapter 8).

4 For the sake of completeness, further details of the flow were sought in a three-dimensional study, also using PHOENICS (Chapter 9).

The next step involves design and fabrication of the test rig, based on the analytical investigation. In this chapter, the design and fabrication of the experimental test rig is described in detail.

10.1 Duct Geometry

It is necessary to decide between two possible duct geometries:

(a) Axisymmetric, or
(b) Planar.

Each geometry has its advantages and drawbacks. An axisymmetric (circular cross-section) duct seems to be the most logical choice for an injection device such as the SAI, which consists of a de Laval nozzle with a centrally located injection tube. Flow in a circular cross section duct does not suffer from the uncertainties and complications associated with recirculation in corners, etc. Moreover, if the device is found commercially feasible in the future, a circular cross-section duct seems the most obvious choice.

However, in the present preliminary study, it was decided to construct a test rig designed to produce a planar or approximately two-dimensional flow. This implies a duct of rectangular cross-section. A rectangular cross-section inevitably gives rise to flow difficulties in the corners, and possibly asymmetry in the boundary layers growing along the duct walls. However, this drawback is outweighed by the fact that it is much easier to fabricate a duct with at least two flat walls. This feature also makes flow visualisation possible, since in the test section, the flat side walls can be glass windows.

In the following sections, the design and fabrication considerations for each component of the SAI are described in detail.

10.2 Stagnation Chamber

Ideally, the primary gas stagnation chamber is an infinitely large reservoir, maintained at the chosen stagnation pressure (~2 bar abs in the present case). In actual practice, a reservoir as large as possible must be used. For reasons of safety, it is necessary to avoid flat walls as far as possible in such a "pressure vessel". A box-shaped stagnation chamber with welded joints was therefore ruled out, since it was thought that the high pressure inside would cause the walls to bulge out to some extent, at the same time putting the welded joints under stress. The bulge, if any, would also be detrimental to the connection between the stagnation chamber and the nozzle duct. For this reason, the wall of the stagnation chamber which is adjacent to the nozzle must necessarily be flat.

A 600 mm length of steel pipe, 270 mm in outer diameter and having wall thickness 10 mm was chosen for the stagnation chamber (Figure 10.1). The stagnation chamber can be maintained at a constant high pressure by connecting it to the main 7 bar air supply via a pressure regulator. The pipe is closed at either end by blank and slip-on flanges (Figure 10.2).

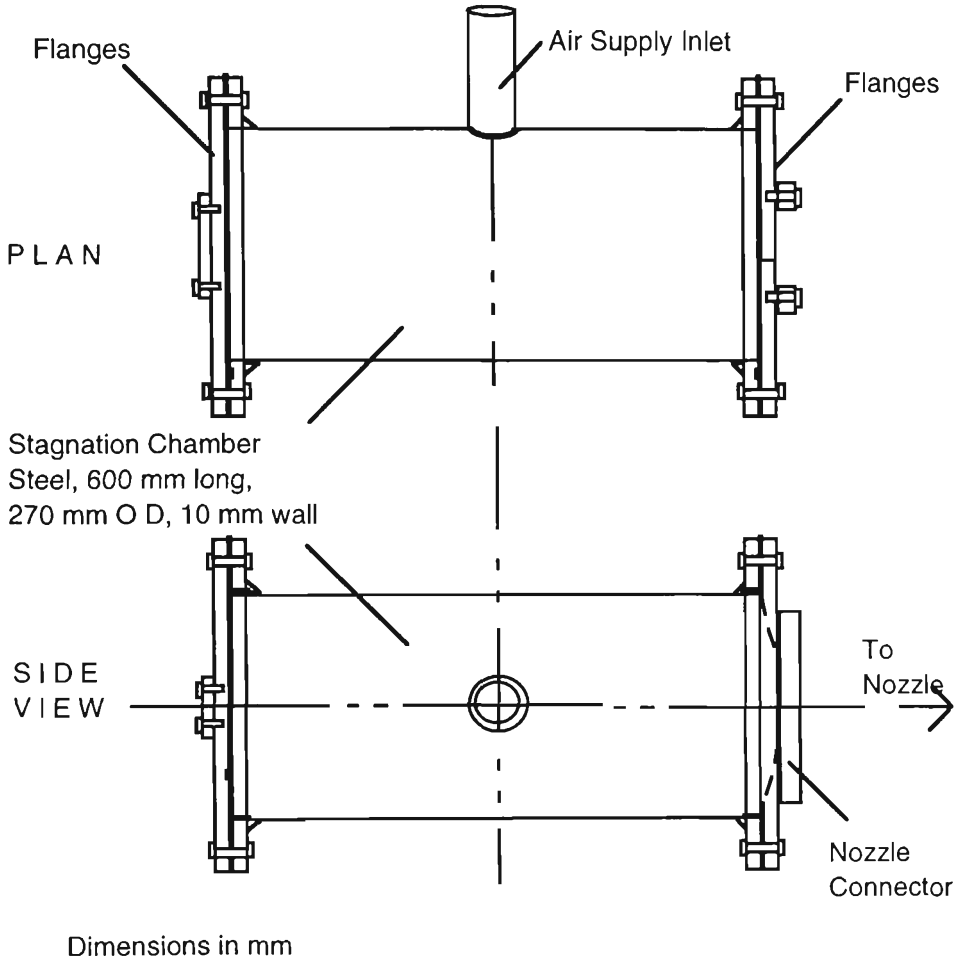

Figure 10.1 Stagnation Chamber

The flanges have appropriately shaped slots as openings for the test section and injection tube respectively (Figure 10.2).

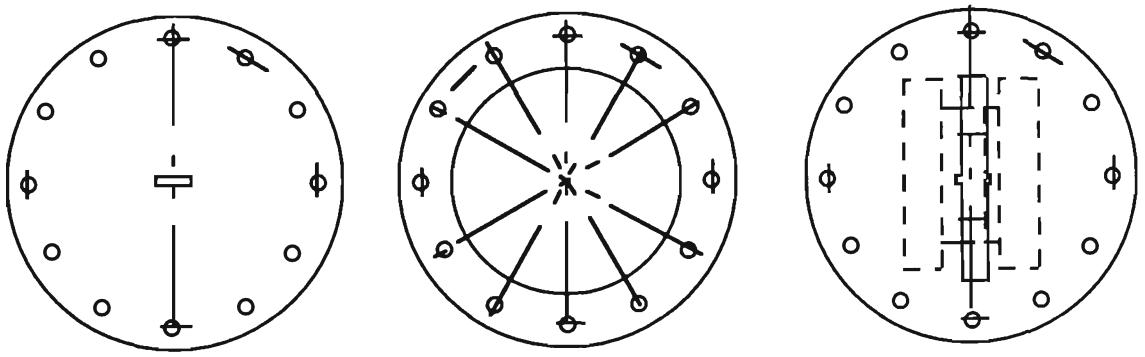

Blank Flange, 400 OD
12 holes
with
rectangular slot
for injection tube

Slip-on Flange
400 OD, 270 ID
12 Holes,
on either side of
Stagn. Chamber

Blank Flange, 400 OD,
12 Holes, with slot for
nozzle opening

Figure 10.2 Flanges on Stagnation Chamber

10.3 Injection Tube

The injection tube is a closed channel of rectangular cross-section measuring 30 mm in width and 5 mm in height. The walls are 3 mm thick on top and bottom and 5 mm thick on the sides. Since an extruded channel of these specifications was not available commercially, the injection tube was fashioned out of a long thick aluminium strip with a milled-out lengthwise channel. The tube is closed at the top by a thinner (3 mm thick) aluminium strip screwed to the channel (Figure 10.3)

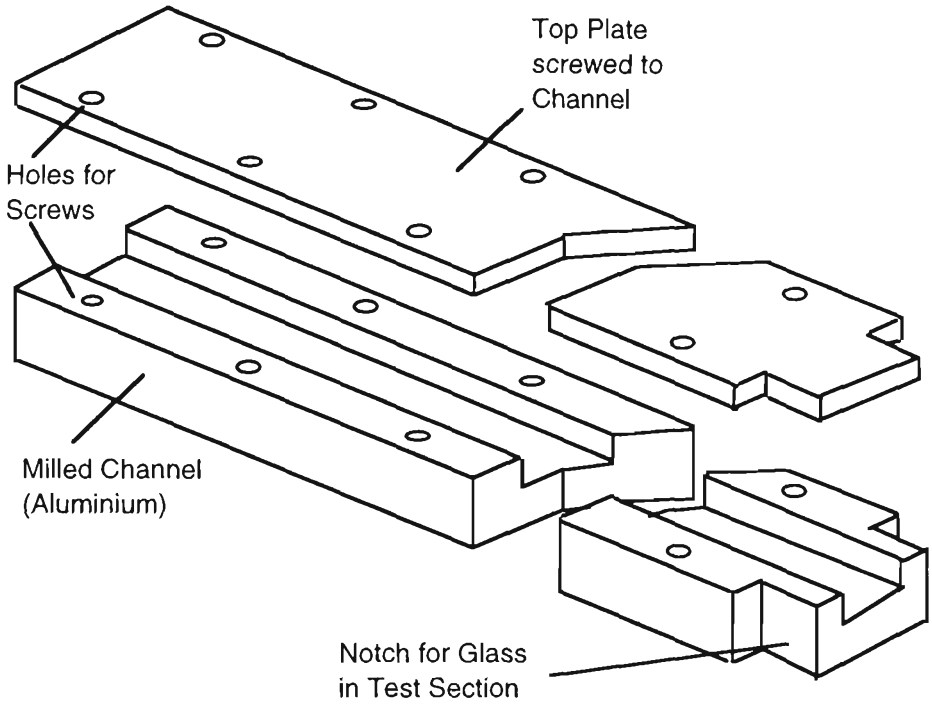

Figure 10.3 Injection Tube - Fabrication Detail -

In order to allow good initial mixing between secondary gas and conveyed solids, the injection tube is provided with two funnel-shaped inlets, one for secondary gas (air) and the other for solids. The secondary gas inlet draws in air from the ambient. As seen in Chapter 3, the funnel-shaped inlet allows smooth entry of air. At the same time it makes possible a relatively high value of initial velocity and Mach number, so that subsequent acceleration to sonic condition at the injection tube exit plane may be facilitated. The solid particles can be gravity-fed into the injection tube via the solids inlet funnel which opens upwards. Near the inlet of the injection tube, a pressure tap is provided to measure pressure at the end of the funnel-shaped nozzle. In order to simplify fabrication of the funnels, it was not thought necessary to have curved walls

(eg a cubic curve) for the air inlet, although such walls will probably be better and minimise initial losses.

Details of the injection tube inlet appear in Figure 10.4. The entire injection tube assembly is shown in Figure 10.5. The injection tube is long enough to pass right through the stagnation chamber and open in the divergent part of the converging-diverging nozzle.

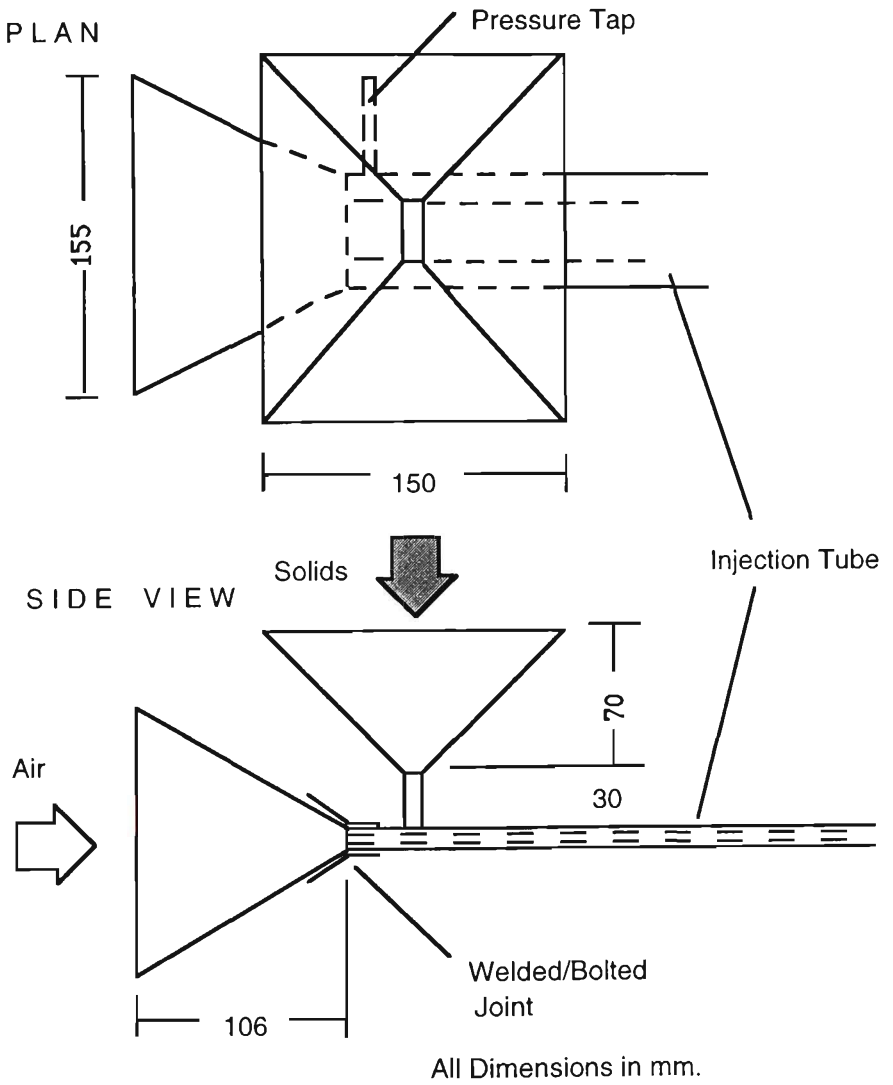

Figure 10.4 Injection Tube - Air and Solids Inlets -

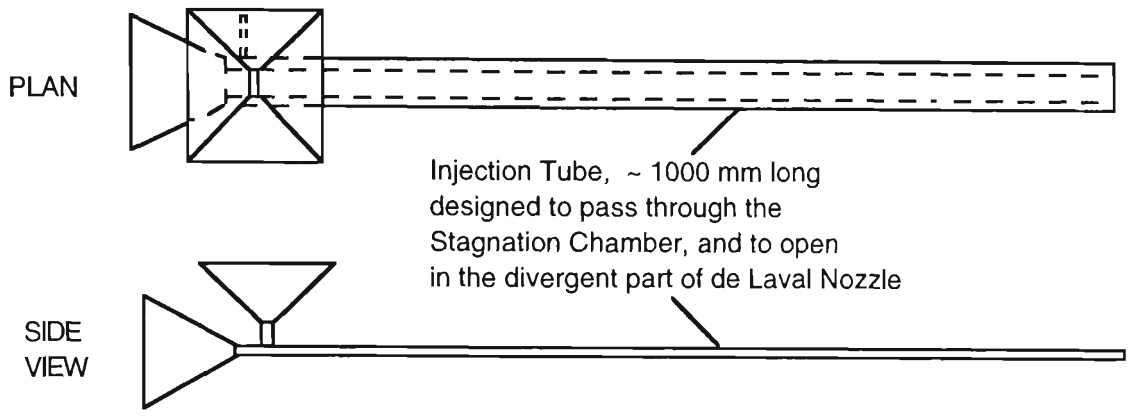

Figure 10.5 Injection Tube Assembly

10.4 Stagnation Chamber-Injection Tube Assembly

The injection tube should be centrally located in the de Laval nozzle, and must open into the divergent (low-pressure, supersonic) part of the nozzle. At the same time, the injection tube must have inlets at the other extremity to admit secondary gas and solids. The de Laval nozzle itself must be connected to the stagnation chamber to draw high-pressure primary gas from it.

To satisfy all these requirements, it is necessary to make the injection tube pass right through the stagnation chamber, with one end opening in the divergent part of the nozzle, and the other end provided with air and solids inlets on the far side of the stagnation chamber. Combined with the requirement that the stagnation chamber itself must be as large as possible, this results in an injection tube about 1 meter in length. Such a long injection tube happens to be compatible with the assumption that the suspension undergoes a Fanno-type flow in it. As seen in Chapter 11, the slenderness ratio of this tube happens to be conducive to producing sonic suspension flow at the exit.

The stagnation chamber-injection tube assembly is shown in Figure 10.6.

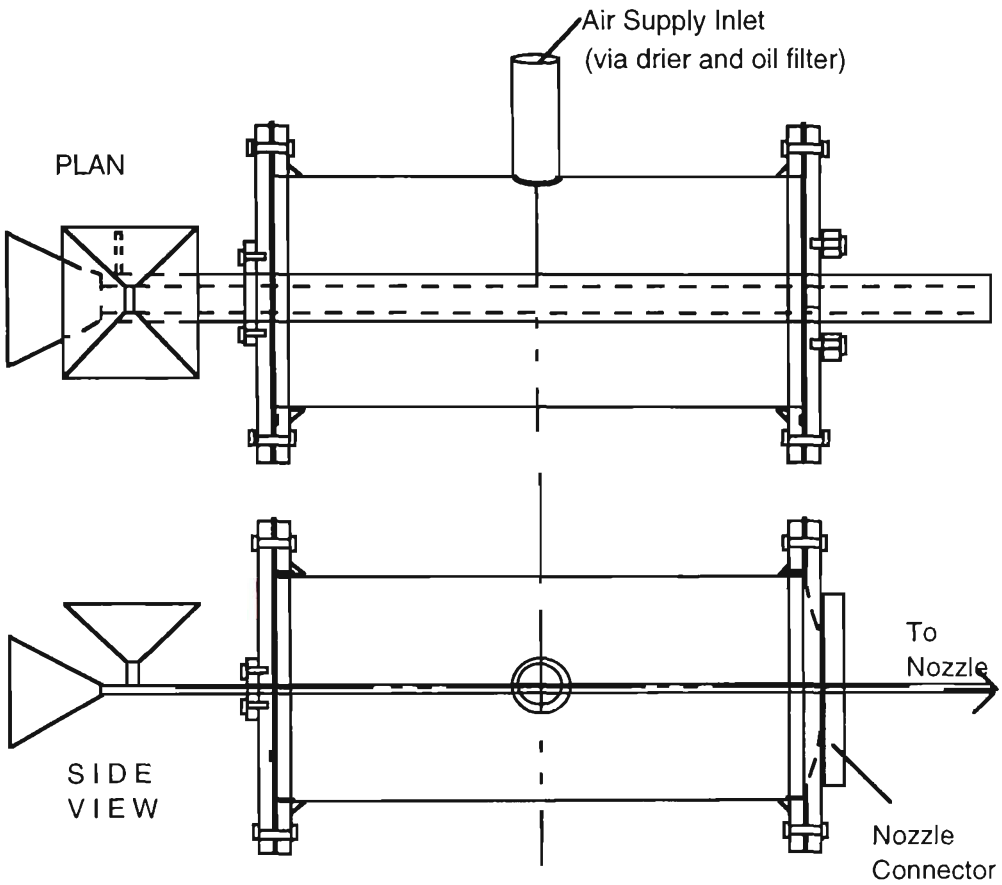

Figure 10.6 Stagnation Chamber-Injection Tube Assembly

As seen in Figure 10.6, the smaller dimension of the injection tube cross-section is made to face the incoming air from the high-pressure supply. This is done to minimise any possible bending of the slender injection tube due to forces exerted upon it by the high-pressure air.

10.5 Main Test Section

10.5.1 de Laval Nozzle

Establishing a supersonic flow is fundamental to the operation of the SAI. Therefore the most crucial part of the SAI duct is the de Laval Nozzle, with its large area variation. Such a nozzle can be much more easily fabricated if the area variation is achieved by varying the duct height only, with the duct width kept constant. The fabrication can be

further simplified by keeping the side walls and the 'floor' flat, with the area variation brought about by curvature in the 'ceiling' only (Figure 10.7).

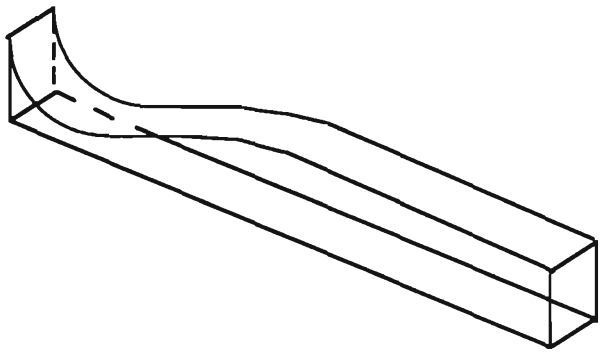

Figure 10.7 Nozzle with Three Flat Walls

In the present application, such a design must be discarded because provision must be made for a 'centrally located' injection tube opening in the divergent part of the nozzle. The asymmetric design in Figure 10.7 would also lead to asymmetric boundary layer growth on the floor and the ceiling.

These considerations call for a nozzle with two flat side walls and having a constant width, with the cross-sectional area variation achieved by symmetrical curvatures in the 'floor' and the 'ceiling'. The width was arbitrarily fixed at 30 mm, based on similar nozzle studies reported in the literature. Due to the large variation in duct height, the aspect ratio of the cross section varies widely. A width of 30 mm is used as a compromise to allow sufficient depth of field, thus approximating a two-dimensional flow to enable flow visualisation. A larger width could also imply prohibitively (and unnecessarily) large air and solids mass flow rates. For the chosen design flow parameters (Chapter 4), these considerations seem to result in an injection tube and de Laval nozzle duct of reasonable shape and dimensions.

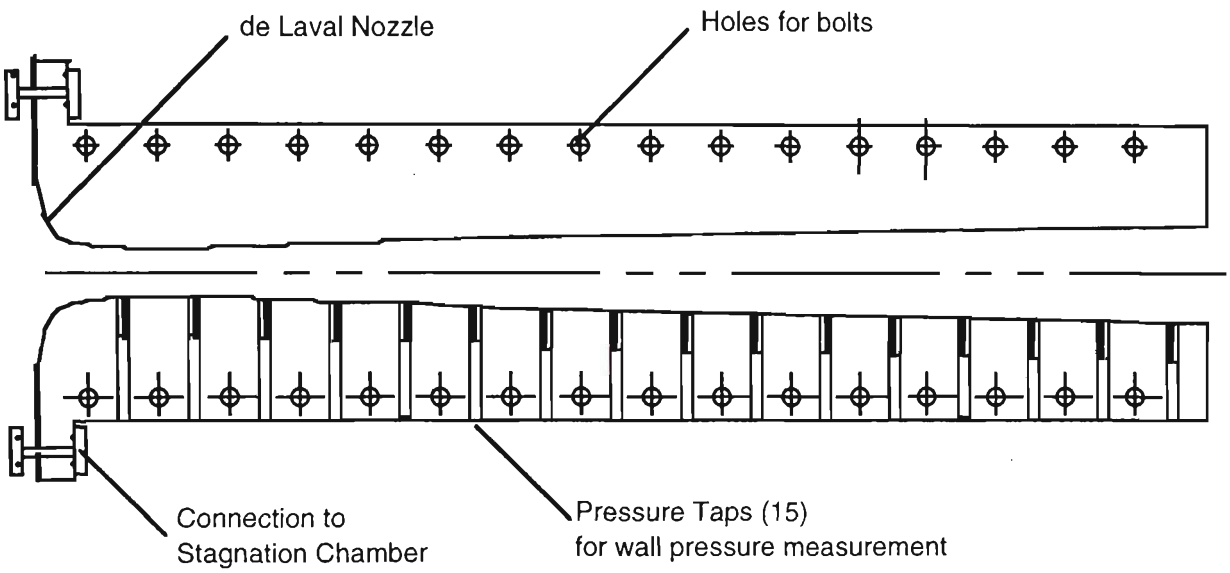

Figure 10.8 de Laval Nozzle

Figure 10.8 shows in side view the symmetrically shaped upper and lower plates which form the de Laval nozzle. The stainless steel plates are 30 mm thick, thus forming a channel of constant 30 mm width between them. Both upper and lower plates are provided with horizontal holes for bolts for the test section assembly. On the lower plate, 15 vertical pressure taps are drilled to allow measurement of wall pressure in the nozzle duct. Detail of a typical pressure tap is shown in Figure 10.9. The pressure tap hole must be small to simulate measurement at a point, but a small long hole would be very difficult to drill in stainless steel. Each pressure tap was therefore drilled in two stages, the smaller tap-hole reaching only part of the way through the plate. The length of the tap-hole is dictated by the length of small drill-bit available. Larger holes drilled from the opposite side are then aligned with the smaller ones. The larger holes are threaded at the open end for connection with push-type tube inserts, which are connected to the pressure measuring device.

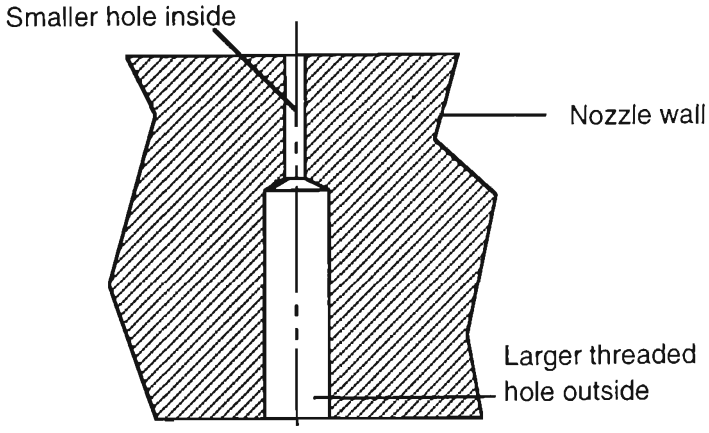

Figure 10.9 Pressure Tap - detail -

10.5.2 Side Walls

To enable relatively easy installation of the injection tube, the side walls of the main test section are provided with grooves in which the injection tube can slide. These grooves hold the injection tube in place, once inserted. For this reason, the side walls of the injection tube are thicker than those at top and bottom, as mentioned in section 10.3. Two vertical toughened glass walls downstream of the injection tube exit make flow visualisation possible. The glass panels and the steel plates forming the nozzle are held together by additional steel plates and bolts. This is done to avoid having to drill holes through the glass. Details of this assembly are shown in Figure 10.10 and 10.11.

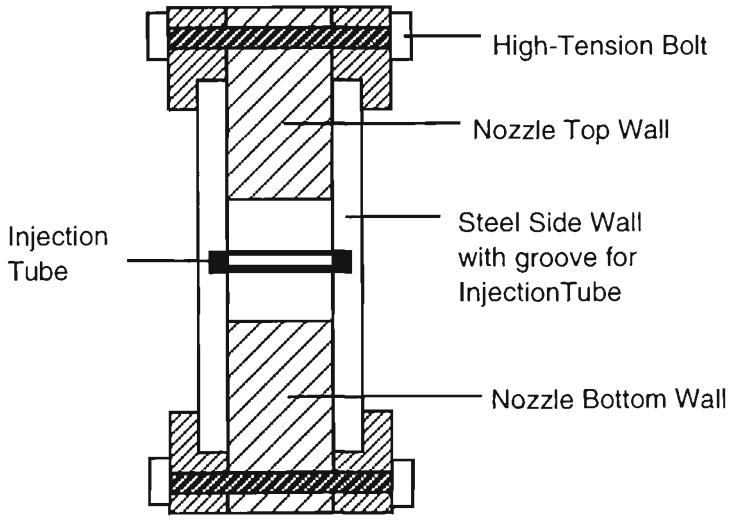

Figure 10.10 Test Section Detail - Upstream -

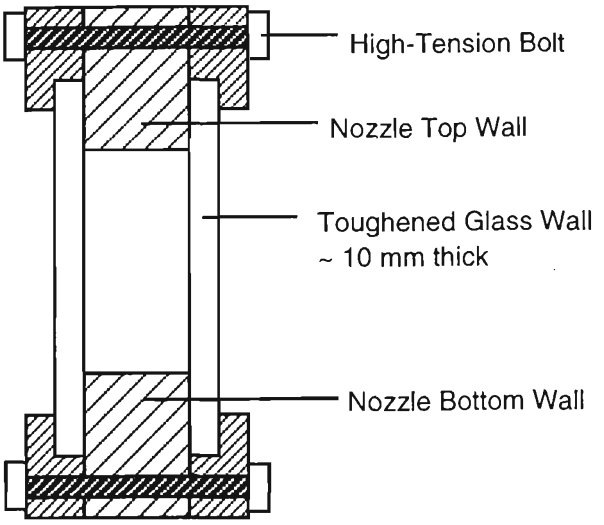

Figure 10.11 Test Section Detail - Downstream -

10.6 Receiving End

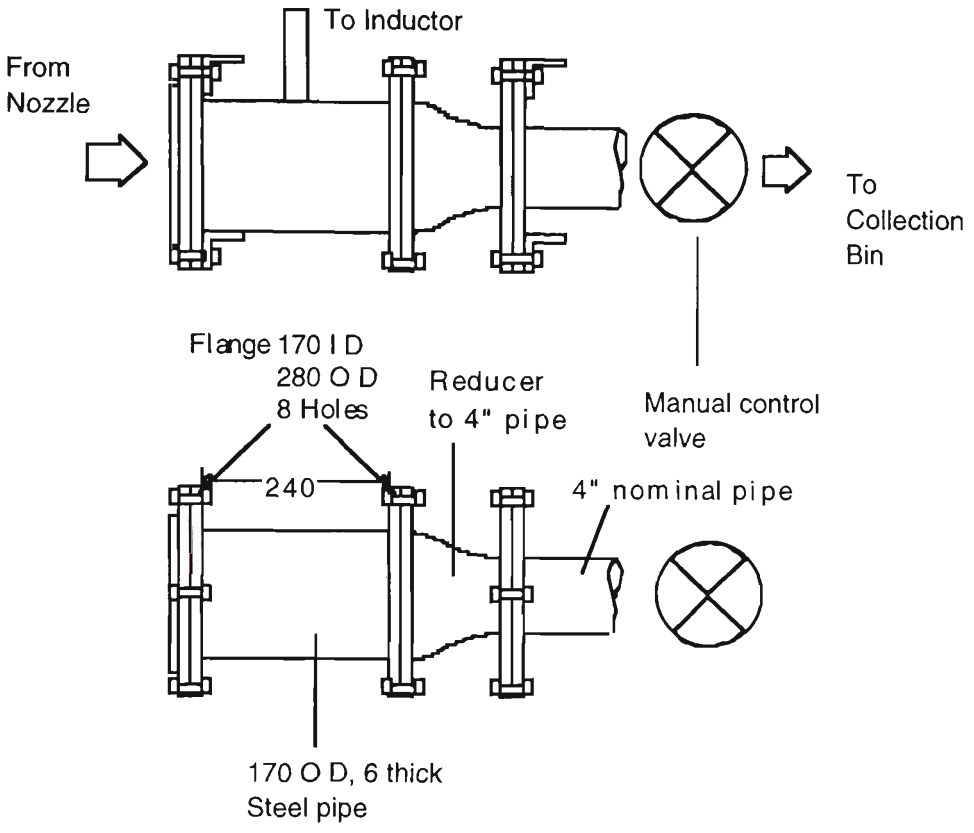

Figure 10.12 Downstream Assembly

Figure 10.12 shows the details of the assembly downstream of the nozzle. It was initially thought that the downstream end would have to be maintained at vacuum pressures to initiate supersonic flow. The connection to the inductor (and an additional plate valve of 'fully open/fully shut' type, not shown in the figure) was provided with this contingency in mind.

It was discovered that the capacity of the available inductors was not nearly large enough to negotiate the high air flow rate (with the stagnation chamber maintained at 2 bar abs. However, such an elaborate arrangement proved to be unnecessary in the end, because the shape of the nozzle itself was found adequate to generate supersonic flow in the nozzle, with the downstream valve(s) fully open. This feature is welcome from a safety point of view. Once supersonic flow is established in the nozzle, the downstream pressure can be easily manipulated using the manual-control valve. This operational simplicity would be important for possible future industrial applications of the device. The flow can be entirely controlled using only two valves, those upstream and downstream of the nozzle.

10.7 Pressure Measurement

A new device was designed and fabricated to enable measurement of wall static pressure at the duct wall. Ideally, a bank of 15 digital pressure gauges is required to measure static pressure at the 15 taps. In the absence of an adequate number of such gauges, it became necessary to use the new pressure measurement manifold. This consists of an arrangement of 16 'on-off' valves interconnected with T sections of compatible PVC tubes with pieces of garden hose (as shown in Figure 10.13).

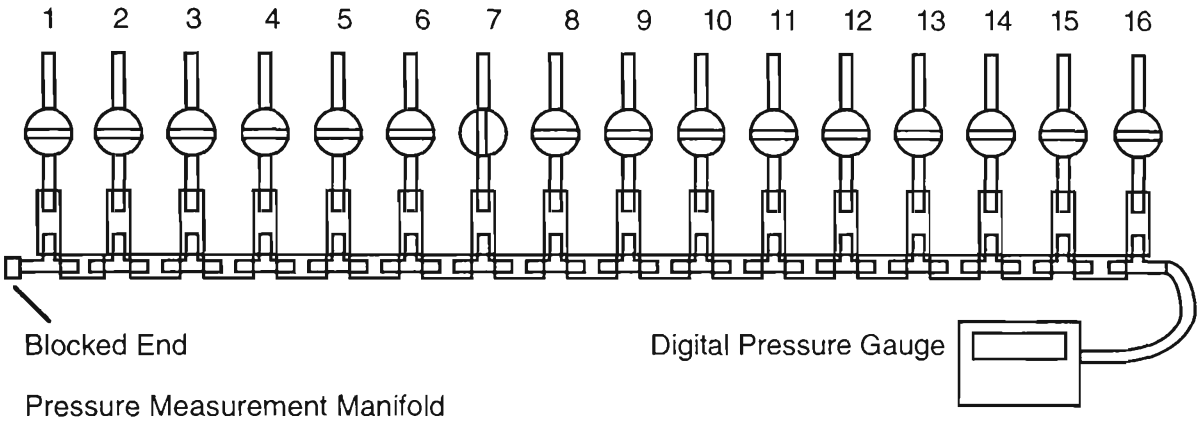

Pressure Measurement Manifold
Valves 1 - 15 are connected to pressure taps on SAI duct.
Opening Valve 16 restores pressure gauge reading to zero between successive readings.

Figure shows Valve 7 open, all others closed. Gauge reads pressure at pressure tap 7.

Figure 10.13 Pressure Measurement Manifold

10.8 Flow Visualisation

The three most commonly used optical methods of investigating compressible flows are [S11]:

1 the Interferometer method
2 the Schlieren method
and
3 the Shadowgraph method.

The working principle in all three techniques is the same: the speed of light depends upon the refractive index of the medium through which it passes, and the refractive index in turn is a function of the density of the medium. Therefore light passing through

a density *gradient* in a transparent gas is deflected in the same way as if it were passing through a prism. Of the three techniques, the Shadowgraph is the easiest to set up, and is reported to be particularly suited to observing flows with shocks, because of the strong density gradients involved in such flows. The disadvantage of this method is that it affords little quantitative information about the flow field. Despite this drawback, since one primary objective in the present project was to investigate whether flow in the SAI contained shocks at all, the Shadowgraph technique was chosen as the optical method of investigation.

10.8.1 Shadowgraph System

In the present experimental arrangement, the shadowgraph system consists of a source of bright light (a 250 W light bulb in a slide projector), placed about 6.25 m away from the SAI duct test section. On the opposite side of the test section, a large white screen is placed parallel to the flow direction, about 1 m from the test section. These distances were fixed after many trials. It was observed that the large physical size of the light source was not suitable. Even with a collimating lens, this resulted in a considerably blurred shadowgraph image. Ideally, an intense 'point' source of light is recommended. An attempt was therefore made to simulate a point source by placing an opaque screen with a small hole in front of the light bulb. If the hole is too small, however, the intensity of light emerging from it is considerably reduced, especially at long distances from the light source. At the same time, the small hole acts like a pin-hole camera, and casts an image of the light filament itself on the screen. A distinct image with relatively sharp edges of shadows cannot be obtained. A working compromise was reached by trying holes of different sizes till the sharpest image was received on the screen. For the distances in the present arrangement, a hole of about 8 mm diameter seems to allow a sufficient amount of light through it to enable optical observation. See Figure 10.14. It was found that a collimating lens was not necessary. This is probably because the included angle between the light rays passing near the upstream and downstream edges of the test section is small enough. This also has the additional advantage of enabling flow visualisation the entire test section at the same time.

Once the flow is established, the light beam passing through it is deflected wherever there is a density gradient. If the density gradient were constant, all light rays would be deflected by the same amount, leaving the resulting illumination on the screen unchanged. However, there will be a change in illumination if there is a *gradient in the density gradient* in a direction perpendicular to the passage of the light rays. If the depth

of field is suitable, therefore, the presence of shocks, if any, should be revealed by a marked difference in illumination on the screen wherever there is a shock.

To obtain a record of the shadowgraph, the image on the screen was photographed at close range with a high-speed (400 ASA) film. To minimise distortion of the photographs, the camera was placed close to the screen in the middle looking slightly up at the shadowgraph on the screen, just out of the path of the light beam. To prevent condensation of atmospheric moisture on the glass windows, an anti-fogging liquid was sprayed on them. The insides of the glass windows were also wiped with this fluid by means of a sponge attached to a long flexible stick. This also enabled cleaning of the glass walls from the inside by reaching in through the stagnation chamber.

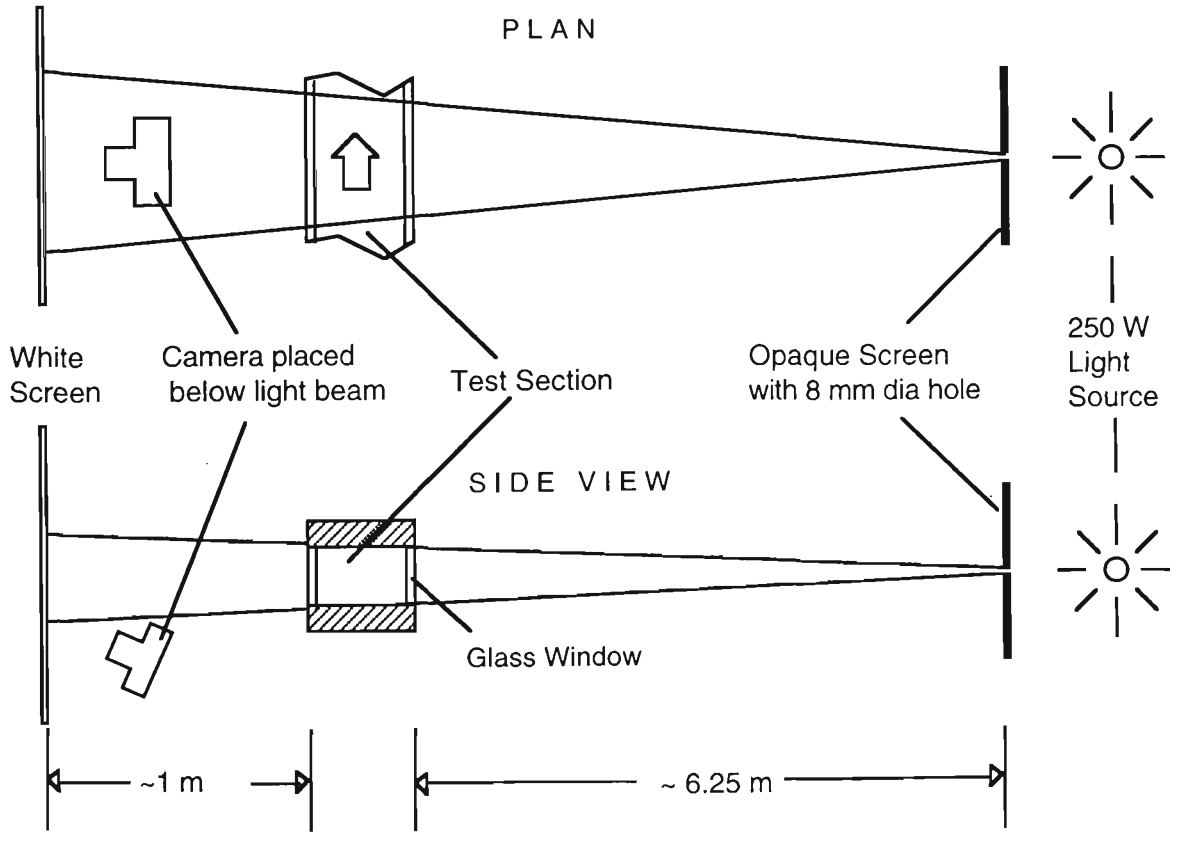

Figure 10.14 Shadowgraph System

It was found that with the experimental arrangement as described above, it was possible to carry out a variety of tasks, viz. regulating the upstream pressure valve to initiate the flow, and obtaining a photographic record of the shadowgraph image on the screen, etc. single-handedly with reasonable ease.

In the next chapter, results of the experimental investigation are presented.

Chapter 11

EXPERIMENTAL INVESTIGATION

Detailed analytical investigation of the SAI seems to indicate that the device is a feasible proposition. In this chapter, results of the experimental investigation are reported.

Establishment of supersonic flow in the de Laval nozzle is a crucial feature of the flow in the SAI. Preliminary 'air-only' tests were conducted to compare the design performance of the nozzle with its actual performance.

11.1 Nozzle Flow

If the pressures at the inlet and outlet of a converging-diverging nozzle are controlled independently, it is possible to get various flow regimes in the nozzle. For example, for a fixed upstream (inlet) pressure, if the back (outlet) pressure is continuously reduced, the pressure along the length of the nozzle varies as shown qualitatively in Figure 11.1.

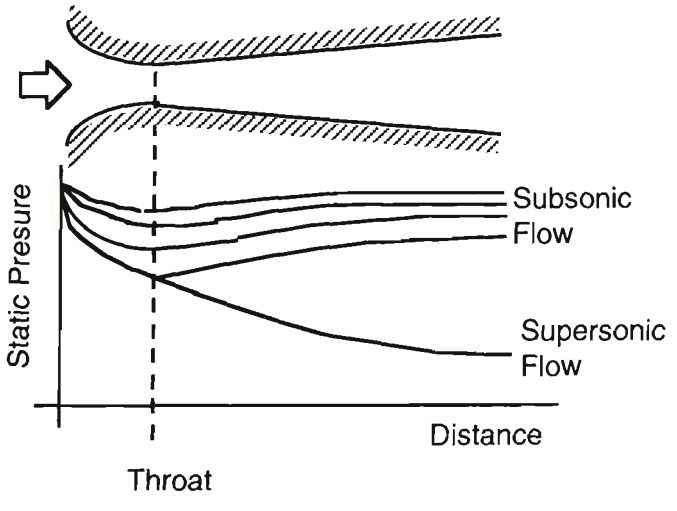

Figure 11.1 de Laval Nozzle Flow

For a relatively small drop in pressure from inlet to outlet, the flow undergoes acceleration in the convergent part of the nozzle with a corresponding drop in pressure, but deceleration accompanied by pressure increase in the divergent part, which acts as a subsonic diffuser. The nozzle behaves as a venturi [F3], and this is characteristic of incompressible flow. This behaviour continues until a point of maximum velocity and minimum pressure is reached at the throat, where the flow attains sonic conditions and the flow is choked. This corresponds to the maximum possible mass flow rate through the nozzle for the given upstream condition. Upon further reduction in back pressure, the flow attains supersonic velocities in the divergent part. The pressure drops continuously throughout the converging-diverging nozzle, provided there is no shock at some point in the divergent part.

From the above, it is seen that if the conditions at the inlet and outlet to the nozzle are adjusted such that a pressure drop is observed in the *divergent* part of the nozzle, it can be concluded that the flow has attained supersonic speeds there, and that the throat is 'choked'. This conclusion, based only on wall pressure measurements, can be subsequently tested by flow visualisation using the shadowgraph technique.

It is assumed in Figure 11.1 that at the downstream end of the given nozzle, a sufficiently powerful device such as a vacuum pump or inductor operates to maintain the back pressure at the required low value. This procedure involving reducing the downstream pressure was attempted initially. However, it was found that with the devices (inductors) available, it was not possible to maintain low pressures at the downstream end. The alternative was to keep the downstream end open to the ambient, and gradually increase the inlet pressure. This was easily possible using the high-pressure air supply available. A pressure regulator at the inlet to the stagnation chamber helps to maintain the high pressure in the stagnation chamber. This procedure does not change the flow qualitatively, because the absolute values of inlet and outlet pressures are not important, but only their relative values. It is also considerably easier to conduct test runs with the downstream end open to atmospheric conditions.

Figure 11.2 shows the result of the above procedure. The static pressure measured at the wall of the nozzle is plotted against the 200 mm distance along the nozzle from the stagnation chamber to the injection tube exit plane. The approximate demarcation between subsonic and supersonic flows is shown. It can be seen that very high suction pressures can be attained at injection tube exit plane.

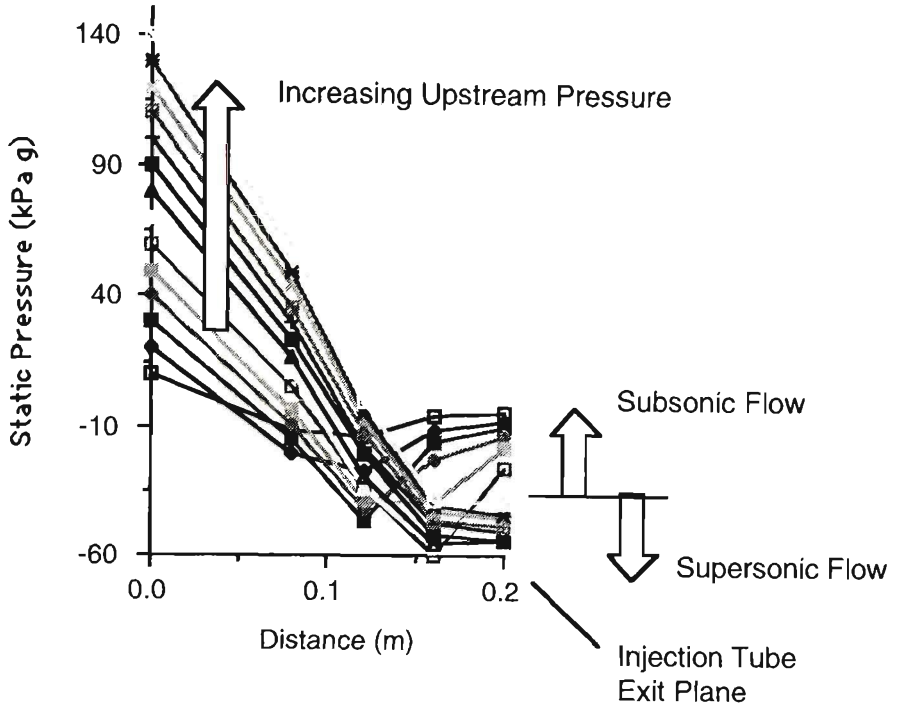

Figure 11.2 Wall Pressure in Nozzle Region

Figure 11.3 shows a comparison between the design pressure variation in the nozzle and interaction regions for air-only flow.

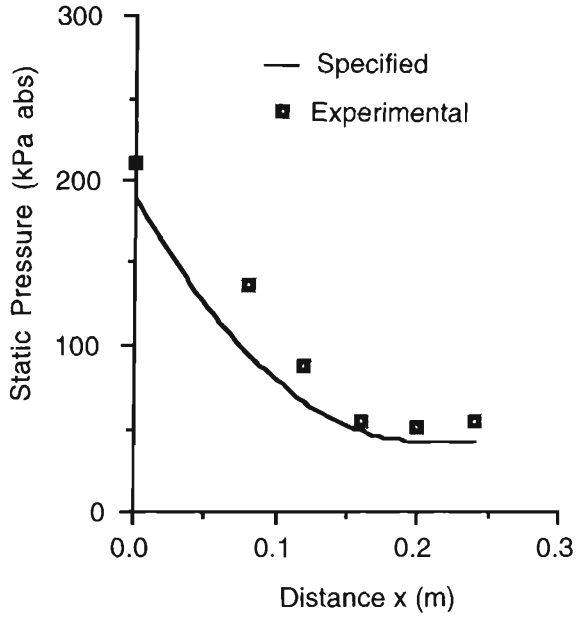

Figure 11.3 Wall Pressure in Nozzle and Interaction Regions

The slight difference between specified and experimental pressure values in the nozzle region ($0 \leq x \leq 0.2$m) can be attributed to frictional effects due to roughness of the nozzle wall. Although wall friction is accounted for while designing the nozzle (Chapter 4), the roughness parameter value used in the computer programme is likely to be different from the actual average height of roughness elements in the nozzle duct.

Also, in the interaction region, ambient air is sucked in due to creation of the relative low-pressure zone at the injection tube exit plane, and this mixes with the supersonic flow in the nozzle. The duct is designed for constant-pressure interaction between the primary air flow and secondary flow in the form of a suspension. In this air-only test, however, a slight increase in pressure in the interaction zone is evident as the slower secondary air mixes with the supersonic primary air. This indicates that the mixing process makes it difficult for the combined flow to reach supersonic speeds, at least in case of air-only flow. To achieve supersonic combined flow for some distance downstream of the injection tube exit plane, a slightly higher stagnation pressure is required, compared with the design value.

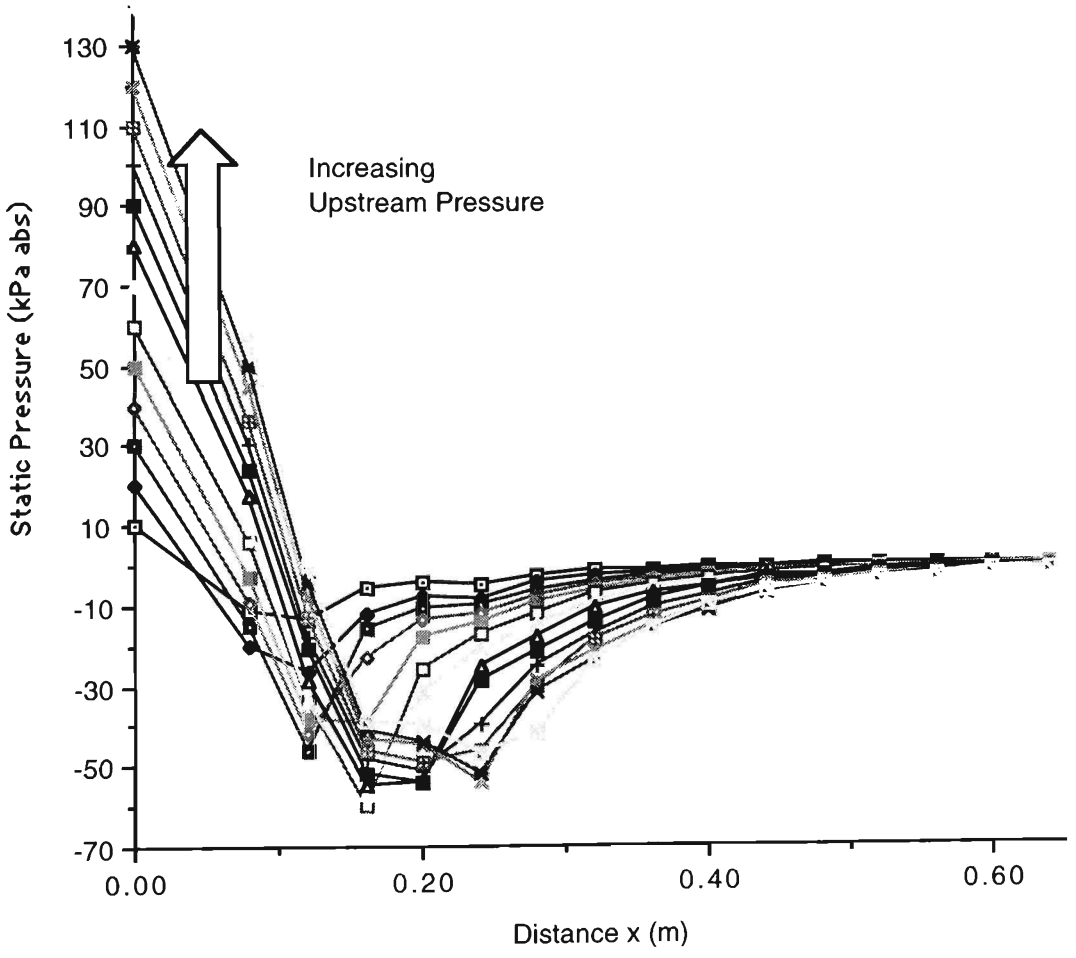

Figure 11.4 Wall Pressure in SAI Duct

Figure 11.4 shows detailed wall pressure measurements along the entire SAI duct for gradually increasing upstream stagnation pressure. The downstream end is maintained at atmospheric conditions by keeping the downstream valve fully open. Once the flow is established, it is a simple matter to raise the downstream pressure by partially closing the manual valve at the downstream end. Because the flow is choked, and supersonic in a large part of the cross section (except the boundary layers), the change in the downstream pressure condition is not communicated upstream. The result is that the

secondary flow, starting at atmospheric conditions, is conveyed to regions of higher pressure. It was found that a maximum downstream pressure of about 150 kPa abs could be attained this way. For a higher downstream pressure, the entire flow suddenly goes subsonic.

The very high suction levels attainable at injection tube exit plane are clearly seen, the minimum observed pressure being about -65 kPa g. Interaction with ambient air drawn in through the injection tube is such that pressure recovery of the combined stream to the final destination takes place as shown.

11.2 Air-Only Flow without Injection Tube

The above observation prompted an air-only test with the injection tube completely removed from the duct. This would eliminate mixing with the secondary flow, and should theoretically make it possible to establish supersonic flow further downstream of the throat with relative ease. Figure 11.5 shows the result of a particular air-only run carried out to test this hypothesis. In such a nozzle flow without the additional complication of the secondary flow, it would also be easier to visualise the shock in the duct. In case a pseudo-shock pattern is observed, it would also be possible to test the models presented in Chapter 6.

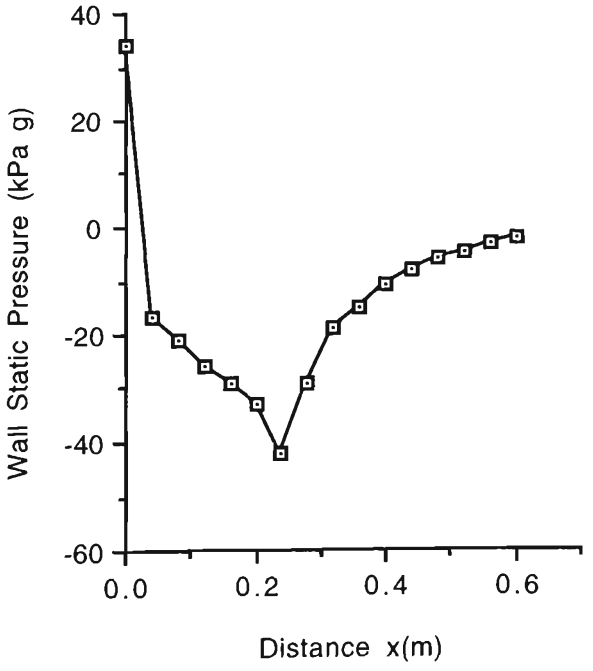

Figure 11.5 Air-Only Flow without Injection Tube

It is clearly seen that establishing supersonic flow (indicated by continuously decreasing pressure values throughout the converging-diverging nozzle to about $x \leq 0.23$ m) is possible with much lower upstream pressures. Figure 11.4 shows a particular case in which a stagnation chamber pressure of only 34 kPa g was sufficient to produce a minimum pressure of -42 kPa g at 0.23 m from the stagnation chamber. This corresponds to an isentropic Mach Number value of about 1.314. Subsequent pressure recovery to ambient conditions at the downstream end is seen to occur gradually, not abruptly, suggesting the existence of a pseudo-shock in the core of the flow.

11.3 Comparison with Diffusion Model

Since at this stage only wall static pressures are available as experimental data, these can be compared with the predictions of the Diffusion Model (Chapter 6). Such a comparison appears in Figure 11.6. The comparison indicates that at least for this moderate upstream Mach number, the diffusion model predicts pressure rise in the upstream part of the compression region with reasonable accuracy. It also appears that the concept of 'hydraulic diameter' can be used to non-dimensionalise distance along the flow in this case of non-axisymmetric flow.

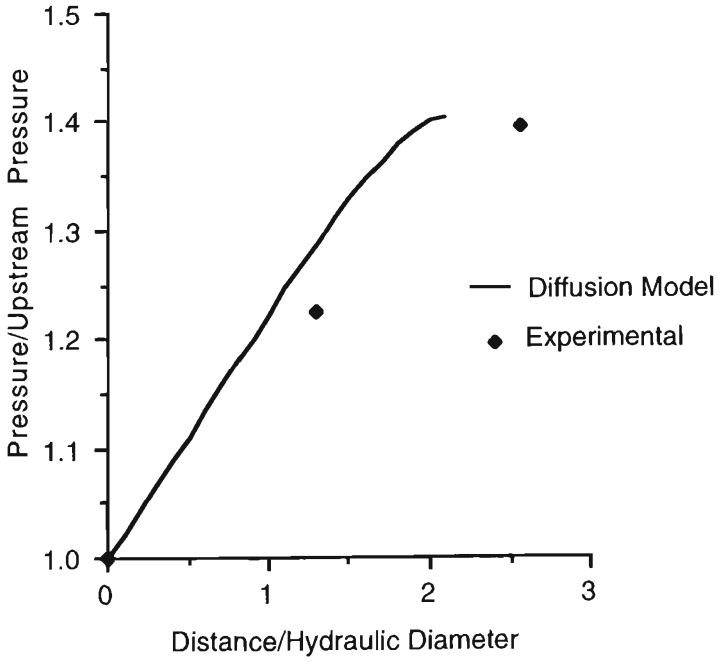

Figure 11.6 Comparison with Diffusion Model

11.4 Pseudo-Shock in Air-Only Flow

Figure 11.7 presents visual evidence of the existence of a series of normal shocks in the SAI duct.

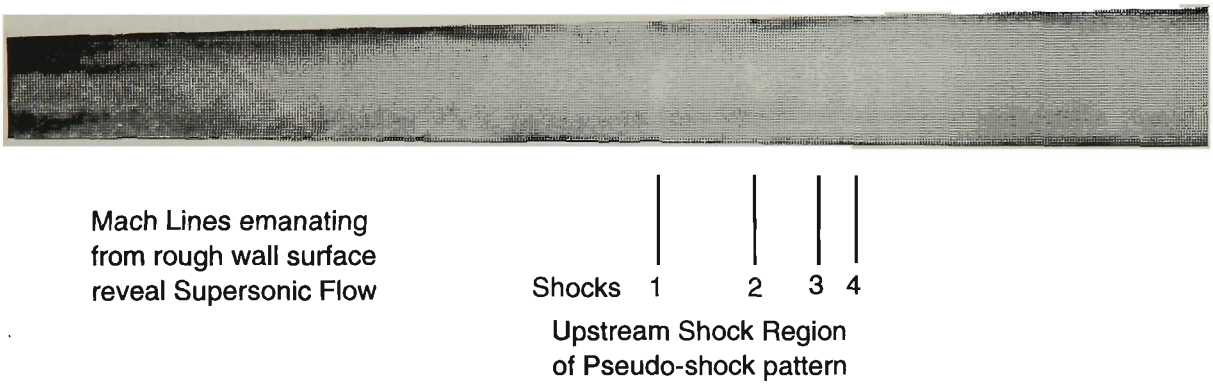

Figure 11.7 Shadowgraph of Pseudo-Shock

Mach lines, or weak oblique shocks emanating from the roughness elements on the upper and lower nozzle walls are seen in the upstream part of the flow. It is noticed that the Mach lines are clearer than the normal shocks comprising the pseudo-shock train. This can be attributed to the fact that the Mach lines are stationary, whereas the normal shocks tend to oscillate about a mean position [I3].

It is possible to estimate the upstream Mach number from the formula [W7]:

$$\text{Mach Number} = \frac{1}{\text{Sin(Mach Angle)}} \tag{11.1}$$

Existence of at least three or four shocks is evident from the bright lines in the core of the flow. Distances between the lines decreases with increasing downstream distance. This confirms the finding reported in the literature [O1, etc] that the inter-shock distance is progressively reduced in a pseudo-shock pattern. The lines are also progressively shorter, indicating gradual reduction in core area downstream of the initial shock. This is the upstream shock region of the pseudo-shock.

It appears that the fourth normal shock could be the 'limiting' shock in the flow. Downstream of this shock, the effect of mixing between core flow and boundary layer flow is such that an 'aerodynamic nozzle' (Chapter 6) is not formed in the core, and the core flow cannot undergo reacceleration to supersonic speed. Downstream of the limiting shock, flow throughout the entire cross section attains sonic conditions. Thereafter, pressure continues to rise in the 'mixing' region of the pseudo-shock, in which the flow is further decelerated to subsonic speeds.

11.4.1 Comparison with 'Modified-Fanno' Model

As seen in Chapter 6, an important feature of the 'Modified-Fanno' model is that it allows prediction of distances between successive shocks in a pseudo-shock pattern. This prediction is based upon a Second Law analysis of the pseudo-shock, and the newly postulated 'core friction factor'. The prediction can be tested using the available shadowgraph record. As in Chapter 6, distance along the flow must be non-dimensionalised with respect to the local hydraulic diameter for the rectangular cross section nozzle duct. The hydraulic diameter is calculated from the formula:

$$\text{Hydraulic Diameter} = \frac{4(\text{Flow Area})}{\text{'Wetted' Perimeter}}$$

$$= \frac{4\,(\text{height})(\text{width})}{2(\text{height} + \text{width})}$$

For an upstream Mach angle of about 46° the corresponding upstream Mach number is about 1.4. For this value of initial Mach number, the modified-Fanno model yields the Mach number variation in the core as shown in Figures 11.8 and 11.9.

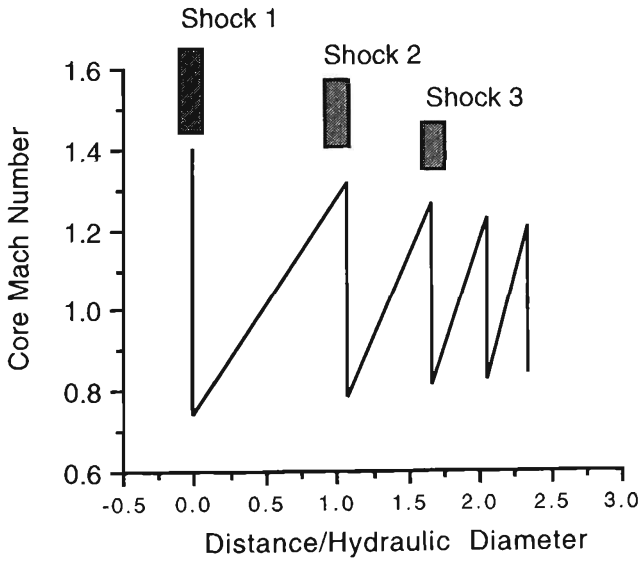

Figure 11.8 Core Mach Number in SAI (Air-Only)

It is seen from Figure 11.8 that the distance between the first and the second shock is calculated to be about 1 hydraulic diameter, and that between the second and the third shock about 0.6 hydraulic diameter. These distances are approximately those seen in the shadowgraph in Figure 11.7. These distances are crucially dependent upon the value of the newly defined 'core friction factor'. This is about 0.1, compared to the value of 0.062 used in Chapter 6.

Figure 11.9 shows a comparison between core Mach number variation as predicted by the Diffusion Model and the Modified-Fanno Model. As seen in Chapter 6, the Diffusion Model, which is an improved version of the 'Shockless' model, does not predict any shocks in the core of the flow, only an overall decrease in core Mach number. It is, however, interesting to note that of the total pseudo-shock length of about 4.6 diameters, the upstream shock region stretches for about 2.5 diameters, at which point the Diffusion model predicts a core Mach number of almost exactly 1. This appears to confirm the reported finding that the pseudo-shock can be divided into two distinct parts, viz. the upstream 'shock region' in which the flow is decelerated to sonic speeds, followed by the 'mixing region' in which the flow is further decelerated to subsonic speeds. The fourth or fifth shock predicted by the modified-Fanno model is likely to be the 'limiting shock'.

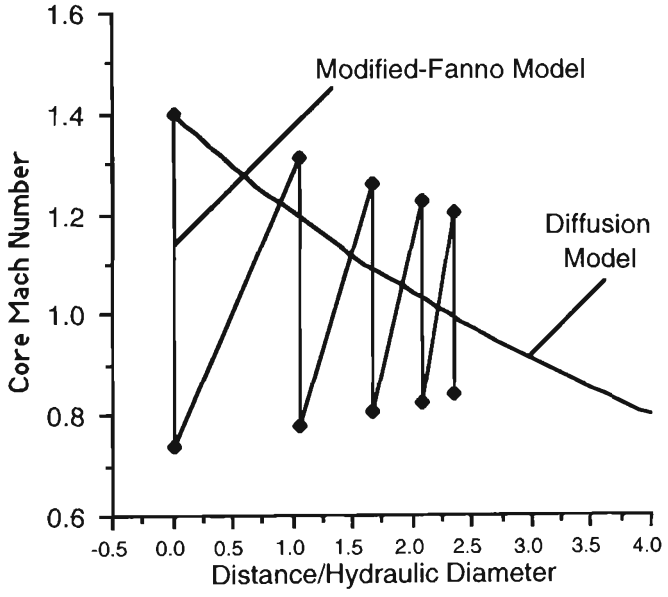

Figure 11.9 Core Mach Number Comparison in Shock Region

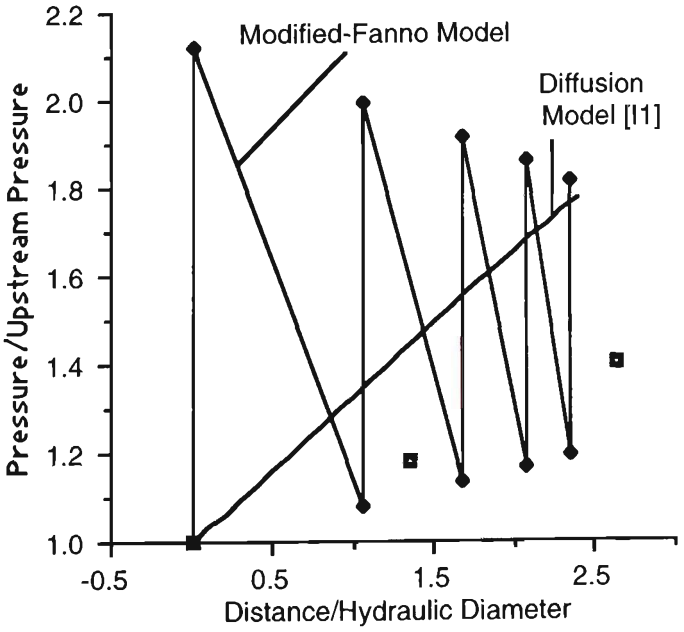

Figure 11.10 Pressure Ratio Comparison in Shock Region

11.5 Air-Only Interaction Region

In the previous sections, existence of a pseudo-shock in the SAI duct was confirmed and an attempt made to reconcile wall pressure readings and shock locations with predictions of available models. To determine the effect of the secondary stream on the flow in the interaction and compression regions, visualisations of air-only flow with the centrally located injection tube in place were carried out. Figures 11.11(a) to 11.14 (b) show the effect of increasing stagnation chamber pressure (100 kPa g to 130 kPa g) on the interaction immediately downstream of injection tube exit. These shadowgraphs show a gradual development of a pattern of shocks between primary-secondary flow interface and the duct wall. Figure 11.11(a) shows a faint pattern of shocks beginning to form on either side of the secondary air emerging from the injection tube. The corresponding wall pressure rise due to these shocks is shown in Figure 11.11(b).

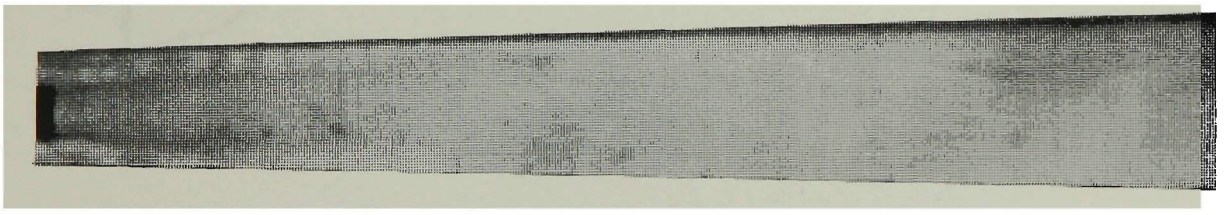

Figure 11.11(a) Interaction and Compression Regions (1)

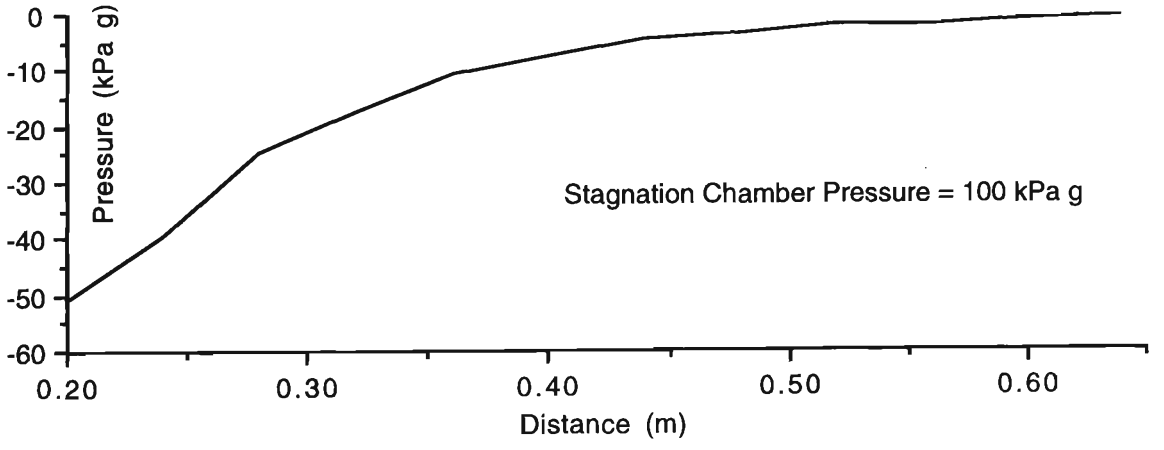

Figure 11.11(b) Wall Pressure in Figure 11.11(a)

The shocks increase in strength with higher upstream stagnation pressure, as seen in the shadowgraph in Figure 11.12(a) and the corresponding slightly more abrupt wall pressure increase in Figure 11.12(b). The abruptness in pressure rise increases in Figures 11.13 (a and b) and 11.14 (a and b) which show the effect of increasing the upstream stagnation pressure further. There is no evidence of shocks in the vicinity of the duct axis, as the combined flow in the core does not reach supersonic speeds

necessary for shock formation. The gradual obliteration of the line marking the interface indicates mixing between primary and secondary streams.

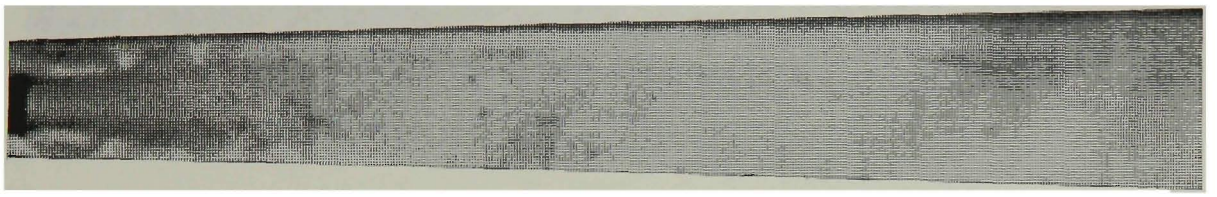

Figure 11.12(a) Interaction and Compression Regions (2)

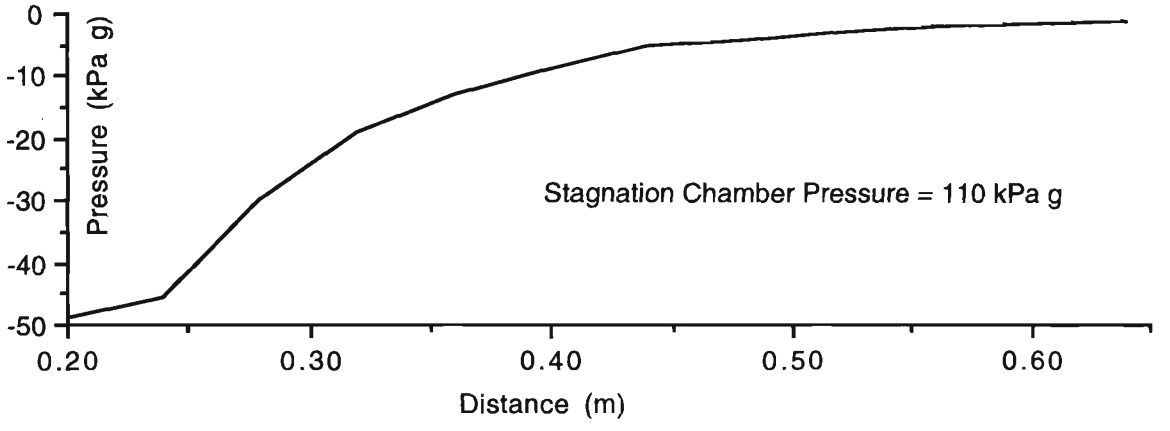

Figure 11.12(b) Wall Pressure in Fig. 11.12(a)

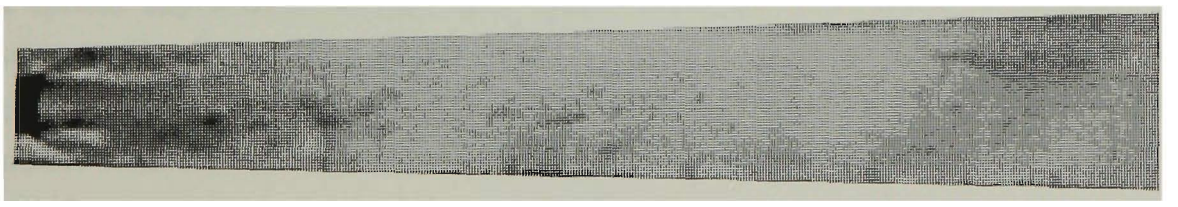

Figure 11.13(a) Interaction and Compression Regions (3)

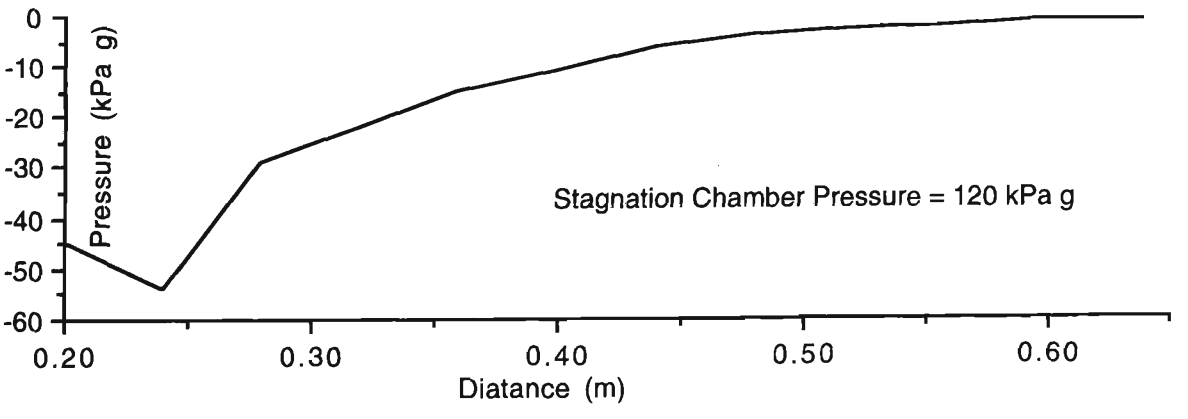

Figure 11.13(b) Wall Pressure in Fig. 11.13(a)

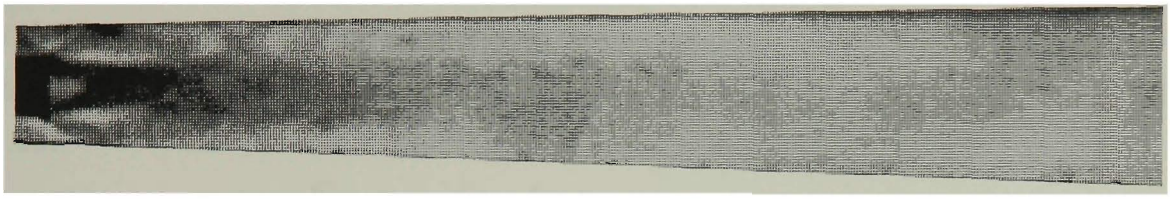

Figure 11.14 Interaction and Compression Regions (4)

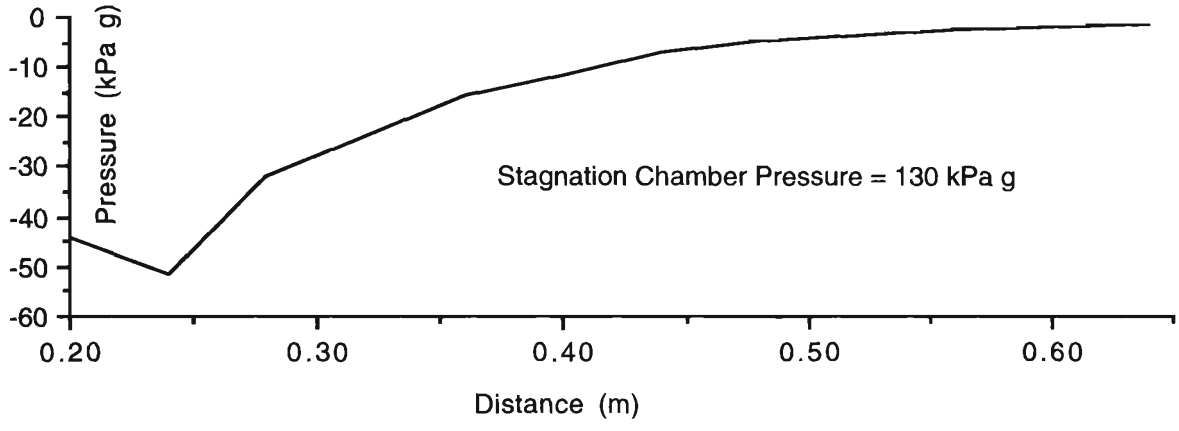

Figure 11.14(b) Wall Pressure in Fig. 11.14(a)

The shape of the line marking the interface suggests that the secondary stream does not spread appreciably in the cross-stream direction. This seems to confirm the assumption made in developing expressions for driving potentials in the interaction region in Chapter 5. It is safe to predict that this observation for an air-only flow will continue to be true for interaction between primary air flow and a heavier suspension flow, due to the greater inertia associated with the suspension flow. The lighter triangular region adjacent to the injection tube exit may reveal the extent of the 'potential core', or the 'initial region' of interaction refereed to in Chapter 5. This potential core seems to be very short, and may provide justification for the assumption made in section 5.4.1 made during the course of developing an expression for the potential core length. It is interesting to compare the shadowgraph in Figure 11.14 with the model for mixing co-flowing streams (Figure 5.2) used for developing expressions of the driving potentials in the interaction region.

11.6 Flow in Injection Tube

An estimate of the nature of flow in the injection tube can be obtained from the observed value of pressure at injection tube inlet. This is observed to decrease with

increasing stagnation chamber pressure, with the minimum value being about -10 kPa g for the maximum stagnation chamber pressure tested. This observation can be used to estimate the velocity of the secondary stream at injection tube inlet, as shown in Figure 11.15.

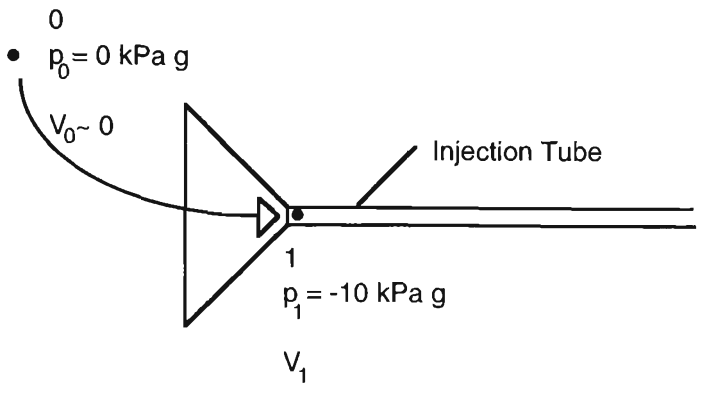

Figure 11.15 Injection Tube Inlet

Figure 11.15 shows a hypothetical streamline in the ambient air flow as air is sucked in due to creation of a low-pressure zone at the injection tube exit. The streamline stretches from point '0' in the stationary atmosphere to point '1' at injection tube inlet. Assuming no losses between these two points, Bernoulli's equation gives:

$$p_0 + \frac{1}{2}\rho_0 V_0^2 = p_1 + \frac{1}{2}\rho_1 V_1^2$$

Assuming $V_0 \sim 0$, an estimate for V_1 is obtained:

$$V_1 = \sqrt{\frac{2(p_0 - p_1)}{\rho_1}}$$

The corresponding inlet Mach number and mass flow rate in the injection tube can be calculated from

Inlet Mach number = $V_1/(\gamma RT)$
and
mass flow rate = ρV_1 (Injection Tube Area)

For increasing stagnation chamber pressure, it is clear that higher levels of suction are achieved at injection tube exit plane. This results in progressively increasing mass flow rates through the injection tube, as it draws in air at atmospheric conditions. Figure 11.16 shows the variation of air mass flow rate through the injection tube with increasing stagnation chamber pressure. The mass flow rate increases and appears to

approach a value of about 0.025 kg/s asymptotically. For this particular injection tube, this value indicated the maximum air mass flow rate, corresponding to a choked flow with sonic conditions at the exit.

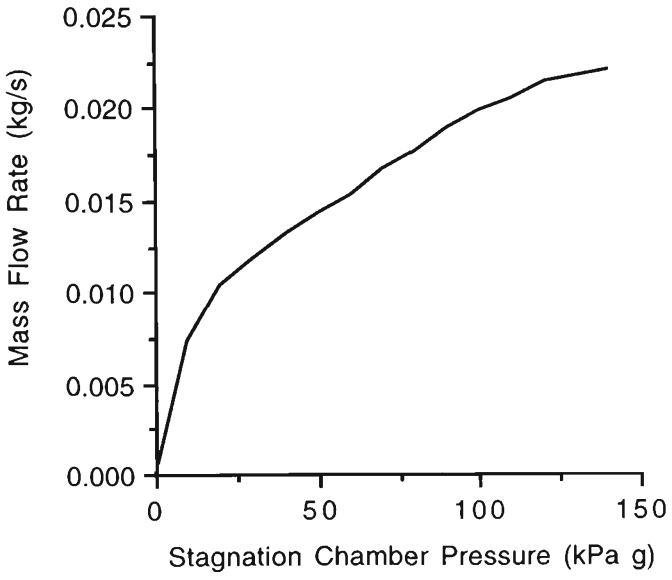

Figure 11.16 Injection Tube Mass Flow Rate

Whether the sonic condition is actually achieved in this particular case depends upon the length of the injection tube. This can be determined by evaluating the initial Mach number of secondary flow at injection tube inlet. Figure 11.17 shows the variation of injection tube inlet Mach number with increasing stagnation chamber pressure.

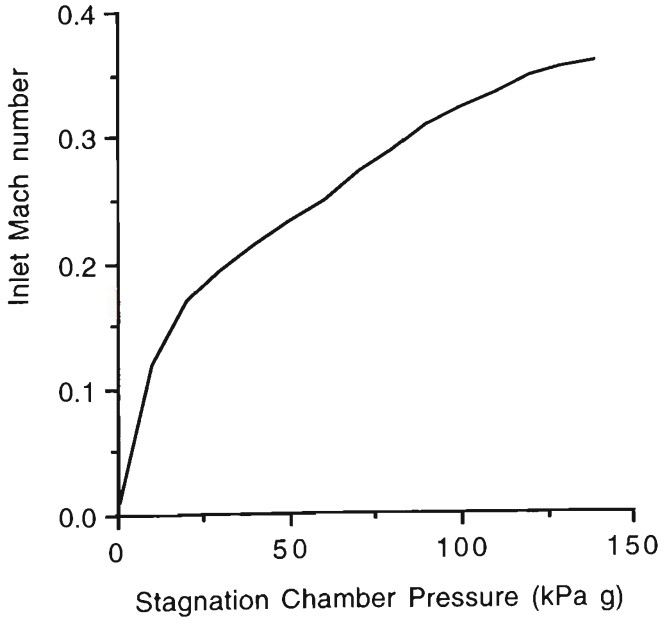

Figure 11.17 Injection Tube Inlet Mach number

For a typical experimentally observed pressure drop of 7 kPa between '0' and '1', this gives V_1 = 126.5 m/s. Again assuming negligible temperature difference between '0' and '1', and that T_0 = 25°C = 298 K, this corresponds to a Mach number of about 0.3 for the incoming clean air. Referring to Figure 11.18, we see that for this initial Mach number, clean air would reach sonic conditions at injection tube exit if the tube were about 200 (hydraulic) diameters long. The actual (Length/Hydraulic Diameter) ratio of the particular injection tube in this project can be calculated: For a width of 30 mm and height of 5 mm (See Chapter 3 for design parameters), the hydraulic diameter is

$$\text{Hydraulic Diameter} = \frac{4(\text{Area})}{\text{Wetted Perimeter}} = 8.57 \text{ mm}$$

so that

$$\frac{\text{Length}}{\text{Hydraulic Diameter}} = 116.7$$

for this meter-long tube.

It can therefore be concluded that this particular injection tube is not long (slender) enough to accelerate clean air to sonic conditions at the exit. However, it appears from the analysis in Chapter 3 and Figure 11.18 that a gas-solids suspension entering at a comparable Mach number can be easily accelerated to its sonic speed at the exit. This lends credence to the initial assumption that the suspension undergoes a Fanno-type flow in the injection tube (Chapter 3).

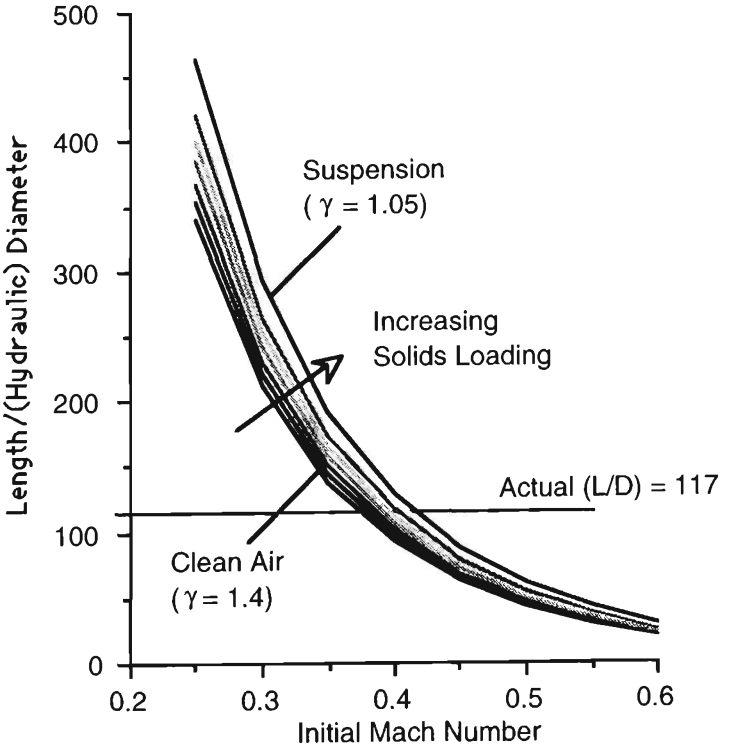

Figure 11.18 Suspension Flow as Fanno Flow

11.7 Introduction of Particles

As mentioned in Chapter 3, the particulate matter chosen for the present study is glass beads of nominal diameter 150 microns. These are introduced into the injection tube by a vibratory feeder perched above the solids inlet funnel, as shown in Figure 11.19.

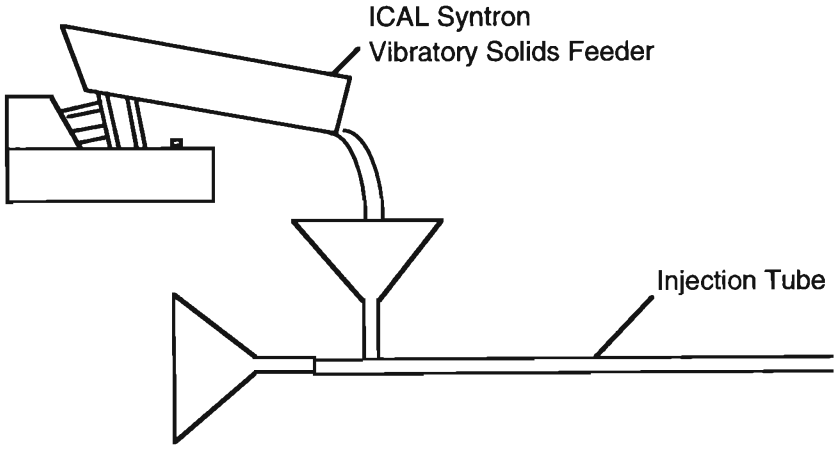

Figure 11.19 Particle Feeding

Preliminary tests were conducted to see the effect of the particles on the shadowgraphs. With the introduction of particles, a sudden shadow appeared on the screen, indicating that light from the source was almost completely cut off from the screen. Later investigation revealed that the shadow was due to a white dusty coating on the inside of the test section glass window. It appears as if there is considerable degradation of the glass 'beads' as they are sucked rapidly into the funnel and sent hurtling down the injection tube. The beads seem to be shattered as they travel along the tube and collide repeatedly with the injection tube walls, and emerge in the form of glass dust. This obliterates the shadowgraph to a great extent, and no useful information can be gathered from the image on the screen.

An attempt was therefore made to photograph the interaction region directly. Figure 11.20 shows a typical example. The shape of the interface suggests that in the vicinity of the point of emergence, the suspension remains confined around the nozzle axis. The spread further downstream could be due to the pressure rise associated with shocks in the flow, and also due to slight asymmetry in the in velocity profile of the primary flow. The shocks, however, cannot be observed in this direct photograph.

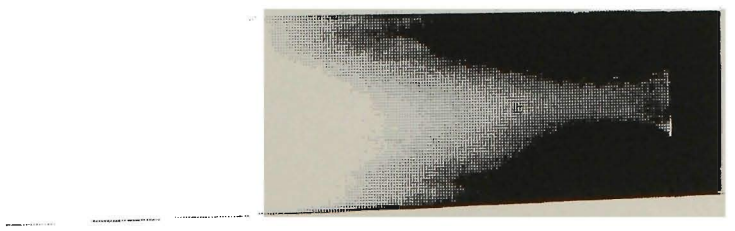

Figure 11.20 Emerging Suspension

Degradation of glass beads as they travel along the injection tube length reduces the size of the emerging particles considerably. However, this circumstance does not affect the properties of the suspension defined in Chapter 3. This is because the properties are defined in terms of the volume fraction occupied by the particles, and the volume fraction is unaffected by particle size. The reduced size will only result in a change in drag experienced by each particle in the interaction region.

Chapter 12

CONCLUSIONS AND FURTHER WORK

Analytical and experimental investigations of a new type of particle injector as reported in the preceding chapters indicate that such a device is feasible. It is also much more easily controllable than originally imagined. This seems to be primarily due to the fact that the shape of the converging-diverging nozzle duct is adequate for producing supersonic flow, and any additional manipulation of upstream and downstream valves is unnecessary. However, to make the operation easier, many design improvements are possible.

12.1 Design Improvements

1 The high-pressure air supply inlet should have a diffuser (a length of gradually diverging duct) leading into the stagnation chamber (Figure 12.1). This will reduce the noise during operation of the device. The noise level even with the present design is tolerable, and seems in large measure due to the high-pressure supply air entering the stagnation chamber via an abrupt opening, impinging thereafter on the opposite wall of the stagnation chamber and on the injection tube which passes through the stagnation chamber.

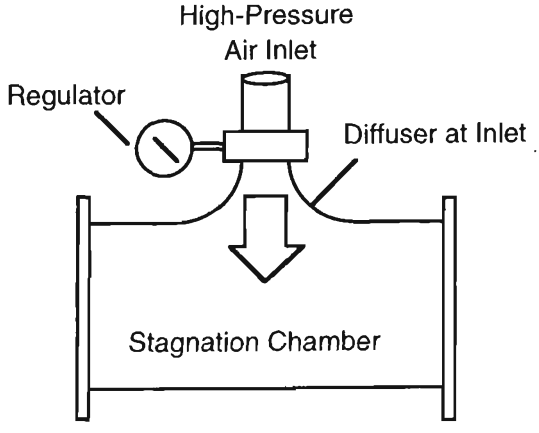

Figure 12.1 Stagnation Chamber Inlet Diffuser

The above design change will lead to further noise reduction, making more comfortable operation possible. This will also bring the air in the chamber closer to the 'stagnation' state without having to have a very large reservoir. With the present design, the air in the reservoir is probably in swirling motion, and perhaps enters the duct with an asymmetric velocity profile at the nozzle inlet, causing the asymmetric spread of suspension emerging from the injection tube.

2 It is found that the glass windows need frequent cleaning and wiping, due to condensation of water vapour in the ambient air drawn in through the injection tube.. Even in tests without the injection tube, condensation is observed on the outer surfaces of the glass windows due to the cooling effect of the high-speed flow inside. Condensation on the outer surfaces can be prevented to a great extent by spraying an anti-fogging fluid on them. The present design is such that the interior of the test section is not easily accessible, and can only be reached by a sponge wiper attached to a long stick through the opening on the far end of the stagnation chamber. The opening could be of a 'snap-on' type (with fewer nuts and bolts) for ease of operation. It should be mentioned that the primary purpose of the glass windows was to enable flow visualisation in this preliminary study. In an actual industrial application (such as inlet to a coal gasifier), glass windows will perhaps be unnecessary, and this particular difficulty will not arise.

3 Simultaneous pressure measurements are not possible with the present pressure measurement manifold. It would be much better to visualise the pressures along the duct using an on-line data logging system. A multi-tube mercury manometer will enable such 'visualisation', but excessively long manometer tubes may be required, especially for higher stagnation chamber pressures. In the present design, pressure taps at 15 stations along the test section could be accommodated. An equal number of pressure taps on the opposite side of the test section will make even more detailed wall pressure readings possible. This refinement would probably be necessary in case of more in-depth investigation of the pseudo-shock pattern.

4 More detailed study of the pseudo-shock will also entail pressure measurements throughout the cross-section of the test section, possibly by means of a pitot-static tube traversing both the streamwise and cross-stream directions.

5 The main reason for opting for a rectangular cross section duct in the present study was to make flow visualisation possible. In actual industrial applications, a circular cross section nozzle with a concentric injection tube would be more advisable.

6 A principal design objective in such a device should be to reduce the initial lag in velocities between primary and secondary streams as much as possible. In the present design, it was somewhat fortuitous that the injection tube is a long one, which enables the suspension flow in the injection tube to approach Fanno-type flow with the suspension emerging at its near-sonic speed. This cannot be regarded as a standard feature of devices of this type. For a constant cross section injection tube, a sonic speed is the maximum that can be attained. This imposes a limit on the initial velocity lag attainable using a constant-area injection tube. The initial velocity lag could be further reduced by designing the injection tube in the form of a concentric de Laval nozzle inside that for the primary flow (Figure 12.2). The suspension would then emerge at a supersonic speed with reduced initial velocity lag between primary and secondary streams.

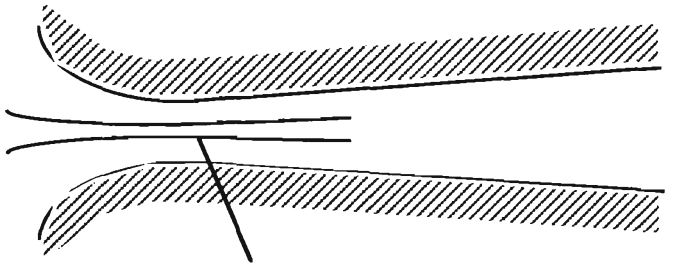

Injection Tube in the form of a de Laval nozzle would enable suspension to emerge at supersonic speed into enveloping primary gas flow, thus reducing initial velocity difference and making subsequent acceleration easier.

Figure 12.2 Injection Tube Design Modification

5 More fine-tuning of visualisation technique is required. The shadowgraph system does allow relatively simple shock visualisation, but it should be possible to obtain sharper images on the screen. It appears that the most important parameters affecting the quality of shadowgraphs are:

1 Distance between light source and test section;
2 Distance between test section and screen;
3 Intensity of light source;
4 Size of aperture between light source and test section.

These variables could be adjusted to maximise shadowgraph clarity.

6 Fine tuning of the photographic technique is also necessary. It should be mentioned that although the shadowgraph appears clear enough to the naked eye, it is less so on the developed film. It can be seen that the Mach waves emanating from wall

roughness elements are stationary, while the bright lines revealing the pseudo-shock pattern oscillate about a mean position. A shutter speed of $^1/_{125}$ s seems to capture the shocks reasonably well, for the light intensity used. A lower shutter speed results with the same light intensity results in less light being transmitted onto the photographic film, making for a darker image.

12.2 Further Research

The present project points beyond itself to a number of related areas in which further research is possible:

1 It was demonstrated that a supersonic flow nozzle can be designed and fabricated using a variation of the Generalised Steady One-Dimensional flow analysis procedure. It may be possible to develop this technique further into a standard nozzle design procedure.

2 A crucial feature of the SAI design has been the assumption (based on reported findings) that the presence of solid particles affects the speed of sound associated with the medium. In a broad sense, this assumption seems to be corroborated by the present investigation. However, detailed analytical and experimental investigation into this aspect of suspensions seems to be necessary, and will presumably find many applications in the pneumatic conveying field [eg G6].

3 It could be in principle possible to derive quantitative information from the shadowgraph record obtained. This would presumably entail digital image processing of the shadowgraph. For example, a certain intensity of illumination on the screen can be associated with a certain value of density, and the entire density (and consequently pressure, etc.) field mapped on the basis of such calibration. Mach number can be easily determined from Mach angle wherever Mach lines are visible. Temperature measurements can yield the sonic speed. Velocity fields can thus be determined from Mach number and sonic speed.

4 The very high suction levels attainable with the device suggest that more efficient and powerful inductors could be fabricated using similar designs.

5 Because flow visualisation is possible with the present experimental facility, its possible use is not confined to the project on hand. It can be easily used as a

supersonic flow testing facility in its own right, as was demonstrated during the investigation of pseudo-shocks in clear air (operation without injection tube).

6 Investigation of the pseudo-shock phenomenon revealed that the upstream shock region of this pattern can be modelled as a 'Modified-Fanno' flow. It was necessary to postulate a 'core friction factor' during the development of this model. In the present version, the core friction factor is assumed to be constant throughout the shock region. No attempt was made to correlate this parameter with variables such as upstream Mach number. For a given pseudo-shock pattern, this parameter could also be a function of distance [Y5]. This investigation was based on a second law analysis of the shock region. Since the second law imposes general restrictions on what is achievable in practice, further study along the same lines (eg. irreversibility and availability analysis) could provide more insight [B5].

7 It is necessary to carry out more research using different particles, to assess the possible industrial applications of the device in gasifiers, etc.

References

A1 Abramovich, G N, *The Theory of Turbulent Jets* , MIT Press ,1963

A2 Anderson, J D, *Modern Compressible flow with Historical perspective* McGraw-Hill, 1982

A3 Alpinieri, L J, *Turbulent mixing of co-axial jets*, AIAA journal, vol 2, No. 9, Sept. 1964, p. 1560-1567

A4 Abbot, S W, Smoot, L D, Schadow, K, *Direct mixing and combustion efficiency measurements in ducted, particle-laden jets* , AIAA Journal, vol 12, no. 3, March 1974

A5 Arastoopour, H, *Pneumatic Transport of Solids*, Chapter 11, p. 349-382, Encyclopaedia of Fluid Mechanics, N P Cheresiminoff, ed., Gulf Publishing House, Houston, Texas, 1986

B1 Boothroyd, R G ,*Similarity in Gas-borne particle suspensions*, Journal for Engineering for Industry, May 1969, p. 303-314

B2 Boothroyd, R G , *Flowing Gas-Solids Suspensions,* Chapman and Hall Ltd, London, 1971

B3 Brodkey, R S, *Turbulent motions, Mixing and kinetics*, Fluid mechanics of mixing, ASME, 1973

B4 Bhattacharya, D, Gauvin, W H, *Modelling of heterogeneous systems in a plasma jet reactor,* AIChE journal, vol 21, No 5, Sept 1975, p. 879-885

B5 Bohnet, M, *Design of gas-solids injectors*, Handbook of fluids in motion, Cheresiminoff & Gupta, eds., Ann Arbor Science, 1986, p. 785-805

B6 Bejan, A, *Entropy generation in heat and fluid flow*, John Wiley & Sons, 1982

B7 Bodle, W, Hueber, W, *Coal Gasification* , Chapter 10, Coal Handbook, R A Meyers ed., Marcel Dekker Inc., 1981, p 494.

C1 Catalano, G D, Morton, J B, Humphris, R R, *Experimental Investigation of an axisymmetric jet in a co-flowing air stream*, AIAA J.,vol 14, no 9, Sept. 1976, p. 1157-1158

C2 Cohen, N S, *A correlation of the spread and decay of turbulent free jets*, AIAA J., vol 4, no 5, May 1966, p. 929-930

C3 Crowe, C T, *Gas-particle flow*, Pulverized coal combustion and gasification, Smoot and Pratt, Plenum press, 1979

C4 Corcos, G M, Sherman, F. S., *The mixing layer - Deterministic models of a turbulent flow*, Part 1-Introduction and the two-dimensional flow, JFM 1984, vol 139, p.29-85

C5 Corcos, G M, Lin, S J, *The mixing layer - Deterministic models of a turbulent flow,* part 2- The origin of three-dimensional motion, JFM 1984, vol 139, p. 67-95

C6 Carrier, G F, *Shock waves in a dusty gas*, J FM, vol 4, p 376-382, 1958

C7 Chanapragada, R S, *Compressible jet spread parameter for mixing zone analysis,* AIAA J., vol. 1, no 9, Sept 1963, p 2138-2190

C8 Cheney, W, Kincaid, D, *Numerical Mathematics and computing,* Brooks-Cole Publishing co., 1985

C9 Carroll, B F, Dutton, J C, *Characteristics of Multiple Shock wave/Turbulent Boundary layer interactions in rectangular duct* , J. Propulsion, vol 6, no 2, p 186-193

C10 Carroll, B. F, Dutton, J C., *Turbulence phenomena in a Multiple Normal shock wave/Turbulent Boundary-layer interaction*, AIAA Journal, vol. 30, no. 1, January 1992, p 43-48

C11 Carroll, B F, Dutton, J C, *Multiple normal shock wave/turbulent boundary-layer interactions*, J Propulsion and Power, vol 8, no 2, Mar-Apr 1992, p 441-448

C12 Carroll, B F, et al, *Computations and Experiments for a Multiple Normal Shock/Boundary Layer Interaction*, J Propulsion and Power, vol 3, May-Jun 1993, p 405-411

D1 Davidson, G A, *Turbulent diffusion in an aerosol jet*, J of Aerosol science, 1975, vol 6, p 227-247

D2 Duggins, R K, *The mixing of a jet with a parallel stream,* The fluid mechanics of Mixing, ASME, 1973

E1 Einstein, A, *A new determination of molecular dimensions,* Investigation on the theory of Brownian motion, R Furth, ed, Dover 1956

F1 Field, M A, Gill D W, Morgan, B B, Hawksley, P G W, *Combustion of pulverized fuel- Pt 2 -Flow patterns and mixing* , The British Coal utilization research association monthly bulletin, vol XXX, No 12, Nov-Dec 1966, part II, p 455-513

F2 Forde, M, *Quasi-one-dimensional gas-particle nozzle flows with shock,* AIAA J, vo; 24, no 7, July 1986, p 1196-1199

F3 Fox, R W, McDonald, A T, *Introduction to Fluid Mechanics,* 4th Edition, John Wiley and Sons, Inc., 1994

G1 Gal, G, *Self preservation in fully expanded turbulent co-flowing jets,* AIAA J, vol 8, no 4, Apr 1970, p 814-815

G2 Gregor, W, *The interaction between particles and gas in an air classifier* ASME 76 WA/FE-32

G3 Griffin, M D, Anderson, J D, *On the application of boundary conditions to the time-dependent computations for quasi-one-dimensional flow,* Computers and fluids, 1977

G4 Gregor, W, *Dispersed two-phase flows at high velocities* , Chapter 13, p. 399-420 Encyclopaedia of Fluid Mechanics, N P Cheresiminoff, ed., Gulf Publishing House, Houston, Texas, 1986

G5 Godbole, A R, Soh, W K, Wypych P W, *The Pseudo-Normal Shock as 'Modified-Fanno' Flow,* Proceedings of IASTED MSO'97, Singapore, 1997, p. 91-95

H1 Harsha, P T, *Free turbulent mixing : a critical evaluation of theory and experiment* , AEDC-TR-71-36

H2. Hedman, P O, Smoot, L D, *Particle-gas dispersion effects in confined coaxial jets*, AIChE J, Vol 21, no 2, March 1975, p 372-379

H3 Hasinger, S H, *A new method for calculating ducted flows* , AIAA Journal, Jan 1984, p 141-143

H4 Hayashi K, Branch, M C,*Concentration, velocity and particle size measurements, in gas-solids two-phase jets* J. Energy, Vol 4, No 5, Sept-Oct 1980, p 193-198

H5 Hunt, V D, *Activity Report - Coal*, Chapter 3, p. 135, Handbook of Energy Technology, part III

I1 Ikui, T, Matsuo, K, Nagai, M, *The mechanism of pseudo-shock waves*, Bulletin of the J S M E, vol 17, no 108, June 1974, p. 731-739

I2 Ishii, R, *Motion of small spheres in a gas flow,* Physics of fluids, 27 (1), Jan 1984, p 33-41

I3 Ikui, T, Matsuo, K, Nagai, M, Honjo, M, *Oscillation phenomena of pseudo-shock waves,* Bulletin of the J S M E, vol 17, no 112, Oct 1974, p 1278-1285

I4 Ishii, R, Umeda, Y *Free jet flows of gas-particle mixtures,* AIAA-86-1371

I5 Imrie, B W, *Compressible fluid flow,* John Wiley and sons, 1973

J1 Jotaki, T, Tomita, Y, *Diffusion of a dusty gas* (Part 1. The velocity distribution of a dusty jet), Bulletin of the JSME, vol 17, no 112, Oct 1974, p. 1267-1271

K1 Keenan, J H, Neumann, E P, *Measurement of friction in a pipe for subsonic and supersonic flow of air*, J of Applied Mechanics, June 1946, A-91-A-100

K2 Kulik, R A, Weinstein, H, *Turbulence measurements in ducted co-axial flows*, Leithem, J, J AIAA J, vol 8, no 9, Sept 1970, p 1694-1696

K3 Kriebel, A R, *Analysis of Normal shock waves in particle-laden gas*, Transactions of ASME, J of Basic Engg, vol 86, no 4, Dec. 1964, p 655-665

K5 Kliegel, J R, *Gas-particle nozzle flows,* 9th Intern. Symp. Combust., p. 811-826, Academic Press, N Y, 1963

K6 Kliegel, JR, *One-dimensional flow of a gas-particle system,* IAS paper no 60-5

L1 Lukasiewicz, J, *Diffusers*, Experimental methods of Hypersonics, Marcel Dekker Inc, N Y, 1973, p 95-101

L2 Laats, M K, *Experimental study of the dynamics of an air-dust jet,* Inzhenerno-Fizicheskii Zhurnal, vol 10, no 1, p 11-15, 1966

L3 Laats, M K, Frishman, F A, *Assumptions in calculating the two-phase jet*, Izv. AN SSSR. Mekhanika Zhidkosti i Gaza, vol 5, no 2, p 186-191, Mar-Apr 1970

L4 Lilly, G P, *Effect of particle size on particle diffusivity*, Ind Eng Chem Fundam, vol 12, no 3, 1973, p 268-275

L5 Lukasiewicz, J, *Diffusers for supersonic wind tunnels,* J of the Aeronautical sciences, Sept 1953, p 617-626

M1 Morganthaler, J H, *Analysis of Two-phase flows in supersonic exhausts*, American Rocket Society, p 1715-1761

M2 Marble, F M, *Dynamics of Dusty Gases*, AIAA J., vol 1, no 12, p 2793-2801, 1963

M3 *Coal Gasification,* McGraw-Hill encyclopaedia of Science and Technology, Vol 4, p 72, 1987

M4 *McGraw-Hill Encyclopaedia of Science and Technology,* 1992

M5 Miyazato, Y, Matsuo, K, *One-Dimensional Flow Model of a Pseudo-Shock Wave in a Constan-Area Duct,* Nippon Kikai Gakkai Ronbunshu B Hen, v 61, no. 592, Dec 1995, p 127-133 (in Japanese)

M6 Matsuo, K, et al, *Oscillatory Characteristics of a Pseudo-Shock Wave in a Rectangular Straight Duct,* Nippon Kikai Gakkai Ronbunshu B Hen, v 57, no. 541, Sept 1991, p 3083-3090, (in Japanese)

N1 Neumann, E P, Lustwerk, F, *Supersonic diffusers for supersonic wind tunnels*, J of App Mech, June 1949, p 195-202

O1 Om, D, Childs, M E, *Multiple transonic shock-wave/turbulent boundary layer interaction in a circular duct*, AIAA J, vol 23, no 10, p 1506-1511

O2 Om, D, Childs, M E, Viegas, J R, *Transonic shock-wave/turbulent boundary layer interaction in a circular duct*, AIAA J, vol 23, no 5, May 1985, p 707-713

P1 Pai, S-I, *Mixture of fluid and solid particles,* Two-phase flows, Vieveg tracts in pure and applied physics, chapter 5, 1977

P2 Peskin, R L, *Numerical solution of particle motion in turbulent gas-solids channel flow,* ASME 76-WA/FE-37

P3 Prince, D C Jr, *Boundary layer development in a converging-diverging channel throat,* AIAA J, Vol 5, no 3, March 1967, p 597-599

P4 Popper, J, Abauff, N, Hestroni, G, *Velocity measurements in a two-phase turbulent jet*, International journal of multiphase flow,, vol 1, p 715-726

P5 Pais, A, *Subtle is the Lord - The Science and life of Albert Einstein,* Oxford University press, 1982

P6 PHOENICS Online Manual, Version 2.2, CHAM, UK

P7 Press, W H et al, *Numerical Recipes in FORTRAN: The Art of Scientific Computing,* Cambridge University Press, 1992

R1 Rudinger, G, Chang, A, *Analysis of non-steady two-phase flow* Physics of Fluids, vol 7, no 11, Nov 1964, p 1747-1754

R2 Rudinger, G, *Gas-particle flow in a converging nozzle at high loading ratios* AIAA J, vol 8, no 7, July 1970, p 1288-1294

R3 Rudinger, G, *Some effects of finite particle volume on the dynamics of gas-particle mixtures,* AIAA J, vol 3, no 7, July 1965, p 1217-1222

R4 Rudinger, G, *Some properties of shock relaxation in gas flows carrying small particles*, Physics of fluids, vol 7, no 5, May 1968, p 658-663

S1 Smoot, L D, Douglas, R A, Simonsen, J M, Tufts, L W, *Development of a model for mixing and combustion of a ducted particle-laden jet,* Dept. of the Navy, 1969

S2 Soo, S L, *Gas-dynamic processes involving suspended solids,* AIChE J, Sept 1961, p 384-387

S3 Smoot, L D, Coates, R L, Simonsen, J M, *Combustion of a particle-laden jet with a secondary stream in a duct*, Dept. of the Navy, 1968

S4 Smoot, L D, Douglas, R A, Simonsen, J M, Tufts, L,W, *A model for mixing and combustion of particle-laden ducted flows*, AIAA paper no 70-736, 1970

S5 Sharma M P,Crowe, C T, *A novel physico-computational model for quasi-one dimensional gas-particle flows*, ASME 76-WA/FE-36

S6 Stowell, D E, Smoot, L D, *Turbulent mixing correlations in free and confined jets*, AIAA paper no 73-1194

S7 Shuen, J-S, Chen, L-D, Faeth, G M, *Predictions of the structure of particle-laden round jets,* AIAA J, vol 21, no 11, Nov 1983, p 1483-1484

S8 Schetz, J A, *Two-phase flows*, Injection and mixing in turbulent flows, Prog Aero Astro Chap 6, Vol 68,

S9 Shuen, J-S, Chen, L-D, Faeth, G M, *Evaluation of a stochastic model of particle dispersion in a turbulent round jet,* AIChE J, vol 29, no 1, Jan 1983, p 167-170

S10 Srivastava, R S, Sharma, J P, *Dispersed shock waves in a gas-particle mixture* AIAA J, vol 23, No 11, Nov 1985, p 1817-1819

S11 Shapiro, A H, *The Dynamics and Thermodynamics of compressible fluid flow* Vol 1, 2, Ronald press, 1953

T1 Tufts, L W, Smoot, L D, *A turbulent mixing coefficient correlation of coaxial jets with and without secondary flows,* AIAA J of spacecraft and rockets, vol 8, no 12, Dec 1971, p 1183-1190

T2 Tamaki, T, Tomita, Y, Yamane, R, *A study of pseudo-shock (first report -λ-type pseudo-shock)*, Bulletin of the JSME, vol 13, no 55, 1970, p 51-58

T3 Tamaki, T, Tomita, Y, Yamane, R, *A study of pseudo-shock (second report -X-type pseudo-shock*,)Bulletin of the JSME, vol 14, no 74, 1971, p 807-817

T4 Trezek, G J, Soo, S L, *Gas dynamics of accelerating particulate flows in circular ducts*, Proc H T & F M Inst. M A Saad, J A Miller eds, 1966, p 148-166

V1 *Van Nostrands Scientific Encyclopaedia,* 5th Ed. , D Considuie, ed., 1976

W1 Wallis, G B, *Suspensions of particles in fluids*, One-dimensional two-phase flows, McGraw-Hill, 1969

W2 Weber, R J, McKay, J S, *An Analysis of Ramjet engines using supersonic combustion,* NACA technical note 4386

W3 Wazzan, A R, Robinson, L B, Diem, H G, *Heat transfer of gas particle flows in a supersonic convergent-divergent nozzle*, App Sci Res 18, Dec. 1964, p 288-308

W4 Witze, P O, *Centerline velocity decay of compressible free jets*, AIAA J, vol 12, no 4, Apr 1874, p 417-418

W5 Witze, P O *A generalised theory of the turbulent mixing of axially symmetric compressible free jets,* The fluid mechanics of mixing, ASME 1973

W6 Willis, D R, Glassman, I, *The mixing of unbounded coaxial compressible streams* ,, Jet propulsion, 27 (1957), p 1241-1248

W7 White, F M, *Fluid Mechanics*, II ed, McGraw-Hill, 1986

W8 Wang, D, *Analysis and Design of Air-Jet Pumps for Pneumatic Transport of Bulk Solids in Pipelines,* Ph D Thesis, University of Wollongong, 1995

W9 Wypych, P W, *Latest Developments in the Pneumatic Pipeline Transport of Bulk Solids,* 5th International Conference on Bulk Material Handling, Storage and Transport, University of Newcastle, Australia, 1995, p 47-56

Y1 Yuu, S, Yasukouchi, N, Hirosawa, Y, Jotaki, T, *Particle turbulent diffuson in a dust-laden round jet*, AIChE J, vol 24, no 3, May 1978, p 509-519

Y2 Yang, J, Kubota, T., Zukoski, E E, *Applications of Shock-induced mixing to supersonic combustion,* AIAA Journal, vol 31, no. 5, May 1993, p 854-862

Y3 Yamane R, *A simple model of the pseudo-shock mechanism*, Bulletin of the Tokyo Institute of Technology, No 100, 1970

Y4 Yamane, R et al, *Numerical Simulation of Pseudoshock in Straight Channels* JSME International Journal, Series B, vol 38, No. 4, 1995, p 549-554

Y5 Yamane, R, *Private Communication*, 1996

Z1 Zucrow, M J, Hoffman, J D, *Gas Dynamics*, Vols 1 and 2, John Wiley and sons, 1976

APPENDIX A

Generalised Steady One-Dimensional Flow Analysis

Equations describing the flow in the SAI are written for the *primary* gas stream, because it is the primary gas stream which provides the suspension with the impetus and conveys it to its destination. The equations are written for a 'one-dimensional fixed' control volume (Figure A1) extending all the way across the flow (except for the Potential Core part of the Interaction Region) and a small distance in the downstream direction. This is because the flow is assumed one-dimensional (as a first approximation) and flow development is to be followed in the downstream direction.

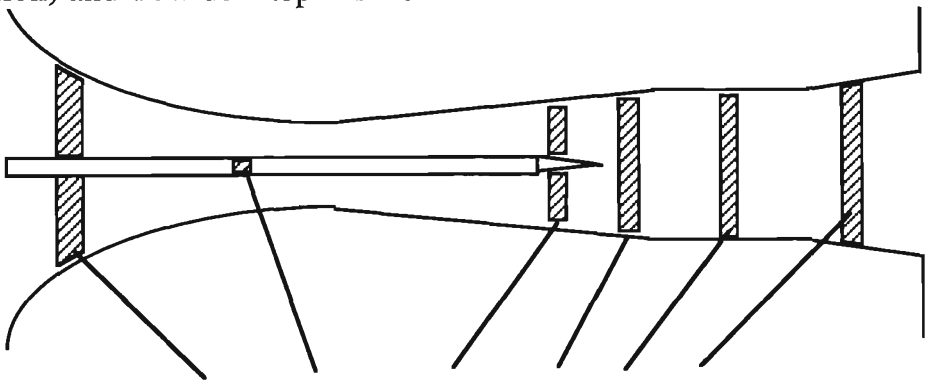

Figure A1 Control Volumes

Following [Z1], let 'B' be any property of the fluid and 'β' (=dB/dm) the corresponding intensive property (amount of B per unit mass in any small portion of fluid). The total amount of B in any control volume is thus

$$B = \int_{CV} \beta \, \rho \, d(vol) \qquad (A.1)$$

Then, using the one-dimensional Reynolds transport theorem for a fixed control volume, the time rate of change of 'B' for a local fluid 'system' is related to the changes within the control volume by

$$\frac{d}{dt}(B_{SYST}) = \frac{d}{dt}\int_{CV} \beta \, \rho \, d(vol) + (\beta \, \rho \, A \, V)_{out} - (\beta \, \rho \, A \, V)_{in} \qquad (A.2)$$

The Continuity Equation

Here, the conserved quantity is mass 'm', so that

$$B = m \; ; \; \beta = \frac{dm}{dm} = 1$$

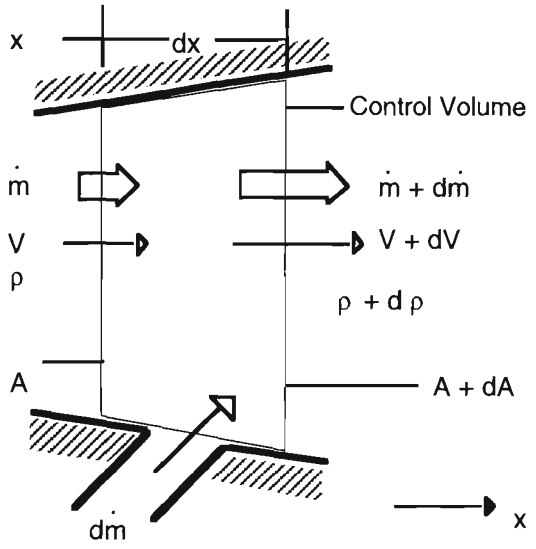

Figure A2 Mass Conservation for a Control Volume

The relevant form of the equation is derived from the expression for mass flow rate :

$$\dot{m} = \rho A V$$

Differentials of both sides :

$$d\dot{m} = d(\rho A V) = A V d\rho + \rho V dA + \rho A dV$$

Division by $\dot{m} = \rho A V$:

$$\frac{d\dot{m}}{\dot{m}} = \frac{d\rho}{\rho} + \frac{dA}{A} + \frac{dV}{V} \qquad \text{(A.3)}$$

Equation (A.3) connects *fractional* changes in mass flow rate, density, cross sectional area and velocity. Here, $d\dot{m}$ is to be interpreted as *rate of mass entrained* into the control volume (Figure A2).

The Momentum Equation

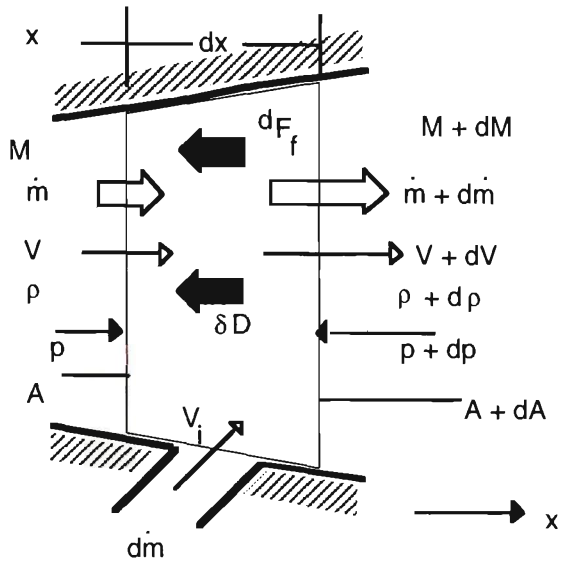

Figure A3 Momentum Equation for a Control Volume

Here, the conserved quantity is fluid momentum 'mV', so that

$$B = mV \; ; \; \beta = \frac{d\,(mV)}{dm} = V$$

$$\frac{d}{dt}(mV)_{SYST} = \frac{d}{dt}\int_{CV} V\,\rho\,d(vol) + (V\,\rho\,A\,V)_{out} - (V\,\rho\,A\,V)_{in}$$

Using $\dot{m} = \rho\,A\,V$,

$$\frac{d}{dt}(m\,V)_{SYST} = \frac{d}{dt}\int_{CV} V\,\rho\,d(vol) + (\dot{m}\,V)_{out} - (\dot{m}\,V)_{in}$$

For steady one-dimensional flow,

$$F_{ext} = \frac{d}{dt}(mV)_{syst} = (\dot{m}V)_{out} - (\dot{m}V)_{in}$$

or,

$$F_{ext} = (\dot{m} + d\dot{m})\,(V + dV) - (\dot{m}\,V + d\dot{m}\,V_i)$$

The net external force affecting the momentum of the fluid system is composed of:

1 *Body. Force* arising from the system being in some external field, such as gravity. In the absence of fields of any other type, or for horizontal flow, this body force can be *assumed negligible.*

2 *Surface Force* due to different pressures acting on different parts of control surface ;

3 *Surface Force* arising from wall friction, on parts of control surface adjacent to wall;

4 *Drag Force* due to obstacles and bodies in relative motion in the stream.

The x-direction momentum equation takes the form:

$$F_{ext,x} = pA - (p + dp)(A + dA) - \delta F_f - \delta D = (\dot{m} + d\dot{m})(V + dV) - (\dot{m}V + d\dot{m}V_{ix})$$

Wall friction force is expressed in terms of an experimentally determined *friction factor 'f '* or *friction coefficient 'cf'*

$$c_f = \frac{\text{wall shear stress}}{\text{velocity head}} = \frac{f}{4} = \frac{\tau_W}{\frac{1}{2}\rho V^2}$$

and hydraulic characteristics of flow passage, defined in terms of 'hydraulic diameter' :

$$\text{Hydraulic Diameter } D_H = \frac{4\,(\text{Flow area})}{\text{'wetted' perimeter}} = \frac{4\,A}{WP}$$

Hence the expression for the wall friction force takes the form :

[wall shear force] = [wall shear stress] [wall area]

$$dF_f = c_f \frac{\rho\, V^2}{2} (WP)\, dx = f \frac{\rho\, V^2}{2} A \frac{dx}{D_H}$$

The momentum equation becomes, *neglecting second-order terms* :

$$Adp + f \frac{\rho\, V^2}{2} A \frac{dx}{D_H} + \delta D + \dot{m}\, dV + d\dot{m}\,(V - V_{ix}) = 0$$

(Interpretation of V_{ix}, $d\dot{m}$, and D_H as applied to flow in the SAI are presented at more appropriate places.)

Division by A :

$$dp + f \frac{\rho V^2}{2} \frac{dx}{D_H} + \frac{\delta D}{A} + \frac{\dot{m}}{A} dV + \frac{d\dot{m}}{A} V \left(1 - \frac{V_{ix}}{V}\right) = 0$$

The momentum equation becomes, in terms of velocity ratio $y = V_{ix}/V$,

$$dp + f \frac{\rho V^2}{2} \frac{dx}{D_H} + \frac{\delta D}{A} + \rho V \, dV + \rho V^2 (1 - y) \frac{d\dot{m}}{\dot{m}} = 0$$

Division by p (since equations connecting *fractional* changes in flow parameters are required):

$$\frac{dp}{p} + f \frac{\rho V^2}{2 p} \frac{dx}{D_H} + \frac{\delta D}{A p} + \frac{\rho V}{p} dV + \frac{\rho V^2}{p} (1 - y) \frac{d\dot{m}}{\dot{m}} = 0$$

For the SAI, this equation can be further modified, since the fluid is compressible and assumed an ideal gas. Hence, the definition of Mach number (V= Ma) and the ideal gas equation of state ($p = \rho RT$) can be used:

Fourth Term:

$$\frac{\rho V}{p} dV = \frac{\rho}{V} d\left(V^2/2\right) = \frac{\rho}{2 p} d\left(V^2\right) = \frac{1}{2 R T} d\left(M^2 a^2\right)$$

Definition of sonic velocity in an ideal gas ($a = \sqrt{\gamma R T}$)

$$\frac{\gamma}{2 T} d\left(M^2 T\right) = \frac{\gamma}{2 T} \left(M^2 dT + T \, dM^2\right) = \frac{\gamma M^2}{2} \frac{dT}{T} + \gamma M^2 \frac{dM}{M}$$

In the second term,

$$\frac{1}{2} \rho V^2 = \frac{1}{2} \gamma p M^2$$

Grouping the second and third term together,

$$\frac{\gamma M^2}{2} \left\{ f \frac{dx}{D_H} + \frac{2}{\gamma M^2} \frac{\delta D}{A p} \right\}$$

Last term :

$$\frac{\rho V^2}{p} (1 - y) \frac{d\dot{m}}{\dot{m}} = \gamma M^2 (1 - y) \frac{d\dot{m}}{\dot{m}}$$

With these modifications, the momentum equation takes on its final useful form :

$$\frac{dp}{p} + \frac{\gamma M^2}{2}\left\{f\frac{dx}{D_H} + \frac{2}{\gamma M^2}\frac{\delta D}{A\,p}\right\} + \frac{\gamma M^2}{2}\frac{dT}{T} + \gamma M^2\frac{dM}{M} + \gamma M^2 (1-y)\frac{d\dot{m}}{\dot{m}} = 0$$

(A.4)

Estimation of Friction Coefficient

At any station in the flow, in general, the value of friction coefficient depends upon:

1 Mach Number (compressibility effects) ;

2 Reynolds Number based on local hydraulic diameter (local condition of flow);

3 Reynolds Number based on streamwise distance measured from some suitable upstream reference point (history of the flow).

It is suggested in the literature that the strongest influence is that due to Reynolds number based on the local hydraulic diameter [S1]. This makes it possible to use the 'Moody chart' in the estimation of the friction coefficient. An alternative formula which gives the friction coefficient *explicitly* in terms of Reynolds number (and surface roughness parameter ε) is 'Haaland's formula' [W7]:

$$f = \left[-1.8\log\left\{\frac{6.9}{Re_{D_H}} + \left(\frac{\varepsilon/D_H}{3.7}\right)^{1.11}\right\}\right]^{-2}$$

This formula is used for estimation of f. The value of the roughness parameter (ε/D_H) is determined empirically, depending on the material of the duct wall..

The Energy Equation

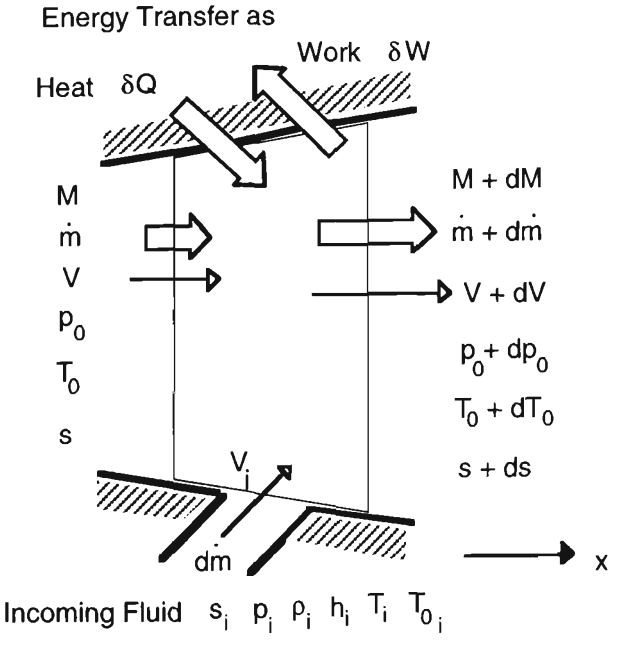

$$\frac{dp}{p} + \frac{\gamma M^2}{2}\left\{ f\frac{dx}{D_H} + \frac{2}{\gamma M^2}\frac{\delta D}{A\,p}\right\} + \frac{\gamma M^2}{2}\frac{dT}{T} + \gamma M^2 \frac{dM}{M} + \gamma M^2 (1-y)\frac{d\dot{m}}{\dot{m}} = 0 \qquad (A.4)$$

Estimation of Friction Coefficient

At any station in the flow, in general, the value of friction coefficient depends upon:

1 Mach Number (compressibility effects) ;
2 Reynolds Number based on local hydraulic diameter (local condition of flow);
3 Reynolds Number based on streamwise distance measured from some suitable upstream reference point (history of the flow).

It is suggested in the literature that the strongest influence is that due to Reynolds number based on the local hydraulic diameter [S1]. This makes it possible to use the 'Moody chart' in the estimation of the friction coefficient. An alternative formula which gives the friction coefficient *explicitly* in terms of Reynolds number (and surface roughness parameter ε) is 'Haaland's formula' [W7]:

$$f = \left[-1.8 \log\left\{ \frac{6.9}{Re_{D_H}} + \left(\frac{\varepsilon/D_H}{3.7} \right)^{1.11} \right\} \right]^{-2}$$

This formula is used for estimation of f. The value of the roughness parameter (ε/D_H) is determined empirically, depending on the material of the duct wall..

The Energy Equation

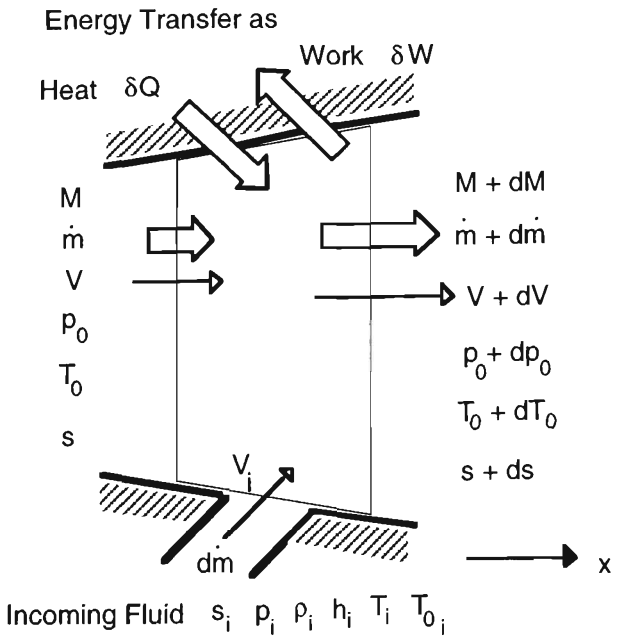

Figure A4 Energy Conservation

Here, the conserved quantity is total energy E, so that

$$B = \text{total energy} = E$$

$$\beta = \frac{dE}{dm} = u + \frac{V^2}{2} + gz$$

$$\frac{d}{dt}(E_{SYST}) = \frac{d}{dt}\int_{CV} e\,\rho\,d(vol) + (\dot{m}\,e)_{out} - (\dot{m}\,e)_{in}$$

Change in total energy is brought about by energy transfers as Heat and Work across the system boundaries (Figure A4). For steady one-dimensional flow,

$$\dot{Q} - \dot{W} = (\dot{m}\,e)_{out} - (\dot{m}\,e)_{in}$$

The total work transfer $\dot{W}$ can be split up into three parts :

$$\dot{W} = \dot{W}_{SHAFT} + \dot{W}_{PRESSURE} + \dot{W}_{VISCOUS}$$

Work done due to pressure forces is

$$\dot{W}_{PRESSURE} = \int_{CS} p\,(V\bullet n)dA = \int_{CS} \frac{p}{\rho}(\rho V\bullet n)\,dA = \left(\frac{p}{\rho}\dot{m}\right)_{out} - \left(\frac{p}{\rho}\dot{m}\right)_{in}$$

The Energy Equation becomes :

$$\dot{Q} - \dot{W} = \left[\dot{m}\left(e + \frac{p}{\rho}\right)\right]_{OUT} - \left[\dot{m}\left(e + \frac{p}{\rho}\right)\right]_{IN}$$

Using the definition of specific enthalpy $h = e + \frac{p}{\rho}$,

$$\dot{Q} - \dot{W} = \left[\dot{m}\left(h + \frac{V^2}{2}\right)\right]_{OUT} - \left[\dot{m}\left(h + \frac{V^2}{2}\right)\right]_{IN}$$

or,

$$\dot{Q} - \dot{W} = \left[(\dot{m} + d\dot{m})\left(h + dh + \frac{V^2}{2} + d\left(\frac{V^2}{2}\right)\right)\right] - \left[\dot{m}\left(h + \frac{V^2}{2}\right)\right] - \left[d\dot{m}\left(h_i + \frac{V_i^2}{2}\right)\right]$$

Dividing by $\dot{m}$, and defining $dh_{0i} = \frac{d\dot{m}}{\dot{m}}(h_0 - h_{0i})$, a measure of difference in stagnation enthalpies of primary and incoming fluids:

$$q - w = dh_0 - dh_{0i} \tag{A.5}$$

The Entropy Equation

Here, the relevant non-conserved quantity is total entropy S, so that
B = total entropy = S

$$\beta = \frac{dS}{dm} = s$$

$$\frac{d}{dt}(S_{SYST}) = \frac{d}{dt}\int_{CV} s\,\rho\,d(vol) + (\dot{m}s)_{out} - (\dot{m}s)_{in}$$

In terms of energy transfer as Heat to the system, in a steady flow, :

$$\frac{d}{dt}(S_{SYST}) = (\dot{m}s)_{out} - (\dot{m}s)_{in} \geq \frac{\dot{Q}}{T}$$

or,

$$(\dot{m} + d\dot{m})(s + ds) - \dot{m}s - d\dot{m}\,s_i \cong \left(ds + \frac{d\dot{m}}{\dot{m}}(s - s_i)\right) \geq \frac{\dot{Q}}{T}$$

Increase in specific entropy across the control volume is brought about by (a) Heat transfer to fluid; (b) entropy of incoming fluid, (c) frictional dissipation:

$$ds = \frac{\dot{Q}}{T} + \frac{d\dot{m}}{\dot{m}}(s_i - s) + ds_{FRICTION+DRAG}$$

However, because specific entropy is, by definition, a state variable, regardless of the type of process which brings about the change 'ds',

$$ds = c_p\frac{dT}{T} - R\frac{dp}{p} \tag{A.6}$$

This is the useful equation, since it contains fractional changes in flow variables. Subsequent analysis automatically reveals contributions to 'ds' of various irreversibility-producing agents (friction, drag, heat transfer, mass entrainment).

Ideal Gas Equation of State

$$p = \rho R_{Gas} T = \rho \frac{R_{univ}}{MW} T \qquad (A.7)$$

Equations (A.3 - A.7) must be supplemented by auxilliary equations defining the following additional quantities :

1 Mach Number = $\frac{\text{flow velocity}}{\text{sonic velocity}} = \frac{V}{a} = \frac{V}{\sqrt{\gamma RT}}$, for an ideal gas.

2 Specific stagnation enthalpy = $h_0 = h + \frac{V^2}{2} \Rightarrow c_p T_0 = c_p T + \frac{V^2}{2}$

3 Stagnation temperature $T_0 = T + \frac{V^2}{2c_p} = T + \frac{1}{2c_p} M^2 a^2 = T + \frac{1}{2c_p} M^2 \gamma RT$

so that, using $R = c_p - c_v$ and $\gamma = c_p/c_v$,

$$T_0 = T\left(1 + \frac{\gamma - 1}{2} M^2\right) \qquad (A.8)$$

Stagnation (total) temperature of the primary gas is affected if there is energy transfer to the stream or if the stream entrains extraneous matter whose stagnation enthalpy is different from that of the primary gas.

4 Stagnation pressure = pressure attained if brought to rest isentropically

For an ideal gas, using the expression for stagnation temperature.

$$p_0 = p\left(\frac{T_0}{T}\right)^{\gamma/\gamma - 1} = p\left(1 + \frac{\gamma - 1}{2} M^2\right)^{\gamma/\gamma - 1}$$

Irreversibilities in the flow contribute to a continuous decline in the value of the stagnation pressure in the streamwise direction. Conversely, decrease in stagnation pressure value is a measure of losses in the flow.

Writing the energy equation as $\delta q - \delta w - dh_{0i} = dh_0 = c_p dT_0$

and using the definition of stagnation temperature, the equation describing fractional change in stagnation temperature becomes :

$$\frac{1}{\psi\, c_p\, T}\left(\delta q - \delta w - dh_{0i}\right) = \frac{dT_0}{T_0} \quad \text{where} \quad \psi = 1 + \frac{\gamma - 1}{2} M^2.$$

Useful forms of these equations are obtained as follows :

1 Ideal gas equation of state

$$p = \rho RT \quad ; \quad dp = d(\rho RT) = R\,T\,d\rho + \rho\,R\,dT$$

Division by $p = \rho\,R\,T$: $\Rightarrow$

$$\frac{dp}{p} = \frac{d\rho}{\rho} + \frac{dT}{T} \tag{A.9}$$

2 From the definition of Mach number ($M = V/a = V/(\gamma RT)^{0.5}$), differentials of both sides and division by the above expression yields:

$$\frac{dM}{M} = \frac{dV}{V} - \frac{1}{2}\frac{dT}{T} \tag{A.10}$$

3 From the definition of stagnation temperature:

$$\frac{dT_0}{T_0} = \frac{dT}{T} + \frac{(\gamma - 1)\,M^2}{\psi}\frac{dM}{M} \tag{A.11}$$

4 From the definition of stagnation pressure:

$$\frac{dp_0}{p_0} = \frac{dp}{p} + \frac{\gamma\,M^2}{\psi}\frac{dM}{M} \tag{A.12}$$

5 From the formula for specific entropy change of an ideal gas,

$$\frac{ds}{c_p} = \frac{dT}{T} - \frac{R}{c_p}\frac{dp}{p} = \frac{dT}{T} - \frac{\gamma - 1}{\gamma}\frac{dp}{p} \tag{A.13}$$

In addition to the above variables, a variable 'Impulse Function' is defined [Z1] as :

$$F = p\,A + \dot{m}\,V = p\,A\left(1 + \frac{\dot{m}\,V}{p\,A}\right) = p\,A\left(1 + \gamma\,M^2\right)$$

Taking differentials and dividing by the above expression yields fractional change in Impulse Function:

$$\frac{dF}{F} = \frac{dp}{p} + \frac{dA}{A} + \frac{2\,\gamma\,M^2}{1+\gamma\,M^2}\,\frac{dM}{M} \qquad (A.14)$$

For a general confined flow, the (fractional) changes in the eight flow properties (dp/p), (dρ/ρ), (dT/T), (dV/V), (dM/M), (dp_0/p_0), (ds/c_p) and (dF/F), considered as *dependent variables*, are brought about due to separate influences of four independent 'driving potentials', considered as *independent variables :*

1 Fractional Mass Addition $d\dot{m}/\dot{m}$;

2 Fractional change in flow cross section area dA/A ;

3 Fractional change in stagnation temperature due to energy transfers as heat and work, and as a result of mass entrainment: $dT_0/T_0 = (\delta q - \delta w - dh_{0i})/\psi\, c_p\, T$

and

4 Wall Friction Force and Drag due to submerged matter in relative motion:

$$\left\{ f\,\frac{dx}{D_H} + \frac{2\,\delta D}{\gamma\,M^2\,p\,A} \right\}$$

(Friction and Drag are clubbed together because both have a retarding influence on the primary stream.)

The equations must now be rearranged so that the dependent variables appear on the left hand side, and the driving potentials on the right hand side of the equality sign :

1 Continuity

$$\frac{d\rho}{\rho} + \frac{dV}{V} = \frac{d\dot{m}}{\dot{m}} - \frac{dA}{A}$$

2 Momentum

$$\frac{dp}{p} + \frac{\gamma\,M^2}{2}\frac{dT}{T} + \frac{\gamma M^2}{2}\frac{dM}{M} = \left\{ -\frac{\gamma M^2}{2}\left(f\,\frac{dx}{D_H} + \frac{2\,\delta D}{\gamma\,M^2\,p\,A} \right) - \gamma\,M^2\,(1-y)\,\frac{d\dot{m}}{\dot{m}} \right\}$$

3 Ideal gas equation of state

$$\frac{dp}{p} - \frac{d\rho}{\rho} - \frac{dT}{T} = 0$$

4 Definition of Mach Number

$$\frac{1}{2}\frac{dT}{T} - \frac{dV}{V} + \frac{dM}{M} = 0$$

5 Definition of Stagnation temperature

$$\frac{dT_0}{T_0} = \frac{1}{\psi\, c_p\, T}\left(\delta q - \delta w - dh_{0i}\right)$$

6 Definition of Stagnation pressure

$$\frac{dp}{p} + \frac{\gamma\, M^2}{\psi}\frac{dM}{M} - \frac{dp_0}{p_0} = 0$$

7 Entropy change

$$\frac{\gamma - 1}{\gamma}\frac{dp}{p} - \frac{dT}{T} + \frac{ds}{c_p} = 0$$

8 Definition of Impulse function

$$-\frac{dp}{p} - \frac{2\,\gamma\, M^2}{1 + \gamma\, M^2}\frac{dM}{M} + \frac{dF}{F} = \frac{dA}{A}$$

Writing the equations in this sequence seems to be convenient for the following reason: When these equations are expressed in matrix form, the coefficient matrix is such that the determinants can be found in a relatively simple way. This leads to a solution of these equations by Cramer's Rule [Z1].

For these equations to be applicable to analysis of flow in the SAI, in which the flow is assumed one-dimensional as a first approximation, the driving potentials are expressed in terms of 'dx', differential increment in the streamwise distance:

1 $\dfrac{dA}{A} = AR \cdot dx \quad$ where $\quad AR = \dfrac{1}{A}\dfrac{dA}{dx}$

2 $f\dfrac{dx}{D_H} = FR \cdot dx \quad$ where $\quad FR = \dfrac{f}{D_H}$

$$\frac{2\,\delta D}{\gamma\, M^2\, p\, A} = DR \cdot dx \quad \text{where} \quad DR = \frac{2}{\gamma\, M^2\, p\, A}\frac{\delta D}{dx}$$

so that

$$f\frac{dx}{D_H} + \frac{2\,\delta D}{\gamma\, M^2\, p\, A} = (FR + DR)\,dx = FD\,dx$$

3 $\dfrac{d\dot{m}}{\dot{m}} = EM \cdot dx \quad$ where $\quad EM = \dfrac{1}{\dot{m}}\dfrac{d\dot{m}}{dx}$

4) $\dfrac{\delta q}{\psi\, c_p\, T} = HT \cdot dx$ where $HT = \dfrac{1}{\psi\, c_p\, T}\dfrac{\delta q}{dx}$;

$\dfrac{\delta w}{\psi\, c_p\, T} = WK \cdot dx$ where $WK = \dfrac{1}{\psi\, c_p\, T}\dfrac{\delta w}{dx}$

and

$$\frac{dh_{0i}}{\psi\, c_p\, T} = \frac{\left(c_p\, T_0 - c_{p_i} T_{0_i}\right)\dfrac{d\dot{m}}{\dot{m}}}{\psi\, c_p\, T} = DHOI\ dx$$

where $$DHOI = \frac{\left(c_p T_0 - c_{p_i} T_{0_i}\right)}{\psi\, c_p\, T}\frac{1}{\dot{m}}\frac{d\dot{m}}{dx}.$$

or $$DHOI = \frac{\left(c_p T_0 - c_{p_i} T_{0_i}\right)}{\psi\, c_p\, T}\, EM.$$

Then,

HT dx - WK dx - DHOI dx = ENER dx

where

HT - WK - DHOI = ENER

Here, the symbols AR, FD, EM and ENER represent driving potentials due to **AR**ea change, **F**riction and **D**rag, **E**ntrained **M**ass and **ENER**gy transfer respectively. In terms of the driving potentials, the governing equations are recast in the following form, assigning mnemonic symbols to the 'influence coefficients'. The nomenclature is descriptive, as shown below for each equation describing the rate of change of each dependent variable with respect to the downstream distance, x :

(1) Rate of Change of Mach Number

dM/dx = EMA*AR + EMFD*FD + EMEN*ENER + EMEM*EM

Here,

EMA = **E**ffect on **M**ach number of **A**rea change $= M\left[\dfrac{-\psi}{1-M^2}\right]$

EMFD = **E**ffect on **M**ach number of **F**riction and **D**rag $= M\left[\dfrac{\gamma M^2 \psi}{2\left(1-M^2\right)}\right]$

EMEN = **E**ffect on **M**ach number of **EN**ergy transfer $= M\left[\dfrac{\left(1+\gamma M^2\right)\psi}{2\left(1-M^2\right)}\right]$

EMEM = **E**ffect on **M**ach number of **E**ntrained **M**ass $= M\left[\dfrac{\left(1+\gamma M^2 - y\,\gamma M^2\right)\psi}{\left(1-M^2\right)}\right]$

(2) Rate of Change of Static Pressure

$dp/dx = EPA*AR + EPFD*FD + EPEN*ENER + EPEM*EM$

Here,

EPA = **E**ffect on **P**ressure of **A**rea change $= p\left[\frac{\gamma M^2}{1 - M^2}\right]$

EPFD = **E**ffect on **P**ressure of **F**riction and **D**rag $= p\left[\frac{-\gamma M^2 \left(1 + (\gamma - 1) M^2\right)}{2\left(1 - M^2\right)}\right]$

EPEN = **E**ffect on **P**ressure of **EN**ergy transfer $= p\left[\frac{-\gamma M^2 \psi}{\left(1 - M^2\right)}\right]$

EPEM = **E**ffect on **P**ressure of **E**ntrained **M**ass $= p\left[\frac{-\gamma M^2 \left(2\psi (1 - y) + y\right)}{\left(1 - M^2\right)}\right]$

(3) Rate of Change of Density

$d\rho/dx = EDA*AR + EDFD*FD + EDEN*ENER + EDEM*EM$

Here,

EDA = **E**ffect on **D**ensity of **A**rea change $= \rho\left[\frac{M^2}{1 - M^2}\right]$

EDFD = **E**ffect on **D**ensity of **F**riction and **D**rag $= \rho\left[\frac{-\gamma M^2}{2\left(1 - M^2\right)}\right]$

EDEN = **E**ffect on **D**ensity of **EN**ergy transfer $= \rho\left[\frac{-\psi}{\left(1 - M^2\right)}\right]$

EDEM = **E**ffect on **D**ensity of **E**ntrained **M**ass $= \rho\left[\frac{-\left((\gamma + 1) M^2 - y\,\gamma M^2\right)}{\left(1 - M^2\right)}\right]$

(4) Rate of Change of Temperature

$dT/dx = ETA*AR + ETFD*FD + ETEN*ENER + ETEM*EM$

Here,

ETA = **E**ffect on **T**emperature of **A**rea change $= T\left[\frac{(\gamma - 1) M^2}{1 - M^2}\right]$

ETFD = **E**ffect on **T**emperature of **F**riction and **D**rag $= T\left[\frac{-\gamma (\gamma - 1) M^4}{2\left(1 - M^2\right)}\right]$

ETEN = **E**ffect on **T**emperature of **EN**ergy transfer $= T\left[\frac{(1 - \gamma M^2)\psi}{\left(1 - M^2\right)}\right]$

ETEM = **E**ffect on **T**emperature of **E**ntrained **M**ass $= T\left[\frac{-(\gamma - 1) M^2 \left(1 + \gamma M^2 - y\,\gamma M^2\right)}{\left(1 - M^2\right)}\right]$

(5) Rate of Change of Velocity

$dV/dx = EVA*AR + EVFD*FD + EVEN*ENER + EVEM*EM$

Here,

EVA = **E**ffect on **V**elocity of **A**rea change $= V\left[\frac{-1}{1-M^2}\right]$

EVFD = **E**ffect on **V**elocity of **F**riction and **D**rag $= V\left[\frac{-\gamma M^2}{2(1-M^2)}\right]$

EVEN = **E**ffect on **V**elocity of **EN**ergy transfer $= V\left[\frac{\gamma}{(1-M^2)}\right]$

EVEM = **E**ffect on **V**elocity of **E**ntrained **M**ass $= V\left[\frac{(1+\gamma M^2 - y\gamma M^2)}{(1-M^2)}\right]$

(6) Rate of Change of Stagnation (Total) Pressure

$dp_0/dx = EP0A*AR + EP0FD*FD + EP0EN*ENER + EP0EM*EM$

Here,

EP0A = **E**ffect on Stagnation Pressure ($\mathbf{p_0}$) of **A**rea change $= 0$

EP0FD = **E**ffect on Stagnation Pressure ($\mathbf{p_0}$) of **F**riction and **D**rag $= p_0\left[\frac{-\gamma M^2}{2}\right]$

EP0EN = **E**ffect on Stagnation Pressure ($\mathbf{p_0}$) of **EN**ergy transfer $= p_0\left[\frac{-\gamma M^2}{2}\right]$

EP0EM = **E**ffect on Stagnation Pressure ($\mathbf{p_0}$) of **E**ntrained **M**ass $= p_0\left[\frac{-\gamma M^2}{(1-y)}\right]$

(7) Rate of Change of Specific Entropy

$ds/dx = ESA*AR + ESFD*FD + ESEN*ENER + ESEM*EM$

Here,

ESA = **E**ffect on Specific Entropy (**s**) of **A**rea change $= 0$

ESFD = **E**ffect on Specific Entropy (**s**) of **F**riction and **D**rag $= c_p\left[\frac{-(\gamma-1)M^2}{2}\right]$

ESEN = **E**ffect on Specific Entropy (**s**) of **EN**ergy transfer $= c_p[\psi]$

ESEM = **E**ffect on Specific Entropy (**s**) of **E**ntrained **M**ass $= c_p\left[(\gamma-1)M^2(1-y)\right]$

(8) Rate of Change of Impulse Function

$dF/dx = EFA*AR + EFFD*FD + EFEN*ENER + EFEM*EM$

Here,

EFA = **E**ffect on Impulse **F**unction of **A**rea change $= F\left[\frac{1}{1+\gamma M^2}\right]$

EFFD = **E**ffect on Impulse **F**unction of **F**riction and **D**rag $= F\left[\frac{-1}{2(1+\gamma M^2)}\right]$

EFEN = **E**ffect on Impulse **F**unction of **EN**ergy transfer $= 0$

EFEM = **E**ffect on Impulse **F**unction of **E**ntrained **M**ass $= F\left[\frac{y\,\gamma M^2}{1+\gamma M^2}\right]$

When these equations are written for specific region of the flow in the SAI, the forms of the Influence Coefficients remain unchanged. Models expressing the Driving Potentials must be developed as they seem relevant to those regions of the flow. A list of significant driving potentials is given in Table A1.

	Nozzle	**Injection Tube**	**Interaction Region**	**Compression Region**	**Diffuser Region**
Area Change	**				
Friction	**	**	**	**	**
Drag			**	**	**
Heat Transfer			**	**	**
Work Transfer			**	**	**
Entrained Mass			**		

Table A1 Summary of Significant Driving Potentials

APPENDIX B

Suspension Flow as Fanno-type flow

For suspension flow in the injection tube, Mach Number and friction factor are related by

$$\frac{2\left(1 - M_S^2\right)}{\gamma_S M_S^3 \psi_S} \frac{dM_S}{dx} = \frac{c_{f_S}}{D_{H_{tube}}}$$

Because the right-hand side must always be positive,

(a) For $M_S < 1$, $M_S^2 < 1$, $\left(1 - M_S^2\right) > 0$

$$\therefore \frac{dM_S}{dx} > 0$$ and M_S increases with increasing x.

(b) For $M_S > 1$, $M_S^2 > 1$, $\left(1 - M_S^2\right) < 0$

$$\therefore \frac{dM_S}{dx} < 0$$ and M_S decreases with increasing x.

Rates of change of specific entropy and Mach number are related by:

$$\frac{ds_S}{dx} = c_{p_S} \frac{\left(\gamma_S - 1\right) M_S^2}{2} \frac{2\left(1 - M_S^2\right)}{\gamma_S M_S^3 \psi_S} \frac{dM_S}{dx}$$

For $M_S = 1$, $ds_S = 0$, showing that $M_S = 1$ is the limiting condition attained by the suspension at the point of exit from the injection tube. As discussed earlier, this is a desirable condition for the proposed device. In this application, it is also necessary to know the static pressure p_S attained by the suspension at the point of exit from the injection tube. The rate of change of suspension pressure with distance is given by [I5]:

$$\frac{dp_S}{dx} = p_S \frac{-\gamma_S M_S^2\left[1 + \left(\gamma_S - 1\right) M_S^2\right]}{2} \frac{2\left(1 - M_S^2\right)}{\gamma_S M_S^3 \psi_S} \frac{dM_S}{dx}$$

Eliminating 'dx' to connect fractional changes in suspension Mach number and M_S and suspension pressure p_S,

$$\frac{dp_S}{p_S} = -\left\{\frac{dM_S}{M_S} + \frac{\frac{\gamma_S - 1}{2} M_S \, dM_S}{1 + \frac{\gamma_S - 1}{2} M_S^2}\right\}$$

Integration of the above equation yields the change in p_S. Because the sonic condition is always attained at the tube exit, this condition, denoted by the suffix '*' is used as one of the limits of integration:

$$\int_{*} \frac{dp_S}{p_S} = -\int_{*} \frac{dM_S}{M_S} - \int_{*} \frac{\frac{\gamma_S - 1}{2} M_S}{1 + \frac{\gamma_S - 1}{2} M_S^2} dM_S$$

This yields

$$\frac{p_S}{p_{S*}} = \frac{1}{M_S} \left\{ \frac{\gamma_S + 1}{1 + \frac{\gamma_S - 1}{2} M_S^2} \right\}^{0.5}$$

Fractional change in stagnation (total) pressure is given by

$$\frac{dp_{0_S}}{p_{0_S}} = \frac{-\gamma_S M_S^2}{2} \frac{c_{f_S}}{D_{H_{tube}}} dx$$

showing that wall friction causes a continuous decline in the value of stagnation pressure in the streamwise direction. At any point in the flow, from the definition of stagnation pressure,

$$\frac{p_{0_S}}{p_S} = \left\{ 1 + \frac{\gamma_S - 1}{2} M_S^2 \right\}^{\frac{\gamma_S}{\gamma_S - 1}}$$

At the sonic condition, $M_S = 1$, so that

$$\frac{p_{0_{S*}}}{p_{S*}} = \left\{ 1 + \frac{\gamma_S + 1}{2} \right\}^{\frac{\gamma_S}{\gamma_S - 1}}$$

Therefore, noting that $p_{0_{S*}} \neq p_{0_S}$,

$$\frac{p_{0_S}}{p_{0_{S*}}} = \frac{p_{0_S}}{p_S} \frac{p_S}{p_{S*}} \frac{p_{S*}}{p_{0_{S*}}} = \frac{1}{M_S} \left[\frac{2 \psi_S}{\gamma_S + 1} \right]^{\frac{\gamma_S + 1}{2(\gamma_S - 1)}}$$

In the present application, it is necessary to know the relation between the suspension stagnation pressure and the suspension static pressure at the point of exit from the tube. This is because the suspension stagnation pressure is a parameter which can be externally controlled.

It is thus necessary to estimate the ratio $\frac{p_{S*}}{p_{0_S}}$.

$$\frac{p_{S*}}{p_{0_S}} = \frac{p_{S*}}{p_{0_{S*}}} \frac{p_{0_{S*}}}{p_{0_S}} = \left[\frac{2}{\gamma_S + 1}\right]^{\frac{\gamma_S}{(\gamma_S - 1)}} M_S \left[\frac{\gamma_S + 1}{2 + (\gamma_S - 1) M_S^2}\right]^{\frac{\gamma_S + 1}{2(\gamma_S - 1)}}$$

This means that the suspension flow must be assumed frictionless from its stagnation chamber upto the point where the Mach Number is M_S. In the present analysis, it is therefore not possible to calculate the losses in this part of the flow. However, an attempt is made to retrieve some lost ground in the following way :
It is seen that

$$\frac{p_{S*}}{p_{0_S}} = \left(\frac{p_{S*}}{p_{0_S}}\right)_{\text{ISENTRIOPIC}} \cdot (\text{Factor})$$

The factor by which the ratio (p_{S*}/p_{0S}) differs from its isentropic value is :

$$\frac{p_{0_{S*}}}{p_{0_S}} = M_S \left[\frac{\gamma_S + 1}{2 + (\gamma_S - 1) M_S^2}\right]^{\frac{\gamma_S + 1}{2(\gamma_S - 1)}}$$

This is a function of both the value of M_S and the value of the suspension 'loading' (which determines the value of γ_S). The value of γ_S must always be greater than the γ value for clean secondary gas (1.4 if the secondary gas is air). Figure B.1 shows a graph of the above Pressure Factor vs γ_S with the initial Mach number as parameter. For example, for an initial Mach number of 0.5, the stagnation pressure drops to about 75% of its initial value. It is not possible to account for this loss in the present model.

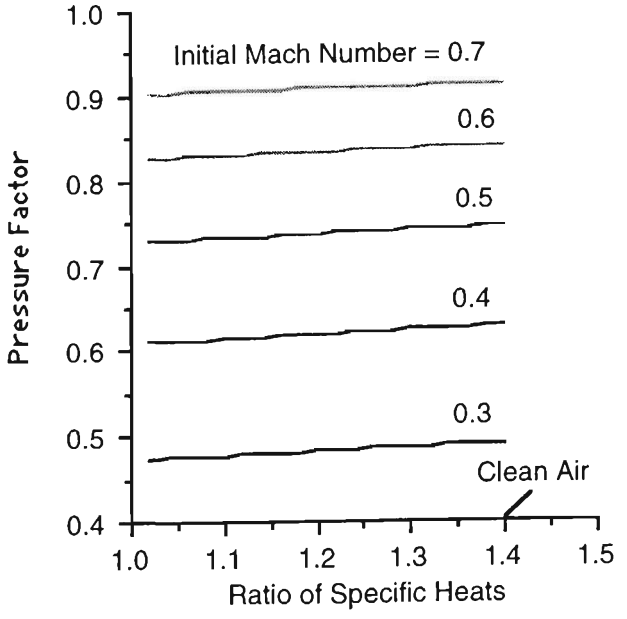

Figure B.1 'Pressure Factor' vs Ratio of Sp Heats

The definition of stagnation temperature uses only the assumption that the flow be adiabatic. At any point in the suspension flow,

$$T_{0_s} = \text{constant} = T_S \left(1 + \frac{\gamma_S - 1}{2} M_S^2\right)$$

At the sonic exit condition, $M_S = 1$. so that

$$T_S = T_{S^*} = \frac{2\, T_{0_s}}{\gamma_S + 1}$$

Appendix C1

```
*  Driver programme for a 4th Order Runge-Kutta routine for solving
*  simultaneous ODEs, representing Nozzle Flow in an SAI.
*Counters
      integer i, k, istep
      integer nstep,nvar,nmax,nstpmx
* Max number of Equations, Max number of Steps, Number of Variables
      parameter(nmax=50,nstpmx=200,nvar=8)
*Constants in Pressure Specification
      real a,b,c
*Matrix definitions
      real vstart(nvar),xx(nstpmx),y(nmax,nstpmx)
      real x1,x2,x3
*Initial (assumed) Mach Number
      real m1
*Initial Pressure, Final Pressure, Pressure Gradient
      real p1,p2,dpdx
*Mach number, Square of Mach number
      real ma,masq
*Stagnation (Total) properties of Primary Stream; Gas CONstant
      real p0,d0,t0,gcon
*Ratio of Sp Heats and recurring Functions thereof
      real gamma, gp1,gm1,rgm1,ggm1,gexp, same
*Sonic Speed and Sonic Speed at Stagn condition
      real sonic,sonic0
*Specific Entropy
      real s
*Geometrical parameters
      real aduct,pi,rtube,atube,rduct,width,hite
*Max Mass Flow Rate
      real maxflo
*Step size, Distance variable, Vectors containing Change in Variable and Variable
      real h,x,dv(nmax),v(nmax)
*Suspension Properties
      real vfp,mfp,mrp,gammas,gcons,texit,pexit,den2e,vexit
*Boundary Layer Calculation Parameters
      real amin,xbl,xbl0,del,delstr,blok

*COMMON Blocks: Presure Gradient, Tube Geometry, Primary Gas, Suspension

      common /prgrd/p1,p2,x1,x2,x3,dpdx
      common /tube/pi,rtube,atube,rduct,aduct,width,hite
      common /gas1/gcon,cp,cv,gamma,gm1,gp1,gp12,rgm1,ggm1,gexp
      common /susp/vfp,mfp,mrp,gammas,gcons,texit,pexit,den2e,vexit

*Definitions of Parameters

      pi = 4.0*atan(1.0)

      nstep = 60

      gcon = 287.0
      cp   = 1004.0
      cv   = 717.0

      gamma = 1.4
      gm1   = gamma - 1.0
```

```
      gp1   = gamma + 1.0
      gp12  = 0.5*gp1
      rgm1  = 1.0/gm1
      ggm1  = gamma/gm1
      gexp  = 0.5*gp1/gm1

*-----Fixing radius of Tube  -----

      rtube = 0.01
      atube = pi*rtube**2

* Uses rk4
*  Starting from initial values vstart(1:nvar) known at x1, use fourth-order
*  Runge-Kutta to advance nstep equal increments to x2. The user-supplied
*  subroutine derivs(h,x,v,dvdx) evaluates derivatives.

      x1 = 0.0
      x2 = 0.2
      x3 = 0.24

      m1 = 0.2

*-----Read suspension properties from SUSPDAT to determine Injection tube exit
conditions
      open(file='SUSPGLS',unit=2)
      do i=1,12
        read(2,*)
      enddo
      read(2,201)vfp,mfp,mrp,gammas,gcons,texit,pexit,den2e,vexit,conp
201   format(10f15.4)

      p2 = pexit

*Setting the initial Mach Number

      ma = m1
      masq = ma*ma

      same = 1.0 + gm1*masq

*--- Setting the initial p0, t0

      p0 = 200000.0

*Different Duct Designs for Different Specified Conditions:

*     do while(p0 .LE. 600000.0)

      t0 = 300.0

*--- Calculation of initial d0

      d0 = p0/(gcon*t0)

*--- Calculation of initial p

      p = p0/same**ggm1
      p1 = p
```

```
*--- Calculation of initial d

      d = d0/same**rgm1

*--- Calculation of initial t

      t = t0/same

*--- Calculation of initial vel

      sonic = sqrt(gamma*gcon*t)
      vel  =  ma*sonic

      sonic0 = sqrt(gamma*gcon*t0)

*--- Setting the initial s
      s = 0.0

*--- Calculation of initial duct size for design mass flow rate
      maxflo = 0.25

*Different Duct Designs for Different Design Mass Flow Rates
*     do while(maxflo .LE. 0.5)

      aduct  = maxflo/(d*vel)

*--- Duct Height for 2D flow, assuming width
      width = 0.030
      hite  = aduct/width

*Outer Radius for Annular Nozzle Duct
      rduct  = sqrt((aduct + atube)/pi)

*----- Calculation of Pressure Gradient

*(Option 1) Linear Pressure Drop in Nozzle region
*     dpdx = (p2-p1)/(x2-x1)
*Different Duct Designs for different injection tube widths
*       do while(width .LE. 0.05)

*----- Load initial values -----

      vstart(1) = ma
      vstart(2) = p
      vstart(3) = d
      vstart(4) = t
      vstart(5) = vel
      vstart(6) = p0
      vstart(7) = s
      vstart(8) = aduct
*     vstart(8) = rduct

*Determining Start of Boundary Layer to Calculate Boundary Layer parameters
      amin = aduct

      do i=1,nvar                    ! Load starting values.
         v(i) = vstart(i)
         y(i,1) = v(i)
```

```
      enddo

      istep = 0

      xx(1) = x1
      x = x1
      h = (x3-x1)/nstep
*     h = 0.01

      k = 0
*Output File
      open(file='CHECK',unit=1)

      write(1,97)width
97    format(/,5x,'2-D Channel Width (const)  = ',f10.3,' m     ',/)
      write(1,98)p0
98    format(/,5x,'Primary Stagnation Pressure = ',f10.3,' Pascals',/)
      write(1,99)maxflo
99    format(/,5x,'Maximum Mass flow Rate     = ',f10.4,' kg/sec ',/)
      write(1,100)
100   format(/,'      x          ma          p          d
     +     t         vel         p0          s     aduct')
      write(1,101)
101   format('-------------------------------------------------------
     +-------------------------------------------------------------
     +-----------',/)
      write(1,102)x,(v(i),i=1,nvar),0.5*v(8)/width

       do k =1,nstep              ! Take nstep steps.
*      do while(p.LE.p2)

*----- Calculation of Pressure Gradient

*          dpdx = (p2-p1)/(x2-x1)
*          dpdx = 0.5*dpdx*pi*sin(pi*x/(x2-x1))

           call derivs(h,x,v,dv)

           call rk4(v,dv,nvar,x,h,v,derivs)

*----- Locating the point of minimum area to start boundary layer calc.

           if(v(8) .LE. amin)then
             amin = v(8)
             xbl0 = x
           endif

           x = x + h
           xx(k+1) = x

           do i=1,nvar
             y(i,k+1) = v(i)
           enddo

           write(1,102)x,(v(j),j=1,nvar),0.5*v(8)/width
102          format(2x,f6.3,9(2x,f12.5))

       enddo
```

```
      write(1,103)
103   format(//,'Suspension Properties',/)
      write(1,104)
104   format('     vfp     mrp     mrp    gammas    gcons    te
     +xit   pexit    den2e    vel2e    conp')
      write(1,105)vfp,mfp,mrp,gammas,gcons,texit,pexit,den2e,vexit,conp
105   format(10f10.4)
      write(1,106)
106   format('*************************************************',//)

*     width = width + 0.01

*     enddo

*     maxflo = maxflo + 0.1

*     enddo

*     p0 = p0 + 100000.0

*     enddo

      end

*****************************************************************
*Standard Fourth-Order Runge-Kutta Suboutine [
      subroutine rk4(y,dydx,n,x,h,yout,derivs)
      integer n,nmax
      real h,x,dydx(n),y(n),yout(n)
      external derivs
      parameter(nmax=50)     ! Max number of functions

*  Given values for the variables y(1:n) and their derivatives dydx(1:n) known
*  at x, use the fourth order Runge-Kutta method to advance the solution over
*  an interval h and return the incremented variables as yout(1:n), which
*  need not be a distinct array from y. The user supplies the subroutine
*  derivs(h,x,y,dydx) which returns derivatives dydx at x.

      integer i
      real h6,hh,xh,dym(nmax),dyt(nmax),yt(nmax)
      hh = 0.5*h
      h6 = h/6.0
      xh = x + hh

      do i=1,n                    ! First Step
        yt(i) = y(i) + hh*dydx(i)
      enddo
      call derivs(h,xh,yt,dyt)

      do i=1,n                    ! Second Step
        yt(i) = y(i) + hh*dyt(i)
      enddo
      call derivs(h,xh,yt,dym)

      do i=1,n                    ! Third Step
        yt(i) = y(i) + h*dym(i)
        dym(i) = dyt(i) + dym(i)
      enddo
```

```
      call derivs(h,x+h,yt,dyt)    ! Fourth Step

      do i=1,n                     ! Accumulate with weightage
       yout(i) = y(i) + h6*(dydx(i) + dyt(i) + 2.0*dym(i))
      enddo

      return
      end

*****************************************************************
*Subroutune for SAI containing Expressions for "Driving Potentials"
      subroutine derivs(h,x,y,dydx)
      integer nmax
      parameter(nmax=50)      ! Max number of functions
      real y(nmax),dydx(nmax)

      real ma,p,d,t,vel,p0,s,aduct,rduct,sonic,rtube
      real x1,x2,x3
      real p1,p2
      real masq,gmsq
      real same1,same2
      real gamma, gp1,gm1,rgm1,ggm1
      real cp,gcon
      real visc,dh,rough,rbydh,redh

      real pi

      real ar,fr,dr,fd,ht,wk,dh0i,ener,em
      real dpdx
      real ff,h
      real far,atube
      real a,b,c
      real vrat
      real ema,emfd,emen,emem
      real epa,epfd,epen,epem
      real eda,edfd,eden,edem
      real eta,etfd,eten,etem
      real eva,evfd,even,evem
      real ep0a,ep0fd,ep0en,ep0em
      real esa,esfd,esen,esem

      common /prgrd/p1,p2,x1,x2,x3,dpdx
      common /tube/pi,rtube,atube,rduct,aduct,width,hite
      common /gas1/gcon,cp,cv,gamma,gm1,gp1,gp12,rgm1,ggm1,gexp
      common /susp/vfp,mfp,mrp,gammas,gcons,texit,pexit,den2e,vexit

*     pi = 4.0*atan(1.0)

*     rtube = 0.01
*     atube = pi*rtube**2

*     x1 = 0.0
*     x2 = 0.2

*     cp = 1004.0
*     gcon = 287.0
*     gamma = 1.4
*     gm1   = gamma - 1.0
```

```
*     gp1  = gamma + 1.0
*     gp12 = 0.5*gp1
*     rgm1 = 1.0/gm1
*     ggm1 = gamma/gm1

      ma   = y(1)
      p    = y(2)
      d    = y(3)
      t    = y(4)

      sonic = sqrt(gamma*gcon*t)
      y(5)  = ma*sonic

      vel  = y(5)
      p0   = y(6)
      s    = y(7)
      aduct = y(8)

      masq = ma*ma
      gmsq = gamma*masq
      same1 = 1.0 + 0.5*gm1*masq
      same2 = 1.0/(1.0-masq)

***** Influence coefficients *****

      vrat = 0.0

      ema  = -ma*same1*same2
      emfd = -ema*0.5*gmsq
      emen = -ema*0.5*(1.0+gmsq)
      emem = -ema*(1.0+gmsq*(1.0-vrat))

      epa  = p*gmsq*same2
      epfd = -0.5*epa*(1.0+gm1*masq)
      epen = -epa*same1
      epem = -epa*(2.0*same1*(1.0-vrat) + vrat)

      eda  = d*masq*same2
      edfd = -0.5*eda*gmsq
      eden = -d*same1*same2
      edem = -d*same2*(gp1*masq - vrat*gmsq)

      eta  = t*gm1*masq*same2
      etfd = -0.5*eta*gmsq
      eten = t*same2*same1*(1.0-gmsq)
      etem = -eta*(1.0+gmsq*(1.0-vrat))

      eva  = -vel*same2
      evfd = -eva*0.5*gmsq
      even = -eva*same1
      evem = -eva*(1.0+gmsq*(1.0-vrat))

      ep0a  = 0.0
      ep0fd = -p0*0.5*gmsq
      ep0en = ep0fd
      ep0em = -p0*gmsq*(1.0-vrat)

      esa  = 0.0
```

```
      esfd = 0.5*cp*gm1*masq
      esen = cp*same1
      esem = cp*gm1*masq*(1.0-vrat)

*----- Driving Potentials -----

*-- Linear (Cos/Parabolic) decrease of Static Pressure from p1 to p2
*---over a distance of (x2-x1) meters - - -

*     dpdx = (p2-p1)/(x2-x1)
*     dpdx = 0.5*dpdx*pi*sin(pi*x/(x2-x1))

      a = (p1-p2)/(x1**2-x2**2 - 2.0*x2*(x1-x2))
      b = -2.0*a*x2

*--- Extending to dpdx = 0 in interaction region -----

      if(x .LE. x2)then
        dpdx = 2.0*a*x + b
      else
        dpdx = 0.0

      endif

*     print *,'dpdx =',dpdx

*----- Calculation of dynamic viscosity -----

      viscon = 1.452e-06          ! Constant for AIR in Sutherland law
      visc = viscon*(t**(1.5)/(t + 110.0))

*----- Calculation of friction factor ff -----

*     dh = 2.0*(rduct - rtube)
*'Wetted Perimeter', Hydraulic Diameter for Rectangular Cross section Nozzle
      wp = 2.0*(width+hite)
      dh = 4.0*aduct/wp
*Height of Roughness Element and Roughness Parameter
      rough = 0.000002
      rbydh = rough/dh
*Reynolds Number based on Hydraulic Diameter; Friction Factor (Haalands Formula
[W7]
*     redh  = d*vel*dh/visc
*     denom = -1.8*alog10((rbydh/3.7)**(1.11) + 6.9/redh)

*----- Assume FULLY ROUGH flow regime -- ff indep of ReDH
      denom = -2.0*alog10(rbydh/3.7)
      ff = (1.0/denom)**2

***** Driving Potentials *****
*FRiction and DRag
      fr = ff/dh
      dr = 0.0
      fd = fr + dr
*ENERgy Transfer as HeaT and/or WorK, or due to Incoming fluid
      ht  = 0.0
      wk  = 0.0
      dh0i = 0.0
```

```
      ener = ht + wk - dh0i
*Entrained Mass
      em = 0.0

      ar = ((dpdx) - (epfd*fd + epen*ener + epem*em))/epa

*----- Factor to calculate Duct Radius from Duct Area

*     far = (rduct**2 - atube)/(2.0*rduct)

***** Differential equations *****
      dydx(1) = ema*ar +  emfd*fd +  emen*ener +  emem*em
      dydx(2) = dpdx
      dydx(3) = eda*ar +  edfd*fd +  eden*ener +  edem*em
      dydx(4) = eta*ar +  etfd*fd +  eten*ener +  etem*em
      dydx(5) = eva*ar +  evfd*fd +  even*ener +  evem*em
      dydx(6) = ep0a*ar + ep0fd*fd + ep0en*ener + ep0em*em
      dydx(7) = esa*ar +  esfd*fd +  esen*ener +  esem*em
      dydx(8) = (aduct/epa)*(dpdx - (epfd*fd + epen*ener + epem*em))

      return
      end
```

Appendix C2

*This programme describes the flow in the Interaction region of the SAI.

```
      integer i, k, istep
      integer nstep,nvar,nmax,nstpmx
      parameter(nmax=50,nstpmx=200,nvar=10)
      real vstart(nvar),xx(nstpmx),y(nmax,nstpmx)
      real x1,x2
      real p1,p2,dpdx
      real ma,masq
      real p0,d0,t0,gcon
      real same1,same2
      real gamma, gp1,gm1,rgm1,ggm1,gexp
      real sonic,sonic0,sonict
      real s
      real aduct,pi,rtube,rthr,athr,atube,rduct,wtube,htube
      real flofac, maxflo
      real h,x,dv(nmax),v(nmax)
      real vfp,mfp,mrp,gammas,gcons,tp,tp1,pexit,den2e,velp1,velp,conp
      real dp,denmp,massp,volp
      real ma,p,d,t,vel,p0,s,rduct,aduct,width,hite
      real ma1,d1,t1,vel1,p01,s1,rduct1

      common /prgrd/p1,p2,x1,x2,dpdx
      common /tube/pi,rtube,atube,htube,wtube,width,hite
      common /gas1/gcon,cp,cv,gamma,gm1,gp1,gp12,rgm1,ggm1,gexp
      common /susp/vfp,mfp,mrp,gammas,gcons,tp1,pexit,den2e,velp1,conp
      common /particle/denmp,dp,cmp,volp,massp
      common /annend/ma1,d1,t1,vel1,p01,s1,aduct1

*-- Primary Gas Properties
      data gcon,cp,cv,gamma/287.0,1004.0,717.0,1.4/
*-- Conveyed particle properties (Coal particles from reference)
*     data denmp,dp,cmp/1360.0,50.0e-06,1255.0/
*-- 150 miccron Glass beads used in experiment
      data denmp,dp,cmp/2480.0,150.0e-06,840.0/
      pi= 4.0*atan(1.0)
      volp = pi*dp**3/6.0
      massp = denmp*volp

      nstep = 10

      gm1   = gamma - 1.0
      gp1   = gamma + 1.0
      gp12  = 0.5*gp1
      rgm1  = 1.0/gm1
      ggm1  = gamma/gm1
      gexp  = 0.5*gp1/gm1

*-- Fixing radius of Tube (for Circular Cross section tube) -----
*     rtube = 0.01
*     atube = pi*rtube**2
*-- Fixing Injection tube cross section -----
      htube = 0.005
      wtube = 0.030
      atube = htube*wtube
```

```
*-- Fixing Nozzle Width -----
     width = wtube

* Uses rk4
*  Starting from initial values vstart(1:nvar) known at x1, use fourth-order
*  Runge-Kutta to advance nstep equal increments to x2. The user-supplied
*  subroutine derivs(h,x,v,dvdx) evaluates derivatives.

*-----Read suspension properties from SUSPDAT as initial suspension parameters
     open(file='SUSPGLS',unit=2)
     do i=1,22
      read(2,*)
     enddo
     read(2,201)vfp,mfp,mrp,gammas,gcons,tp1,pexit,den2e,velp1,conp
201   format(10f15.4)

*-----Read Initial Primary Gas parameters from EXP2D
     open(file='EXP2D',unit=3)
     do i=1,63
      read(3,*)
     enddo
     read(3,301)x1,ma1,p1,d1,t1,vel1,p01,s1,aduct1
301   format(f8.3,8f14.5)

     ma    = ma1
     p     = p1
     d     = d1
     t     = t1
     vel   = vel1
     p0    = p01
     s     = s1
     aduct = aduct1
     velp  = velp1
     tp    = tp1

     x2 = x1 + 0.04

     masq = ma*ma
     same1 = 1.0 + gm1*masq
     same2 = 1.0/(1.0-masq)
*----- Setting of Zero Pressure Gradient in Interaction Region
     p2 = p1
     dpdx = (p2 -p1)/(x2 - x1)
*----- Load initial values -----
     vstart(1)  = ma
     vstart(2)  = p
     vstart(3)  = d
     vstart(4)  = t
     vstart(5)  = vel
     vstart(6)  = p0
     vstart(7)  = s
     vstart(8)  = aduct
     vstart(9)  = velp
     vstart(10) = tp

     do i=1,nvar                    ! Load starting values.
        v(i) = vstart(i)
        y(i,1) = v(i)
```

```
      enddo

      istep = 0

      xx(1) = x1
      x = x1
      h = (x2-x1)/nstep

      k = 0

      open(file='INTP1',unit=1)

      write(1,100)
100   format(/,'      x          ma          p          d
     +      t         vel         p0          s      aduct
     +  velp         tp')
      write(1,101)
101   format('----------------------------------------------------------
     +-------------------------------------------------------------
     +-------------------',/)
      write(1,102)x,(v(i),i=1,nvar),0.5*v(8)/width

       do k =1,nstep              ! Take nstep steps.
*       do while(x.LE.x2)

          call derivs(h,x,v,dv)

          call rk4(v,dv,nvar,x,h,v,derivs)

          x = x + h
          xx(k+1) = x

          do i=1,nvar
            y(i,k+1) = v(i)
          enddo

          write(1,102)x,(v(j),j=1,nvar),0.5*v(8)/width
102         format(2x,f6.3,11(2x,f12.5))

       enddo
      end

**********************************************************************

      subroutine rk4(y,dydx,n,x,h,yout,derivs)
      integer n,nmax
      real h,x,dydx(n),y(n),yout(n)
      external derivs
      parameter(nmax=50)     ! Max number of functions

*  Given values for the variables y(1:n) and their derivatives dydx(1:n) known
*  at x, use the fourth order Runge-Kutta method to advance the solution over
*  an interval h and return the incremented variables as yout(1:n), which
*  need not be a distinct array from y. The user supplies the subroutine
*  derivs(h,x,y,dydx) which returns derivatives dydx at x.

      integer i
      real h6,hh,xh,dym(nmax),dyt(nmax),yt(nmax)
```

```
      hh = 0.5*h
      h6 = h/6.0
      xh = x + hh

      do i=1,n                    ! First Step
       yt(i) = y(i) + hh*dydx(i)
      enddo
      call derivs(h,xh,yt,dyt)

      do i=1,n                    ! Second Step
       yt(i) = y(i) + hh*dyt(i)
      enddo
      call derivs(h,xh,yt,dym)

      do i=1,n                    ! Third Step
       yt(i) = y(i) + h*dym(i)
       dym(i) = dyt(i) + dym(i)
      enddo
      call derivs(h,x+h,yt,dyt)   ! Fourth Step

      do i=1,n                    ! Accumulate with weightage
       yout(i) = y(i) + h6*(dydx(i) + dyt(i) + 2.0*dym(i))
      enddo

      return
      end

**********************************************************************
* This subroutine calculates driving potentials for flow in the Interaction Region of
* the SAI.

      subroutine derivs(h,x,y,dydx)
      integer nmax
      parameter(nmax=50)     ! Max number of functions
      real y(nmax),dydx(nmax)

      real ma,p,d,t,vel,p0,s,rduct,sonic,rtube
      real atube,wtube,htube,width,hite,aduct,width
      real m1,m2,x1,x2
      real p1,p2
      real masq,gmsq
      real same1,same2
      real gamma, gp1,gm1,rgm1,ggm1
      real cp,gcon
      real visc,dh,rough,rbydh,redh
      real vinf,kf,kfcon,xcore,cd,vrel,nu
      real ma1,d1,t1,vel1,p01,s1,aduct1
      real denmp,dp,cmp,volp,massp

      real pi

      real ar,fr,dr,fd,ht,wk,dh0i,ener,em
      real dpdx
      real ff,h
      real far,atube

      real vrat
      real ema,emfd,emen,ememm
```

```
      real epa,epfd,epen,epem
      real eda,edfd,eden,edem
      real eta,etfd,eten,etem
      real eva,evfd,even,evem
      real ep0a,ep0fd,ep0en,ep0em
      real esa,esfd,esen,esem

      common /prgrd/p1,p2,x1,x2,dpdx
      common /tube/pi,rtube,atube,htube,wtube,width,hite
      common /gas1/gcon,cp,cv,gamma,gm1,gp1,gp12,rgm1,ggm1,gexp
      common /susp/vfp,mfp,mrp,gammas,gcons,tp1,pexit,den2e,velp1,conp
      common /particle/denmp,dp,cmp,volp,massp
      common /annend/ma1,d1,t1,vel1,p01,s1,aduct1

      ma   = y(1)
      p    = y(2)
      d    = y(3)
      t    = y(4)

      sonic = sqrt(gamma*gcon*t)
      y(5)  = ma*sonic

      vel   = y(5)
      p0    = y(6)
      s     = y(7)
      aduct = y(8)
      velp  = y(9)
      tp    = y(10)

*     aduct = pi*rduct**2

      masq = ma*ma
      gmsq = gamma*masq
      same1 = 1.0 + 0.5*gm1*masq
      same2 = 1.0/(1.0-masq)

*----- Influence coefficients -----

      vrat = 0.0

      ema  = -ma*same1*same2
      emfd = -ema*0.5*gmsq
      emen = -ema*0.5*(1.0+gmsq)
      emem = -ema*(1.0+gmsq*(1.0-vrat))

      epa  = p*gmsq*same2
      epfd = -0.5*epa*(1.0+gm1*masq)
      epen = -epa*same1
      epem = -epa*(2.0*same1*(1.0-vrat) + vrat)

      eda  = d*masq*same2
      edfd = -0.5*eda*gmsq
      eden = -d*same1*same2
      edem = -d*same2*(gp1*masq - vrat*gmsq)

      eta  = t*gm1*masq*same2
      etfd = -0.5*eta*gmsq
      eten = t*same2*same1*(1.0-gmsq)
```

```
      etem = -eta*(1.0+gmsq*(1.0-vrat))

      eva  = -vel*same2
      evfd = -eva*0.5*gmsq
      even = -eva*same1
      evem = -eva*(1.0+gmsq*(1.0-vrat))

      ep0a  = 0.0
      ep0fd = -p0*0.5*gmsq
      ep0en = ep0fd
      ep0em = -p0*gmsq*(1.0-vrat)

      esa  = 0.0
      esfd = 0.5*cp*gm1*masq
      esen = cp*same1
      esem = cp*gm1*masq*(1.0-vrat)

*----- Driving Potentials -----


*----- Calculation of dynamic viscosity, thermal conductivity -----

      viscon = 1.452e-06          ! Constant for AIR in Sutherland law
      visc = viscon*(t**(1.5)/(t + 110.0))
*----- Calculate thermal conductivity kf from Prandtl No = 0.71
      kf  =  visc*cp/0.71

*----- Calculation of friction factor ff -----

      hite = aduct/width
      dh = 0.5*aduct/(width+hite)
      rough = 0.000002
      rbydh = rough/dh

      redh  = d*vel*dh/visc
*     denom = -1.8*alog10((rbydh/3.7)**(1.11) + 6.9/redh)

*----- Assume FULLY ROUGH flow regime -- ff indep of ReDH
      denom = -2.0*alog10(rbydh/3.7)
      ff = (1.0/denom)**2

      fr = ff/dh

*----- Calculating the extent of Initial region (Potential Core Xc)-----

      vbar = velp1/vel1
      rhobar = den2e/d1

*     vbar = vel1/velp1
*     rhobar = d1/den2e

      xcore = 4.0*htube*(1.0 + vbar*rhobar)/((1.0-vbar)*(1.0+rhobar))
      print *, 'core length = ', xcore

*----- Specifying Drag Coeff and Nusselt No for small particles = Stokes values

      cd = 1.0        !Ratio cd/cdstokes
      nu = 1.0        !Ratio nu/nustokes
```

```
*----- Specifying driving potentials in Initial Region and Main Region -----

      if(x-x1 .LE. xcore) then          ! Initial Region

*       vinf = atube*(1.0-(1.0-(x-x1)/xcore)**2)
        vinf = atube*(x-x1)/xcore
        vrel = vel - velp
        tdiff = tp - t

        dr = 3.0*pi*visc*cd*dp*vrel*conp*vinf
        dr = dr/(gamma*masq*p*aduct*massp)

        ht = 2.0*nu*kf*dp*tdiff*conp*vinf
        ht = ht/(massp*same1*cp*t*d*vel*aduct)

        wk = 3.0*pi*visc*cd*dp*vrel*conp*vinf*velp
        wk = wk/(massp*same1*cp*t*d*vel*aduct)

        em = 2.0*den2e*velp*atube*(1.0-x/xcore)/(xcore*same1*cp*t)

*       dh0i = (cp*t0 - cps*t0s)*em/(same1*cp*t)

        ener = ht - wk - dhoi

      else                              ! Main Region

        vinf = atube
        vrel = vel - velp
        tdiff = tp - t

        dr = 3.0*pi*visc*dp*vrel*conp*vinf
        dr = dr/(gamma*masq*p*aduct*massp)

        ht = 2.0*nu*kf*dp*tdiff*conp*vinf
        ht = ht/(massp*same1*cp*t*d*vel*aduct)

        wk = 3.0*pi*visc*cd*dp*vrel*conp*vinf*velp
        wk = wk/(massp*same1*cp*t*d*vel*aduct)

        em = 0.0
        dh0i = 0.0
        ener = ht - wk - dhoi

      endif

      fd = fr + dr

      ar = ((dpdx) - (epfd*fd + epen*ener + epem*em))/epa

*----- Factor to calculate Duct Radius from Duct Area

*     far = (rduct**2 - atube)/(2.0*rduct)

*-- Differential equations -----

      dydx(1) = ema*ar +  emfd*fd +  emen*ener +  emem*em
      dydx(2) = dpdx
      dydx(3) = eda*ar +  edfd*fd +  eden*ener +  edem*em
```

```
dydx(4) = eta*ar +  etfd*fd +  eten*ener +  etem*em
dydx(5) = eva*ar +  evfd*fd +  even*ener +  evem*em
dydx(6) = ep0a*ar + ep0fd*fd + ep0en*ener + ep0em*em
dydx(7) = esa*ar +  esfd*fd +  esen*ener +  esem*em
dydx(8) = (aduct/epa)*(dpdx - (epfd*fd + epen*ener + epem*em))
dydx(9) = (18.0*visc*cd/(denmp*dp**2))*(vel - velp)/velp
dydx(10)= -12.0*nu*kf*tdiff/(denmp*cmp*velp*dp**2)

return
end
```

Appendix C3

```
* Suspension Properties in terms of Particle Volume fraction

      real mp,mfp,vfp, mrp,mwp,mws,mwg2,mstart,masq
      real mflux, mflow, mflowp
      real mug,mus,nug,nus
      real gcons
      real rtube,atube,htube,wtube

***** Particle properties *****

*     denmp = density of particle material (kg/m3)
*     dens  = density of suspension (kg/m3)
*     dp    = particle diameter (m)
*     cmp   = specific heat of particle material(J/kgK)
*     mp    = mass of a particle (kg)
*     mwp   = molecular weight of particle (kg/kgmole)

***** Suspension Properties *****

*     mws   = molecular weight of suspension (kg/kgmole)
*     nus   = kinematic viscosity of suspension
*     mus   = dynamic viscosity of suspension

***** Gas Properties *****

*     nug   = kinematic viscosity of gas
*     mug   = dynamic viscosity of gas

*     data denmp,dp,pi,cmp/1360.0,50.0e-06,3.141593,1255.0/

*Properties of Glass beads in Lab

      data denmp,dp,pi,cmp/2480.0,150.0e-06,3.141593,840.0/

***** Secondary gas (air) properties *****

      data gcong2,gg2,mwg2,cpg2,cvg2/287.0,1.4,28.96,1005.0,718.0/
      data runiv/8314.0/

***** Injection Tube Area _____

*     rtube = 0.005
*     atube = pi*rtube**2

      htube = 0.005
      wtube = 0.010
      atube = htube*wtube

      crat = cmp/cpg2

      data mug/1.5e-05/

***** Stagnation values *****
      data p02,t02/100000.0,300.0/
      deng02 = p02/(gcong2*t02)
```

```
      mp  = pi*dp**3*denmp/6.0
      mwp = mp/1.67e-27

***** Initial values for particle volume fraction and mach number *****

      mstart = 0.6
      masq = mstart**2

      open(file='SUSPGLS',unit=3)
C
      write(3,101)dp,denmp,mwp,htube,wtube
101   format(5x,'        Particle Diameter =',f10.5,'m',//,
     +       5x,'        Particle Density  =',f10.5,'kg/m3',//,
     +       5x,' Particle Molecular Weight  =',e10.5,'kg/kgmole',//,
     +       5x,'    Injection Tube Height  =',f10.5,'m',/,
     +       5x,'    Injection Tube Width   =',f10.5,'m',/)
*    +       5x,'    Injection Tube Radius  =',f10.5,'m',/)
      write(3,102)
102   format(/,'          vfp          mfp          mrp          ga
     +mmas          gcons          texit          pexit          den2e
     +          vexit          conp          mflow      ptons/h',/)

      vfp = 0.0

      do while(vfp.LE.0.05)

        onemv = 1.0 - vfp
        conp = denmp*vfp
        cong02 = deng02*onemv
        den02  = conp + cong02
        mfp = conp/den02
        onemm = 1.0 - mfp
        mrp = mfp/onemm
        mws = 1.0/(mfp/mwp + onemm/mwg2)
        gcons = runiv/mws
        gammas = gg2*(1.0 + mrp*crat)/(1.0 + gg2*mrp*crat)
        g2p1 = gammas + 1.0
        g2m1 = gammas - 1.0
        gexp1 = gammas/g2m1
        gexp2 = 0.5*gexp1

***** Temperature at injection tube exit *****

        t2e = 2.0*t02/g2p1
        v2e = sqrt(gammas*gcons*t2e)

***** Pressure at injection tube exit *****

        p2ep02 = mstart*(2.0/g2p1)**gexp1
        p2ep02 = p2ep02*(g2p1/(2.0+g2m1*masq))**gexp2
        p2e = p2ep02*p02
        den2e = p2e/(t2e*gcons)
        mflux = den2e*v2e
        mflow = mflux*atube

* Particle mass flow rate in Tonnes per hour
        mflowp = mfp*mflow*3.6
        mus    = mug*(1.0 + 2.5*vfp)
```

```
      nus    = mus/den02
      write(4,99)vfp,mus,nus
99      format(f12.4,5x,2(e15.4))

     write(3,103)vfp,mfp,mrp,gammas,gcons,t2e,p2e,den2e,v2e,conp,mflow,
    +mflowp
103     format(12(f15.4))

       vfp = vfp + 0.001

     enddo
     end
```

Appendix C4

```
* In this programme, the multiple-shock region in a confined, initially
* supersonic flow is modelled as a 'modified' Fanno flow.
* In the region of supersonic-to-sonic deceleration, it is assumed that
* after each successive normal shock, only a fraction of the mass flow
* is subject to further acceleration to a supersonic speed before the
* next normal shock is encountered.
* But, as the area available to the core flow also decreases due to the
* growing boundary layers along the walls, we assume that these two
* effects are such that the mass FLUX remains constant. This allows the
* core flow to be modelled as a Fanno flow.

* It is found that each shock is weaker than the previous one. The flow
* approaches sonic velocity asymptotically.

* The values obtained in this model are applicable to the core flow.
* specifically, on the centerline in an axisymmetric/rectangular cross section flow.

* The data is taken from Om, Childs, Ref [O1], and from SAI Experiment.

      real ma1,ma2,ma, masq, mflux, msqm1,maav,maav2
      real cp,dxdh,xdh

      data p0i, t0i/1.332e+05,300.0/      ! Assume GAUGE pressure in (6).
      data dh/0.0519/
      data r,cp/287.0,1004.0/
      data gamma/1.4/

* Stagnation Parameters.....
      d0 = p0i/(r*t0i)
      p0 = p0i
      t0 = t0i

* Compute constants to be used repeatedly .....
      gm1  = gamma - 1.0
      gp1  = gamma + 1.0
      gm12 = 0.5*gm1
      gp12 = 0.5*gp1
      ggm1 = gamma/gm1
      rgm1 = 1.0/gamma
      gexp = gp12/gm1

* Assuming isentropic flow upto the occurence of the first shock,
* calculate static properties .....
* Assume initial Mach number value.
* 'Ma1' means Mach number before a shock.

      open(file='MFANNO',unit = 1)

      ma  = 1.49
      ma1 = ma

* Starting value of entropy assumed zero ...

      s = 0.0

* Call this value of entropy 's1', meaning 'before the shock'
```

```
      s1 = s

*  Start of the Multiple-Shock region ... (non-dim. distance x/dh)

      xdh = 0.0

      write(1,10) ma
10    format(1h1,10x,'Initial Mach Number  = ',f6.4)

      write(1,20) p0,t0
20    format(//,5x,'Stagnation Condition : ',f10.2,' N/m2  ',f6.2,'K')

      write(1,30)
30    format(//,5x,'Mach No.   Temp    Press.  Entropy    p/p0i
     +   p0/p0i    p/p0    xdh ',//)

*  Start of repeated calculations ....

       niter = 1

       do while(niter.le.10)

        ma1 = ma
        masq  = ma*ma
        same  = 1.0 + gm12*masq
        gmsq  = gamma*masq
        msqm1 = masq - 1.0

        t    = t0/same
        d    = d0/same**rgm1
        p    = p0/same**ggm1
        pp0  = p/p0
        p0p0i = p0/p0i
        pp0i  = p/p0i

        t1 = t
        d1 = d
        p1 = p

*  Compute sonic velocity, velocity, mass flux .....

        svel  = sqrt(gamma*r*t)
        vel   = svel*ma
        mflux = vel*d

*  Calculate Dynamic Viscosity from 'Sutherland Law' for clean air .....
        emu1 = (t**(1.5)/(t + 110.0))*1.452e-06

*  Calculate 'Unit Reynolds number' (based on length = 1)
        re1 = mflux/emu1

        write(1,60)ma,t,p,s,pp0i,p0p0i,pp0,xdh
60      format(5x,f6.4,3x,f7.3,3x,f9.2,3x,f8.3,4(3x,f8.4))

*  Assume that a normal shock occurs at this point, and compute
*  properties across the shock .....
```

```
*  Stagnation pressure ratio in 2 steps because long formula ....
       p0rat = (gm1/gp1+2.0/(gp1*masq))**gamma
       p0rat = (p0rat*(2.0*gamma*masq-gm1)/gp1)**(-1/gm1)

*  Subsonic Mach number .....
       ma = ((gm1*masq + 2.0)/(2.0*gamma*masq - gm1))**0.5
       ma2 = ma
       maav = (ma1 + ma2)*0.5
       masq = ma*ma
       same = 1.0 + gm12*masq

*  Changed values of stagnation pressure and density after shock .....
*  stagnation temperature remains constant, because adiabatic flow .....
       p0 = p0*p0rat
       d0 = p0/(r*t0)

*  Changed value of static pressure due to shock (prat = p2/p1).....
       prat = (2.0*gamma*masq - gm1)/gp1
       p = p*prat

*  Entropy calculation ..... only due to normal shock .....
       ds  = -r*alog(p0rat)
       dsn = ds
       s = s + ds

*** Distance between shocks ***
    ff = 0.10
    maav = 0.5*(ma1 + ma2)
    maav2 = maav*maav
    dxdh =  2.0*ds/(cp*gm12*maav2*ff)
    xdh = xdh + dxdh

*Static Temperature, density, pressure .....
       t = t0/same
       d = d0/same**rgm1
       p = p0/same**ggm1

       pp0 = p/p0
       p0p0i = p0/p0i
       pp0i = p/p0i

       t2 = t
       d2 = d
       p2 = p

       emu2 = (t**(1.5)/(t + 110.0))*1.452e-06

*Sonic velocity, velocity, Mass flux .....
       svel  = sqrt(gamma*r*t)
       vel   = svel*ma
       re2 = mflux/emu2

       write(1,60)ma,t,p,s,pp0i,p0p0i,pp0

*  Area ratio corresponding to supersonic Mach number [W7].....

       aastar = (same/gp12)**gexp/ma
```

```
*  Corresponding supersonic Mach number .....
*  This is the isentropic supersonic Mach number [W7].....

        if (aastar.LE.2.90) then
          ma = 1.0 + 1.2*sqrt(aastar - 1.0)
        else
          ma = (216.0*aastar - 254.0*aastar**(0.6667))**(0.2)
        end if

        niter = niter + 1

      end do
    stop
    end
```

Appendix C5

```
*--- This is an extension of the "Modified Fanno" model to dilute suspensions.

      real vfp,mfp,mrp,onemv,onemm
      real dp,denmp,cmp,volp,mwp,massp,conp,crat

      real ma1,ma2,ma, masq, mflux, msqm1,maav,maav2,mwg,mws
      real cp,dxdh,xdh

      data p0i, t0i/1.332e+05,300.0/      ! Assume GAUGE pressure in (6).
      data dh/0.0519/
      data r,cp,gamma,mwg,runiv/287.0,1004.0,1.4,28.96,8314.0/
      data denmp,dp,cmp/2840.0,50.0e-6,1255.0/

      pi = 4.0*atan(1.0)

      deng0 = p0i/(r*t0i)

      volp = pi*dp**3/6.0
      massp = denmp*volp
      mwp = massp/1.67e-27

      crat = cmp/cp

      open(file='SFANNO',unit = 1)

      vfp = 0.0

      do while (vfp .LE. 0.05)

       onemv = 1.0 - vfp
       conp  = denmp*vfp
       cong0 = deng0*onemv

       den0 = conp + cong0

       mfp = conp/den0
       onemm = 1.0 - mfp
       mrp = mfp/onemm

       mws = 1.0/(mfp/mwp + onemm/mwg)
       r = runiv/mws

       gammas = gamma*(1.0 + mrp*crat)/(1.0 + gamma*mrp*crat)
       cps = (cp + mrp*cmp)/(1.0 + mrp)

       g2p1 = gammas + 1.0
       g2m1 = gammas - 1.0
       gexp1 = gammas/g2m1
       gexp2 = 0.5*gexp1

*  Compute stagnation density .....

       d0 = p0i/(r*t0i)
       p0 = p0i
       t0 = t0i
```

```
*  Compute constants to be used repeatedly .....
      gm1  = gammas - 1.0
      gp1  = gammas + 1.0
      gm12 = 0.5*gm1
      gp12 = 0.5*gp1
      ggm1 = gammas/gm1
      rgm1 = 1.0/gammas
      gexp = gp12/gm1

*  Assuming isentropic flow upto the occurence of the first shock,
*  calculate static properties .....
*  Assume initial Mach number value.
*  'Ma1' means Mach number before a shock.

      ma  = 1.5
      ma1 = ma

*  Starting value of entropy assumed zero ...

      s = 0.0

*  Call this value of entropy 's1', meaning 'before the shock'

      s1 = s

*  Start of the Multiple-Shock region ... (non-dim. distance x/dh)

      xdh = 0.0

      write(1,9)
9      format(10x,'==================================',/)
      write(1,10) ma
10     format(10x,'INITIAL MACH NUMBER     = ',f6.4)

      write(1,11) vfp
11     format(10x,'Solids Volume Fraction  =',f6.4)

      write(1,12) gammas
12     format(10x,'Isentropic Exponent  = ',f6.4)

      write(1,20) p0,t0
20     format(//,5x,'STAGN COND : ',f10.2,' N/m2  ',f6.2,'K')

      write(1,30)
30     format(//,5x,'Mach No.   Temp    Press.  Entropy    p/p0i
     +   p0/p0i    p/p0     xdh ',//)


*  Start of repeated calculations ....

      niter = 1

      do while(niter.le.10)
        ma1 = ma
        masq  = ma*ma
        same  = 1.0 + gm12*masq
        gmsq  = gammas*masq
        msqm1 = masq - 1.0
```

```
      t    = t0/same
      d    = d0/same**rgm1
      p    = p0/same**ggm1
      pp0  = p/p0
      p0p0i = p0/p0i
      pp0i  = p/p0i

      t1 = t
      d1 = d
      p1 = p

*  Compute sonic velocity, velocity, mass flux .....

      svel  = sqrt(gammas*r*t)
      vel   = svel*ma
      mflux = vel*d

*  Calculate Dynamic Viscosity from 'Sutherland Law' for clean air .....

      emu1 = (t**(1.5)/(t + 110.0))*1.452e-06

*  Calculate 'Unit Reynolds number' (based on length = 1)

      re1 = mflux/emu1

      write(1,60)ma,t,p,s,pp0i,p0p0i,pp0,xdh
60      format(5x,f6.4,3x,f7.3,3x,f9.2,3x,f8.3,4(3x,f8.4))

*  Assume that a normal shock occurs at this point, and compute
*  properties across the shock .....

*  Stagnation pressure ratio in 2 steps because long formula ....
      p0rat = (gm1/gp1+2.0/(gp1*masq))**gammas
      p0rat = (p0rat*(2.0*gammas*masq-gm1)/gp1)**(-1/gm1)

*  Subsonic Mach number .....
      ma = ((gm1*masq + 2.0)/(2.0*gammas*masq - gm1))**0.5
      ma2 = ma
      maav = (ma1 + ma2)*0.5
      masq = ma*ma
      same = 1.0 + gm12*masq

*  Changed values of stagnation pressure and density after shock .....
*  stagnation temperature remains constant, because adiabatic flow .....
      p0 = p0*p0rat
      d0 = p0/(r*t0)

*  Changed value of static pressure due to shock (prat = p2/p1).....
      prat = (2.0*gammas*masq - gm1)/gp1
      p = p*prat

*  Entropy calculation ..... only due to normal shock .....
      ds  = -r*alog(p0rat)
      dsn = ds
      s = s + ds

*** Distance between shocks ***
```

```
      ff = 0.10
      maav = 0.5*(ma1 + ma2)
      maav2 = maav*maav
      dxdh =  2.0*ds/(cps*gm12*maav2*ff)
      xdh = xdh + dxdh

*     Static Temperature, density, pressure .....

        t = t0/same
        d = d0/same**rgm1
        p = p0/same**ggm1

        pp0 = p/p0
        p0p0i = p0/p0i
        pp0i = p/p0i

        t2 = t
        d2 = d
        p2 = p

        emu2 = (t**(1.5)/(t + 110.0))*1.452e-06

*     Sonic velocity, velocity, Mass flux .....

        svel  = sqrt(gammas*r*t)
        vel   = svel*ma
        re2 = mflux/emu2

        write(1,60)ma,t,p,s,pp0i,p0p0i,pp0

*     Area ratio corresponding to supersonic Mach number [W7].....
        aastar = (same/gp12)**gexp/ma

*     Corresponding supersonic Mach number .....
*     This is the isentropic supersonic Mach number [W7] .....

        if (aastar.LE.2.90) then
          ma = 1.0 + 1.2*sqrt(aastar - 1.0)
        else
          ma = (216.0*aastar - 254.0*aastar**(0.6667))**(0.2)
        end if

        niter = niter + 1

      end do

      vfp = vfp + 0.001

    enddo

    stop
    end
```

Appendix C6

```
*This programme calculates core mass flow rate, etc. with downstream distance
*(x/DH) according to Ikui et al.

*FURTHER MODIFICATION TO TEST PSHOCKS IN MULTIPHASE FLOWS
*TEST FOR GAMMA FROM 1.4 TO 1.1

*DECLARATIONS
*Stagnation and Static Parameters; sonic speed
      real p0,t0,rho0,rho,t,vel,sonic
*Gas Constant, Ratio of Sp Heats, Recurring parameters
      real gcon,cp,gamma,gm1,rgm1,ggm1,gm12,gp1,gp12,gm12g,gp12g
*Crocco Number, in Core and Boundary Later Flow
      real w1,wstar2,w2,c,x,wp,wpp,ws2wp,ws2wpp,ws2w1,delw,wstar
      real w12,wpwpp
*Impulse Functions in Core and Boundary Layer Flow
      real jpj1n,jppj1n,jpj1d,jppj1d,jpj1,jppj1
*Mass Flow Rate Ratio
      real mu,mun,mud,mcorem
*Mach Numbers in Core and Boundary Layer Flows
      real ma,map,mapp
*Area Ratios in Core and Boundary Layer Flows
      real apa1,appa1
*Pressure Ratios in Core and Boundary Layer Flows
      real pp1n,pp1d,pp1,p1,p0p,p0pp
*Geometrical Parameters and
      real pi, rad, area, mflo,mcore
*Pseudo-shock length
      real len
*Recurring function of gamma and Mach number in Core and Boundary Layer Flow
      real same, samep,samepp

      pi = 4.0*atan(1.0)
      rad = 0.02595              ! Duct Radius in meters
      area = pi*rad**2

      data p0,t0/1.3325e+05,300.0/   ! Data from Om, Childs..p0 assumed gauge

      gcon  = 287.0
      cp    = 1004.0
      gamma = 1.4

      open(file='MCORE',unit=1)

      do while(gamma .GE. 1.1)

        gm1   = gamma - 1.0
        rgm1  = 1.0/gm1
        ggm1  = gamma/gm1
        gm12  = 0.5*gm1
        gm12g = gm12/gamma
        gp1   = gamma + 1.0
        gp12  = 0.5*gp1
        gp12g = gp12/gamma

        wstar2 = gm1/gp1
        wstar  = sqrt(gm1/gp1)
```

```
      c  = 0.114                ! Constant in Ikui's Model

      ma = 1.49
      same = 1.0 + gm12*ma*ma

*----- Static Pressure just before first shock

      p1 = p0/same**ggm1
      print *, 'p1 =  ',p1

* -- Calculate total mass flow rate 'mflo'

      rho0 = p0/(gcon*t0)

      rho  = rho0/same**rgm1
      t    = t0/same
      sonic = sqrt(gamma*gcon*t)

      vel  = ma*sonic

      mflo = vel*rho*area

      w1 = sqrt(gamma*gcon/(2.0*cp))*ma/sqrt(same)
      w12 =  w1**2
      w2 = wstar2/w1
      delw = w1 - w2

      len = delw/(c*wstar)        ! Total pseudo-shock length (Ikui's model)

      ws2w1 = wstar2/w1

      write(1,97)
97     format(//,'-------------------------------------------------',//)

      write (1,98)gamma,ma,mflo,len
98     format(5x,'gamma  =',f5.3,/
     +        'Initial Mach Number =',f5.3,/,
     +        'Mass Flow Rate     =',f10.5,'  kg/sec',/
     +        '    Pshock length      =',f10.5,'  diameters',//)

      write (1,99)
99     format('     x        wp        wpp        mu      mcorem
     +  jp/j1     jpp/j1       map       mapp       apa1      ap
     +pa1       pp1        p        p0p       p0pp      mcore',/
     +)

      x = 0.0

      do while(x.LE.len)

        wp = w1*exp(-c*x)
        ws2wp = wstar2/wp

        wpp = (wstar2/(w1 - ws2w1))*(1.0 - exp(-c*x))
        ws2wpp = wstar2/wpp

        wpwpp = wp*wpp
```

```
      mun = (ws2wp + wp) - (ws2w1 + w1)
      mud = (ws2wp + wp) - (ws2wpp + wpp)

      mu = mun/mud
      mcorem = 1.0 - mu
      mcore  = mflo*mcorem

      jpj1n = mcorem*(gp12g*wp + gm12g/wp)
      jpj1d = gp12g*w1 + gm12g/w1
      jpj1  = jpj1n/jpj1d

      jppj1n = mu*(gp12g*wpp + gm12g/wpp)
      jppj1d = jpj1d
      jppj1  = jppj1n/jppj1d

      map = wp*sqrt(2.0/(gm1*(1.0 - wp**2)))
      mapp = wpp*sqrt(2.0/(gm1*(1.0 - wpp**2)))

      samep  = 1.0 + gm12*map**2
      samepp = 1.0 + gm12*mapp**2

      pp1n = (wstar2+w12)*(1.0+wpwpp)-w1*(wstar2+1.0)*(wp+wpp)
      pp1d = (1.0-w12)*(wstar2-wpwpp)
      pp1  = pp1n/pp1d
      p    = pp1*p1

      p0p  = p*samep**ggm1
      p0pp = p*samepp**ggm1
     print *,'p =',p
     print *,'  map =',map,'     samep =',samep,'     p0p  =',p0p
     print *,' '

      apa1 = (mcorem/pp1)*(1.0-wp**2)*w1/((1.0-w12)*wp)
      appa1 = (mu/pp1)*(1.0-wpp**2)*w1/((1.0-w12)*wpp)

      write(1,100)x,wp,wpp,mu,mcorem,jpj1,jppj1,map,mapp,apa1,appa1,
     +          pp1,p,p0p,p0pp,mcore

      x = x + 0.1

    enddo

    gamma = gamma - 0.05

    enddo

100  format(f7.3,15f15.5)

    stop
    end
```

Appendix C7

PHOENICS Input Language Listing of Q1 file for 2D Simulation of Compression Region

```
TALK=T;RUN(1,1)
  GROUP 1. Run title and other preliminaries
  Declaration of non-PHOENICS variables
  ny1 = number of y-cells inside injection tube
  nyt = number of y-cells making up injection tube wall
  ny2 = number of y-cells in nozzle
  len = length of computational domain (x-direction)
  htube = half height of injection tube
  ttube = thickness of injection tube wall
  hite1 = width of computational domain at inlet
  hite2 = width of computational domain at exit
  uin = x-component of velocity at inlet
  denin = fluid density at inlet
  hin = specific enthalpy at inlet
  tin = static temperature at inlet
  kein = turbulent kinetic energy at inlet
  epin = rate of dissipation of kein at inlet

integer(ny1,nyt,ny2)
real(len,htube,ttube,hite1,hite2)
real(uin,denin,hin,tin)
real(kein,epin)

htube = 0.0025
ttube = 0.001

hite1 = 0.0125;hite2 = 0.0205
len = 0.46
kein = 1.0e-6;epin = 1.0e-6

  GROUP 2. Transience; time-step specification

  GROUP 3. X-direction grid specification
nx = 350

  GROUP 4. Y-direction grid specification
ny1 = 5;nyt = 5;ny2 = 10
ny = ny1 + nyt + ny2

  GROUP 5. Z-direction grid specification

  GROUP 6. Body-fitted coordinates or grid distortion

rset(d,pshock,len,hite2,0.03)

bfc = t
nogrid = t

if(.NOT.nogrid)then
  Setting points
gset(p,A1,0.0,0.0,0.0);gset(p,A2,0.0,hite1,0.0)
gset(p,B1,len,0.0,0.0);gset(p,B2,len,hite2,0.0)
```

```
  Defining lines between points
gset(l,A1A2,A1,A2,ny,0.7);gset(l,B1B2,B1,B2,ny,0.7)
gset(l,A1B1,A1,B1,nx,1.0);gset(l,A2B2,A2,B2,nx,1.0)
  Defining 'frames'
gset(f,fr1,A1,-,B1,-,B2,-,A2,-)
  Matching frame to rectangular grid
gset(m,fr1,+i+j,1,1,1,trans)
  Copying grid to create second side boundary
gset(c,k2,f,k1,1,nx,1,ny,+,0,0,0.03,INC,1.0)

view(k,1)
view(k,2)

endif

  stop

   GROUP 7. Variables stored, solved & named
solve(p1,u1,v1,h1)
solutn(p1,y,y,y,n,n,n)
store(den1,tmp1)
store(enut)

   GROUP 8. Terms (in differential equations) & devices

   GROUP 9. Properties of the medium (or media)
rho1 = grnd5
rho1a = 0.0;rho1b = 3.48e-3;rho1c = 0.0

press0 = 1.0e+5

tmp1 = grnd2
  tmp1a = 300.0
tmp1b = 9.95e-4

  el1 = grnd4

 *** Sutherland Viscosity Law ***
enul = grnd6
enula = 0.08499;enulb = 110.0

enul = 1.5e-5
  enut = 100.0*enul

drh1dp = grnd5

turmod(kechen)

   GROUP 10. Inter-phase-transfer processes and properties

   GROUP 11. Initialization of variable or porosity fields
uin = 430.0;denin = 0.6875
tin = 200.0;hin = 1005.0*tin

fiinit(h1) = hin
fiinit(ke) = kein
fiinit(ep) = epin
  fiinit(enut) = 1.5e-3
```

```
restrt(p1,u1,v1,h1)
  restrt(ke,ep,enut)

    GROUP 12. Patchwise adjustment of terms (in differential equations)

    GROUP 13. Boundary conditions and special sources
inlet(in,west,1,1,1,ny,1,nz,1,1)
value(in,p1,denin*uin)
value(in,u1,uin)
value(in,h1,hin)
value(in,ke,kein)
value(in,ep,epin)

outlet(out,east,nx,nx,1,ny,1,nz,1,1)
value(out,p1,20000.0)

wall(top,north,1,nx,ny,ny,1,nz,1,1)

    GROUP 14. Downstream pressure for PARAB=.TRUE.

    GROUP 15. Termination of sweeps
lsweep = 20

    GROUP 16. Termination of iterations

    GROUP 17. Under-relaxation devices
real(fdt);fdt = len/(nx*uin)
relax(p1,linrlx,0.7)
relax(u1,falsdt,fdt);relax(v1,falsdt,fdt)
relax(ke,falsdt,0.01*fdt);relax(ep,falsdt,0.01*fdt)

    GROUP 18. Limits on variables or increments to them
    GROUP 19. Data communicated by satellite to GROUND
    GROUP 20. Preliminary print-out
    GROUP 21. Print-out of variables
    GROUP 22. Spot-value print-out
    GROUP 23. Field print-out and plot control
output(p1,n,y,y,y,y,y)
output(u1,n,y,y,y,y,y)
output(v1,n,y,y,y,y,y)
output(h1,n,y,y,y,y,y)
output(ke,n,y,y,y,y,y)
output(ep,n,y,y,y,y,y)
output(enut,n,y,y,y,y,y)

    GROUP 24. Dumps for restarts
STOP
```

Appendix C8

PHOENICS Input Language Listing of Q1 file for 3D SImulation of Flow Compression Region.

```
TALK=T;RUN(1,1)
  GROUP 1. Run title and other preliminaries
integer(ny1,nyt,ny2)
real(len,htube,ttube,hite1,hite2)
real(win,denin,hin,tin)
real(kein,epin)

htube = 0.0025
ttube = 0.001

hite1 = 0.0125;hite2 = 0.0144
len = 0.46
kein = 1.0e-6;epin = 1.0e-6

  GROUP 2. Transience; time-step specification

  GROUP 3. X-direction grid specification
nx = 15

  GROUP 4. Y-direction grid specification
ny1 = 4;nyt = 3;ny2 = 10
ny = ny1 + nyt + ny2

  GROUP 5. Z-direction grid specification
 Direction of Flow
nz = 150

  GROUP 6. Body-fitted coordinates or grid distortion

rset(d,pshock,len,hite2,0.03)

bfc = t
 nogrid = t

if(.NOT.nogrid)then

gset(p,A1,0.0,0.0,0.0);gset(p,A2,0.0,hite1,0.0)
gset(p,B1,0.0,0.0,len);gset(p,B2,0.0,hite2,len)

gset(l,A1A2,A1,A2,ny,0.7);gset(l,B1B2,B1,B2,ny,0.7)
gset(l,A1B1,A1,B1,nz,1.0);gset(l,A2B2,A2,B2,nz,1.0)

gset(f,fr1,A1,-,B1,-,B2,-,A2,-)

gset(m,fr1,+k+j,1,1,1,trans)

gset(c,i:nx+1:,f,i1,1,ny,1,nz,+,0.03,0,0.0,INC,s1.5)

view(i,1)
view(i,2)
view(k,1)
```

```
endif

stop

   GROUP 7. Variables stored, solved & named
solve(p1,u1,v1,w1,h1)
solutn(p1,y,y,y,n,n,n)
store(den1,tmp1)
  store(enut)

   GROUP 8. Terms (in differential equations) & devices

   GROUP 9. Properties of the medium (or media)
rho1 = grnd5
rho1a = 0.0;rho1b = 3.48e-3;rho1c = 0.0

press0 = 1.0e+5

tmp1 = grnd2
  tmp1a = 300.0
tmp1b = 9.95e-4

  el1 = grnd4

 *** Sutherland Viscosity Law ***
  enul = grnd6
  enula = 0.08499;enulb = 110.0

enul = 1.5e-5
enut = 100.0*enul

drh1dp = grnd5

  turmod(kemodl)

   GROUP 10. Inter-phase-transfer processes and properties

   GROUP 11. Initialization of variable or porosity fields
win = 430.0;denin = 0.6875
tin = 200.0;hin = 1005.0*tin

fiinit(h1) = hin
  fiinit(ke) = kein
  fiinit(ep) = epin

restrt(p1,u1,v1,w1,h1)
  restrt(ke,ep,enut)

   GROUP 12. Patchwise adjustment of terms (in differential equations)

   GROUP 13. Boundary conditions and special sources
inlet(in,low,1,nx,1,ny,1,1,1,1)
value(in,p1,denin*win)
value(in,w1,win)
value(in,h1,hin)
  value(in,ke,kein)
  value(in,ep,epin)
```

```
outlet(out,high,1,nx,1,ny,nz,nz,1,1)
  value(out,p1,20000.0)

wall(top,north,1,nx,ny,ny,1,nz,1,1)
wall(left,west,1,1,1,ny,1,nz,1,1)
wall(rite,east,nx,nx,1,ny,1,nz,1,1)

   GROUP 14. Downstream pressure for PARAB=.TRUE.

   GROUP 15. Termination of sweeps
lsweep = 20

   GROUP 16. Termination of iterations

   GROUP 17. Under-relaxation devices
real(fdt);fdt = len/(nz*win)
relax(p1,linrlx,0.7)
relax(u1,falsdt,fdt)
relax(v1,falsdt,fdt)
relax(w1,falsdt,fdt)
   relax(ke,falsdt,0.001*fdt);relax(ep,falsdt,0.001*fdt)

   GROUP 18. Limits on variables or increments to them
   GROUP 19. Data communicated by satellite to GROUND
   GROUP 20. Preliminary print-out
   GROUP 21. Print-out of variables
   GROUP 22. Spot-value print-out

   GROUP 23. Field print-out and plot control
output(p1,n,y,y,y,y,y)
output(u1,n,y,y,y,y,y)
output(v1,n,y,y,y,y,y)
output(w1,n,y,y,y,y,y)
output(h1,n,y,y,y,y,y)
  output(ke,n,y,y,y,y,y)
  output(ep,n,y,y,y,y,y)
  output(enut,n,y,y,y,y,y)

   GROUP 24. Dumps for restarts
STOP
```

Appendix C9

PHOENICS Input Language Listing of Grid Generation file for 3D Simulation of Flow in SAI.

```
TALK=T;RUN(1,1)
  Declaration of non-PHOENICS parameters
  nzan = number of z-cells in 'annular' nozzle region (in 4 parts)
  nzint = number of z-cells in interaction region
  nzdif = number of z-cells in diffuser region
  nyan = number of y-cells in 'annular' nozzle region
  nyt  = number of y-cells in injection tube
  angint = angle (degrees) of divergence of wall in interaction region
  angdif = angle (degrees) of divergence of wall in diffusion region
  ltube = length of injection tube (nozzle region) from stagnation chamber
  lint  = length of interaction region
  lsh  = length of pseudo-shock region
  ldif  = length of diffuser region

integer(nzan1,nzan2,nzan3,nzan4,nzan,nzint,nzsh,nzdif)
integer(nyan,nyt)
real(pi,angint,angdif)
real(ltube,lint,lsh,ldif)
real(htube,hint,hsh,hdif)
real(width)
pi = 4.0*atan(1.0)
angint = 5.0*pi/180.0
angdif = 10.0*pi/180.0
width  = 0.03
htube = 0.0025
ltube = 0.20
lint  = 0.05
lsh   = 0.05
ldif  = 0.05

   GROUP 1. Run title and other preliminaries
   GROUP 2. Transience; time-step specification
   GROUP 3. X-direction grid specification
nx = 10
   GROUP 4. Y-direction grid specification
nyt  = 3
nyan = 15

ny = nyt + nyan
   GROUP 5. Z-direction grid specification
nzan1 = 15;nzan2 = 15;nzan3 = 15;nzan4 = 15
nzan  = nzan1 + nzan2 + nzan3 + nzan4
nzint = 20
nzsh  = 20
nzdif = 20
nz = nzan + nzint + nzsh + nzdif
   GROUP 6. Body-fitted coordinates or grid distortion
rset(d,gdi,ltube+lint+lsh+ldif,0.05,0.05)
bfc = t
  ---Points on the axis ; Points on Tube
  nogrid = t
```

```
if(.NOT.nogrid)then

gset(p,A0, 0.0  ,0.0,0.0);gset(p,B0 ,0.0  ,htube,0.0)
gset(p,A14,0.0,0.0,0.056);gset(p,B14,0.0,htube,0.056)
gset(p,A26,0.0,0.0,0.104);gset(p,B26,0.0,htube,0.104)
gset(p,A38,0.0,0.0,0.152);gset(p,B38,0.0,htube,0.1520)
gset(p,A50,0.0,0.0,ltube);gset(p,B50,0.0,htube,ltube)

 ----- Points on Nozzle (from Chapter 4)-----

gset(p,C0, 0.0,htube+0.0271,0.0)
gset(p,C1, 0.0,htube+0.0268,0.004)
gset(p,C2, 0.0,htube+0.0258,0.008)
gset(p,C3, 0.0,htube+0.0244,0.012)
gset(p,C4, 0.0,htube+0.0228,0.016)
gset(p,C5, 0.0,htube+0.0212,0.020)
gset(p,C6, 0.0,htube+0.0197,0.024)
gset(p,C7, 0.0,htube+0.0182,0.028)
gset(p,C8, 0.0,htube+0.0170,0.032)
gset(p,C9, 0.0,htube+0.0159,0.036)
gset(p,C10,0.0,htube+0.0149,0.040)
gset(p,C11,0.0,htube+0.0141,0.044)
gset(p,C12,0.0,htube+0.0133,0.048)
gset(p,C13,0.0,htube+0.0127,0.052)
gset(p,C14,0.0,htube+0.0121,0.056)
gset(p,C15,0.0,htube+0.0116,0.060)
gset(p,C16,0.0,htube+0.0112,0.064)
gset(p,C17,0.0,htube+0.0109,0.068)
gset(p,C18,0.0,htube+0.0105,0.072)
gset(p,C19,0.0,htube+0.0102,0.076)
gset(p,C20,0.0,htube+0.0100,0.080)
gset(p,C21,0.0,htube+0.0099,0.084)
gset(p,C22,0.0,htube+0.0097,0.088)
gset(p,C23,0.0,htube+0.0096,0.092)
gset(p,C24,0.0,htube+0.0095,0.096)
gset(p,C25,0.0,htube+0.0094,0.100)
gset(p,C26,0.0,htube+0.0094,0.104)
gset(p,C27,0.0,htube+0.0094,0.108)
gset(p,C28,0.0,htube+0.0094,0.112)
gset(p,C29,0.0,htube+0.0094,0.116)
gset(p,C30,0.0,htube+0.0094,0.120)
gset(p,C31,0.0,htube+0.0095,0.124)
gset(p,C32,0.0,htube+0.0096,0.128)
gset(p,C33,0.0,htube+0.0097,0.132)
gset(p,C34,0.0,htube+0.0098,0.136)
gset(p,C35,0.0,htube+0.0100,0.140)
gset(p,C36,0.0,htube+0.0101,0.144)
gset(p,C37,0.0,htube+0.0103,0.148)
gset(p,C38,0.0,htube+0.0105,0.152)
gset(p,C39,0.0,htube+0.0107,0.156)
gset(p,C40,0.0,htube+0.0109,0.160)
gset(p,C41,0.0,htube+0.0111,0.164)
gset(p,C42,0.0,htube+0.0113,0.168)
gset(p,C43,0.0,htube+0.0116,0.172)
gset(p,C44,0.0,htube+0.0118,0.176)
gset(p,C45,0.0,htube+0.0120,0.180)
gset(p,C46,0.0,htube+0.0121,0.184)
gset(p,C47,0.0,htube+0.0123,0.188)
```

```
gset(p,C48,0.0,htube+0.01245,0.192)
gset(p,C49,0.0,htube+0.01253,0.196)
gset(p,C50,0.0,htube+0.01259,ltube)

gset(p,A51,0.0,0.0,ltube+lint)
gset(p,B51,0.0,htube,ltube+lint)

hint = htube + 0.01259 + lint*tan(angint)

gset(p,C51,0.0,hint,ltube+lint)

gset(p,A52,0.0,0.0,ltube+lint+lsh)
gset(p,B52,0.0,htube,ltube+lint+lsh)
gset(p,C52,0.0,hint,ltube+lint+lsh)

hdif = hint + ldif*tan(angdif)

gset(p,A53,0.0,0.0,ltube+lint+lsh+ldif)
gset(p,B53,0.0,htube,ltube+lint+lsh+ldif)
gset(p,C53,0.0,hdif,ltube+lint+lsh+ldif)

  Defining z-direction lines
gset(l,A014 ,A0 ,A14,nzan1,1.2)
gset(l,A1426,A14,A26,nzan2,1.0)
gset(l,A2638,A26,A38,nzan3,1.0)
gset(l,A3850,A38,A50,nzan4,1.0)
gset(l,A5051,A50,A51,nzint,1,0)
gset(l,A5152,A51,A52,nzsh,1.0)
gset(l,A5253,A52,A53,nzdif,1,0)

gset(l,B014 ,B0, B14,nzan1,1.2)
gset(l,B1426,B14,B26,nzan2,1.0)
gset(l,B2638,B26,B38,nzan3,1.0)
gset(l,B3850,B38,B50,nzan4,1.0)
gset(l,B5051,B50,B51,nzint,1,0)
gset(l,B5152,B51,B52,nzsh, 1.0)
gset(l,B5253,B52,B53,nzdif,1,0)

gset(v,noz1,C0,C1,C2,C3,C4,C5,C6,C7,C8,C9,C10,C11,C12,C13,C14)
gset(l,C014,C0,C14,nzan1,1.0,CRV,noz1)

gset(v,noz2,C14,C15,C16,C17,C18,C19,C20,C21,C22,C23,C24,C25,C26)
gset(l,C1426,C14,C26,nzan2,1.0,CRV,noz2)

gset(v,noz3,C26,C27,C28,C29,C30,C31,C32,C33,C34,C35,C36,C37,C38)
gset(l,C2638,C26,C38,nzan3,1.0,CRV,noz3)

gset(v,noz4,C38,C39,C40,C41,C42,C43,C44,C45,C46,C47,C48,C49,C50)
gset(l,C3850,C38,C50,nzan4,1.0,CRV,noz4)

gset(l,C5051,C50,C51,nzint,1.0)
gset(l,C5152,C51,C52,nzsh,1.0)
gset(l,C5253,C52,C53,nzdif,1.0)

 ----- Setting y-lines -----

gset(l,A0B0  ,A0 ,B0 ,nyt,1.0)
gset(l,A14B14,A14,B14,nyt,1.0)
```

```
gset(l,A26B26,A26,B26,nyt,1.0)
gset(l,A38B38,A38,B38,nyt,1.0)
gset(l,A50B50,A50,B50,nyt,1.0)
gset(l,A51B51,A51,B51,nyt,1.0)
gset(l,A52B52,A52,B52,nyt,1.0)
gset(l,A53B53,A53,B53,nyt,1.0)

gset(l,B0C0  ,B0 ,C0 ,nyan,s1.5)
gset(l,B14C14,B14,C14,nyan,s1.5)
gset(l,B26C26,B26,C26,nyan,s1.5)
gset(l,B38C38,B38,C38,nyan,s1.5)
gset(l,B50C50,B50,C50,nyan,s1.5)
gset(l,B51C51,B51,C51,nyan,s1,5)
gset(l,B52C52,B52,C52,nyan,s1.5)
gset(l,B53C53,B53,C53,nyan,s1.5)

 ----- Setting and Matching Frames -----
gset(f,frt1,A0,-,A14,-,B14,-,B0,-)
gset(f,frt2,A14,-,A26,-,B26,-,B14,-)
gset(f,frt3,A26,-,A38,-,B38,-,B26,-)
gset(f,frt4,A38,-,A50,-,B50,-,B38,-)
gset(m,frt1,+k+j,1,1,1,trans)
gset(m,frt2,+k+j,1,1,nzan1+1,trans)
gset(m,frt3,+k+j,1,1,nzan1+nzan2+1,trans)
gset(m,frt4,+k+j,1,1,nzan1+nzan2+nzan3+1,trans)

gset(f,fra1,B0,-,B14,-,C14,-,C0,-)
gset(f,fra2,B14,-,B26,-,C26,-,C14,-)
gset(f,fra3,B26,-,B38,-,C38,-,C26,-)
gset(f,fra4,B38,-,B50,-,C50,-,C38,-)
gset(m,fra1,+k+j,1,nyt+1,1,trans)
gset(m,fra2,+k+j,1,nyt+1,nzan1+1,trans)
gset(m,fra3,+k+j,1,nyt+1,nzan1+nzan2+1,trans)
gset(m,fra4,+k+j,1,nyt+1,nzan1+nzan2+nzan3+1,trans)

gset(f,fri1,A50,-,A51,-,B51,-,B50,-)
gset(f,fri2,B50,-,B51,-,C51,-,C50,-)
gset(m,fri1,+k+j,1,1,nzan+1,trans)
gset(m,fri2,+k+j,1,nyt+1,nzan+1,trans)

gset(f,frs1,A51,-,A52,-,B52,-,B51,-)
gset(f,frs2,B51,-,B52,-,C52,-,C51,-)
gset(m,frs1,+k+j,1,1,nzan+nzint+1,trans)
gset(m,frs2,+k+j,1,nyt+1,nzan+nzint+1,trans)

gset(f,frd1,A52,-,A53,-,B53,-,B52,-)
gset(f,frd2,B52,-,B53,-,C53,-,C52,-)
gset(m,frd1,+k+j,1,1,nzan+nzint+nzsh+1,trans)
gset(m,frd2,+k+j,1,nyt+1,nzan+nzint+nzsh+1,trans)

gset(c,i:nx+1:,f,i1,1,ny,1,nz,+,width,0,0,INC,1.0)

endif

view(i,1)

  stop
```